UNIVERSIDAD D SEVILLA

FACULTY OF BIOLOGY

DEPARTMENT OF GENETICS

Interplay between Endoplasmic Reticulum and Cellular Homeostasis

Leticia Lemus Rodríguez

Seville, 2017

PhD Program in Integrated Biology
University of Seville

Interplay between Endoplasmic Reticulum and Cellular Homeostasis

Dissertation submitted to the
Faculty of Biology, University of Seville, Spain by

Leticia Lemus Rodríguez

for the degree of Doctor of Natural Sciences

Dr. Veit Goder
Director
Dpt. of Genetics

Leticia Lemus Rodríguez
PhD student
Dpt. of Genetics

Seville, 30th May, 2017

To my Teachers, Classmates and Friends.

“Its pictures had for me the effect of the song of a mermaid: irresistible and half transparent”.

George E. Palade
(Palade, 1975)
Recalling EM pictures of the rough endoplasmic reticulum.

“Essential… will be the development… of devices… to visualize the dynamic machinery of autophagy in higher spatiotemporal resolution”.

Yoshinori Ohsumi
(Ohsumi, 2014)

Summary

Autophagy and ERAD (endoplasmic reticulum-associated protein degradation) are stress response pathways required for cell homeostasis. These two clearance pathways involve the trafficking and degradation of cellular components.

Autophagy is characterized by the engulfment of the targeted cargo by cytosolic double membrane vesicles: autophagosomes. Our group has identified the *Saccharomyces cerevisiae* ER-localized Qa-SNARE Ufe1p, as a novel component, needed in autophagy. In *ufe1-1* cells expressing GFP-Atg8, there is no generation of free GFP at the non-permissive temperature, indicating impairment in the autophagic flux. Furthermore, the analysis of the electron microscopy images of this conditional mutant strain revealed a significant reduction in number and size autophagosomes. Moreover, the number of autophagic bodies is almost absent in this mutant. Together, these results indicate that Ufe1p plays a role in autophagosome biogenesis and autophagy flux.

Furthermore, we investigate the degradation mechanisms of post-translational modified misfolded proteins by ERAD. Glycosylphosphatidylinositol-anchored proteins (GPI-APs) are secretory proteins anchored to the luminal leaflet of the ER membrane. It has been recently enquired whether GPI-APs may be refractory to degradation by ERAD because of their covalently attached glycolipid, which might poses a topologic problem for ERAD. We have identified that the yeast misfolded GPI-AP, Gas1*p, it is indeed degraded by ERAD and additional mechanisms might be implicated in its turnover, like autophagy.

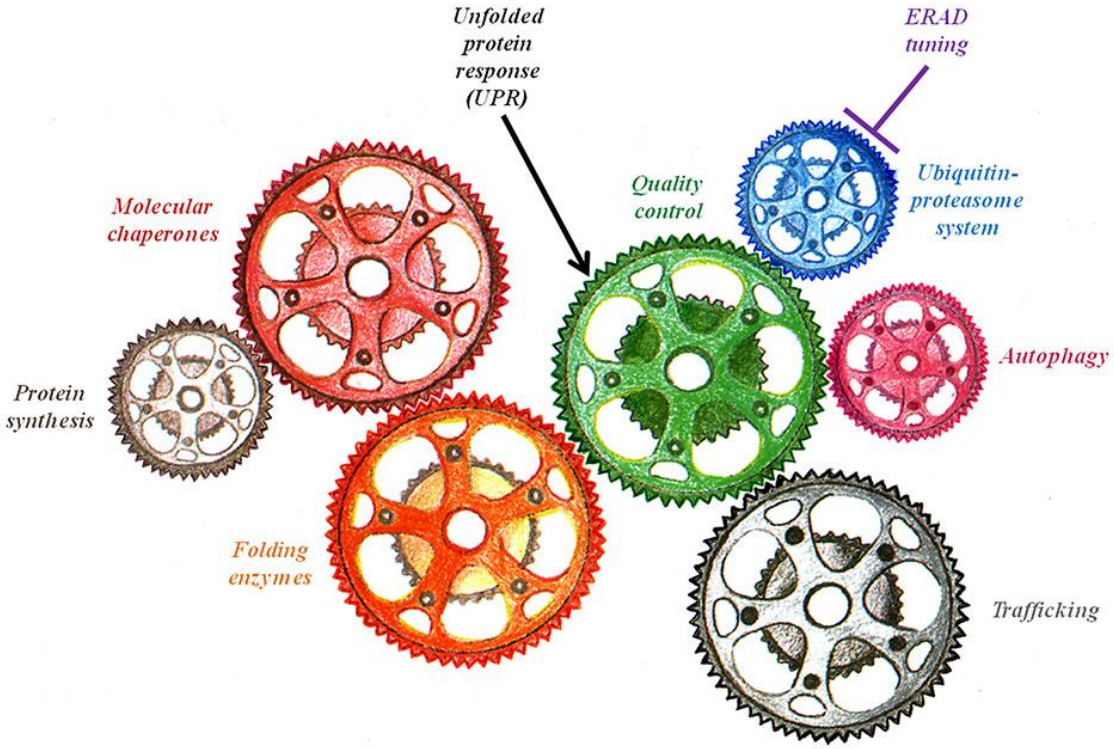

Noack, *et al.*, **Swiss Med Wkly**, 2014

Preface

This thesis has been entirely conducted in the Integral Biology Program, Cell and Molecular Biology research field at the Department of Genetics under the supervision of Dr. Veit Goder.

The results of the work presented here illustrate, first, a previously unreported explanation for the limiting of GPI-anchored proteins as ERAD substrate; second, a novel role for the ER-localized SNARE Ufe1p in autophagy.

TABLE OF CONTENTS

Abbreviations

aa	aminoacid
AB	autophagic body
AP	autophagosome
Ape1	aminopeptidase 1
Atg	autophagy-related (Atg) protein
BiP	binding immunoglobulin protein
COPI	coatomer protein I-mediated retrograde transport
COPII	coatomer protein II-mediated anterograde transport
CRT	calreticulin
Cvt	cytoplasm to vacuole targeting
CXN	calnexin
DAG	diacylglycerol
DRM	detergent resistant membrane
ER	endoplasmic reticulum
ERES	ER exit sites
ERQC	ER quality control
EtNP	phosphoethanolamine
GlcN	N - acetylated glucosamine
GPI	glycosylphosphatidylinositol
GPI-AP	GPI-anchored protein
Hsp	heat shock protein
Ino	inositol phospholipid
IRE1	inositol-requiring enzyme-1
LC3	microtubule-associated protein 1 light chain 3
Man	mannose
MVB	Multivesicular body
OST	oligosaccharyltransferase
PAS	pre-autophagosomal structure or phagophore assembly site
PDI	protein disulfide isomerase
PE	phosphatidylethanolamine
PI-PLC	phosphoinositol-specific phospholipase C
PLC	phospholipase C
PMT	protein *o*-mannosyltransferase
PTMs	post-translational modifications

RER	rough endoplasmic reticulum
SER	smooth endoplasmic reticulum
SNARE	SNAP (Soluble NSF Attachment Protein) REceptor
SRP	signal recognition particle
SS	signal sequence
TAP	tandem affinity purification
TCR	T cell antigen receptor
TEM	transmission electron microscopy
TMD	transmembrane domain
Ub	ubiquitin
UBC	ubiquitin carrier protein
UGGT	UDP-glucose:glycoprotein transferase
UPR	unfolded protein response
UPS	ubiquitin-proteasome system
WT	wild type

INTRODUCTION

The Endoplasmic Reticulum (ER).

Eukaryotic cells have a complex internal structure that contains many membrane-limited compartments known as organelles. One of the most remarkable organelles is the endoplasmic reticulum (ER) whose labyrinthine spaces encompass more than half of the total area of membrane in a eukaryotic cell (Figure 1, A). Pioneering work of George E. Palade, by using electron microscopy techniques, demonstrated that it is involved in secretory processes (Palade, 1956).

The ER possesses several subdomains with distinct morphology, composition, and function (Lynes and Simmen, 2011; Voeltz et al., 2002). It is organized into a netlike of tubules and flattened sacs extending from the nuclear envelop throughout the cytosol forming two plastic sub-compartments: the rough (RER) and the smooth ER (SER) (Shibata et al., 2006). The first is studded with ribosomes, which is the first station of the secretory pathway for protein synthesis; the latter is devoid of ribosomes and is the site of synthesis for lipids and several of its related metabolites (Figure 1, B and C).

More light was shed on the role of the ER in protein processing and sorting through the findings made by G. E. Palade and his colleagues in the early 1960s (Caro and Palade, 1964; Siekevitz and Palade, 1962). Proteins that are destined to become part of the Golgi apparatus, endosomes, vacuole, plasma membrane and obviously those ER-resident proteins are first targeted to the ER in order to enter into the secretory pathway.

Altogether, membrane and secretory proteins represent up to 30% of total protein in a eukaryotic cell (Diehn et al., 2006), and they are mostly co-translationally translocated into the ER. That is, the protein is being synthesized in the cytosol and emerging from the ribosome, while the N-terminal[1] signal sequence (SS) of the nascent polypeptide is recognized by the signal recognition particle (SRP) that in turn interacts with the SRP receptor, which is embedded in the ER membrane. Thus, the ribosome-nascent chain complex will be anchored to the ER membrane. (Ogg et al., 1992).

[1] or also internal signal sequence in the case of transmembrane proteins.

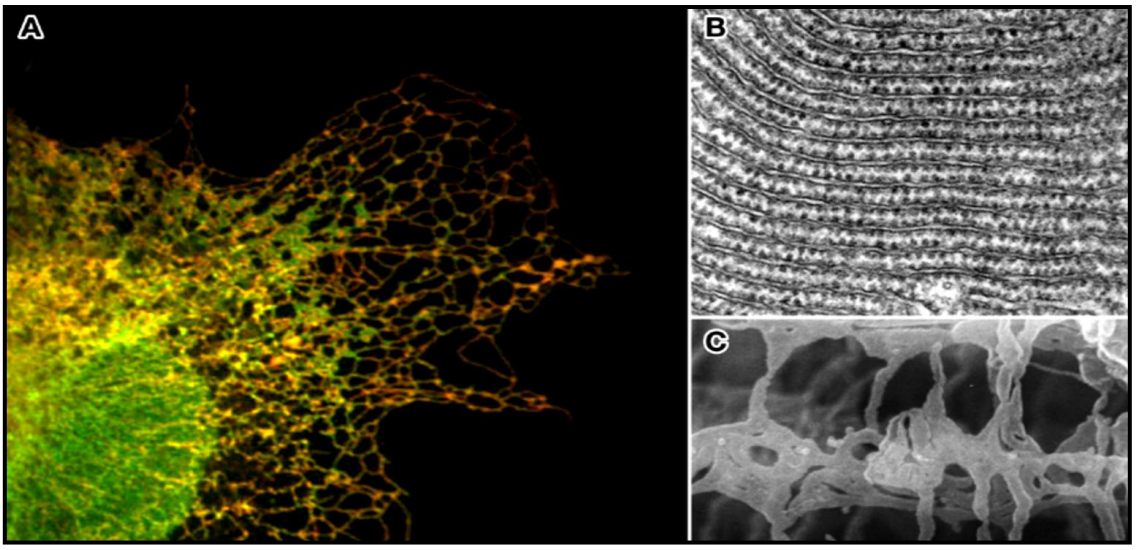

Figure 1. Endoplasmic reticulum and its different structural subdomains.
(A) A cultured cell line coexpressing Rtn4c (red, tubules) and Sec61β (green, sheets) shows the huge membrane extension of the ER. (B) Thin-section electron micrograph of the RER in secretory cells from the silk glands of the silkworm. (C) Scanning electron micrograph of the SER in the sarcoplasmic reticulum of rat white skeletal muscle fibers. Note that the RER in (B) appears as sheets, whereas the SER in (C) is tubular. (Shibata et. al., 2006).

The SRP is released and the nascent polypeptide is targeted to a protein-conducting channel formed by a heterotrimeric membrane-protein complex, the Sec61 complex[2] or "translocon", which mediates the integration or translocation of the polypeptide chain, into or across the ER membrane respectively (Rapoport, 2007). Namely, two kinds of proteins are moved from the cytosol to the ER: on one hand water-soluble proteins will cross completely the ER membrane and will be released into the ER lumen, and on the other hand, transmembrane proteins will partially cross the ER membrane and will become embedded in it.

When protein folding fails and terminally misfolded proteins start to accumulate in the lumen of the ER, several stress response are triggered in order to maintain the ER homeostasis. There are two major pathways of intracellular protein degradation: the ubiquitin-proteasome system (UPS) and autophagy (Ciechanover, 2012). They encompass the unfolded protein response (UPR), which induces the expression of chaperones and proteins involved in the recovery of the ER proteostasis. Next, if the stress is prolonged and ER function cannot be restored, two catabolic processes are triggered: the ER-associated protein degradation (ERAD) and autophagy (Nedelsky et al., 2008; Pisoni and Molinari, 2016; Senft and Ronai, 2015).

[2] Sec61 complex is the translocase heterotrimeric complex composed of alpha, beta, and gamma subunits (Sec61p-Sss1p-Sbh1p) in eukaryotes and the SecY in prokaryotes.

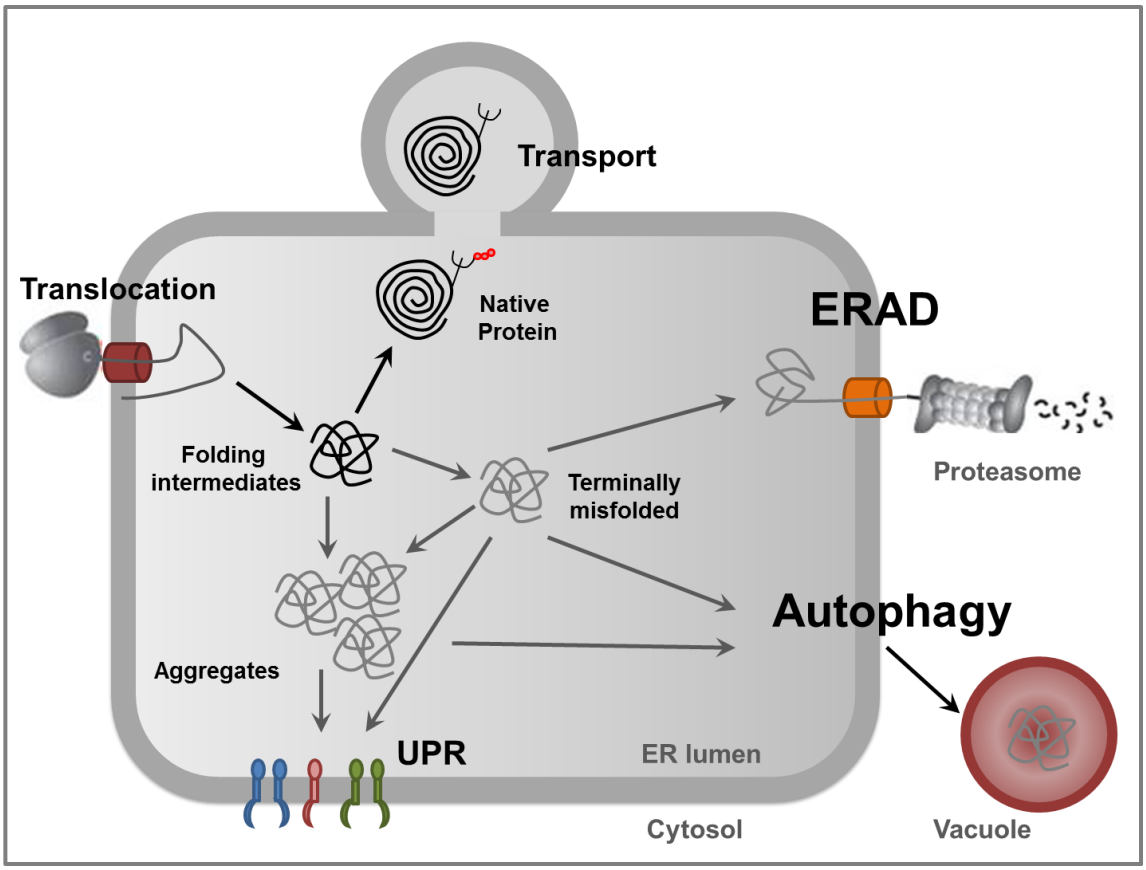

Figure 2. Proteostasis networks in the ER.
Newly synthesized secretory proteins are translocated into the ER in an unfolded state. ER chaperones and other folding enzymes involved in post-translationally modification participate in the folding process to attained the native conformation of the protein which will be transported to its final location. When proteins are terminally misfolded or form aggregates, they will accumulate and will result in ER stress. Subsequently, the unfolded protein response (UPR) is triggered and eventually, terminally misfolded proteins and/or aggregates are transported out of the ER in order to undergo degradation processes. Namely, the ER-association protein degradation (ERAD) targets misfolded proteins to the proteasome. Additionally, autophagy targets misfolded proteins and aggregates to the vacuole/lysosome in a mechanism that remains in part elusive.

We have focused on two major proteolytic processes: ERAD and autophagy. And we have used the eukaryotic model organism *Saccharomyces cerevisiae,* which has been a driving force in the discovery and elucidation of both ERAD (Hiller et al., 1996; Lippincott-Schwartz et al., 1988; Sommer and Wolf, 1997) (Vembar and Brodsky, 2008) and autophagy (Baba et al., 1994; Ohsumi, 2014; Takeshige et al., 1992).

The first part of this work encompasses the quality control mechanism of the glycosylphosphatidylinositol (GPI)-anchored proteins (GPI-APs), Gas1*p, one of the most abundant secretory proteins in the baker's yeast, in order to decipher the molecular mechanism of its degradation, focusing in the ERAD pathway (Sikorska et al., 2016).

A special secretory protein are the GPI-APs (Figure 8) which play a wide variety of physiological roles, as nutrient uptake, hydrolytic enzymes, cell surface antigens,

signaling receptors, cell adhesion, migration molecules, protease inhibitors, etc. (Kinoshita, 2014). Consequently, defects in GPI-APs causes several pathological conditions being many of them neurophysiological diseases, suggesting that GPI synthesis is critical for the correct development of the nervous system (Kato et al., 2014; Ng et al., 2012) (Paladino et al., 2015). In the yeast *S. cerevisiae*, and probably most fungi, GPI anchors are used to target certain mannoproteins for covalent incorporation into the β-glucan cell wall (Ferguson et al., 2009).

In virtue of the implication of GPI-APs in prominent diseases, their intracellular quality control mechanisms have been extensively studied. It has been shown that some misfolded GPI-APs accumulate in the presence of proteasome inhibitors, indicating that ERAD might be involved in their turnover (Ma and Lindquist, 2001; Wang et al., 2014). However, other studies have reported that GPI-APs may be poor ERAD substrates because the GPI moiety could be a sterical hindrance for ERAD, being predominantly targeted to the lysosome for its degradation (Satpute-Krishnan et al., 2014).

The second part of this work deals with the subject of autophagy. The word “autophagy” was coined by Christian de Duve in 1963 (de Duve, 1963) in a conference on lysosomes and the term originates from the Greek words *auto*-, meaning "self", and *phagein*, meaning "to eat". Thus, autophagy is the degradation process of cytoplasmic constituents delivered to the vacuole/lysosome in double-membrane vesicles called autophagosomes (Ohsumi, 2014).

Namely, we have centered in determining the role of Ufe1p, an ER-localized SNARE[3] in the biogenesis and completion of autophagosomes.

Both, ERAD and autophagy are proteolytic processes within the cell involved in proteostasis and associated with numerous physiological and pathological human conditions. Thus, disruption of ER homeostasis is linked to many human diseases as diverse as diabetes, neurodegeneration (Creutzfeldt–Jakob, Alzheimer, Parkinson’s and Huntington’s disease), heart and kidney disease, viral and bacterial infections cancer, atherosclerosis, etc. (Ciechanover, 2012; Whatley et al., 2008) and reviewed in (Guerriero and Brodsky, 2012).

Therefore, studies on ER homeostasis broaden the knowledge about the mechanisms that lead organisms to disease or to health.

[3] SANRE: **SNA**P (Soluble NSF Attachment Protein) **RE**ceptor

PART I

Role of the Endoplasmic Reticulum in Protein Quality Control

Endoplasmic Reticulum Quality Control (ERQC)

The ER is an organelle where about 30% of all cellular protein synthesis, folding, and traffic is orchestrated. As with every biological process, protein biogenesis is prone to errors. Thus, several quality control mechanisms are to be performed in the ER to assure that only correctly folded, assembled, and modified proteins are transported along the secretory pathway (Ellgaard and Helenius, 2003). Consequently, folding and aid in oligomerization are controlled by a system of sequential checkpoints that recognize topologically distinct domains of the protein (Vashist and Ng, 2004). Therefore, both processes, protein folding and protein quality control are to be tightly intertwined (Figure 3).

The key step in ERQC is the assistance in proteostasis by a battery of chaperones, folding enzymes and folding sensors present in the lumen and/or in the membrane of the ER (Ellgaard et al., 2016; Halperin et al., 2014; Houck and Cyr, 2012). Hence, chaperones will interact with nascent polypeptides, or with intermediate folding states or with terminally misfolded structures. Accordingly, chaperones in the ER have a wide range of functions. Likewise, they can be sorted in three main groups: first, the heat shock protein (Hsp70, Hsp90) family and its co-chaperones (Hsp40), second, the lectin-like chaperones (calnexin (CNX), calreticulin (CRT)) and third, the thiol oxidoreductases (protein disulfide isomerase, PDI family) (Nishikawa et al., 2005; Stolz and Wolf, 2010).

Thus, in a first instance, chaperones facilitate protein folding, oligomerization, maturation, and post-translational modifications by interacting with hydrophobic patches that are exposed in the newly synthetized polypeptide or with specific polypeptide sequence (Guerriero and Brodsky, 2012; Nishikawa et al., 2001; Pincus, 2016; Stolz and Wolf, 2010).

Once proteins have attained their native structure, they will be released from chaperones, exit the ER and transported through the secretory pathway till eventually they reach their final location (Figure 3, (2d), (3f), (4) and (6)).

Despite the aid of different cellular components, substantial fraction (40% or more) of newly synthesized native proteins are translated, folded or assembled with low efficiency and fail to mature due to errors in these processes or because of genetic mutations (Ellgaard and Helenius, 2003; Schubert et al., 2000).

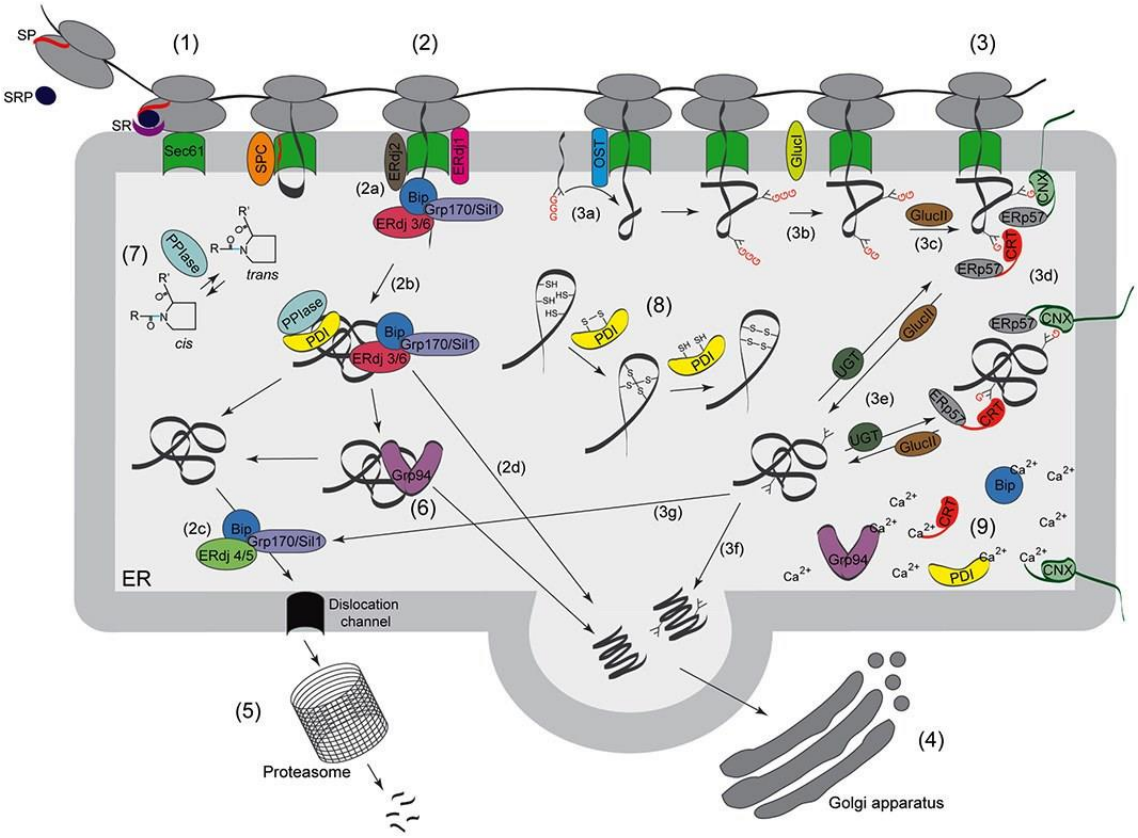

Figure 3. Protein folding in the ER and ERQC.

Nascent polypeptides are translocated in an unfolded state into the ER (1). BiP/Kar2 (2) and calnexin (CNX)/calreticulin (CRT) (3) are two of the main chaperone system in the ER. BiP functions together with other co-chaperones depending on the process: either translocation, or protein folding or degradation (2a, 2b and 2c, respectively). CNX and CRT, both lectins, assist the folding of glycoproteins that carry mono-glucosylated N-linked glycans (3d), a moiety that initially contains 3 glucoses and that is added to secreted proteins by the ER resident oligosaccharyltransferase (OST) (3a). Other folding factors include Grp94 (6), peptidyl-prolyl isomerases (PPIases) (7), and protein disulfide isomerases (PDIs) (8), assists also folding of proteins. Terminally misfolded proteins (2c, 3g) are targeted to a dislocation channel and retrotranslocated into the cytosol for degradation by the proteasome (5), a process called ER-associated protein degradation or ERAD (Ellgaard et al., 2016).

Such unfolded or misfolded species are then retained in the ER by some of the major ER-resident chaperone system: BiP (Kar2 in baker's yeast) and CNX/ CRT. The latter is best studied in mammalian cells where repetitive binding and release of these chaperones to substrates is dependent on protein folding and is regulated by a distinct set of the N-glycan remodeling steps by glycosidases (glucosidase I and II) and by the UDP-glucose:glycoprotein glucosyltransferase (UGGT) (Ellgaard and Helenius, 2003; Lemus and Goder, 2014).

A canonical CNX/CRT mechanism does not exist in yeast because it lacks the orthologue of the key enzyme UGGT. Nevertheless, the presence of calnexin in yeast suggests that a simpler mechanism of protein folding based on binding to sugar residues is present in most eurkaryotes (Jakob et al., 2001). Together this process is

also known as the calnexin/calreticulin cycle (Hammond et al., 1994; Hebert et al., 1995) (Figure 3, (3a-3e)).

Protein *o*-mannosylation is essential for viability of cells, due to their role in the stability, localization and/or function of various secretory and membrane proteins. It is known that protein *o*-mannosyltransferase (PMT) are upregulated during ER stress by the UPR (Travers et al., 2000). Therefore, this post-translational modification is also involved in ER homeostasis. It has been shown that *o* -mannosylation of misfolded proteins retained in the ER, increases and it is a signal for targeting terminally misfolded proteins to ERAD or for post-ER degradation processes (Goder and Melero, 2011; Nakatsukasa et al., 2004). Moreover, additional protein quality control mechanisms occur along the secretory pathway downstream the ER (Arakawa et al., 2016; Arvan et al., 2002; Kadowaki et al., 2015; Wang and Ng, 2010; Zhao et al., 2013).

Eventually and after passing all this scrutiny of the ERQC, if proteins do not attain their native state they will end up terminally misfolded and are ultimately eliminated. Degradation of terminally misfolded proteins from the ER can occur via either of the two major intracellular protein degradation systems: the ubiquitin-proteasome system (UPS) and/or autophagy. The latter will be discussed in more detail in Part II p. 77.

The UPS is linked to the degradation of misfolded ER proteins as part of an ER-specific degradation pathway called ER-associated protein degradation or ERAD (it will be discussed in the next chapter p.21) in which terminally misfolded proteins are retrotranslocated to the cytosol and targeted to the proteasome for degradation (Figure 3, (5)).

Endoplasmic Reticulum-Associated Protein Degradation (ERAD)

The first evidence connecting the ER with protein degradation was observed with newly synthesized T cell antigen receptor (TCR) subunits in which the non-glycosylated precursors of the single alpha monomers of the multimeric complex were undergoing degradation (Lippincott-Schwartz et al., 1988). That suggested that "some" proteolytic processes were occurring prior to reach the Golgi and consequently somewhere between ER and Golgi.

These results indicated the existence of a selective degradation of unassembled or incomplete assembled TCR complexes in a lysosome-independent manner (Bonifacino et al., 1989). By that time, the site of the nonlysosomal degradation was uncertain and it was thought to be either located “within” or closely related to the ER (Bonifacino and Lippincott-Schwartz, 1991). Many important studies were directed to elucidate the location, the machinery and the protease(s) that were involved in the newly-found degradation pathway (reviewed in (Needham and Brodsky, 2013)).

Next, in a seminal work carried out in yeast, it was determined that proteins that failed to pass the ERQC are targeted to ER resident factors and surprisingly, this malfolded species were returned to the cytoplasm, a step called retro-translocation, and degraded by the proteasome. Since ER-associated components were required for this degradation, the process was named ER-associated degradation, or simply ERAD (Werner et al., 1996).

The capacity of the cell to perform ERAD is part regulated by a pathway named the unfolded protein response (UPR). In yeast, the accumulation of misfolded polypeptides in the ER is detected directly and indirectly by the conserved ER membrane-embedded protein kinase Ire1p which, upon activation, leads to an unconventional splicing of the transcript for the transcription factor Hac1p which induces the expression of the so-called UPR target genes. Many of these upregulated genes are ER chaperones and several ERAD components (Cox and Walter, 1996; Travers et al., 2000) (Figure 4).

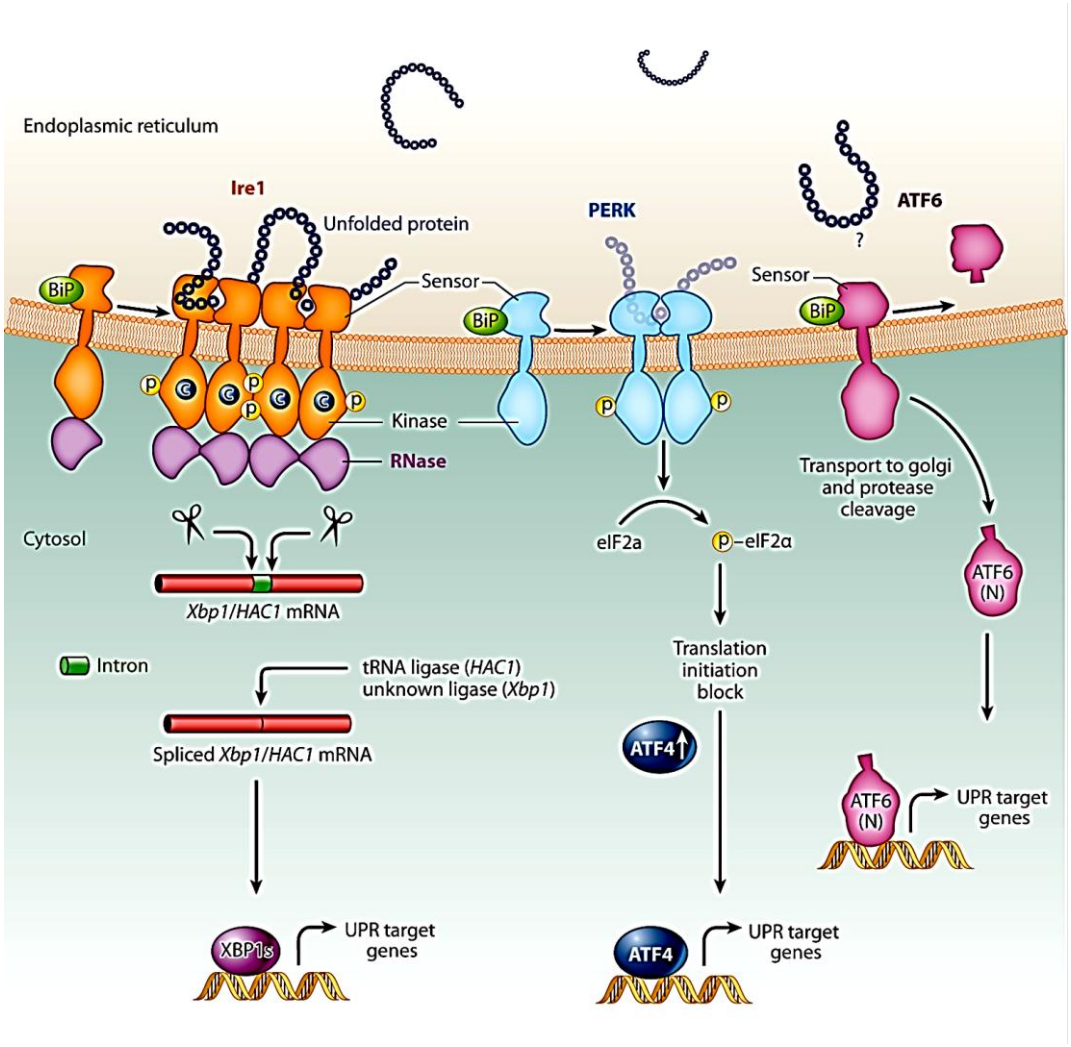

Figure 4. The three unfolded protein response (UPR) branches in higher eukaryotes.
Ire1, PERK, and ATF6 are three sensors of unfolded proteins located in the ER membrane. They activate transcriptional and translational processes aiming to attain the native state of the proteins. Upon activation, Ire1 assembles into high-order oligomers and PERK into dimers. Signaling in the Ire1 branch proceeds via the nonconventional splicing of Xbp1 or (in yeast) HAC1 mRNA. Signaling in the ATF6 branch utilizes regulated proteolysis of ATF6 to liberate its cytosolic domain, which then functions as a transcription activator in the nucleus (Korennykh and Walter, 2012).

This conserved response leads to an increase in the folding capacity of the ER and activates the clearance of accumulating misfolded proteins by ERAD (Figure 6) (Hoseki et al., 2010).

At the same time, it became clear that ubiquitination plays an important role in ER protein degradation (Sommer and Jentsch, 1993). ER membrane-embedded E3 ubiquitin ligases were identified as key components in ERAD (Foresti et al., 2014; Hampton et al., 1996; Swanson et al., 2001).

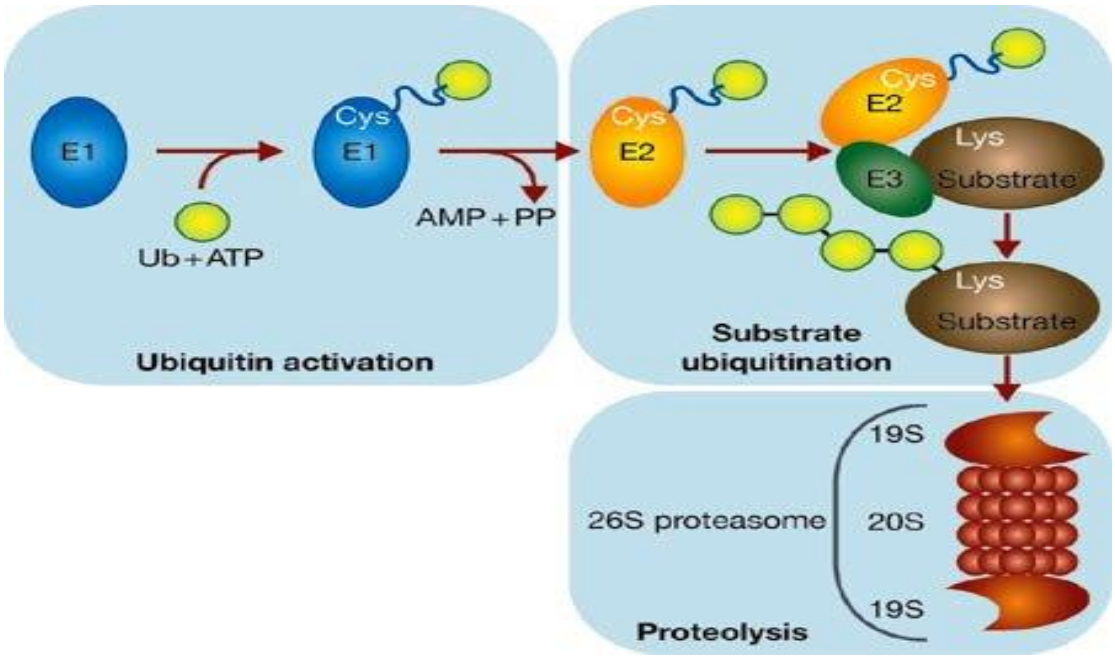

Figure 5. The ubiquitin-proteasome system (UPS).

Ubiquitin (Ub) are activated for transfer by ubiquitin-activating enzyme (E1). Next, activated Ub (E1~Ub) is transferred in thioester linkage from the active-site cysteine of E1 to the active-site cysteine of an ubiquitin-conjugating enzyme (E2). The E2~Ub thioester next interacts with an ubiquitin ligase (E3), which transfers the Ub from E2~Ub to a lysine residue of a proteins substrate. Ubiquitinated proteins are recognized by specific subunits in the 19S capping complexes of the 26S proteasome (Meusser et al., 2005).

Ubiquitination of proteins is a post-translational modification that occurs in the cytosol and nucleoplasm of eukaryotic cells in a multistep transfer between a series of ubiquitin ligases (Hershko and Ciechanover, 1998). First, ubiquitin-activating enzymes (E1s) will activate ubiquitin molecules by the coupling of a thiol group of a specific cysteine in E1 to the ATP-dependent C-terminus of the ubiquitin molecule. Second, ubiquitin will be transferred to the ubiquitin conjugating enzymes (E2s, also referred to as ubiquitin carrier proteins or UBCs). Finally, ubiquitin-protein ligases (E3s) bind to specific protein substrates and either promote the transfer of ubiquitin (RING-E3) (Metzger et al., 2014) or serve as catalytic intermediates (HECT-E3) from a thioester to amide linkages (*ε*-amino group of internal lysines) to proteins or to polyubiquitin chains. (Metzger et al., 2012) (Lemus and Goder, 2014). These modifications can be reversed by deubiquitinating enzymes (DUBs), which also play important roles in establishing the ubiquitin code (Komander and Rape, 2012).

In yeast, there is a large number of known E3 ligases, however only three RING E3 ligase are know so far that have a function in ERAD: Hrd1, Doa10 and Asi1 (Carvalho et al., 2006; Foresti et al., 2014). These ligases form membrane-associated complexes that specifically recognize and ubiquitinate lumenal and membrane misfolded proteins for targeting to the proteasome.

The elucidation of a variety of associated factors in the ER lumen and in the ER membrane in the last years has led to an emerging model of how misfolded ER proteins are recognized, retrotranslocated into the cytosol and targeted to the proteasome for degradation, (see Figure 3, reviewed in (Lemus and Goder, 2014) and (Mehnert et al., 2010).

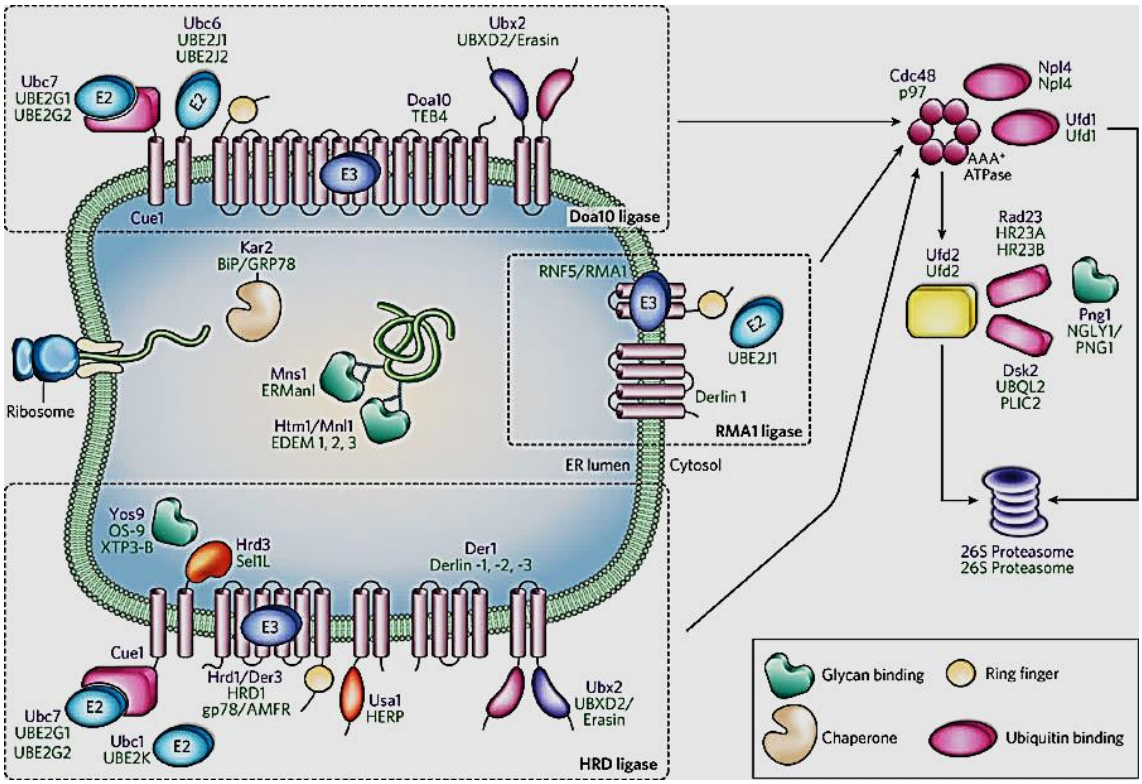

Figure 6. Mechanism of protein degradation in yeast and mammalian cells.
Misfolded proteins are detected by molecular chaperones and other folding sensor factors (like glycosylhydrolases, Msn1 and Htm1) and direct them to ER-membrane associated ubiquitin ligase complexes that specifically recognize the targeted substrate. These degradation machineries comprise an ubiquitin-ligase enzyme (E3), ubiquitin-conjugating enzymes (E2) and additional factors. The substrates are ubiquitinated by E3 ligases during or after retrotranslocation. Additional protein factors (Rad23, Dsk2 Ufd1, Ufd2, etc.) are involved in targeting the ubiquitinated substrate to the 26S proteasome for degradation (Hirsch et al., 2009).[4]

[4] Asi complex, another recently discovered ERAD machinery is not depicted in this figure

ERAD substrates

Terminally misfolded proteins, either soluble in the lumen (nontransmembrane) or integrated into the membrane of the ER, are subjected to ERAD. Moreover, it has been observed that ERAD substrates are sorted out in three different pathways depending on the domain where they have the lesion: either in the lumen (ERAD-L), or in the membrane (ERAD-M) or in the cytosol (ERAD-C) they will be recognized by specific degradation machineries (Carvalho et al., 2006). Namely, ERAD-L targets soluble and membrane-integrated proteins with a misfolded domain localized to the ER lumen. In yeast, ERAD-L requires the E3 ligase, Hrd1 and the associated components Hrd3, Usa1 and Der1 (Figure 7).

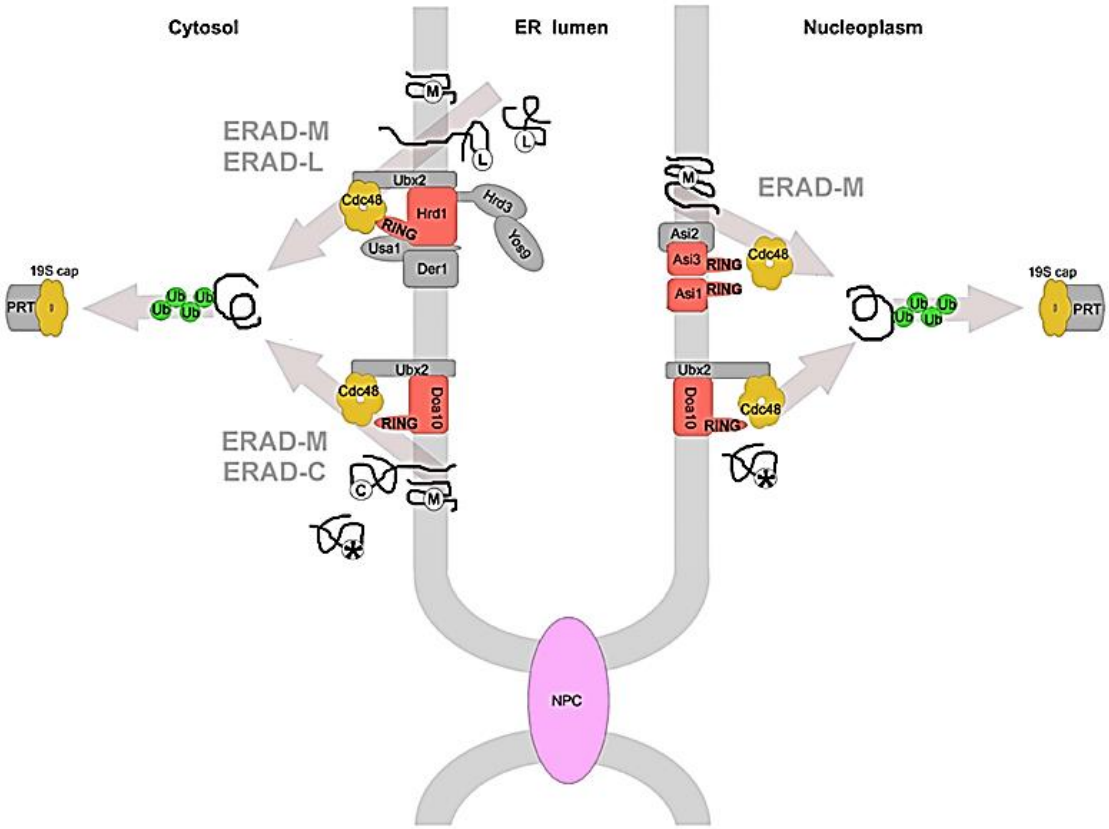

Figure 7. Distinct ERAD substrates and pathways.
The location of the misfolded lesion (L, M, or C) dictates the required ERAD machinery. Namely, soluble or transmembrane proteins with the misfolded domains in the lumen (ERAD-L) or in the membrane (ERAD-M) of the ER are directed to the Hrd1 complex. ERAD-M substrates from the inner nuclear membrane are targeted to Asi1 complex. Membrane proteins with the misfolded lesion in the cytosol (ERAD-C) are directed to the Doa10 complex.

ERAD-M targets membrane-integrated proteins with a misfolded domain inside the ER membrane and does not depend on Usa1 and Der1 for efficient degradation. The third pathway, ERAD-C, targets membrane-integrated components with a misfolded domain localized to the cytosol and depends on the E3 ligase Doa10 (Figure 7).

Recently, an additional ERAD complex containing the E3 ligase Asi1, was identified and operates exclusively in the inner nuclear membrane in yeast (Figure 7). So far, the substrates identified for the Asi complex, point towards a role in degrading membrane proteins with unassembled or mislocalized membrane domains, thus being part of an ERAD-M pathway (Foresti et al., 2014).

The correlation between the localization of the misfolded lesion and its targeting to a specific ERAD machinery have been also observed in mammalian cells, although its characterization is a more complex subject (Bernasconi et al., 2010; Hebert et al., 2010; Olzmann et al., 2013)

Glycosylphosphatidylinositol-anchored proteins (GPI-APs).

Post-translational modifications (PTMs) are chemical modifications of the proteins after their translation and it is estimated to exist more than 200 types of them in the proteome (Walsh, 2006). Consequently, PTMs increase greatly the functionality and complexity of the proteome (Khoury et al., 2011; Tripodi et al., 2015). Proteins of the secretory pathway commonly undergo several type of glycosylation[5] in the ER and in the Golgi that direct quality control of the proteins. These multiple PTMs have general functions in protein folding by promoting binding to chaperones and can also act as intrinsic sorting signal which are recognized by transport machineries for the correct delivery to their final cellular location (Xu and Ng, 2015).

The glycosylphosphatidylinositol (GPI) anchor is an evolutionary conserved and unique PTM occurring in about 60 proteins in budding yeasts and about 150 different proteins in mammalian cells (Fujita et al., 2015). It constitutes a complex membrane-embedded glycolipid structure (Figure 8).

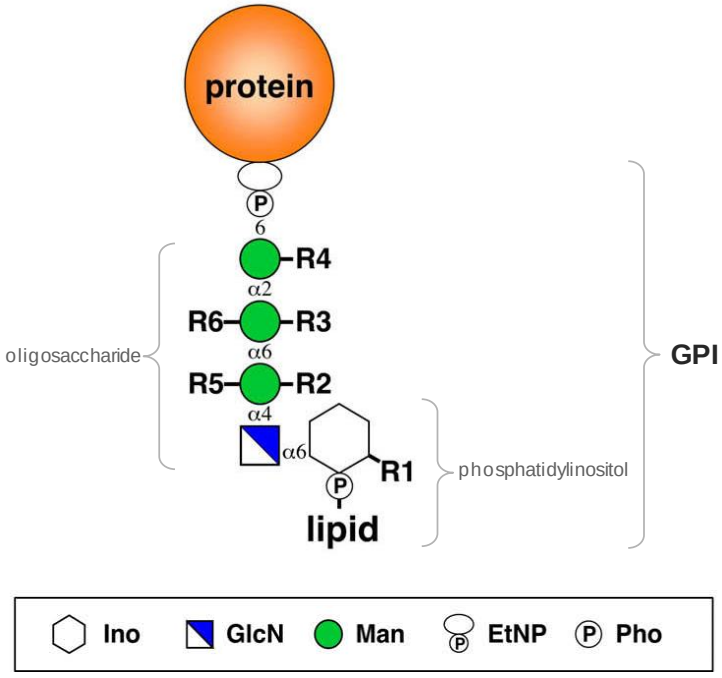

Figure 8. Core structure of the GPI moiety anchored to a protein.
GPI anchors share a common core consisting of ethanolamine-PO4-6Manα1–2Manα1–6Manα1–4GlcNα1–6myo-inositol-1-PO4-lipid. R1–R6, side-chains; Ino, inositol; GlcN, glucosamine; Man, mannose; EtNP, phosphoethanolamine; Pho, phosphate. Adapted from (Fujita and Kinoshita, 2010)

[5] *N*-, *O*- and *C*-glycosylation.

GPIs in almost all organisms have a common backbone consisting of phosphoethanolamine (EtNP), three mannoses (Mans), one non-N-acetylated glucosamine (GlcN), and inositol phospholipid (Ino) (Fankhauser et al., 1993; Ferguson et al., 1988). The backbone can be modified with glycans, phosphoethanolamine, and/or palmitate side-branches (Figure 8, R1-R6) depending on the organism, cell type, and protein (Fujita and Kinoshita, 2010) (Paulick and Bertozzi, 2008).

GPI anchoring to proteins stands out among the glycosylations because the sugar residues are not directly attached to the protein. Rather GPI anchors are linked to the C-terminus of the protein via an amide bond with the phosphoethanolamine (EtNP) of the third mannose (Figure 8).

GPI-APs were originally described 30 years ago (Futerman et al., 1985; Tse et al., 1985). They are initially synthesized as precursors, containing a signal-anchor domain at the C-terminus known as GPI anchoring site or the omega site (ω)[6] (Figure 9).

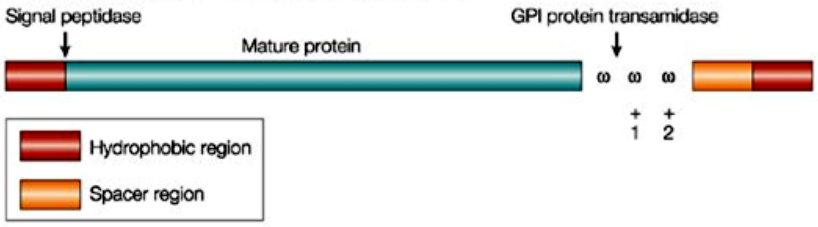

Figure 9. GPI-AP precursor.
A cleavable, hydrophobic amino-terminal signal peptidase targets the protein to the lumen of the (ER) and a cleavable, carboxy-terminal signal sequence (ω-site) directs GPI anchoring. Adapted from (Mayor and Riezman, 2004)

GPI-APs also have an N-terminal signal for ER translocation. After translocation into the ER lumen, the N-terminal signal is removed. The C-terminal signal is recognized by a GPI transamidase that cleaves the peptide bond between ω and ω+1 amino acids, generating an amide linkage with the EtNP of the third mannose of the GPI moiety that is transferred *en bloc* to the C-terminus of the protein (Mayor and Riezman, 2004) (Figure 10).

GPI-APs are targeted to the outer leaflet of the cell surface where they are diffusely distributed. This led to the hypothesis, and later on to the demonstration that these glycolipid-linked proteins are assembled in lipid rafts. Namely, GPI-APs are assembled in cholesterol-dependent submicron-sized domains enriched in glycosphingolipids,

[6] ω-site (ω / ω+1, ω+2), near the carboxy-terminal end of the protein.

sterols, and certain types of lipidated protein (Mayor and Riezman, 2004; Saha et al., 2015; Varma and Mayor, 1998).

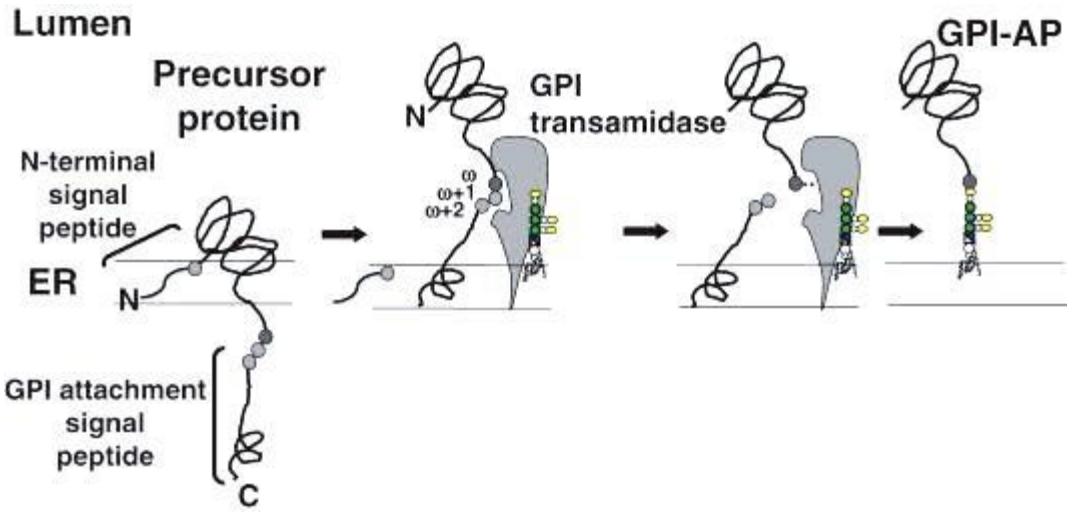

Figure 10. Attachment of GPI moiety to proteins by GPI transamidase**.**
After translocation of GPI-anchor precursors into the ER, the ω-site is cleaved, then the C-terminal TMD is removed and the luminal part of the protein is attached to a GPI by a transamidase, generating GPI-AP (Kinoshita, 2014).

The GPI anchor moiety is subject to various remodeling reactions on the glycan and lipid moieties (Reggiori et al., 1997; Umemura et al., 2007). Variations in the decoration of the GPI core can occur by addition of extra sugars or phosphoethanolamines to the mannose residues, acylation of the inositol ring, changes in the fatty acids (length, saturation, hydroxylation), or the types of linkage to the glycerol backbone (acyl to alkyl), or remodeling of the entire diacylglycerol (DAG) to ceramide (Figure 8 and Figure 11).

In yeast GPI remodeling occurs exclusively in the ER, whereas in mammals this process completes in the Golgi (Fujita et al., 2006a; Maeda et al., 2007; Tashima et al., 2006). The first structural remodeling step of the lipid moiety of GPI-APs in yeast is the removal of the unsaturated acyl chain from the inositol-ring. Bst1p mediates this inositol deacylation reaction. Next, Per1p and Gup1p, both are involved in the remodeling of the sn2-linked fatty acid, removing C18:1 and replacing it by a C26:0 fatty acid, respectively. Later, Cwh43p replaces the DAG of the lipid moiety by ceramide. The lipid moieties of mature GPI-anchors of *S. cerevisiae* usually do not contain the DAG present on the original transferred GPI lipid to the protein. Instead, most mature GPI-AP of yeast contain a ceramide (Reggiori et al., 1997; Umemura et al., 2007).

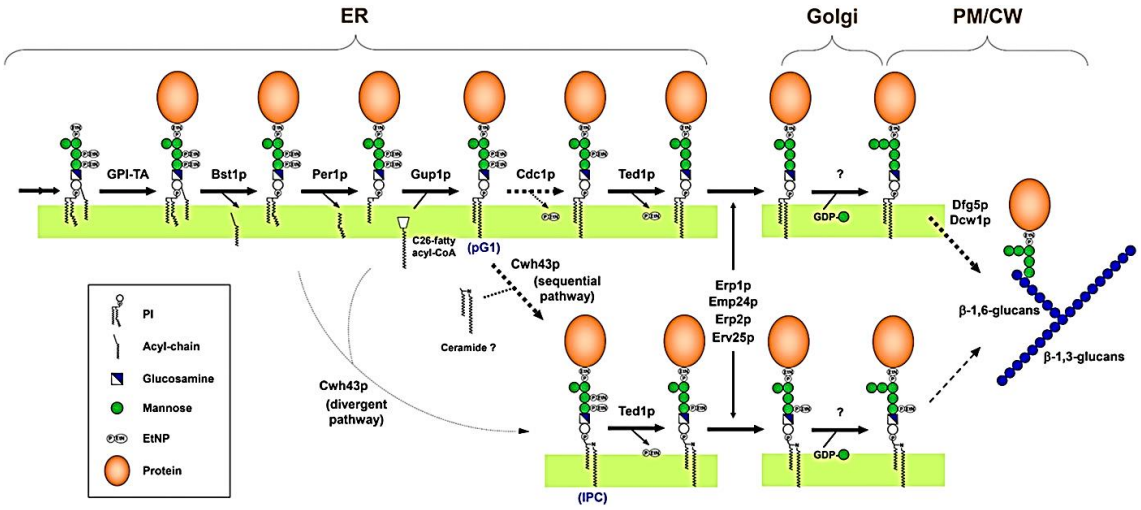

Figure 11. Lipid and glycan remodeling of GPI-APs in yeast *Saccharomyces cerevisiae*.
After attachment of GPI to proteins by the GPI transamidase complex (GPI-TA), Bst1p eliminates the acyl chain linked to inositol. Next, Per1p and Gup1p perform the fatty acid remodeling. In many GPI-APs of yeast, the diacylglycerol (DAG) moiety is exchanged with ceramide by Cwh43p. Depending on the GPI-AP substrate, removal of the side-chain EtNP attached to Man1 is performed most likely by Cdc1p and the one attached to Man2 is removed by Ted1p enabling efficient binding to the p24 complex for ER export. After GPI-APs are transported to the Golgi, additional Man is transferred to the Man4. On the cell surface, many GPI-APs are cleaved and cross-linked to glucans on the cell wall (Kinoshita and Fujita, 2016).

The role of p24 complex in GPI-AP trafficking has been extensively studied (Fujita and Kinoshita, 2012; Fujita et al., 2009; Muniz et al., 2000). It has been reported that Ted1p acts together with Emp24p and Erv25p, and that Cdc1p functions after Per1p and Gup1p in the same pathway, which suggests that they are involved in GPI remodeling. Side-chain EtNPs on the first and second mannoses are required for ceramide remodeling, whereas it remains unclear whether the side-chain EtNPs are eliminated (Kinoshita and Fujita, 2016).

Despite continued attempts to determine the functions of GPI-AP and uncovered several of them, still the possible roles of the GPI moiety have to be elucidated at a molecular level. Yet, one well-known evident significance of the GPI anchor is to provide a stable membrane anchoring, which is resistant to most extracellular proteases and lipases (Low and Saltiel, 1988). Besides being consider a primarily sorting signals for targeting proteins to the cell surface, GPI-APs may play other biological functions in the cell (Paulick and Bertozzi, 2008). They may also have a specific role in lipid homeostasis (Loizides-Mangold et al., 2012) and may also influence the conformation and structure of its associated protein (Butikofer et al., 2001; Seong et al., 2013).

Moreover, GPI-Aps may be involved in signal transduction at the so-called, GPI-hotspots[7] (Smith and Marshall, 2010; Stefanova et al., 1991; Suzuki et al., 2007). Furthermore, the GPI anchor confers high lateral mobility[8] to the attached protein at the cell surface and may facilitate inter-cellular communication (Low and Saltiel, 1988; Saha et al., 2015).

GPI-anchored proteins are known to critically regulate a wide range of physiological functions from nutrient uptake to cell migration to immune recognition. Therefore, it is obvious that perturbation resulting in altered GPI-anchored protein trafficking as well as plasma membrane organization can lead to several diseases (Saha et al., 2015).

In summary, GPI remodeling inside the ER regulates the ER export of GPI-APs and they intracellular trafficking (Castillon et al., 2011; Fujita and Kinoshita, 2012; Manzano-Lopez et al., 2015).

[7] regions on the cell surface, which have a high local concentration of GPI clusters.
[8] about ~ 2-5 fold faster than transmembrane proteins Zhang F, Crise B, Su B, Hou Y, Rose JK, Bothwell A, and K, J. (1991). Lateral diffusion of membrane-spanning and glycosylphosphatidylinositol- linked proteins: toward establishing rules governing the lateral mobility of membrane proteins. The Journal of Cell Biology *115*, 75-84..

Controversy in GPI-APs degradation pathways.

ERAD machinery handles poorly the aggregation of misfolded or unassembled proteins which form large ER luminal deposits, requiring therefore the activity of the vacuole/lysosome for their clearance. Therefore, some misfolded proteins may use alternative post-ER degradation pathways, being eventually targeted for vacuolar degradation (Coughlan et al., 2004; Goder and Melero, 2011; Hong et al., 1996). Correspondingly, it has been shown that GPI-APs may be refractory to degradation by ERAD presumably, because as the targeted-for-degradation protein has to be retrotranslocated across the ER membrane to the cytosol, the GPI moiety might result in a steric hindrance for the ERAD machinery (Ashok and Hegde, 2008; Satpute-Krishnan et al., 2014).

Previous work have shown that the turnover rate of Gas1*p in cells where ERAD components has been genetically impaired[9] is similar than for wild type cells or only showing a small stabilization (Fujita et al., 2006b)[10](Goder and Melero, 2011)[11]. This indicates that another or more than one degradation pathways are involved in Gas1*p turnover which do not required ERAD components. Accordingly, when components of the p24 complex, involved in the ER export of GPI-APs (Muniz et al., 2000) (Watanabe and Riezman, 2004) are impaired, Gas1*p is very much stabilized (Goder and Melero, 2011). This result points to a post-ER degradation pathway. It is known that some misfolded proteins exit the ER and are degraded in the vacuole/lysosome instead (Coughlan et al., 2004) (Kincaid and Cooper, 2007; Satpute-Krishnan et al., 2014).

However, in previous works in yeast using single mutant *pep4*Δ cells, that is defective in vacuolar protease activity, it was found that Gas1*p turnover does not differ from the wild type. This led to the conclusion that Gas1*p was either not degraded in the vacuole (Fujita et al., 2006b), or whose vacuolar degradation was dependent of other factors like *o*-mannosylation (Hirayama et al., 2008).

Therefore, the mechanism of the limiting ERAD for GPI-APs and evidences of their vacuolar degradation were still lacking. We were aimed at unraveling a possible quality control mechanism of ERAD for GPI-APs as well.

[9] However, in cells where specifically the function of the proteasome is affected, Gas1*p can be stabilized (MG-132, *rpn3*Δ, *rpn12*Δ) Fujita, M., Yoko, O. T., and Jigami, Y. (2006b). Inositol deacylation by Bst1p is required for the quality control of glycosylphosphatidylinositol-anchored proteins. Mol Biol Cell *17*, 834-850..
[10] *hrd1*Δ, *doa10*Δ, *rpn12*Δ
[11] *hrd1*Δ, *doa10*Δ, *hrd3*Δ, *der3*Δ, *dfm1*Δ, *usa1*Δ

Goals

General:

To study the quality control of misfolded GPI-APs centered on Gas1*.

Specifics:

1- To confirm that the misfolded GPI-AP, GFP-HA-Gas1* undergoes the replacement of its transmembrane domain by a GPI anchor moiety like the native protein as well.

2- To determine that GPI remodeling also occurs in misfolded GPI-APs.

3- To verify that the ER-exported Gas1* is ultimately targeted to the vacuole.

4- To address the mechanism of ER export for misfolded GPI-APs.

5- To demonstrate that misfolded GPI-APs may also be ERAD substrates.

6- To quantify the preferentially routing of Gas1* to ERAD in strains where the ER export is impaired.

7- To identify the underlying mechanisms by which GPI-APs may be preferentially targeted to ERAD instead of being targeted to the vacuole.

Results

Part I

J Cell Biol. 2016 Jun 20;213(6):693-704. doi: 10.1083/jcb.201602010.

Limited ER quality control for GPI-anchored proteins.

Sikorska N*, **Lemus L***, Aguilera-Romero A, Manzano-Lopez J, Riezman H, Muñiz M, Goder V.

*equal contribution

Highlights of Sikorska/Lemus *et al*., 2016

We reported for the first time the following experimental evidences:

1. Misfolded Gas1*p is GPI-anchored.

   Cells expressing HA-Gas1*p after being treated with Triton X-114, resulted in this protein render more abundant in the detergent fraction, confirming the lipophilic nature of the protein. Hence, HA-Gas1* is GPI-anchored. On the other hand, when cells were treated with phosphoinositol-specific phospholipase C (PI-PLC) previously to the treatment with Triton X-114, cell lysate rendered a HA-Gas1* more abundant in the aqueous fraction showing the property of a GPI-AP of being cleaved by a phospholipase and rendering a water-soluble protein. Therefore these results confirmed that Gas1*p despite being misfolded, it is attached to a GPI moiety (Fig. 4).

2. Gas1*p undergoes GPI remodeling in spite of being misfolded.

   We have shown that in wild type cells the misfolded Gas1* is as abundant as the native Gas1p in the upper fraction of the density gradient ultracentrifugation assay being partitioned together with DRM and ceramides. Furthermore, when the GPI-lipid remodeling is disturbed in bst1Δ cells, the distribution of both the native and the unfolded protein changed and both are now found in the bottom fraction of the gradient (Fig. 6). This result indicates that Gas1p and Gas1*p undergoes GPI-remodeling alike.

3. Misfolded GPI-AP, Gas1*p is routed to the vacuole for degradation.

   There is a significant increase in protein stability in double mutant cells (hrd1Δ/pep4Δ) in comparison with the faster degradation rate of the corresponding single mutants. (Fig. 2, A and B).

4. GPI-APs can be indeed degraded by ERAD.

   Therefore, the GPI moiety does not represent a hindrance for it, as it was proposed in other previous works. We showed that in double mutant cells defected for ERAD and impaired for ER export (either hrd1Δemp24Δ or hrd1Δted1Δ) Gas1* turnover is significantly reduced in comparison with the single mutants (Fig. 3, E and F).

5. GPI moiety not only does not obstruct ERAD but also plays a role as an ER exit signal even for misfolded GPI-APs.

   We have shown for the first time that the GPI moiety of a misfolded protein (Gas1*) also undergoes remodeling which enable the protein to interact with the p24 complex component, Emp24 for ER export (Fig.8). Therefore, GPI remodeling is not only crucial for the ER export of correctly folded proteins but also for those misfolded since GFP-Gas1*p is retained in the ER in those cells impaired for GPI remodeling (ted1Δ, bst1Δ, cwh43Δ) (Fig. 3 B, Fig. 5 A, Fig. 7 B).

6. Targeting of misfolded GPI-APs is increased to ERAD when GPI remodeling and/or ER export are disturbed.

   Gas1*p turnover rate in the double mutant background for ERAD and GPI remodeling (hrd1Δ/bst1Δ and hrd1Δ/cwh43Δ) lowers much more than for the corresponding single mutants (Fig. 7 C and D). This stabilization of the protein indicates that Gas1*p is more readily targeted to ERAD when remodeling of the GPI moiety is impaired and consequently its ER export. In fact, when GPI remodeling (bst1Δ and cwh43Δ) along with ER export (emp24Δ) are impaired the degradation rate is even faster than for WT cells (Fig. 7 E and F). Noteworthy is the maximum stabilization of the protein in emp24Δ single mutant indicating how GPI remodeling slows down ERAD.

Published June 20, 2016

Limited ER quality control for GPI-anchored proteins

Natalia Sikorska,[1]* Leticia Lemus,[1]* Auxiliadora Aguilera-Romero,[4,5] Javier Manzano-Lopez,[2,3] Howard Riezman,[4,5] Manuel Muñiz,[2,3] and Veit Goder[1]

[1]Department of Genetics and [2]Department of Cell Biology, University of Seville, 41012 Seville, Spain
[3]Instituto de Biomedicina de Sevilla, Hospital Universitario Virgen del Rocío, Consejo Superior de Investigaciones Científicas, University of Seville, 41013 Seville, Spain
[4]National Centre of Competence in Research, Chemical Biology and [5]Department of Biochemistry, Sciences II, University of Geneva, 1211 Geneva 4, Switzerland

Endoplasmic reticulum (ER) quality control mechanisms target terminally misfolded proteins for ER-associated degradation (ERAD). Misfolded glycophosphatidylinositol-anchored proteins (GPI-APs) are, however, generally poor ERAD substrates and are targeted mainly to the vacuole/lysosome for degradation, leading to predictions that a GPI anchor sterically obstructs ERAD. Here we analyzed the degradation of the misfolded GPI-AP Gas1* in yeast. We could efficiently route Gas1* to Hrd1-dependent ERAD and provide evidence that it contains a GPI anchor, ruling out that a GPI anchor obstructs ERAD. Instead, we show that the normally decreased susceptibility of Gas1* to ERAD is caused by canonical remodeling of its GPI anchor, which occurs in all GPI-APs and provides a protein-independent ER export signal. Thus, GPI anchor remodeling is independent of protein folding and leads to efficient ER export of even misfolded species. Our data imply that ER quality control is limited for the entire class of GPI-APs, many of them being clinically relevant.

Introduction

Proteins of the secretory pathway are often modified after translocation across or insertion into the membrane of the ER (Braakman and Bulleid, 2011). A subclass of proteins that are to be targeted to the cell surface are attached to a specific membrane-embedded glycolipid, the GPI anchor (Mayor and Riezman, 2004). After attachment, the GPI anchor is subject to a series of remodeling steps on both its lipid and sugar moieties. In yeast, remodeling occurs exclusively inside the ER (Fig. 1). The sequential actions of the lipid remodeling enzymes Bst1, Per1, Gup1, and Cwh43 catalyze the addition of a long unsaturated fatty acid at the sn-2 position of the diacylglycerol (DAG) of the GPI anchor or, in most cases, the exchange of the DAG for ceramide (Reggiori et al., 1997; Umemura et al., 2007; Fujita and Kinoshita, 2012). In addition, the phosphoethanolamine from the second mannose of the GPI anchor is removed by the sugar remodeling enzyme Ted1, which promotes binding of GPI-anchored proteins (GPI-APs) to the receptor p24 complex for vesicular export from the ER (Fujita et al., 2009; Fujita and Kinoshita, 2012; Manzano-Lopez et al., 2015). In mammalian cells, GPI anchor remodeling inside the ER is catalyzed by PGAP1 (Bst1) and PGAP5 (Ted1), the latter of which promotes ER export analogous to yeast, whereas additional lipid remodeling occurs inside the Golgi (Tashima et al., 2006; Fujita and Jigami, 2008; Fujita et al., 2009).

If proteins to be exported from the ER fail to acquire their native fold, they are efficiently retained inside the ER by quality control mechanisms. Ultimately, they will be retrotranslocated and/or extracted from the membrane into the cytosol and targeted to the proteasome for degradation, a process called ER-associated degradation (ERAD; Meusser et al., 2005; Vembar and Brodsky, 2008). The Hrd1 complex is one of several conserved ERAD machineries in the ER and promotes the degradation of misfolded ER luminal and membrane proteins (Carvalho et al., 2006; Gauss et al., 2006; Mehnert et al., 2010). Interestingly, ER export can compete with retention mechanisms, as illustrated by findings that selected ERAD model substrates leave the ER to a significant extent if ER export signals are appended or upon overexpression (Haynes et al., 2002; Spear and Ng, 2003; Kincaid and Cooper, 2007). The eukaryotic cell possesses additional protein quality control mechanisms in the secretory pathway downstream of the ER; these mechanisms target substrates to the proteasome independently of ERAD or to the vacuole/lysosome (Arvan et al., 2002; Wang and Ng, 2010; Zhao et al., 2013).

Because of the roles of GPI-APs in prominent human diseases, including malaria (Davidson and Gowda, 2001) and neurodegenerative prion diseases (Puig et al., 2014; Victoria and Zurzolo, 2015), the intracellular quality control of selected GPI-

*N. Sikorska and L. Lemus contributed equally to this paper.

Correspondence to Veit Goder: vgoder@us.es

N. Sikorska's present address is Institut de Biologie Moléculaire des Plantes du Centre National de la Recherche Scientifique, University of Strasbourg, 67081 Strasbourg, France.

Abbreviations used in this paper: CHX, cycloheximide; coIP, coimmunoprecipitation; DAG, diacylglycerol; ERAD, ER-associated degradation; ERES, ER exit site; GPI-AP, GPI-anchored protein; PI-PLC, phosphoinositol-specific phospholipase C; TAP, tandem affinity purification; TMD, transmembrane domain; UPR, unfolded protein response.

Supplemental Material can be found at:
/content/suppl/2016/06/13/jcb.201602010.DC1.html
/content/suppl/2016/06/20/jcb.201602010.DC2.html

The Rockefeller University Press $30.00
J. Cell Biol. Vol. 213 No. 6 693–704
www.jcb.org/cgi/doi/10.1083/jcb.201602010

Published June 20, 2016

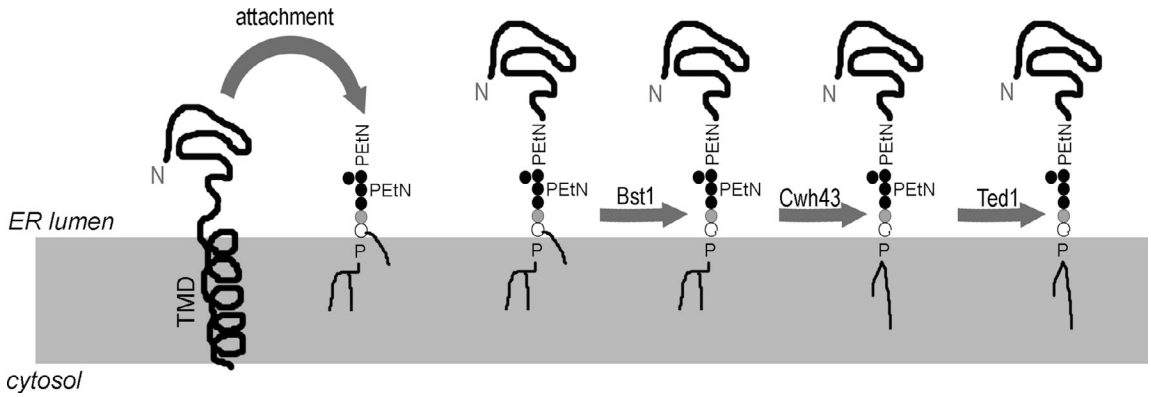

Figure 1. **GPI anchor remodeling in the yeast ER.** After translocation into the ER, the C-terminal TMD is removed and the luminal part of the protein is attached to a GPI anchor via a phosphoethanolamine (PEtN). After attachment, the sugar and lipid moieties of the GPI anchor undergo remodeling. Bst1 removes the acyl chain from the inositol (open circle), a step required for downstream lipid remodeling. Cwh43 exchanges the diacylglycerol for ceramide, the major lipid on remodeled GPI anchors in yeast. For simplicity, Per1 and Gup1, which catalyze intermediate lipid remodeling steps, are not shown. Ted1 removes a PEtN on the second mannose (closed circles), enabling efficient binding to the p24 complex for ER export.

APs has been studied extensively. Various misfolded GPI-APs accumulate in the presence of proteasome inhibitors, suggesting that ERAD is involved in their turnover (Ma and Lindquist, 2001; Yedidia et al., 2001; Petris et al., 2014; Wang et al., 2014). However, this view was challenged by the observation that the proteasome also degrades nontranslocated species, and recent studies suggested that ER-localized misfolded GPI-APs are predominantly routed to lysosomes for degradation (Drisaldi et al., 2003; Ashok and Hegde, 2008; Satpute-Krishnan et al., 2014).

Recent work with yeast to study the quality control of misfolded GPI-APs centered on Gas1*, a mutant version of the β-1,3-glucanosyltransferase Gas1, which normally functions in cell wall assembly. Gas1* contains a single point mutation (G291R) that renders the protein unstable and leads to its degradation (Fujita et al., 2006). Subsequent work showed that, like degradation of misfolded GPI-APs in mammalian cells, only a minor fraction of Gas1* was routed to ERAD, whereas most of its degradation depended on ER export and probably occurred inside the vacuole, although evidence for vacuolar degradation of Gas1* is still lacking (Fujita et al., 2006; Hirayama et al., 2008; Goder and Melero, 2011).

Altogether, these data suggest that misfolded GPI-APs are generally rather poor ERAD substrates, but the reasons for this phenomenon are unclear. Interestingly, misfolded mutant versions of the prion protein could be efficiently routed to ERAD when GPI anchor attachment was prevented (Ashok and Hegde, 2008). In combination with a more recent study, this result led to the postulation that the presence of a GPI anchor might generally obstruct ERAD for sterical reasons (Satpute-Krishnan et al., 2014). However, this would be in conflict with the observation that at least a minor fraction of Gas1* in yeast is a substrate for Hrd1-dependent ERAD (Goder and Melero, 2011). To address these uncertainties and the mechanisms that determine the degradation pathways of misfolded GPI-APs, we performed a detailed analysis of the degradation of the misfolded GPI-AP Gas1* in yeast.

Results

We have previously shown that Gas1* can be degraded by several cellular pathways in parallel, including Hrd1-dependent ERAD and post-ER degradation involving ER export that is dependent on the p24 protein complex component Emp24 (Goder and Melero, 2011). Although *Δhrd1Δemp24* cells showed stronger stabilization of Gas1* than individual single mutants, suggesting that ER-exported Gas1* was not rerouted to the ER for ERAD, it was not clear whether Gas1* was ultimately targeted to the vacuole (Goder and Melero, 2011). Indeed, earlier results showed that Gas1* was not stabilized in a *Δpep4* mutant, in which vacuolar proteases are inactive (Fujita et al., 2006). When we expressed HA-tagged Gas1* (HA-Gas1*) and measured protein turnover using the translation elongation inhibitor cycloheximide (CHX) in wild-type cells and *Δpep4* cells, we obtained similar results, with no visible protein stabilization in the *Δpep4* mutant (Fig. 2, A [lanes 1–9] and B). However, when we measured the effect of *Δpep4* deletion in the *Δhrd1* background, which on its own showed only marginal Gas1* stabilization, we found a significant increase in protein stability compared with the individual single mutants, showing that a fraction of Gas1* is routed to the vacuole for degradation (Fig. 2, A [lanes 10–18] and B). These data reinforce the idea that Gas1* can be degraded dynamically by several simultaneously operating degradation pathways, one of them being ERAD and another depending on ER export and leading to the vacuole (Fig. 2 C). These results also explain why blockage of only one of these pathways in single mutants might not (necessarily) be sufficient to significantly reduce the global degradation rate.

Important for resolving whether a GPI anchor obstructs ERAD is to determine whether Gas1* routed to this pathway contains a GPI anchor or still a transmembrane domain (TMD; Fig. 2 C, dashed arrows). To address this, we were initially looking for mutants in which the routing of Gas1* to the vacuole is reduced in favor of increased ERAD. We expressed a GFP-tagged version of Gas1* for a comparative analysis of protein targeting to the vacuole by live cell fluorescence microscopy (Fig. 3, A and B). Wild-type cells showed a strong vacuolar signal, in agreement with a significant fraction of Gas1* being routed to the vacuole despite ERAD being fully operational (Fig. 3 B, wild type). The faint perivacuolar puncta could be post-ER trafficking intermediates (Fig. 3 B, wild type). In the absence of the p24 complex component Emp24, when GPI-AP–specific ER export is impaired and Gas1* degradation is reduced (Muñiz et al., 2000; Goder and Melero, 2011), the vacuolar signal was decreased and the perinuclear and cortical

Published June 20, 2016

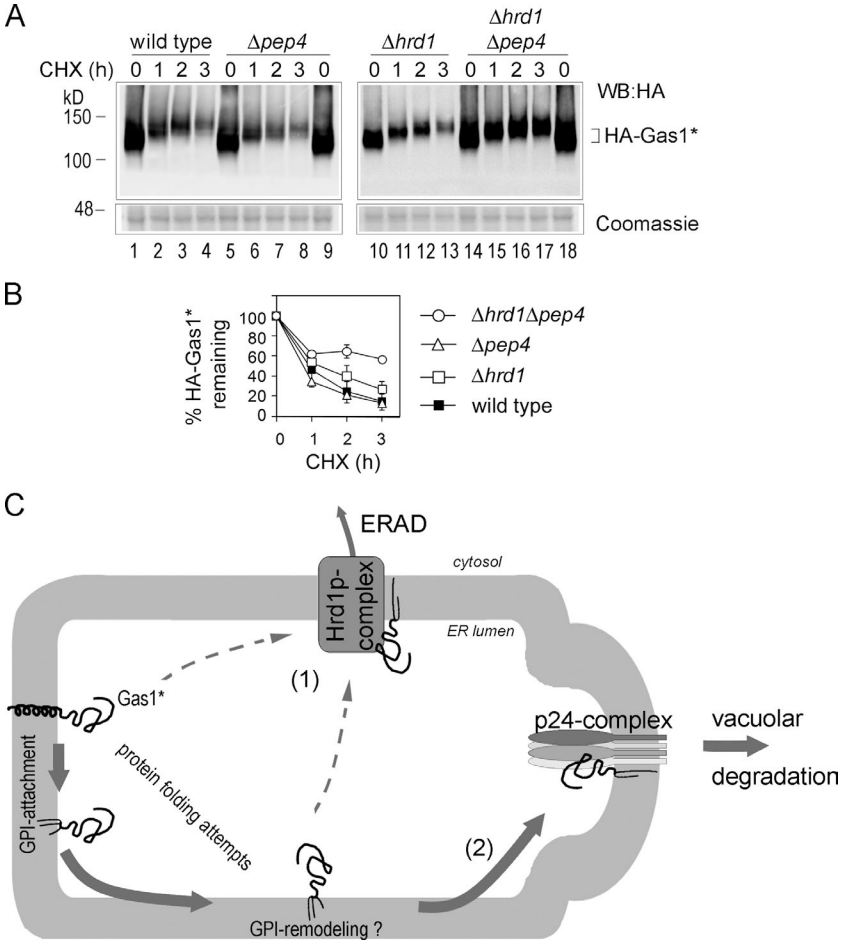

Figure 2. **Dynamic routing of the misfolded GPI-AP Gas1* to ERAD and/or the vacuole for degradation.** (A) Wild-type cells and the indicated single and double mutant cells expressing HA-Gas1* were subjected to CHX shut-off experiments. Cells were lysed, and the remaining HA-Gas1* was measured by SDS-PAGE and Western blotting (WB) with antibodies against HA. Accumulation of higher-molecular-weight species during chase periods is caused by protein *O*-mannosylation (Goder and Melero, 2011). A lower part of the gel was separately stained with Coomassie as loading control. (B) Quantifications of results from experiments shown in A. Mean values and SDs from at least three individual experiments are shown. (C) Schematic representation of the degradation pathways of Gas1* in wild-type cells. (1) A fraction of Gas1* is routed to the Hrd1-dependent ERAD machinery, retrotranslocated, and degraded by the proteasome (not shown). It is unclear whether Gas1* can be routed to ERAD only before or also after attachment to the GPI anchor (dashed lines). (2) A larger fraction of Gas1* is exported from the ER and routed to the vacuole for degradation. ER export of Gas1* depends in part on the p24 complex, but it is unknown whether and to what extent the GPI anchor of Gas1* is remodeled.

ER was stained more strongly, suggesting a reduction in ER export of GFP-Gas1* (Fig. 3 B, *Δemp24*). A similar phenotype was seen in the absence of the GPI anchor remodeling enzyme Ted1, which acts immediately upstream of Emp24 (Fig. 3 B, *Δted1*). The fact that *Δted1* cells phenocopied *Δemp24* cells suggests that the GPI anchor of Gas1* undergoes sugar remodeling. Remaining vacuolar staining likely arises from the ER export of GPI-APs by bulk-flow mechanisms (Manzano-Lopez et al., 2015). Cells with deleted Hrd1, lacking Hrd1-dependent ERAD, showed vacuolar staining similar to that of wild-type cells (Fig. 3 B, *Δhrd1*). Increased staining of the perinuclear ER in *Δhrd1* cells compared with wild-type cells might reflect elevated nonspecific ER retention of misfolded proteins by the up-regulated unfolded protein response (UPR) in this ERAD mutant (Jonikas et al., 2009). However, UPR activation does not cause the major differences in Gas1* ER export in the distinct mutants, because the UPR is less elevated in *Δted1* cells than in *Δhrd1* cells (Jonikas et al., 2009). To quantify the differences in GFP-Gas1* targeting to the vacuole in the distinct mutants, we measured free GFP that resisted vacuolar proteolysis as a remnant of GFP-Gas1*. Free GFP was reduced up to 50% in *Δemp24* and in *Δted1* cells compared with wild-type and *Δhrd1* cells (Fig. 3, C and D).

Next we tested whether more Gas1* was routed to ERAD in *Δemp24* and *Δted1* cells compared with wild-type cells. We expressed HA-tagged Gas1* and measured protein turnover using CHX. Deletion of *HRD1* in the *Δted1* or *Δemp24* background showed a much stronger stabilizing effect than the *HRD1* deletion in wild-type cells (Fig. 3, E–G). Quantification revealed that ERAD is the major degradation pathway for Gas1* in *Δemp24* and in *Δted1* cells, with more than 50% of protein turnover being dependent on Hrd1 (Fig. S1).

Next, we measured the amount of cellular Gas1* that contained a GPI anchor under these conditions. We used phosphoinositol-specific phospholipase C (PI-PLC), which cleaves the phosphate diester of the GPI anchor at the sn-3 position, thereby removing the lipophilic DAG or ceramide and rendering a GPI-AP water soluble. In combination with Triton X-114 phase separation, we found that more than 90% of HA-Gas1* was recovered in the aqueous phase after treatment of lysates with PI-PLC, irrespective of the tested strain (Fig. 4, A and B, HA-Gas1*). As a control, we expressed HA-Gas1*TMD in *Δemp24* cells, a construct in which the exchange of the TM domain for the GPI anchor is prevented by a specific mutation (N528Q), therefore rendering HA-Gas1*TMD a type I TM protein. As expected, HA-Gas1*TMD was not recovered in the aqueous phase after PI-PLC treatment, validating the functionality of the assay (Fig. 4, A and B, HA-Gas1*TMD). This result shows that Gas1* is efficiently attached to a GPI anchor in all tested strains, including those in which >50% of Gas1* is routed to Hrd1-dependent ERAD. Therefore, the Hrd1-machinery can mediate ERAD of a misfolded GPI-AP.

Because our data ruled out that sterical obstructions limit ERAD of a misfolded GPI-AP, the question remained as to why misfolded GPI-APs are often exported from the ER and predominantly degraded inside the vacuole/lysosome. In striking resemblance to results obtained in mammalian cells with mutant prion proteins lacking the GPI anchor (Ashok and Hegde,

Published June 20, 2016

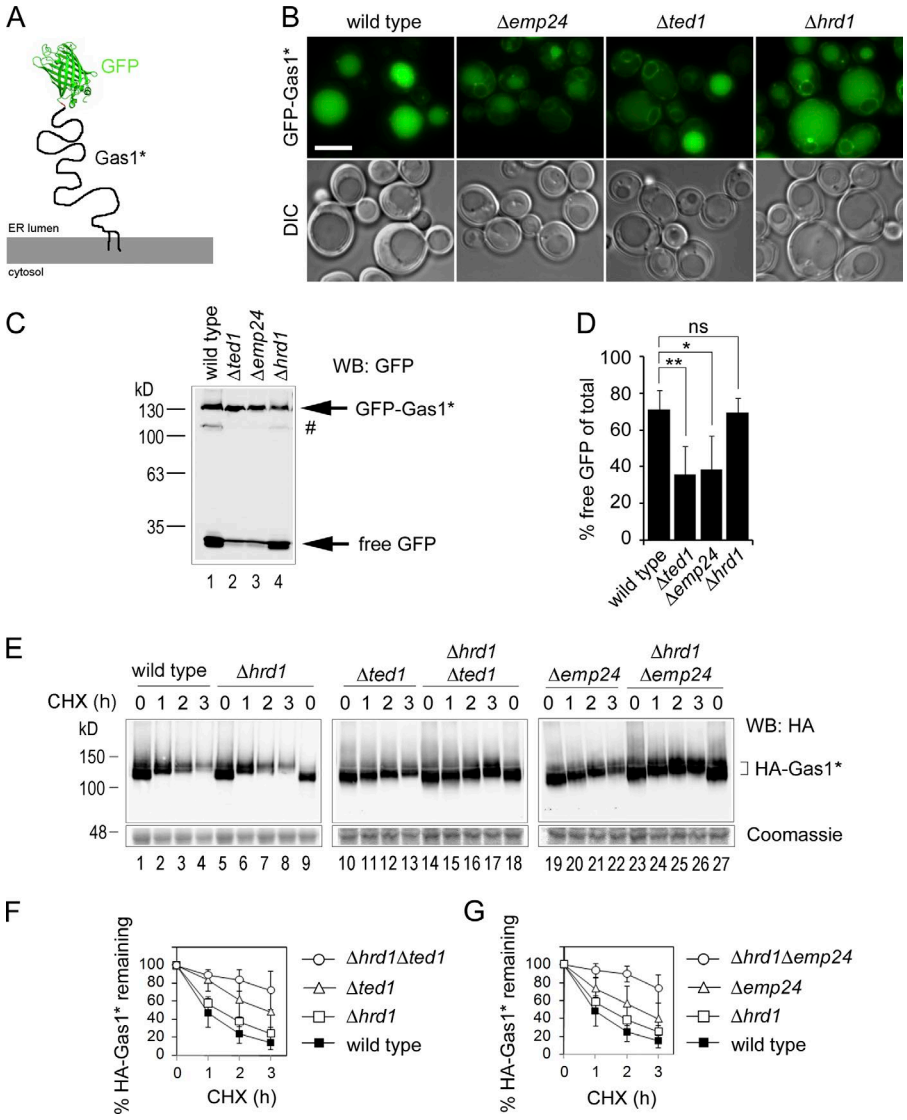

Figure 3. **Increased targeting of Gas1* to ERAD in *Δemp24* and *Δted1* cells.** (A) Schematic representation of the fusion construct GFP-Gas1*. The GFP moiety was fused to the N-terminus domain of Gas1*, downstream of the signal sequence. The C-terminal GPI anchor extends into the luminal leaflet of the ER membrane. (B) Wild-type and indicated mutant cells expressing GFP-Gas1* were analyzed by live cell fluorescence microscopy. DIC = Nomarski image. Bar, 2 µm. (C) GFP-cleavage assay. Cells used for microscopy in B were lysed in equal amounts and analyzed by SDS-PAGE in combination with Western blotting (WB) with antibodies against GFP. The hashtag indicates a minor fraction of the fusion protein that likely has not been translocated into the ER. (D) Quantification and statistical analysis of results from experiments shown in C. Mean values and SDs from at least three individual experiments are shown. ns, not significant. *, $P < 0.05$; **, $P < 0.01$ (unpaired two-tailed Student's *t* test). (E) Wild-type cells and the indicated single and double mutant cells expressing HA-Gas1* were subjected to CHX shut-off experiments. A lower part of the gel was separately stained with Coomassie as loading control. (F and G) Quantifications of results from experiments shown in E. Mean values and SDs from at least three individual experiments are shown.

2008), we found that significantly less GFP-Gas1*TMD was targeted to the vacuole and more retained inside the ER compared with GFP-Gas1* in wild-type cells, as shown by fluorescence microscopy (Fig. 5 A). Similar results were obtained with GFP-Gas1*ΔTMD, in which the C-terminal TMD was deleted, rendering the construct a soluble ER luminal

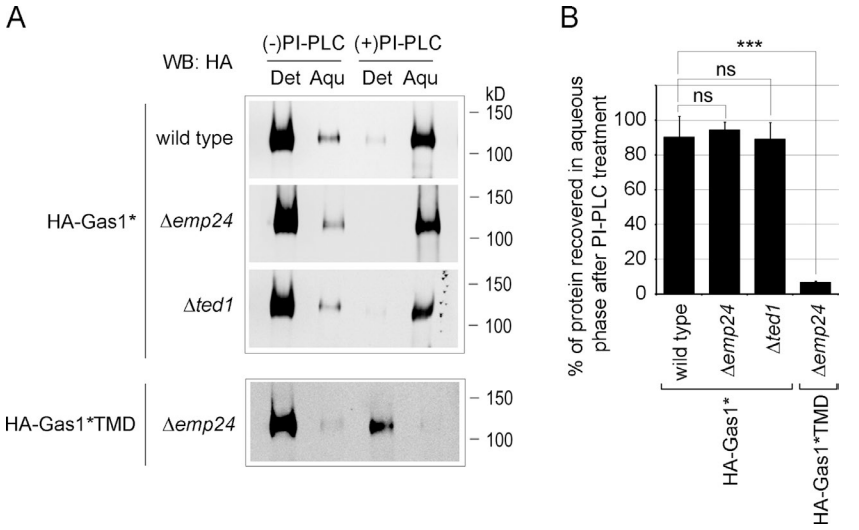

Figure 4. **Gas1* is efficiently attached to the GPI anchor.** (A) Triton X-114 extracts from wild-type cells and the indicated single mutant cells expressing HA-Gas1* or HA-Gas1*TMD were treated with PI-PLC or mock-treated. Detergent (Det) and aqueous (Aqu) phases were separated and analyzed by SDS-PAGE and Western blotting (WB) with antibodies against HA. (B) Quantification of the relative amounts of HA-Gas1* and HA-Gas1*TMD recovered in the aqueous phase compared with total signal after treatment with PLC from experiments shown in A. Mean values and SDs from two to five individual experiments are shown. ns, not significant. ***, $P < 0.001$ (unpaired two-tailed Student's *t* test).

Published June 20, 2016

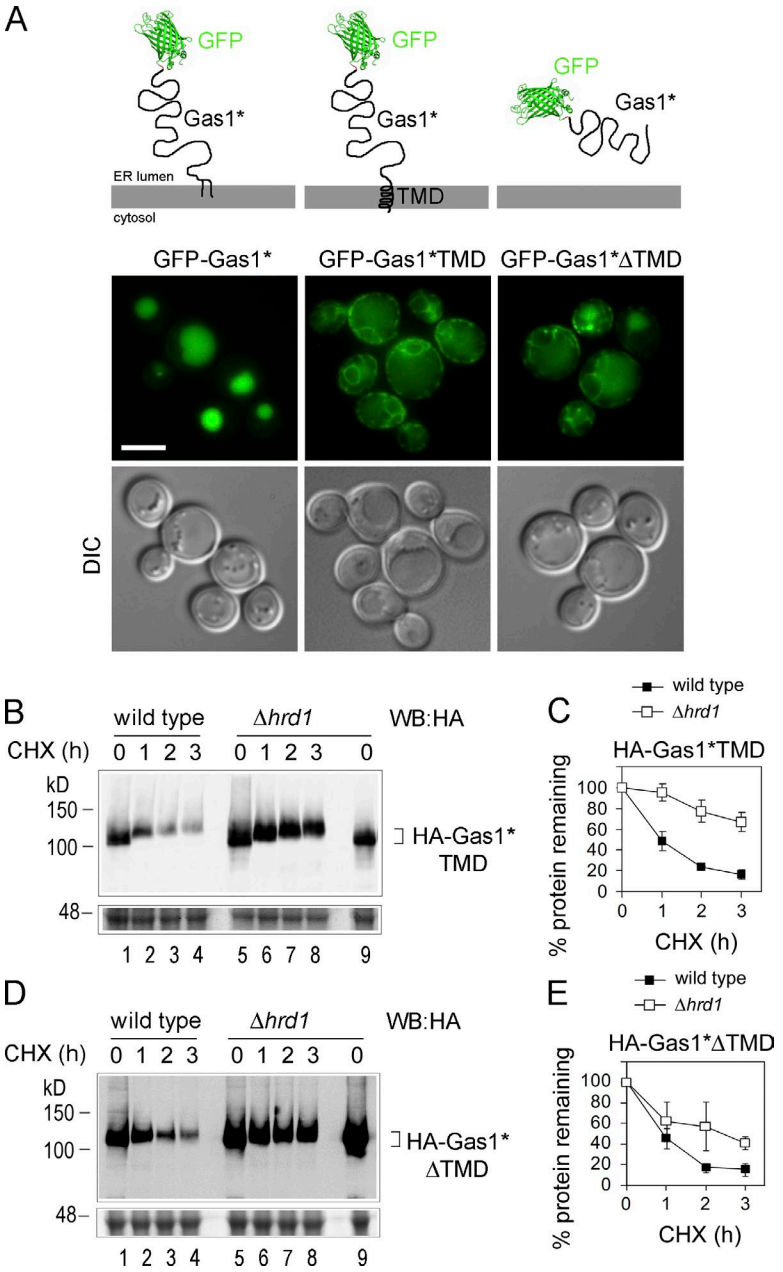

Figure 5. **Preventing GPI anchor attachment increases ER retention and routing of Gas1* to ERAD.** (A) Live cell fluorescence microscopy of wild-type cells expressing the indicated GFP-Gas1* fusion constructs. Schematic illustrations of the various constructs are shown above the microscopy images. DIC = Nomarski image. Bar, 2 µm. (B–E) Wild-type cells and *Δhrd1* cells expressing HA-Gas1*TMD and HA-Gas1*ΔTMD were subjected to CHX shut-off experiments. A lower part of the gel was separately stained with Coomassie as loading control. The graphs illustrate the obtained degradation rates and show the mean values and SDs from at least three individual experiments.

misfolded protein (Fig. 5 A). In addition, the stabilizing effect of the Hrd1 deletion was significantly larger for the HA-tagged versions of both constructs lacking the GPI anchor compared with HA-Gas1* (Fig. 5, B and C, versus Fig. 3, E and F). In light of these data, it appears that a GPI anchor reduces the routing of misfolded proteins to ERAD by limiting ER retention or by promoting ER export.

Recent data suggested that GPI-APs would mix with free ceramides inside the ER and promote the cotransport of free ceramides in vesicles from the ER to the Golgi (Loizides-Mangold et al., 2012). We considered the possibility that Gas1*, albeit misfolded, would function in ceramide cotransport by virtue of its GPI anchor. Such a function could bypass ER-retention mechanisms and explain the universally observed reduction in ERAD. However, a combination of experiments, including lipid analysis in which we determined the ceramide and sphingolipid profiles of *Δgas1* cells expressing HA-Gas1 or HA-Gas1* or the anchorless versions HA-Gas1TMD and HA-Gas1*TMD, did not provide any evidence for a role of Gas1* in ceramide cotransport (Fig. S2).

It has been shown that ER export of (correctly folded) GPI-APs is directly coupled to GPI anchor remodeling (Castillon et al., 2009, 2011; Fujita et al., 2009; Manzano-Lopez et al., 2015). In fact, the remodeled GPI anchor is the major, if not the only, ER export signal of GPI-APs. GPI anchor lipid remodeling promotes the concentration of GPI-APs in specific ER exit sites (ERESs) where binding to the p24 complex is thought to occur (Castillon et al., 2009). p24 proteins can bind to synthetic remodeled but not unremodeled glycostructures of the GPI anchor and to specific sphingolipids that contain ceramide, a lipid also present in remodeled GPI anchors (Contreras et al., 2012; Manzano-Lopez et al., 2015). The observed reduction in ER export of Gas1* in *Δted1* cells indicates that its GPI anchor undergoes sugar remodeling (Fig. 3, E and F). To test whether the GPI anchor of Gas1* undergoes lipid remodeling as well, we used a flotation assay (Castillon et al., 2011). HA-Gas1*

Published June 20, 2016

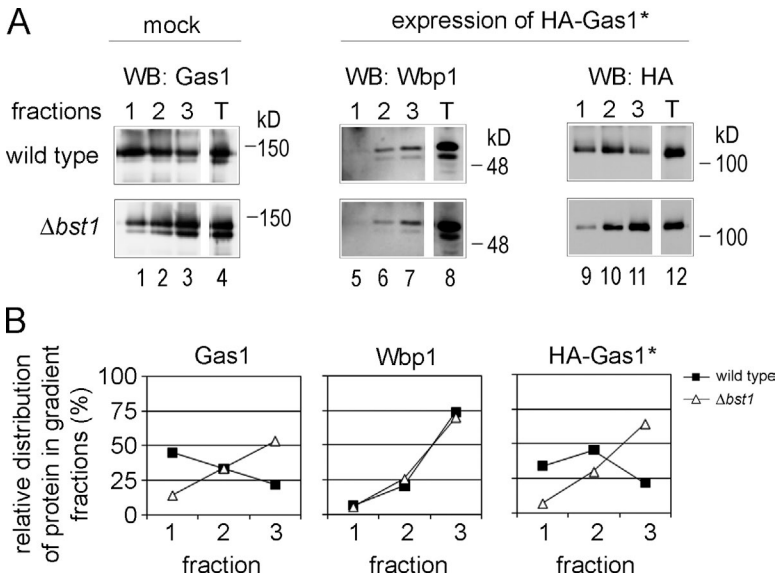

Figure 6. **The GPI anchor of Gas1* undergoes lipid remodeling.** (A) Lysates of wild-type cells and *Δbst1* cells with or without expression of HA-Gas1* were subjected to flotation in an Optiprep gradient. The three top fractions of the gradient as well as the total (T) were analyzed by SDS-PAGE and Western blotting (WB) with the indicated antibodies. (B) Graphical display of the results shown in A. The relative distribution of each individually analyzed protein in the three top fractions is plotted after quantifying protein bands from the WBs shown in A.

and Gas1, but not the control TM protein Wbp1, were recovered in the top gradient fractions (fraction 1), indicating the presence of a long-chain fatty acid that promotes association with membrane rafts (Fig. 6, A and B, wild type). The amount of HA-Gas1* and Gas1 in the top gradient fractions was strongly reduced in *Δbst1* cells, in which lipid remodeling of the GPI anchor is blocked genetically, indicating that the GPI anchor of Gas1* was lipid-remodeled in wild-type cells (Fig. 6, A and B, *Δbst1*). Thus, Gas1*, like Gas1, undergoes sugar and lipid remodeling. This scenario could explain why Gas1*, despite being misfolded, is efficiently exported from the ER although being a substrate for ERAD.

To investigate this further, we tested whether inhibition of GPI anchor remodeling would increase the routing of Gas1* to ERAD. This was true for *Δted1* cells, where sugar remodeling is blocked (Fig. 3, E and F). We extended this test and measured the degradation of Gas1* in the lipid-remodeling mutants *Δbst1* and *Δcwh43*. The global degradation rate of HA-Gas1* was not affected in the single mutants (Fig. 7, A and D). However, expression of GFP-Gas1* revealed that less protein was routed to the vacuole and more was retained inside the ER in both mutants compared with wild-type cells (Fig. 7 B). At the same time, more Gas1* was now degraded by ERAD, because *Δhrd1Δbst1* and *Δhrd1Δcwh43* double mutants showed a marked increase in protein stability compared with the individual single mutants (Fig. 7, C and D). Conversely, Gas1* degradation was not affected when Emp24-dependent export was blocked in the same mutants, consistent with the predominant routing of Gas1* to ERAD (Fig. 7, E and F). Interestingly, *Δemp24Δbst1* and *Δemp24Δcwh43* mutants showed faster Gas1* turnover than *Δemp24* cells (Fig. 7 E). This could indicate that routing of GPI-APs to ERAD is more efficient for GPI-APs that are not yet lipid-remodeled compared with lipid-remodeled species that accumulate in *Δemp24* cells. It is known that lipid-remodeled species tend to localize to membrane rafts and to GPI-AP–specific ERESs (Castillon et al., 2011), which might be less accessible for the ERAD machinery. This could explain why the global degradation rate of Gas1* is decreased in *Δemp24* and, analogously, in *Δted1* cells, compared with *Δbst1* or *Δcwh43* cells (compare Fig. 7 A with Fig. 3 E). Future studies will address these questions in detail.

To address the mechanism of ER export of Gas1*, we assayed its binding to the p24 complex component Emp24. Binding of a GPI-AP to Emp24 was previously shown to depend on anchor remodeling (Castillon et al., 2011; Manzano-Lopez et al., 2015). Using tandem affinity purification (TAP)-tagged Emp24, we could efficiently coimmunoprecipitate (coIP) the ER form of HA-Gas1* (Fig. 8 A, lane 12). Importantly, the efficiency of coIP was comparable to that of Gas1, supporting the conclusion that the GPI anchor was remodeled independently of protein folding (Fig. 8 A, compare lanes 10 and 12). The binding to the anchorless mutants HA-Gas1*TMD and HA-Gas1TMD was strongly reduced, confirming that the interaction between Gas1 or Gas1* and Emp24 was mainly GPI anchor dependent (Fig. 8 A, lanes 14 and 16; Castillon et al., 2011). Interestingly, higher-molecular-weight versions of Gas1* and Gas1 constructs, which correspond to forms that have undergone further glycosylation in the Golgi, were also immunoprecipitated with Emp24-TAP in a manner that was independent of the presence of the GPI anchor (Fig. 8, [post-]Golgi forms). This is in agreement with a proposed function of the p24 complex in retrieval of misfolded or incompletely remodeled GPI-APs from the Golgi to the ER by a mechanism that does not depend on anchor remodeling (Castillon et al., 2011).

Because a conserved mechanism for the ER export of GPI-APs in yeast and mammals consists of Ted1/PGAP5-mediated sugar remodeling of the GPI anchor, we tested whether binding of Gas1* to Emp24 was dependent on Ted1. Indeed, binding of the ER form of HA-Gas1* to Emp24-TAP was strongly reduced in *Δted1* cells, supporting the idea that ER exit of Gas1* is mediated by canonical GPI anchor remodeling that seemingly occurs irrespective of the state of protein folding (Fig. 8 B).

To generalize these findings, we performed additional experiments with an entirely distinct misfolded protein. We used CPY*, a mutant version of the soluble vacuolar carboxypeptidase Y and classic Hrd1-dependent ERAD substrate (Bordallo et al., 1998). To directly evaluate whether a GPI anchor would induce the targeting of CPY* to the vacuole, we generated the fusion proteins GFP-CPY*TMD and GFP-CPY*GPI, which differ only in the nature of their membrane anchors. Live cell fluorescence microscopy revealed that GFP-CPY*TMD, which lacks a GPI anchor, was retained rather efficiently inside the

Published June 20, 2016

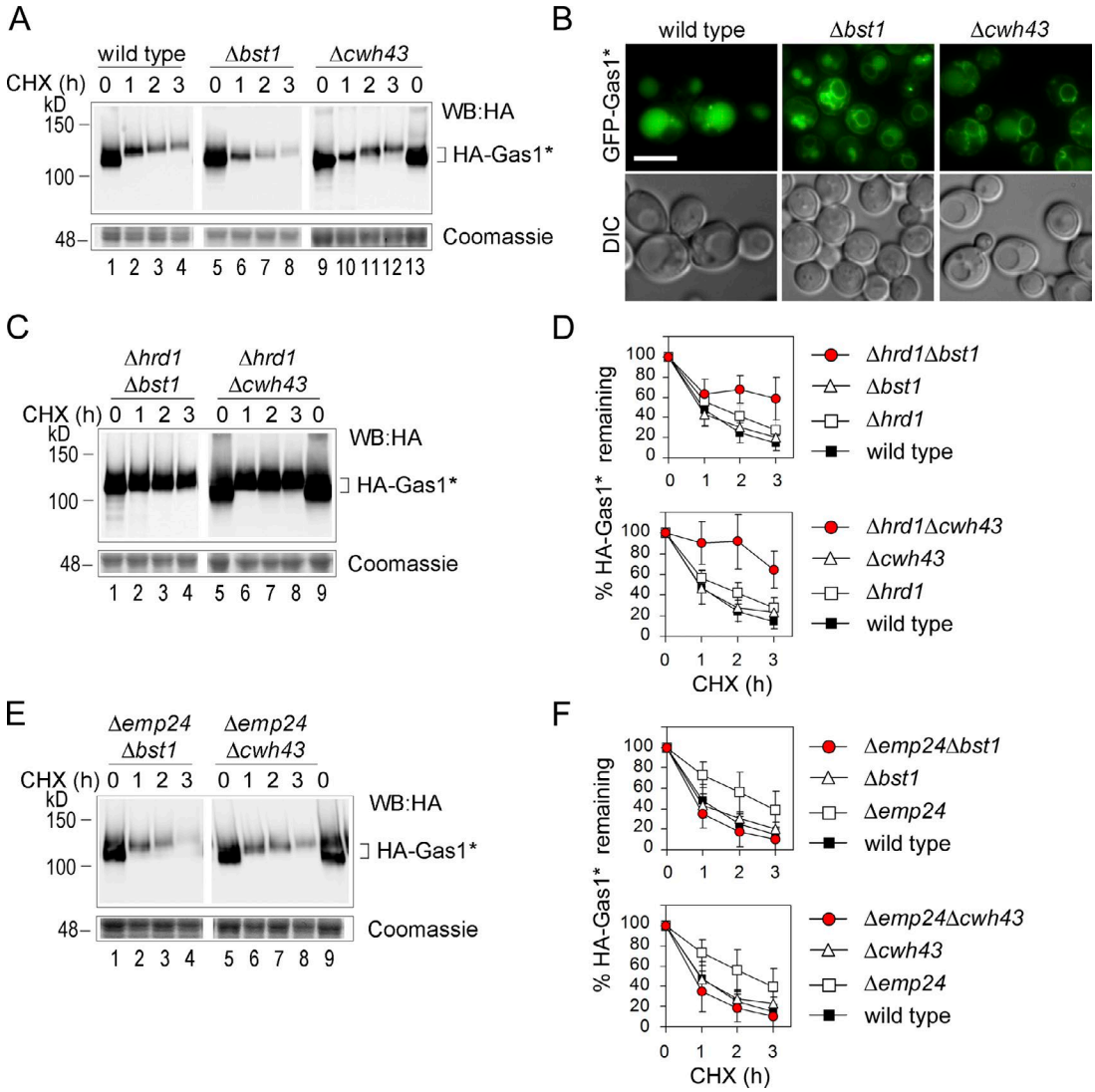

Figure 7. **Increased targeting of Gas1* to ERAD in GPI anchor lipid remodeling mutants.** (A) CHX shut-off experiments with wild-type cells and remodeling mutants expressing HA-Gas1*. The lower part of the gel was separately stained with Coomassie as loading control. (B) Live cell fluorescence microscopy with wild-type cells and remodeling mutants expressing GFP-Gas1*. DIC = Nomarski image. Bar, 3 µm. (C–F) CHX shut-off experiments with the indicated double mutants expressing HA-Gas1*. The lower parts of the gels were separately stained with Coomassie as loading control. For quantification and statistical analysis, results from experiments shown in A as well as from those shown in Fig. 3 E (*Δhrd1* and *Δemp24* cells) were used. Mean values and SDs from at least three individual experiments are shown. Red circles are used to highlight the degradation rates in the double mutants.

ER, with only weak vacuolar signal, indicating minor trafficking to the vacuole (Fig. 9 A, GFP-CPY*TMD). In contrast, the attachment of the GPI anchor resulted in a prominent vacuolar signal and reduced ER membrane staining, indicating increased targeting to the vacuole of this construct (Fig. 9 A, GFP-CPY*GPI). Moreover, the GFP cleavage assay revealed a significant increase in the production of free GFP with GFP-CPY*GPI in comparison to GFP-CPY*TMD, showing that the presence of the GPI anchor led to a global increase in vacuolar degradation of the CPY* fusion protein (Fig. 9, B [compare lanes 1 and 3] and C). The near-absence of free GFP when the same constructs were expressed in the *Δpep4* strain confirmed that free GFP produced in wild-type cells originated from the vacuole (Fig. 9, B [compare lanes 1 and 3 with lanes 2 and 4] and C). In addition to an increase in vacuolar degradation in the presence of the GPI anchor, measurements of Hrd1-dependent degradation using HA-tagged versions of the fusion constructs revealed that the exchange of a TMD for a GPI anchor resulted in a significant drop in ERAD (Fig. 9, D and E). Together, the data obtained with CPY* corroborate those obtained with Gas1* and show that the presence of a GPI anchor on a misfolded ER protein generally causes a reduction in ER retention and ERAD in favor of an increase in ER export, followed by ultimate degradation inside the vacuole.

Discussion

Our data demonstrate that a GPI anchor does not pose a sterical obstruction for the degradation of a misfolded GPI-AP through a canonical ERAD pathway. In contrast to degradation of a misfolded GPI-AP inside the vacuole, where the GPI anchor may be removed by lipases and/or glycosidases, degradation of the same substrate through ERAD hints at the existence of a

Published June 20, 2016

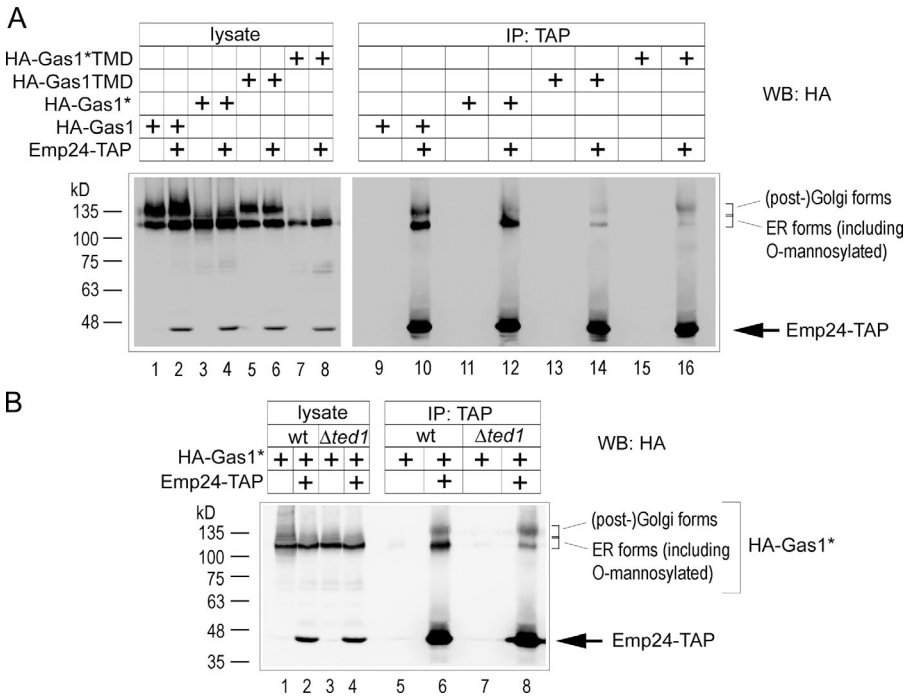

Figure 8. **GPI anchor remodeling-dependent binding of Gas1* to Emp24.** (A) Wild-type cells coexpressing chromosomally TAP-tagged Emp24 and the indicated Gas1 or Gas1* constructs and control cells were subjected to co-immunoprecipitation (IP) experiments followed by SDS-PAGE and Western blotting (WB) with antibodies against HA. Emp24-TAP was recognized by the secondary antibody. (B) As in A, with wild-type cells and *Δted1* cells coexpressing Emp24-TAP and HA-Gas1* or control cells.

yet-unknown cellular mechanism for the removal of the GPI anchor during or after protein retrotranslocation to allow degradation by the proteasome. The presence of such a mechanism is also implied by observation that other posttranslational protein modifications such as glycans on retrotranslocated proteins are removed by a conserved specific cytosolic glycanase before proteasomal degradation (Katiyar et al., 2004). We are currently pursuing the identification of cellular components involved in the removal of a GPI anchor during ERAD.

Remodeled GPI anchors on (correctly folded) GPI-APs were previously known to be recognized by the p24 complex ER export machinery, thereby connecting GPI anchor remodeling with ER export. Our finding that a GPI anchor is remodeled irrespective of protein (mis)folding reveals that a potent ER export signal is also generated on a misfolded protein. We furthermore showed that the remodeled GPI anchor of misfolded Gas1* promotes binding to Emp24, which suggests that inefficient ER retention and ERAD of the tested misfolded GPI-APs are a consequence of efficient GPI anchor–mediated ER export. Although we observed variations in the degree of ER retention, ERAD, and degradation inside the vacuole between different tested constructs, we found in all cases that the presence of a GPI anchor resulted in a larger fraction of the misfolded protein to be exported from the ER and routed to the vacuole compared with the same protein when membrane-anchored via a TMD or when soluble. These observations combined suggest that the ER residence time for misfolded GPI-APs is mainly determined by remodeling of the GPI anchor and only to a minor degree by protein folding.

On a speculative note, it could be possible that ER protein-retention mechanisms, which are largely based on protein–protein and protein–glycan interactions between substrates and chaperones, are in competition with lipid-based sorting mechanisms connected to membrane homeostasis or membrane traffic. For instance, the particular lipids that are part of the GPI anchor, in particular after anchor remodeling, are likely to affect ER membrane homeostasis at least locally and might necessitate efficient export from the ER (Copic et al., 2009). Alternatively, the known segregation of GPI-APs from other membrane and soluble proteins inside the ER as part of a sorting mechanism linked to membrane traffic might limit the access of misfolded GPI-APs to particular cellular components involved in ER retention and protein quality control (Muñiz et al., 2001; Castillon et al., 2009). Future work will address these possibilities.

Based on our results, we propose that canonical GPI anchor remodeling universally limits the ER quality control of GPI-APs. This provides a unifying model for the increasing number of observations in various organisms that misfolded GPI-APs are rather poor ERAD substrates. Interference with GPI anchor remodeling could thus also be a relevant approach in an attempt to increase ERAD of certain disease-prone mutant prion proteins that are converted into pathogenic aggregates only after ER exit (Victoria and Zurzolo, 2015). Finally, our data also illustrate the importance of post-ER quality control mechanisms, about which much is still to be learned, that have particular relevance for the entire class of GPI-APs.

Materials and methods

Yeast strains

A detailed list of yeast strains used in this study is found in Table S1.

Construction of plasmids

All constructs used in this study were expressed from integrative plasmids under the control of the endogenous *GAS1* promoter. Plasmid markers are indicated in the list of yeast strains (Table S1). The construct for the expression of HA-Gas1*, pMF616, was a gift from the Jigami laboratory (Fujita et al., 2006). A construct expressing HA-Gas1 was generated from pMF616 by changing the single point mutation (G291R) back to wild-type sequence using the primers 5′-GATGTC TGGTCTGGTGGTATCGTATACATGTAC-3′ and 5′-GTACATGTA TACGATACCACCAGACCAGACATC-3′ in combination with the Quikchange protocol from Agilent Technologies, yielding NSp17. To

Published June 20, 2016

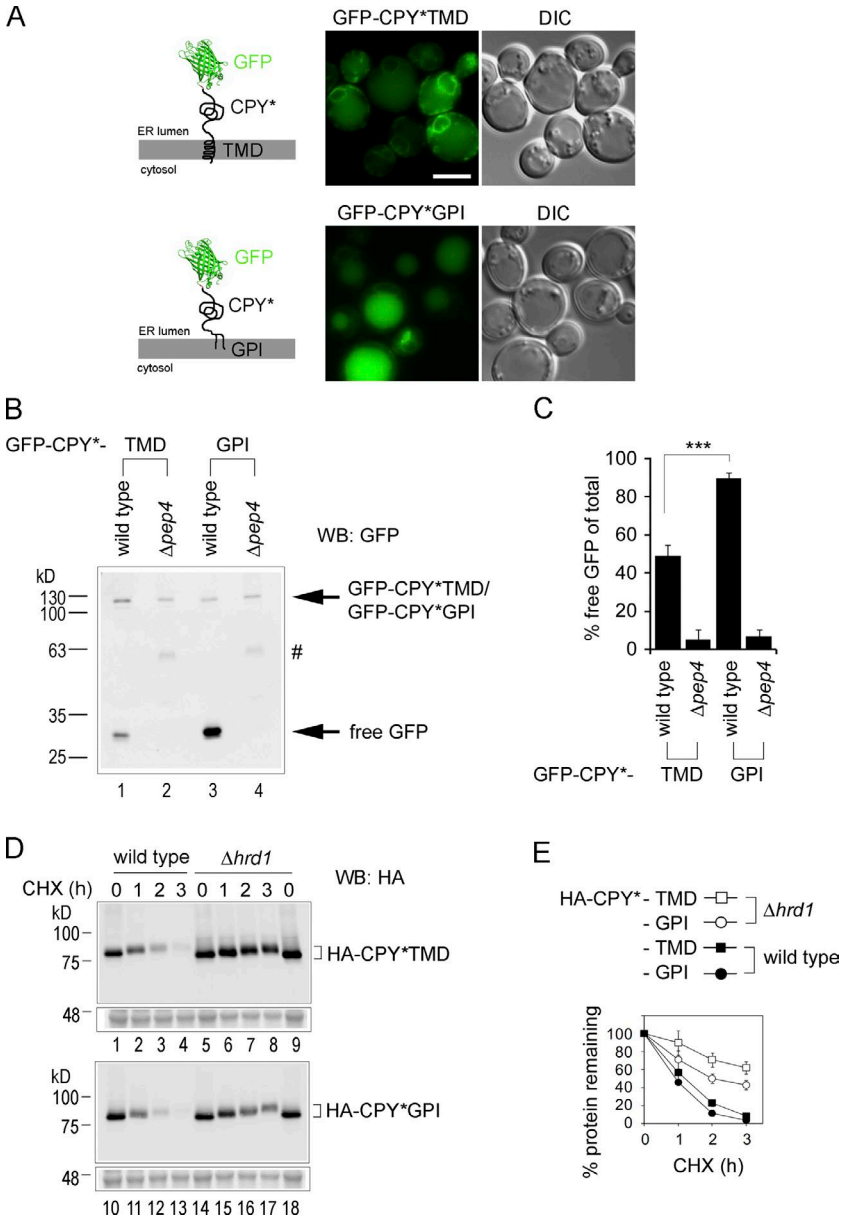

Figure 9. **The presence of a GPI anchor on CPY* causes an increase in vacuolar degradation and a parallel decrease in ERAD compared with CPY* with a TMD.** (A) Live cell fluorescence microscopy of wild-type cells expressing the indicated GFP-CPY* fusion constructs. Schematic illustrations of the various constructs are shown. From previously used GFP-Gas1* fusion constructs, the Gas1* moiety, with the exception of 57 amino acids comprising its C-terminal domain containing the GPI anchoring signal, was exchanged with CPY*; for details see Materials and methods. DIC = Nomarski image. Bar, 2 µm. (B) GFP-cleavage assay. Cells used for microscopy in A and *Δpep4* cells expressing the same constructs were lysed in equal amounts and analyzed by SDS-PAGE in combination with Western blotting (WB) with antibodies against GFP. The hashtag indicates a non-specific protein that accumulated in *Δpep4* cells. (C) Quantification and statistical analysis of results from experiments shown in B. Mean values and SDs from at least three individual experiments are shown. ***, $P < 0.001$ (unpaired two-tailed Student's *t* test). (D) Wild-type cells and the indicated mutant cells expressing HA-CPY*TMD and HA-CPY*GPI were subjected to CHX shut-off experiments. Protein *O*-mannosylation occurs within the serine-rich region proximal to the GPI anchoring site that is part of the C-terminal 57 amino acids of the fusion proteins that originate from Gas1 (Gatti et al., 1994). A lower part of the gel was separately stained with Coomassie as loading control. (E) Quantification of results from experiments shown in D. Mean values and SDs from at least three individual experiments are shown.

generate constructs for the expression of mutants lacking GPI anchors, the point mutations K526R and N528Q were simultaneously introduced into pMF616 and NSp17 using PCR-based single primer site-directed mutagenesis and the primer 5′-CAGCTTCATCTTCATCTTCTTCGC GAAAGCAAGCTGCCACCAACGTTAAAGC-3′, yielding NSp23 (HA-Gas1*TMD) and NSp20 (HA-Gas1TMD). To generate the soluble version HA-Gas1*ΔTMD, a stop codon was introduced into the coding region of the protein just upstream of the TMD using the same method in combination with pMF616 as template and the primer 5′-CTTCATCTT CTAGCAAGAAGTAAAAGGCCTCGACACATACATAATAACT-3′, yielding VGp256. To generate GFP-tagged constructs, the GFP sequence was amplified from pKT128 (EUROSCARF Collection Center) with the primers 5′-GCGACGCGTTCTAAAGGTGAAGAATTATTC-3′ and 5′-GCGACGCGTTTTGTACAATTCATCCATACC-3′. The PCR product was cut with MluI and inserted into pMF616, NSp17, NSp20, NSp23, and VGp256 to yield NSp19 (GFP-Gas1*), LLp16 (GFP-Gas1), LLp17 (GFP-Gas1TMD), LLp18 (GFP-Gas1*TMD), and clone374 (GFP-Gas1*ΔTMD). To generate fusion constructs with CPY*, HA-Gas1* and HA-Gas1*TMD were first subcloned into pRS314 (*TRP1*, CEN) using XmaI and SacI, yielding VGp257 and VGp258. The coding sequence for 81 amino acids downstream of a unique BsrGI site in Gas1* was then removed in both constructs using PCR-based single primer site-directed mutagenesis and the primer 5′-CAAAGGAACAGCTATCTT TCTCCAGTTCTTCTTCTTCTTC-3′, leaving the coding region for the 57 C-terminal amino acids of HA-Gas1* and HA-Gas1*TMD, yielding clone390 and clone391. The CPY* moiety was amplified with PCR using the primers 5′-GCGCATATGTCATTGCAAAGACCGTTG-3′ and 5′-GCGTGTACATAAGGAGAAACCACCGTG-3′ from VGp173, cut with NdeI and BsrGI, and pasted into clone390 and clone391, yielding HA-CPY*GPI (clone392) and HA-CPY*TMD (LLp43). To obtain the GFP-tagged constructs, LLp18 was cut with MluI to release the GFP moiety. The fragment was purified, pasted into clone392 and LLp43, and cut with the same enzyme, yielding GFP-CPY*GPI (LLp47) and GFP-CPY*TMD (LLp45). To generate integrative plasmids containing these fusion constructs, they were subcloned into pRS306 using XmaI and SacI, yielding clone409 and clone410, respectively.

For lipidomics analysis, the various constructs expressing HA-tagged Gas1 derivatives together with the adjacent *URA3* gene were

Published June 20, 2016

amplified from the integrated plasmids using the primers 5′-CTGATA AAACAAAAACAACAAACACAGCTAAATCTCAACAATGTTGTT TAAATCCCTTTCD-3′ and 5′-CTCATCGAGCATCAAATGAAACTG CAATTTATTCATATCAGATTGTACTGAGAGTGCACC-3′. The PCR products were transformed into the *Δgas1* strain, replacing the *KANMX*6 cassette in the *GAS1* locus by homologous combination.

Antibodies

Primary antibodies for Western blotting and immunoprecipitation experiments were polyclonal rabbit antibodies from our laboratories (against Wbp1 and Gas1) and commercially available antibodies against HA or GFP (Roche). Secondary antibodies for Western blot analysis were peroxidase-coupled anti-mouse or anti-rabbit antibodies from Sigma-Aldrich.

CHX shut-off experiments

The experiments were started with exponentially growing cells in rich medium with an OD of 0.5 to 0.8. Translation was stopped by addition of CHX to a final concentration of 200 µg/ml. Equal-volume aliquots of cell culture were removed at indicated time points and moved to ice. Cells were lysed using 150 mM NaOH, followed by adding sample buffer containing 2% SDS and heating. Samples were analyzed by SDS-PAGE followed by Western blotting using the indicated primary antibodies, peroxidase-coupled secondary antibodies (Sigma-Aldrich), and ECL (Thermo Fisher Scientific) as substrate. Images were taken with a LAS-3000 mini-imaging system (Fujifilm), and bands were quantified using Multi-Gauge software (Fujifilm).

Fluorescence microscopy

Cells were grown overnight, diluted to OD 0.3, regrown for 4 h, washed with PBS, and immediately analyzed by fluorescence microcopy at RT. Cells were observed with an Olympus BX61 microscope equipped with a 100×/1.4 PlanApo oil-immersion lens and a conventional FITC cube as well as a DIC prism and polarizer for Nomarski imaging. Images were acquired using a DP70 camera and the DPcontroller software (Olympus).

Probing for GPI anchor attachment

20 OD of exponentially growing cells were lysed by bead beating in cold TEPI buffer in presence of 150 mM NaCl and protease inhibitor cocktail (Roche). 1 ml lysate was incubated with 1% of precondensed Triton X-114 (Fluka) at 4°C for 30 min with rotation and cleared by spinning at 14,000 *g* for 15 min at 4°C. Cleared lysates were split into two equal parts. One sample was incubated with 0.1 units PI-PLC (Thermo Fisher Scientific), and the second sample was mock-treated. Samples were incubated for 12 h at 4°C on a rocker. Phase separation was achieved by heating to 32°C followed by brief spinning. Phases were split, reextracted twice, and precipitated with trichloroacetic acid (TCA). Finally, SDS sample buffer containing 2% and 6 M urea was added, and samples were analyzed by SDS-PAGE and Western blotting.

GFP processing assay

Cells were grown overnight, diluted to OD 0.3, and regrown for 4 h. Before removal of aliquots, cells were incubated with CHX to a final concentration of 200 µg/ml and incubated for 15 min to allow for completion of posttranslational protein translocation across the ER membrane. Aliquots were removed, transferred to ice, lysed by alkaline treatment (Kushnirov, 2000), and resuspended in a cell density–normalized volume of loading buffer, followed by SDS-PAGE and Western blotting using anti-GFP antibody (Roche), HRP-conjugated anti-mouse secondary antibody (Sigma-Aldrich), and ECL as substrate. Images were taken with a LAS-3000 mini-imaging system, and bands were quantified using Multi-Gauge software.

Optiprep gradient flotation assay

10 OD of exponentially growing cells were harvested at OD 0.1, washed in ice cold water, and lysed by bead beating in TNE buffer (50 mM Tris-HCl, pH 7.4, 150 mM NaCl, and 5 mM EDTA) containing a protease inhibitor cocktail (Roche). The lysate was cleared, washed, and resuspended in 300 µl TNE buffer. Triton X-100 was added to 1% final concentration and incubated on ice for 30 min. Optiprep solution (Nycomed) was added to 40% final concentration, and the resulting solution was divided into two parts with equal volume. One part was considered "total"; the other part was overlaid with 1.2 ml of 30% Optiprep in TXNE (TNE with 1% Triton X-100) and finally with 200 µl TXNE. The samples were centrifuged at 55,000 rpm for 2 h in a TLS55 rotor (Beckman Coulter). Six fractions (360 µl each) were collected from top to bottom. Protein contents were precipitated by adding TCA to 15%, washed, and resuspended in SDS-PAGE loading buffer, followed by SDS-PAGE and Western blot analysis.

CoIP

200 ml of cell culture was grown to mid-log phase, washed, and lysed by bead beating with glass beads in lysis buffer (1× PBS, 1 mM EDTA, 1 mM PMSF, and protein inhibitor cocktail [Roche]). Lysates were cleared, solubilized by addition of 1% digitonin (EMD Millipore) for 30 min, and cleared by centrifugation for 20 min at 100,000 *g*, followed by incubation with magnetic beads (Thermo Fisher Scientific) coupled to rabbit IgG (Sigma-Aldrich) for 2 h at 4°C. Washing was done in lysis buffer with 0.5% digitonin followed by elution in SDS-loading buffer.

Lipid extraction protocols

Yeast culture, lipid extraction of sphingolipid and glycerophospholipids, and mass spectrometry analysis were performed as described (da Silveira Dos Santos et al., 2014). In brief, strains were grown in rich medium (yeast extract/peptone/dextrose) at 30°C to early exponential growth phase. 25 600-OD units were collected, and metabolism was stopped using TCA and cooling on ice. Samples were resuspended in extraction solvent (ethanol, water, diethylether, pyridine, and ammonium hydroxide). Internal standards were added, and the samples were broken through mechanical disruption using glass beads. Cell debris was pelleted by centrifugation, and the supernatant was collected. Lipid extract was divided into two aliquots for analysis of glycerophospholipids and sphingolipids. Mild alkaline hydrolysis was performed on the sphingolipid fraction. Finally, both fractions were desalted using water saturated *n*-butanol. Mass spectrometry analysis was done using direct infusion in negative and positive mode. The lipid species were identified by the *m*/*z* of the lipid and relevant fragment, and their amount was calculated by their signal intensities relative to the standards. Three independent biologic replicates were analyzed. The amount of ceramide and IPC species were summed to obtain the total amount of each lipid class, and the samples were normalized by the total amount of inorganic phosphate.

Determination of total phosphorus

Glycerophospholipid lipid extract was resuspended in 500 µl chloroform:methanol (1:1, vol/vol), and 50 µl was placed in 13-mm disposable Pyrex tubes. After solvent evaporation, 20 µl of water and 140 µl of 70% perchloric acid were added to the tubes. Samples were heated for 1 h at 180°C in a hood. Tubes were allowed to cool for 5 min at RT. Next, 800 µl of freshly prepared water:1.25% NH_4 molybdate: 1.67% ascorbic acid (5:2:1, vol/vol) was added to the tubes, followed by 5 min of heating at 100°C. Tubes were cooled at RT, and 100 µl was used for measurement of absorbance at 820 nm. A standard curve was generated with KH_2PO_4 standard solution and processed identically.

Online supplemental material

Fig. S1 shows the degradation rates of HA-Gas1* in single- and double-deletion mutants, highlighting the contribution of Hrd1-dependent ERAD to global protein degradation. Fig. S2 shows lipid profiles of *Δgas1* cells in dependence on expressing various Gas1* and Gas1 constructs along with control experiments. Table S1 shows a detailed list of yeast strains used in this study. Online supplemental material is available at http://www.jcb.org/cgi/content/full/jcb.201602010/DC1.

Acknowledgments

We thank the Jigami laboratory for plasmids and Martin Spiess and Robert Ernst for critical reading of the manuscript.

This work was supported by the Swiss National Center for Competence in Research (Chemical Biology) and the Schweizerischer Nationalfonds zur Förderung der Wissenschaftlichen Forschung to H. Riezman and the Ministerio de Ciencia e Innovación (BFU2009-07290 and BFU2014-59309-P) and the Junta de Andalucia (P09-CVI-4503) to M. Muñiz and V. Goder.

The authors declare no competing financial interests.

Author Contributions: N. Sikorska, L. Lemus, A. Aguilera-Romero, M. Muñiz, and V. Goder designed experiments. N. Sikorska, L. Lemus, A. Aguilera-Romero, J. Manzano-Lopez, and V. Goder performed experiments. N. Sikorska, L. Lemus, A. Aguilera-Romero, J. Manzano-Lopez, H. Riezman, M. Muñiz, and V. Goder evaluated data. V. Goder wrote the manuscript.

Submitted: 3 February 2016
Accepted: 26 May 2016

References

Arvan, P., X. Zhao, J. Ramos-Castaneda, and A. Chang. 2002. Secretory pathway quality control operating in Golgi, plasmalemmal, and endosomal systems. *Traffic.* 3:771–780. http://dx.doi.org/10.1034/j.1600-0854.2002.31102.x

Ashok, A., and R.S. Hegde. 2008. Retrotranslocation of prion proteins from the endoplasmic reticulum by preventing GPI signal transamidation. *Mol. Biol. Cell.* 19:3463–3476. http://dx.doi.org/10.1091/mbc.E08-01-0087

Bordallo, J., R.K. Plemper, A. Finger, and D.H. Wolf. 1998. Der3p/Hrd1p is required for endoplasmic reticulum-associated degradation of misfolded lumenal and integral membrane proteins. *Mol. Biol. Cell.* 9:209–222. http://dx.doi.org/10.1091/mbc.9.1.209

Braakman, I., and N.J. Bulleid. 2011. Protein folding and modification in the mammalian endoplasmic reticulum. *Annu. Rev. Biochem.* 80:71–99. http://dx.doi.org/10.1146/annurev-biochem-062209-093836

Carvalho, P., V. Goder, and T.A. Rapoport. 2006. Distinct ubiquitin-ligase complexes define convergent pathways for the degradation of ER proteins. *Cell.* 126:361–373. http://dx.doi.org/10.1016/j.cell.2006.05.043

Castillon, G.A., R. Watanabe, M. Taylor, T.M. Schwabe, and H. Riezman. 2009. Concentration of GPI-anchored proteins upon ER exit in yeast. *Traffic.* 10:186–200. http://dx.doi.org/10.1111/j.1600-0854.2008.00857.x

Castillon, G.A., A. Aguilera-Romero, J. Manzano-Lopez, S. Epstein, K. Kajiwara, K. Funato, R. Watanabe, H. Riezman, and M. Muñiz. 2011. The yeast p24 complex regulates GPI-anchored protein transport and quality control by monitoring anchor remodeling. *Mol. Biol. Cell.* 22:2924–2936. http://dx.doi.org/10.1091/mbc.E11-04-0294

Contreras, F.X., A.M. Ernst, P. Haberkant, P. Björkholm, E. Lindahl, B. Gönen, C. Tischer, A. Elofsson, G. von Heijne, C. Thiele, et al. 2012. Molecular recognition of a single sphingolipid species by a protein's transmembrane domain. *Nature.* 481:525–529. http://dx.doi.org/10.1038/nature10742

Copic, A., M. Dorrington, S. Pagant, J. Barry, M.C. Lee, I. Singh, J.L. Hartman IV, and E.A. Miller. 2009. Genomewide analysis reveals novel pathways affecting endoplasmic reticulum homeostasis, protein modification and quality control. *Genetics.* 182:757–769. http://dx.doi.org/10.1534/genetics.109.101105

da Silveira Dos Santos, A.X., I. Riezman, M.A. Aguilera-Romero, F. David, M. Piccolis, R. Loewith, O. Schaad, and H. Riezman. 2014. Systematic lipidomic analysis of yeast protein kinase and phosphatase mutants reveals novel insights into regulation of lipid homeostasis. *Mol. Biol. Cell.* 25:3234–3246. http://dx.doi.org/10.1091/mbc.E14-03-0851

Davidson, E.A., and D.C. Gowda. 2001. Glycobiology of *Plasmodium falciparum*. *Biochimie.* 83:601–604. http://dx.doi.org/10.1016/S0300-9084(01)01316-5

Drisaldi, B., R.S. Stewart, C. Adles, L.R. Stewart, E. Quaglio, E. Biasini, L. Fioriti, R. Chiesa, and D.A. Harris. 2003. Mutant PrP is delayed in its exit from the endoplasmic reticulum, but neither wild-type nor mutant PrP undergoes retrotranslocation prior to proteasomal degradation. *J. Biol. Chem.* 278:21732–21743. http://dx.doi.org/10.1074/jbc.M213247200

Fujita, M., and Y. Jigami. 2008. Lipid remodeling of GPI-anchored proteins and its function. *Biochim. Biophys. Acta.* 1780:410–420. http://dx.doi.org/10.1016/j.bbagen.2007.08.009

Fujita, M., and T. Kinoshita. 2012. GPI-anchor remodeling: Potential functions of GPI-anchors in intracellular trafficking and membrane dynamics. *Biochim. Biophys. Acta.* 1821:1050–1058. http://dx.doi.org/10.1016/j.bbalip.2012.01.004

Fujita, M., T. Yoko-O, and Y. Jigami. 2006. Inositol deacylation by Bst1p is required for the quality control of glycosylphosphatidylinositol-anchored proteins. *Mol. Biol. Cell.* 17:834–850. http://dx.doi.org/10.1091/mbc.E05-05-0443

Fujita, M., Y. Maeda, M. Ra, Y. Yamaguchi, R. Taguchi, and T. Kinoshita. 2009. GPI glycan remodeling by PGAP5 regulates transport of GPI-anchored proteins from the ER to the Golgi. *Cell.* 139:352–365. http://dx.doi.org/10.1016/j.cell.2009.08.040

Gatti, E., L. Popolo, M. Vai, N. Rota, and L. Alberghina. 1994. O-linked oligosaccharides in yeast glycosyl phosphatidylinositol-anchored protein gp115 are clustered in a serine-rich region not essential for its function. *J. Biol. Chem.* 269:19695–19700.

Gauss, R., T. Sommer, and E. Jarosch. 2006. The Hrd1p ligase complex forms a linchpin between ER-lumenal substrate selection and Cdc48p recruitment. *EMBO J.* 25:1827–1835. http://dx.doi.org/10.1038/sj.emboj.7601088

Goder, V., and A. Melero. 2011. Protein *O*-mannosyltransferases participate in ER protein quality control. *J. Cell Sci.* 124:144–153. http://dx.doi.org/10.1242/jcs.072181

Haynes, C.M., S. Caldwell, and A.A. Cooper. 2002. An HRD/DER-independent ER quality control mechanism involves Rsp5p-dependent ubiquitination and ER-Golgi transport. *J. Cell Biol.* 158:91–101. http://dx.doi.org/10.1083/jcb.200201053

Hirayama, H., M. Fujita, T. Yoko-o, and Y. Jigami. 2008. *O*-mannosylation is required for degradation of the endoplasmic reticulum-associated degradation substrate Gas1*p via the ubiquitin/proteasome pathway in *Saccharomyces cerevisiae*. *J. Biochem.* 143:555–567. http://dx.doi.org/10.1093/jb/mvm249

Jonikas, M.C., S.R. Collins, V. Denic, E. Oh, E.M. Quan, V. Schmid, J. Weibezahn, B. Schwappach, P. Walter, J.S. Weissman, and M. Schuldiner. 2009. Comprehensive characterization of genes required for protein folding in the endoplasmic reticulum. *Science.* 323:1693–1697. http://dx.doi.org/10.1126/science.1167983

Katiyar, S., G. Li, and W.J. Lennarz. 2004. A complex between peptide:N-glycanase and two proteasome-linked proteins suggests a mechanism for the degradation of misfolded glycoproteins. *Proc. Natl. Acad. Sci. USA.* 101:13774–13779. http://dx.doi.org/10.1073/pnas.0405663101

Kincaid, M.M., and A.A. Cooper. 2007. Misfolded proteins traffic from the endoplasmic reticulum (ER) due to ER export signals. *Mol. Biol. Cell.* 18:455–463. http://dx.doi.org/10.1091/mbc.E06-08-0696

Kushnirov, V.V. 2000. Rapid and reliable protein extraction from yeast. *Yeast.* 16:857–860. http://dx.doi.org/10.1002/1097-0061(20000630)16:9<857::AID-YEA561>3.0.CO;2-B

Loizides-Mangold, U., F.P. David, V.J. Nesatyy, T. Kinoshita, and H. Riezman. 2012. Glycosylphosphatidylinositol anchors regulate glycosphingolipid levels. *J. Lipid Res.* 53:1522–1534. http://dx.doi.org/10.1194/jlr.M025692

Ma, J., and S. Lindquist. 2001. Wild-type PrP and a mutant associated with prion disease are subject to retrograde transport and proteasome degradation. *Proc. Natl. Acad. Sci. USA.* 98:14955–14960. http://dx.doi.org/10.1073/pnas.011578098

Manzano-Lopez, J., A.M. Perez-Linero, A. Aguilera-Romero, M.E. Martin, T. Okano, D.V. Silva, P.H. Seeberger, H. Riezman, K. Funato, V. Goder, et al. 2015. COPII coat composition is actively regulated by luminal cargo maturation. *Curr. Biol.* 25:152–162. http://dx.doi.org/10.1016/j.cub.2014.11.039

Mayor, S., and H. Riezman. 2004. Sorting GPI-anchored proteins. *Nat. Rev. Mol. Cell Biol.* 5:110–120. http://dx.doi.org/10.1038/nrm1309

Mehnert, M., T. Sommer, and E. Jarosch. 2010. ERAD ubiquitin ligases: Multifunctional tools for protein quality control and waste disposal in the endoplasmic reticulum. *BioEssays.* 32:905–913. http://dx.doi.org/10.1002/bies.201000046

Meusser, B., C. Hirsch, E. Jarosch, and T. Sommer. 2005. ERAD: the long road to destruction. *Nat. Cell Biol.* 7:766–772. http://dx.doi.org/10.1038/ncb0805-766

Muñiz, M., C. Nuoffer, H.P. Hauri, and H. Riezman. 2000. The Emp24 complex recruits a specific cargo molecule into endoplasmic reticulum-derived vesicles. *J. Cell Biol.* 148:925–930. http://dx.doi.org/10.1083/jcb.148.5.925

Muñiz, M., P. Morsomme, and H. Riezman. 2001. Protein sorting upon exit from the endoplasmic reticulum. *Cell.* 104:313–320. http://dx.doi.org/10.1016/S0092-8674(01)00215-X

Petris, G., A. Casini, L. Sasset, F. Cesaratto, M. Bestagno, A. Cereseto, and O.R. Burrone. 2014. CD4 and BST-2/tetherin proteins retro-translocate from endoplasmic reticulum to cytosol as partially folded and multimeric molecules. *J. Biol. Chem.* 289:1–12. http://dx.doi.org/10.1074/jbc.M113.512368

Puig, B., H. Altmeppen, and M. Glatzel. 2014. The GPI-anchoring of PrP: Implications in sorting and pathogenesis. *Prion.* 8:11–18. http://dx.doi.org/10.4161/pri.27892

Reggiori, F., E. Canivenc-Gansel, and A. Conzelmann. 1997. Lipid remodeling leads to the introduction and exchange of defined ceramides on GPI proteins in the ER and Golgi of *Saccharomyces cerevisiae*. *EMBO J.* 16:3506–3518. http://dx.doi.org/10.1093/emboj/16.12.3506

Satpute-Krishnan, P., M. Ajinkya, S. Bhat, E. Itakura, R.S. Hegde, and J. Lippincott-Schwartz. 2014. ER stress-induced clearance of misfolded GPI-anchored proteins via the secretory pathway. *Cell.* 158:522–533. http://dx.doi.org/10.1016/j.cell.2014.06.026

Spear, E.D., and D.T. Ng. 2003. Stress tolerance of misfolded carboxypeptidase Y requires maintenance of protein trafficking and degradative pathways. *Mol. Biol. Cell.* 14:2756–2767. http://dx.doi.org/10.1091/mbc.E02-11-0717

Tashima, Y., R. Taguchi, C. Murata, H. Ashida, T. Kinoshita, and Y. Maeda. 2006. PGAP2 is essential for correct processing and stable expression of GPI-anchored proteins. *Mol. Biol. Cell.* 17:1410–1420. http://dx.doi.org/10.1091/mbc.E05-11-1005

Umemura, M., M. Fujita, T. Yoko-O, A. Fukamizu, and Y. Jigami. 2007. *Saccharomyces cerevisiae* CWH43 is involved in the remodeling of the lipid moiety of GPI anchors to ceramides. *Mol. Biol. Cell.* 18:4304–4316. http://dx.doi.org/10.1091/mbc.E07-05-0482

Vembar, S.S., and J.L. Brodsky. 2008. One step at a time: Endoplasmic reticulum-associated degradation. *Nat. Rev. Mol. Cell Biol.* 9:944–957. http://dx.doi.org/10.1038/nrm2546

Victoria, G.S., and C. Zurzolo. 2015. Trafficking and degradation pathways in pathogenic conversion of prions and prion-like proteins in neurodegenerative diseases. *Virus Res.* 207:146–154. http://dx.doi.org/10.1016/j.virusres.2015.01.019

Wang, S., and D.T. Ng. 2010. Evasion of endoplasmic reticulum surveillance makes Wsc1p an obligate substrate of Golgi quality control. *Mol. Biol. Cell.* 21:1153–1165. http://dx.doi.org/10.1091/mbc.E09-10-0910

Wang, Y.J., B.O. Tayo, A. Bandyopadhyay, H. Wang, T. Feng, N. Franceschini, H. Tang, J. Gao, Y.J. Sung, R.C. Elston, et al. COGENT BP consortium. 2014. The association of the vanin-1 N131S variant with blood pressure is mediated by endoplasmic reticulum-associated degradation and loss of function. *PLoS Genet.* 10:e1004641. http://dx.doi.org/10.1371/journal.pgen.1004641

Yedidia, Y., L. Horonchik, S. Tzaban, A. Yanai, and A. Taraboulos. 2001. Proteasomes and ubiquitin are involved in the turnover of the wild-type prion protein. *EMBO J.* 20:5383–5391. http://dx.doi.org/10.1093/emboj/20.19.5383

Zhao, Y., J.A. Macgurn, M. Liu, and S. Emr. 2013. The ART-Rsp5 ubiquitin ligase network comprises a plasma membrane quality control system that protects yeast cells from proteotoxic stress. *eLife.* 2:e00459. http://dx.doi.org/10.7554/eLife.00459

Sikorska et al., http://www.jcb.org/cgi/content/full/jcb.201602010/DC1

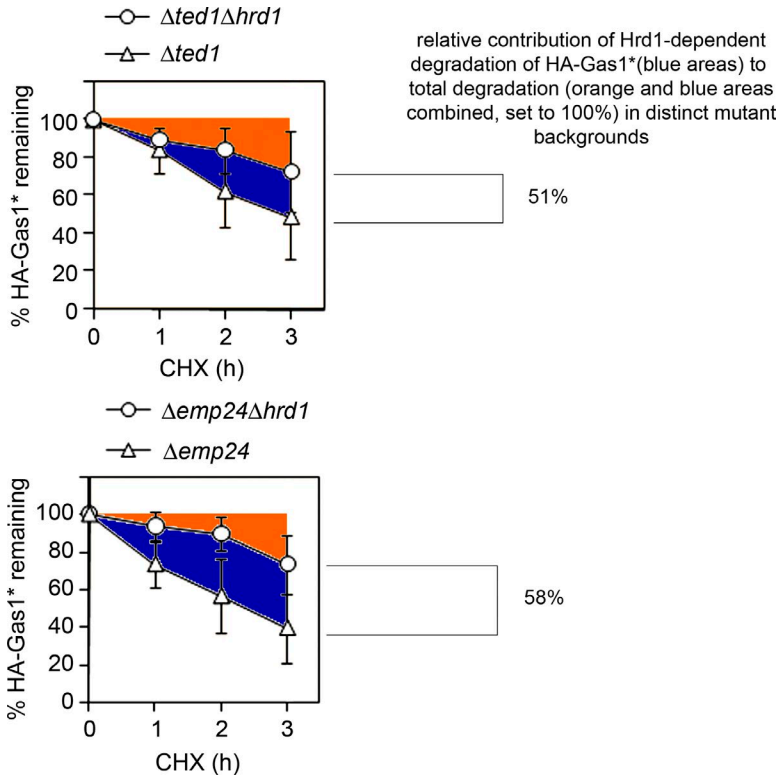

Figure S1. **ERAD is the major degradation pathway for HA-Gas1* in *Δted1* and *Δemp24* cells.** Graphical display of the degradation rates of HA-Gas1* in the indicated mutant strains from experiments described in Fig. 3 (E–G). The degradation rates of HA-Gas1* in the single and double mutants were determined by regression of linear trendlines. The degradation rate of HA-Gas1* in each individual single mutant was set to 100%. The extent of reduction in HA-Gas1* degradation in the double mutant compared with the single mutant is indicated in percent. Mean values and SDs from at least three individual experiments are shown.

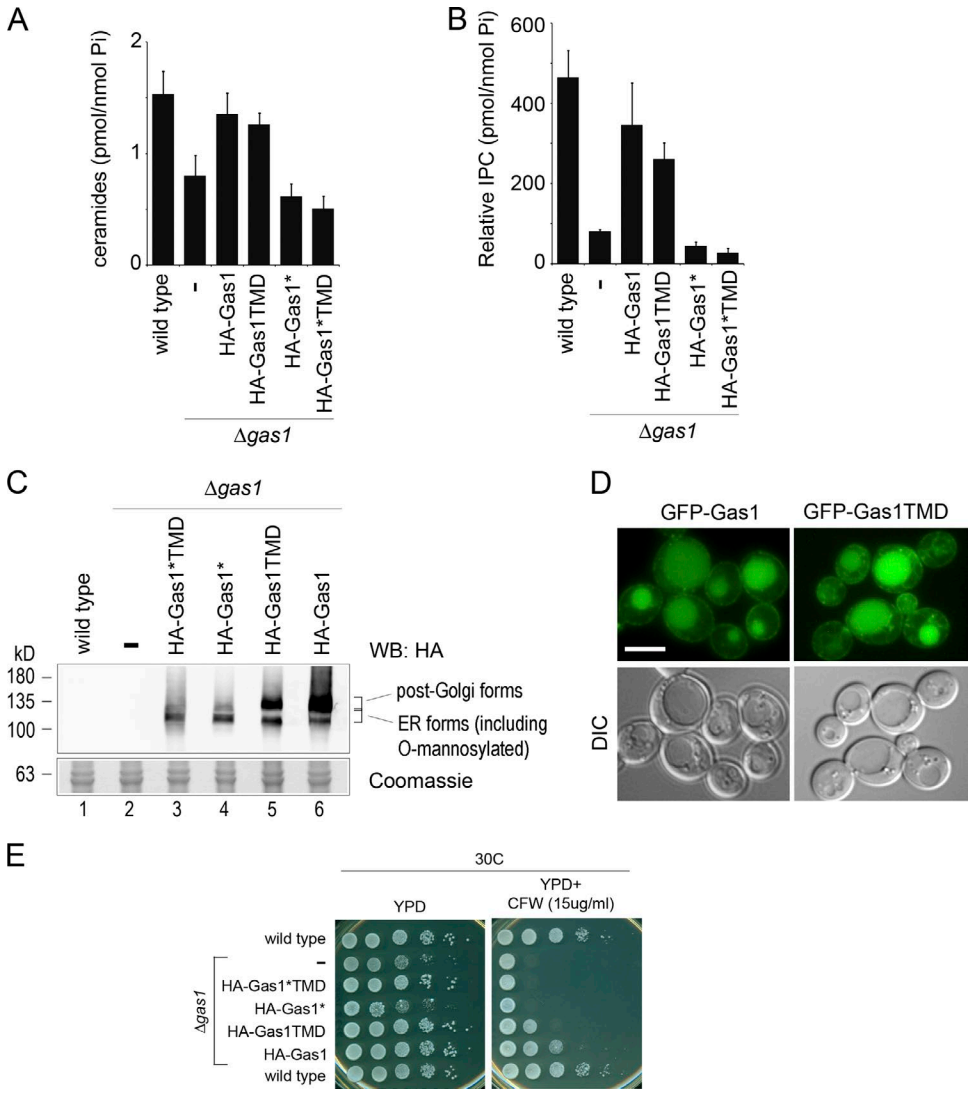

Figure S2. **Lack of evidence for a role of Gas1* in cellular ceramide cotransport.** (A) Ceramide profile of wild-type cells, *Δgas1* cells, and *Δgas1* cells expressing the indicated chromosomally integrated constructs. Three biological replicates were used for quantification, and mean values and SDs are indicated. *Δgas1* cells showed a drop in total cellular ceramide that could be partially reversed by expressing HA-Gas1 or HA-Gas1TMD but not HA-Gas1* or HA-Gas1*TMD. (B) Inositol phosphoceramide C (IPC) profiles of cells used in A. IPC levels were normalized to inorganic phosphate (see Materials and methods). Three biological replicates were used for quantification, and mean values and SDs are indicated. (C) Expression test for different Gas1 and Gas1* constructs in cells used in A and B. Exponentially growing cells were lysed and analyzed by SDS-PAGE and Western blotting (WB) with antibodies against HA. The lower part of the gel was separately stained with Coomassie as loading control. (D) Live cell fluorescence microscopy of wild-type cells expressing GFP-Gas1 and GFP-Gas1TMD. Both constructs are in part degraded inside the vacuole, likely because of tagging, in agreement with only partial complementation of cell wall defects (E). However, both constructs also show localization at the plasma membrane, demonstrating that Gas1TMD, despite lacking the GPI anchor, can be targeted to the plasma membrane, probably by bulk-flow mechanisms, explaining the observed post-Golgi glycosylation pattern of a fraction of the protein (C, lanes 5 and 6) and partial complementation of cell wall defects (E). DIC = Nomarski image. Bar, 3 µm. (E) Drop assay with cells used in A–C in the presence or absence of calcofluor white. Plates were imaged after 2 d (yeast extract peptone dextrose) or 4 d (yeast extract peptone dextrose plus calcofluor white). Gas1 can compensate in part for cell wall defects as well as ceramide and IPC alterations independent of the GPI anchor, suggesting that the observed changes in lipid profiles in *Δgas1* cells are not caused by a deficiency in (GPI-dependent) ceramide cotransport but rather by lack of Gas1 enzymatic activity. In any case, expression of Gas1* did not restore lipid profile to those found in wild-type cells.

Table S1. **Yeast strains used in this study**

Strain	Genotype	Source
VGY100	MATa; BY background	Laboratory strain
VGY302	MATx; BY background	Laboratory strain
VGY381	MATa; W303 background	Laboratory strain
VGY382	MATx; W303 background	Laboratory strain
VGY1204	MATa; W303 background, *Δpep4::KanMX6, Δhrd1::HygrB,* containing *HA-Gas1** (pMF616, YIp, *URA3*)	This study
VGY1206	MATx; W303 background, *Δpep4::KanMX6,* containing *HA-Gas1** (pMF616, YIp, *URA3*)	This study
VGY1242	MATa; W303 background, *Δbst1::KanMX6*	This study
VGY1403	MATa; W303 background, containing *GFP-Gas1** (NSp19, YIp, *URA3*)	This study
VGY1487	MATa; W303 background, *Δhrd1::HygrB,* containing *HA-Gas1*TMD* (NSp23, YIp, *URA3*)	This study
VGY1489	MATa; W303 background, *Δhrd1::HygrB, Δbst1::KanMX6,* containing *HA-Gas1** (pMF616, YIp, *URA3*)	This study
VGY1490	MATa; W303 background, containing *HA-Gas1*TMD* (NSp23, YIp, *URA3*)	This study
VGY1491	MATa; W303 background, *Δemp24::HIS,* containing *Gas1*TMD* (NSp23, YIp, *URA3*)	This study
VGY1492	MATa; W303 background, *Δemp24::HIS, Δbst1::HygrB,* containing *HA-Gas1** (pMF616, YIp, *URA3*)	This study
VGY1737	MATa; W303 background, *Δhrd1::HygrB, Δcwh43::HIS,* containing *HA-Gas1** (pMF616, YIp, *URA3*)	This study
VGY1746	MATa; W303 background, *Δemp24::HygrB, Δcwh43::KanMX6,* containing *HA-Gas1** (pMF616, YIp, *URA3*)	This study
VGY2612	MATx; BY background, *Δgas1::KanMX6*	This study
VGY2617	MATx; BY background, *Δgas1::HA-Gas1*TMD* (*URA3*)	This study
VGY2620	MATx; BY background, *Δgas1::HA-Gas1TMD* (*URA3*)	This study
VGY2622	MATx; BY background, *Δgas1::HA-Gas1* (*URA3*)	This study
VGY2626	MATx; BY background, *Δgas1::HA-Gas1** (*URA3*)	This study
VGY2799	MATa; W303 background, *Δcwh43::HIS,* containing *GFP-Gas1** (NSp19, YIp, *URA3*)	This study
VGY2894	MATa; W303 background, containing *HA-Gas1*ΔTMD* (VGp256, YIp, *URA3*)	This study
VGY2895	MATa; W303 background, *Δhrd1::HygrB,* containing *HA-Gas1*ΔTMD* (VGp256, YIp, *URA3*)	This study
VGY2897	MATa; W303 background, containing *HA-CPY*GPI* (clone392, CEN, *TRP1*)	This study
VGY2898	MATa; W303 background, *Δhrd1::HygrB,* containing *HA-CPY*GPI* (clone392, CEN, *TRP1*)	This study
VGY2900	MATa; W303 background, containing *HA-CPY*TMD* (LLp43, CEN, *TRP1*)	This study
VGY2901	MATa; W303 background, *Δhrd1::HygrB,* containing *HA-CPY*TMD* (LLp43, CEN, *TRP1*)	This study
VGY2925	MATx; W303 background, *Δpep4::KanMX6,* containing *GFP-CPY*TMD* (LLp45, CEN, *TRP1*)	This study
VGY2926	MATx; W303 background, *Δpep4::KanMX6,* containing *GFP-CPY*GPI* (LLp47, CEN, *TRP1*)	This study
VGY2934	MATa; W303 background, containing *GFP-CPY*GPI* (clone409, YIp, *URA3*)	This study
VGY2935	MATx; W303 background, *Δpep4::KanMX6,* containing *GFP-CPY*GPI* (clone409, YIp, *URA3*)	This study
VGY2936	MATa; W303 background, containing *GFP-CPY*TMD* (clone410, YIp, *URA3*)	This study
VGY2937	MATx; W303 background, *Δpep4::KanMX6,* containing *GFP-CPY*TMD* (clone410, YIp, *URA3*)	This study
LLY140	MATa; W303 background, containing *GFP-Gas1* (LLp16, YIp, *URA3*)	This study
LLY143	MATa; W303 background, containing *GFP-Gas1TMD* (LLp17, YIp, *URA3*)	This study
LLY147	MATa; W303 background, containing *GFP-Gas1*TMD* (LLp18, YIp, *URA3*)	This study
LLY303	MATa; W303 background, containing *GFP-CPY*TMD* (LLp45, CEN, *TRP1*)	This study
LLY306	MATa; W303 background, containing *GFP-CPY*GPI* (LLp47, CEN, *TRP1*)	This study
NY283	MATa; W303 background, containing *HA-Gas1** (pMF616, YIp, *URA3*)	This study
NY285	MATx; W303 background, *Δted1::HIS,* containing *HA-Gas1** (pMF616, YIp, *URA3*)	This study
NY286	MATa; W303 background, *Δbst1::KanMX6,* containing *HA-Gas1** (pMF616, YIp, *URA3*)	This study
NY287	MATa; W303 background, *Δgup1::KanMX6,* containing *HA-Gas1** (pMF616, YIp, *URA3*)	This study
NY289	MATa; W303 background, *Δcwh43::KanMX6,* containing *HA-Gas1** (pMF616, YIp, *URA3*)	This study
NY290	MATa; W303 background, *Δemp24::HygrB,* containing *HA-Gas1** (pMF616, YIp, *URA3*)	This study
NY297	MATa; W303 background, *Δhrd1::HygrB,* containing *HA-Gas1** (pMF616, YIp, *URA3*)	This study
NY302	MATa; W303 background, *Δhrd1::HygrB, Δted1::HIS,* containing *HA-Gas1** (pMF616, YIp, *URA3*)	This study
NY381	MATa; W303 background, *Δhrd1::HygrB, Δemp24::HIS,* containing *HA-Gas1** (pMF616, YIp, *URA3*)	This study
NY428	MATa; W303 background, *Δted1::HIS,* containing *GFP-Gas1** (NSp19, YIp, *URA3*)	This study
NY430	MATa; W303 background, *Δbst1::KanMX6,* containing *GFP-Gas1** (NSp19, YIp, *URA3*)	This study
NY443	MATx; W303 background, *EMP24-TAP(HIS3),* containing *HA-Gas1** (pMF616, YIp, *URA3*)	This study
NY444	MATx; W303 background, *EMP24-TAP(HIS3), Δted1::HIS,* containing *HA-Gas1** (pMF616, YIp, *URA3*)	This study
NY472	MATa; W303 background, containing *HA-Gas1* (NSp17, YIp, *URA3*)	This study
NY474	MATa; W303 background, containing *HA-Gas1TMD* (NSp20, YIp, *URA3*)	This study
NY476	MATa; W303 background, containing *HA-Gas1*TMD* (NSp23, YIp, *URA3*)	This study
NY478	MATx; W303 background, *EMP24-TAP(HIS3),* containing *HA-Gas1* (NSp17, YIp, *URA3*)	This study
NY480	MATx; W303 background, *EMP24-TAP(HIS3),* containing *HA-Gas1TMD* (NSp20, YIp, *URA3*)	This study
NY482	MATx; W303 background, *EMP24-TAP(HIS3),* containing *HA-Gas1*TMD* (NSp23, YIp, *URA3*)	This study
NY567	MATa; W303 background, *Δhrd1::HygrB,* containing *GFP-Gas1** (NSp19, YIp, *URA3*)	This study
NY568	MATa; W303 background, *Δemp24::HIS,* containing *GFP-Gas1** (NSp19, YIp, *URA3*)	This study

Chromosomal tagging of proteins and gene deletions and integrations were performed using PCR (if needed) in combination with standard homologous recombination techniques.

Cells. 2014 Aug 5;3(3):824-47. doi: 10.3390/cells3030824.

Regulation of Endoplasmic Reticulum-Associated Protein Degradation (ERAD) by Ubiquitin.

Lemus L, Goder V.

Cells **2014**, *3*, 824-847; doi:10.3390/cells3030824

OPEN ACCESS

cells

ISSN 2073-4409
www.mdpi.com/journal/cells

Review

Regulation of Endoplasmic Reticulum-Associated Protein Degradation (ERAD) by Ubiquitin

Leticia Lemus and Veit Goder *

Department of Genetics, University of Seville, Av. Reina Mercedes 6, 41012 Seville, Spain

* Author to whom correspondence should be addressed; E-Mail: vgoder@us.es; Tel.: +34-954-556-230.

Received: 6 June 2014; in revised form: 9 July 2014 / Accepted: 20 July 2014 / Published: 5 August 2014

Abstract: Quality control of protein folding inside the endoplasmic reticulum (ER) includes chaperone-mediated assistance in folding and the selective targeting of terminally misfolded species to a pathway called ER-associated protein degradation, or simply ERAD. Once selected for ERAD, substrates will be transported (back) into the cytosol, a step called retrotranslocation. Although still ill defined, retrotranslocation likely involves a protein conducting channel that is in part formed by specific membrane-embedded E3 ubiquitin ligases. Early during retrotranslocation, reversible self-ubiquitination of these ligases is thought to aid in initiation of substrate transfer across the membrane. Once being at least partially exposed to the cytosol, substrates will become ubiquitinated on the cytosolic side of the ER membrane by the same E3 ubiquitin ligases. Ubiquitin on substrates was originally thought to be a permanent modification that (1) promotes late steps of retrotranslocation by recruiting the energy-providing ATPase Cdc48p/p97 via binding to its associated adaptor proteins and that (2) serves to target substrates to the proteasome. Recently it became evident, however, that the poly-ubiquitin chains (PUCs) on ERAD substrates are often subject to extensive remodeling, or processing, at several stages during ERAD. This review recapitulates the current knowledge and recent findings about PUC processing on ERAD substrates and ubiquitination of ERAD machinery components and discusses their functional consequences.

Keywords: ubiquitin; ERAD; Cdc48; p97; proteasome; E3 ubiquitin ligase; deubiquitinase

---

1. ER Protein Quality Control and ERAD

Up to 30% of all proteins in the eukaryotic cell are targeted to the secretory pathway. The initial translocation across or insertion into the membrane of the endoplasmic reticulum (ER) is mediated by the protein conducting Sec61-channel or "translocon". It has only a narrow pore and requires that proteins cross the membrane in an unfolded state [1]. Consequently, proteins fold post-translocationally inside the ER, a process that is aided and controlled by a battery of chaperones. Folding, however, is still inefficient and many proteins fail to acquire their native three-dimensional structure. A major cellular pathway is dedicated to remove terminally misfolded proteins from the lumen or the membrane of the ER and targets them for regulated degradation. The pathway is conserved among eukaryotes and has been named ER-associated (protein) degradation, or simply ERAD [2–4].

During ERAD, misfolded proteins are retrotranslocated back to the cytosol where they will undergo ubiquitination. Initially it was thought that ubiquitination of ERAD substrates serves exclusively as a tag for ultimate recognition by the proteasome. However, as it will be discussed in this review, accumulating evidence shows that ubiquination has various additional roles for ERAD. This is mainly linked to the findings that deubiquitinating enzymes (DUBs) are required for ERAD. DUBs remove single or multiple ubiquitins from polyubiquitin chains (PUCs), implying that PUCs on substrates are processed prior to their removal upon protein degradation by the proteasome. Moreover, it appears that PUCs can be processed during ERAD at several stages. This includes initial phases of ERAD where proteins are triaged for degradation and subsequent phases such as protein retrotranslocation across the ER membrane. Finally, ubiquitin also appears to be important for ERAD by regulating the composition or conformation of machinery components thereby controlling ERAD efficiency and substrate retrotranslocation.

2. Ubiquitination in ERAD

Ubiquitination is a post-translational modification that occurs in the cytosol and nucleoplasm of eukaryotic cells and requires a cascade of reactions [5–7]. Briefly, ubiquitin is activated by its ATP-dependent C-terminal coupling to the thiol group of a specific cysteine of a so-called E1 enzyme. Subsequently, ubiquitin is transferred to a specific cysteine of an E2 enzyme and finally to the substrate, usually to the ε-amino group of internal lysines, which is presented to the E2-linked ubiquitin by an E3 ubiquitin ligase. In yeast, there are one E1 enzyme, thirteen E2 enzymes and a much larger number of E3 ligases. A similar ratio between these families is found in mammalian cells although more individual enzymes from each class are present. Whereas E1 and E2 enzymes are common to many individual reactions, the large number of E3 ligases is likely because many of them are specific for only one or few particular cellular substrate(s). In contrast, only a small number of E3 ligases have a function in ERAD but they catalyze the ubiquitination of a large variety of distinct substrates. Consequently, these E3 ligases have much broader specificities for substrates.

In yeast, the known E3 ligases with a function in ERAD are Doa10p and Hrd1p. They are involved in the degradation of essentially all identified ERAD substrates so far and they are the core components of two individual protein complexes consisting of several membrane integrated proteins and associated components in the ER lumen as well in the cytosol. These complexes have been named

accordingly, Doa10-complex and Hrd1-complex [8–10]. Doa10p and Hrd1p themselves are multispanning ER membrane proteins and belong to the family of RING ligases, named after the presence of the RING (Really Interesting New Gene) domain on their cytosolic C-terminus which catalyzes the transfer of ubiquitin from the E2 directly to the substrate [7]. The E2 enzymes with a function in ERAD are Ubc6p and Ubc7p (for Doa10p) and Ubc1p and Ubc7p (for Hrd1p) [11]. Mammalian cells possess ERAD-specific membrane protein complexes with homologues components and almost identical functions compared to yeast but also have additional E3 ligases with roles in ERAD that are less well characterized, reviewed in [11]. Interestingly, many of the key components that mediate ERAD not only have a role in clearing the ER from misfolded proteins but they are also involved in regulating metabolic pathways. For instance, the production of sterols in eukaryotic cells is tightly controlled at several points by metabolite-triggered ERAD of regulatory elements [8,12]. These observations illustrate that a common pathway can serve distinct functional purposes.

It has been observed that the location of misfolded domain(s) on ERAD substrates is decisive for which ERAD machinery complex is used for their subsequent degradation. Based on this, three major ERAD pathways have been defined (Figure 1). Membrane proteins with a misfolded cytosolic domain are generally targeted to the Doa10-complex, a pathway termed ERAD-C (C for cytosolic) [13]. Membrane proteins with a misfolded luminal domain are generally targeted to the Hrd1-complex, a pathway termed ERAD-L (L for luminal) [13]. The same pathway degrades soluble misfolded proteins of the ER lumen. Finally, membrane proteins with a misfolded region in their transmembrane domain(s) are also targeted to the Hrd1-complex. However, in this case, fewer associated components are required for the degradation of these substrates; this pathway was termed ERAD-M (M for membrane) [14–16]. The correlation between substrate class and "choice" of pathway is strongest in yeast but is also found in mammalian cells, albeit to a lesser extent.

A common mechanism of how individual misfolded proteins in the ER are first recognized is not known but it likely involves several criteria such as the exposure of hydrophobic patches and the dwell time of binding to chaperones. The selected substrates are then targeted to the membrane-embedded E3 ligase complexes where they undergo ubiquitination on their cytosolically exposed protein domains during or after retrotranslocation.

Generally, the 76 amino acid long ubiquitin is coupled to mostly ε-amino groups of internal lysine residues in substrates, via an isopeptide bond. In particularly prepared model substrates for ERAD that lacked lysine residues, ubiquitin could also be coupled to the hydroxyl groups of serine or threonine side chains, or to the sulfhydryl group of cysteine, forming ester bonds [17–19]. After initial (mono-)ubiquitination, substrates can be further modified with additional ubiquitins leading to the formation of PUCs. PUCs can occur in a very large number of different chain conformations because ubiquitins can attach to one another in several ways. The C-terminal glycine of the donor ubiquitin can be attached to the α-amino group of the N-terminus of the acceptor ubiquitin, *via* a peptide bond, or to any of its seven internal lysines (K6, K11, K27, K29, K33, K48 and K63), via an isopeptide bond. A PUC with identical linkages between the ubiquitin moieties is called homotypic whereas different linkages lead to the formation of heterotypic chains, reviewed in [20].

It is currently unclear whether the ERAD-specific E3 ligases mono-ubiquitinate substrates or whether they generate PUCs with specific linkage types or chain lengths. *In vitro* experiments with components from yeast and mammalian cells suggested that poly-ubiquitin chains can form on

substrates in a single step. For instance, ERAD E3 ligases could catalyze the *en bloc* transfer of preassembled PUCs from E2 enzymes directly to substrates [21,22]. E2-specific cofactors are also thought to stimulate PUC formation by increasing the E2 activity [23]. Finally, certain E2 cofactors, such as Cue1p in yeast, have been shown to stabilize PUCs by binding to them and are therefore thought to promote PUC formation on substrates [24].

Figure 1. Distinct endoplasmic reticulum-associated degradation (ERAD) pathways. Three main ERAD pathways in yeast are classified based on substrates and the components that are involved in their degradation. ERAD-L degrades membrane integrated or soluble proteins with misfolded domains in the ER lumen, marked with (L). All depicted constituents of the Hrd1-complex are required for the efficient degradation of these substrates. ERAD-M degrades membrane integrated proteins with misfolded regions in their transmembrane domain(s), marked with (M). Proteins of this class are degraded via the Hrd1-complex but do not require Usa1p and Der1p for efficient degradation. ERAD-C degrades membrane integrated proteins with misfolded domains in the cytoplasm, marked with (C). These proteins are degraded via the Doa10-complex. All ERAD pathways require cytosolic Cdc48p for substrate retrotranslocation and extraction from the ER membrane. The substrate is ubiquitinated by the E3 ligases during or after retrotranslocation and is targeted to the proteasome (PRT) for degradation. Cdc48p and the 19S cap of the proteasome have structural and functional similarities. The classification for the different ERAD pathways also exists in mammalian cells albeit it is less stringent. RING = RING domain of the E3 ligases that are shown in red. The associated constituents of the individual complexes are shown in grey. Ub = ubiquitin. See text for details.

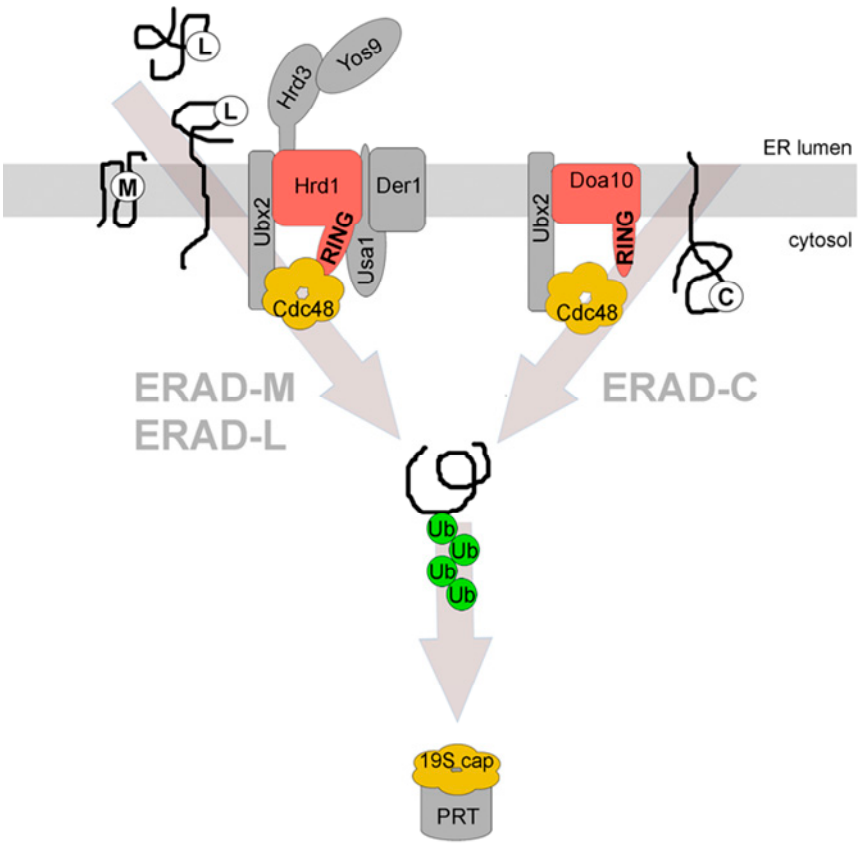

3. Deubiquitination in ERAD

Deubiquitinating enzymes (DUBs) comprise a large protein family that can be subdivided further into five subfamilies: ubiquitin C-terminal hydrolases (UCHs), ubiquitin-specific proteases (USPs), ovarian tumor proteases (OTUs), Josephins (Josephins) and JAB1/MPN/MOV34 (JAMMs) [25]. Only a few identified DUBs have so far been shown to be clearly relevant for ERAD. They are, however, not restricted to a particular family as they belong to the USPs (Usp13, Usp25), Josephins (Ataxin3), and OTUs (YOD1) families [26–30]. Additional DUBs might play a yet insufficiently characterized role during ERAD, such as USP19, USP50 and VCPIP1 [31–33].

Although a detailed understanding for the function of DUBs in ERAD is far from being complete, the general emerging picture is that their actions allow the constant remodeling of PUCs on substrates in combination with ubiquitination reactions. Such PUC remodeling would allow more selective and efficient recognition of substrates and the regulation of transport to the proteasome for their subsequent turnover. Recent evidence indicates that similar cycles of ubiquitination and deubiquitination reactions also occur on ERAD machinery components. This might be yet another important mechanism for the regulation of ERAD. In the following, examples from recent studies with specific relevance to these mechanisms will be discussed in more detail.

4. PUC Processing as a Mechanism for ER Membrane Protein Quality Control

ER membrane proteins are often directly accessible to the cytosolic ubiquitination machinery through their cytosolic domains and ubiquitination of these domains could result in a direct signal for ERAD. Recently, however, ubiquitination of cytosolic domains of ER membrane proteins was proposed to have a function prior to their degradation and would instead be involved in their quality control [34]. In this particular case, the authors investigated the traffic of mammalian lipoprotein receptor-related protein-6 (LRP6) [35]. LRP6 is a type I membrane protein with a large luminal domain and a shorter cytoplasmic tail. It is constitutively palmitoylated at one or possibly two juxtamembranous cysteines, and is normally targeted to the plasma membrane for its function in Wnt signaling. Abrogation of palmitoylation by mutating the critical cysteine residues resulted in mono-ubiquitination on a proximal lysine residue [35]. However, mono-ubiquitination did not trigger ERAD but resulted in protein retention inside the ER. The authors suggested that the observed initial mono-ubiquitination would be a first and critical step in the quality control of particular membrane proteins and would prevent the protein from being prematurely exported from the ER. In addition to that, mono-ubiquitinated substrate would also allow recruitment of yet-to-be defined cytosolic quality control components, potentially including chaperones and folding sensors [34]. Prolonged retention of the protein in the ER will lead to the extension of mono-ubiquitin by E3 ligases and to the formation of PUCs. Initially this could be reversed by DUBs but eventually, in case that protein folding attempts repeatedly fail, PUCs would form which are recognized by the ERAD system (Figure 2). Clearly, the model is still very hypothetical and needs more experimental backup for validation. For instance, it is still unclear which E3 ligases or DUBs are involved in modifying LRP6. Despite all these uncertainties, the model is appealing with the concept that E3 ligases and DUBs are involved in modifying PUCs on cytosolic domains of ER membrane proteins in a similar manner and with similar consequences like

ER luminal UDP-glucose:glycoprotein glucosyltransferase (GT) and Glucosidase II, which are involved in modifying N-glycans on proteins for quality control in the ER lumen [36].

Figure 2. A model for poly-ubiquitin chain (PUC) processing as a mechanism for coupling ER protein quality control with ERAD. Membrane proteins with exposed cytosolic domains are ubiquitinated by E3 ligases. Due to topological confinement of membrane proteins and membrane integrated E3 ligases to the same bilayer, ubiquitination might occur frequently, even on correctly folded proteins. DUBs can remove ubiquitins, favoring ER export of correctly folded species. Reoccurring ubiquitination due to prolonged ER retention as a result of misfolding (in the cytosol or ER lumen) will favor the assembly of PUCs to induce targeting to the proteasome, thereby favoring ERAD. A similar mechanism might occur for soluble proteins prior to their post-translational translocation across the ER membrane, a pathway called prERAD. See text for details. E3 = E3 ligase. DUB = deubiquitinase. Filled green circles: ubiquitin.

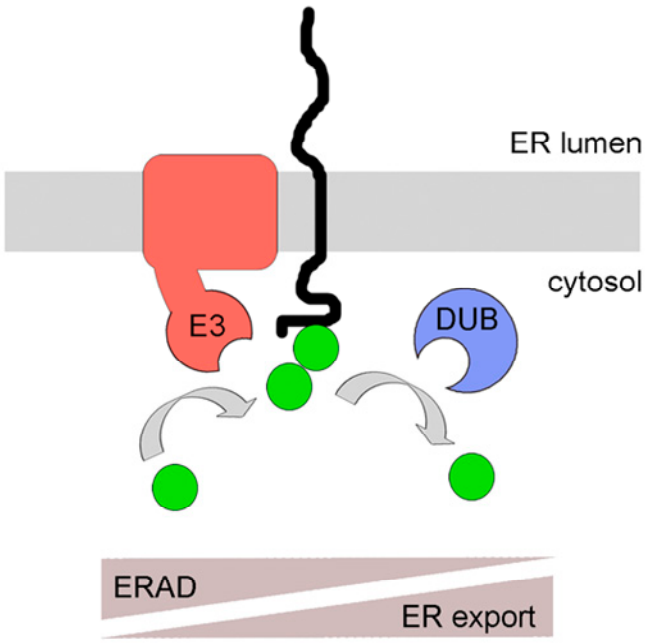

Another recent study highlighted the kinetic aspect of protein quality control *versus* ERAD and the roles of E3 ligases and DUBs in these processes [37]. The authors addressed an issue that is particular relevant for E3 ligases involved in ERAD since they are very promiscuous due to the large number of substrates they have to deal with. It is predictable that these ligases posses different affinities to particular substrates, yet all substrates have to be efficiently ubiquitinated for degradation. Whereas soluble ER luminal proteins are only getting access to the E3 ligases after being selected for ERAD and targeted to the membrane, ER membrane proteins have to fold in the neighborhood of these E3 ligases. Thus, the chances for encounter and ubiquitination are high even if the substrate might not end up terminally misfolded. Due to the limitations to purify defined misfolded proteins the authors used a viral system where correctly folded mammalian CD4, a membrane protein with a sizable cytosolic tail, is targeted by the HIV-encoded membrane protein Vpu to the cytosolic SCF E3 ligase, leading to ubiquitination, extraction of CD4 from the ER membrane and proteasomal degradation [37]. This

system recapitulates cellular ERAD. It turned out that the observed ubiquitination state of particular CD4 mutants could only be explained by kinetic modeling incorporating DUB activity. This was supported by subsequent *in vitro* and *in vivo* experiments using DUB inhibitors [37]. Based on their observations the authors proposed a model where frequent ubiquitination is occurring on many cellular substrates, in particular on those that are restricted to the membrane and thus are in constant vicinity to membrane-embedded E3 ligases, such as those involved in ERAD. Properly folded substrates would have weaker affinity to E3 ligases resulting in shorter PUCs. Importantly, these PUCs would be further shortened or removed by DUBs, preventing protein degradation. In contrast, substrates with higher dwell time with an E3 ligase would result in longer PUCs, ultimately resulting in proteasomal degradation of the substrate (Figure 2). This system would thus resemble important aspects of the earlier discussed quality control mechanism proposed for mammalian LRP6 [34].

A recent report revealed yet another mechanism for the connection of ER quality control and ERAD [38]. The authors proposed that ER proteins are quality controlled even prior to membrane insertion or translocation, a mechanism they called prERAD [38]. This mechanism seems to occur when proteins translocate post-translationally, *i.e.*, after protein synthesis. In such cases, some proteins associate transiently with the cytosolic leaflet of the ER membrane. They are then scrutinized by the E3 ligase Doa10p and, interestingly, by the DUB Ubp1p [38]. Again, it was proposed that an interplay between ubiquitination and deubiquitination reactions as a result of yet unknown determinants of protein quality would determine whether the protein will be degraded by the proteasome or translocated across or inserted into the ER membrane [38].

5. PUC Processing as a Mechanism to Promote Protein Retrotranslocation

Shortly after the discovery of ERAD it became clear that ubiquitination of substrates has an important role not only for their ultimate degradation by also for their retrotranslocation [39–41]. Major insights into the mechanism that links ubiquitination with retrotanslocation came from the discovery that Cdc48p (p97 in mammals), a well-conserved hexameric AAA-ATPase, is involved in ERAD [42,43]. Cdc48p is a very abundant protein found in the cytosol and nucleus, and it has multiple cellular functions beyond ERAD. They involve control of the cell cycle, membrane fusion, autophagy and DNA repair, reviewed in [44]. The distinct cellular roles of Cdc48p are determined through binding to different co-factors. This is particularly relevant for the recruitment of Cdc48p to ubiquitin. Although it has been shown that Cdc48p itself can bind to ubiquitin via its N-domain, its ERAD-specific co-factors Npl4p and Ufd1p (Npl4 and Ufd1) provide additional binding sites to ubiquitin [45]. For instance, mammalian Npl4 possesses a ubiquitin-binding zinc finger motif (which is not present in the yeast orthologue) whereas Ufd1p has a conserved so-called UT3 motif. This UT3 motif makes Ufd1p to prefer the binding to poly-ubiquitin over mono-ubiquitin, suggesting that some PUCs have formed on substrates at the stage when it connects to Cdc48p [46]. Important for the proposed role of Cdc48p in substrate retrotranslocation is also the finding that it is recruited to the ER membrane via direct binding to E3 ligases such as Hrd1p (and gp78) or, independently, via binding to one of its co-factors and integral membrane protein Ubx2p (UbxD8), which is part of both the Hrd1- and Doa10-complexes [47–50]. Thus, by binding to ubiquinated substrates on the one hand and to the ER membrane on the other hand, Cdc48p might pull substrates out of or across the membrane like a

molecular ratchet, fueled by repeating cycles of ATP hydrolysis and the accompanying conformational changes (Figure 3A) [51,52]. Whether substrate ubiquitination generally precedes binding to Cdc48p and its co-factors or whether initial binding of non-ubiquitinated substrates to Cdc48p would facilitate their subsequent ubiquitination by E3 ligases, especially with respect to the build-up of PUCs on substrates, is still not clear. However, several recent reports place Cdc48p in the center of the processing of PUCs. This has important implications for mechanistic aspects of ERAD and provides new models for how substrates are retrotranslocated and how they are targeted to the proteasome after retrotranslocation.

Figure 3. Models for PUC processing as a mechanism for protein retrotranslocation. (**A**) Ubiquitination of the substrate on the cytosolic side of the ER membrane by an E3 ligase promotes binding to the hexameric Cdc48p, via its ubiquitin-binding cofactors Npl4p and Ufd1p. ATP hydrolysis by Cdc48p is thought to promote the complete retrotranslocation and substrate extraction from the ER membrane. See text for details. (**B**) In the mammalian system, the p97-associated DUB Ataxin-3 acts downstream of protein retrotranslocation and might promote the removal of ubiquitins from longer PUCs. This is thought to be required for the generation of PUCs with optimal binding affinities to proteasomal shuttle factors or to the proteasome itself. See text for details. (**C**) The p97-associated DUB YOD1 is thought to act upstream of protein retrotranslocation. Its activity was suggested to be needed for the complete removal of PUCs to allow passage of the substrate through the pore of p97. ATP hydrolysis would then couple protein retrotranslocation with protein unfolding. Subsequently, reubiquitination by an E3 ligase would allow substrate targeting to the proteasome. See text for details.

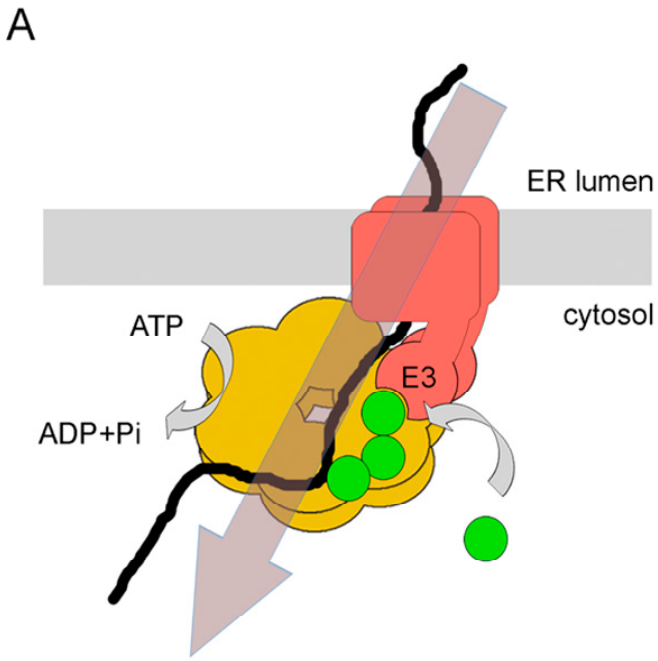

Figure 3. *Cont.*

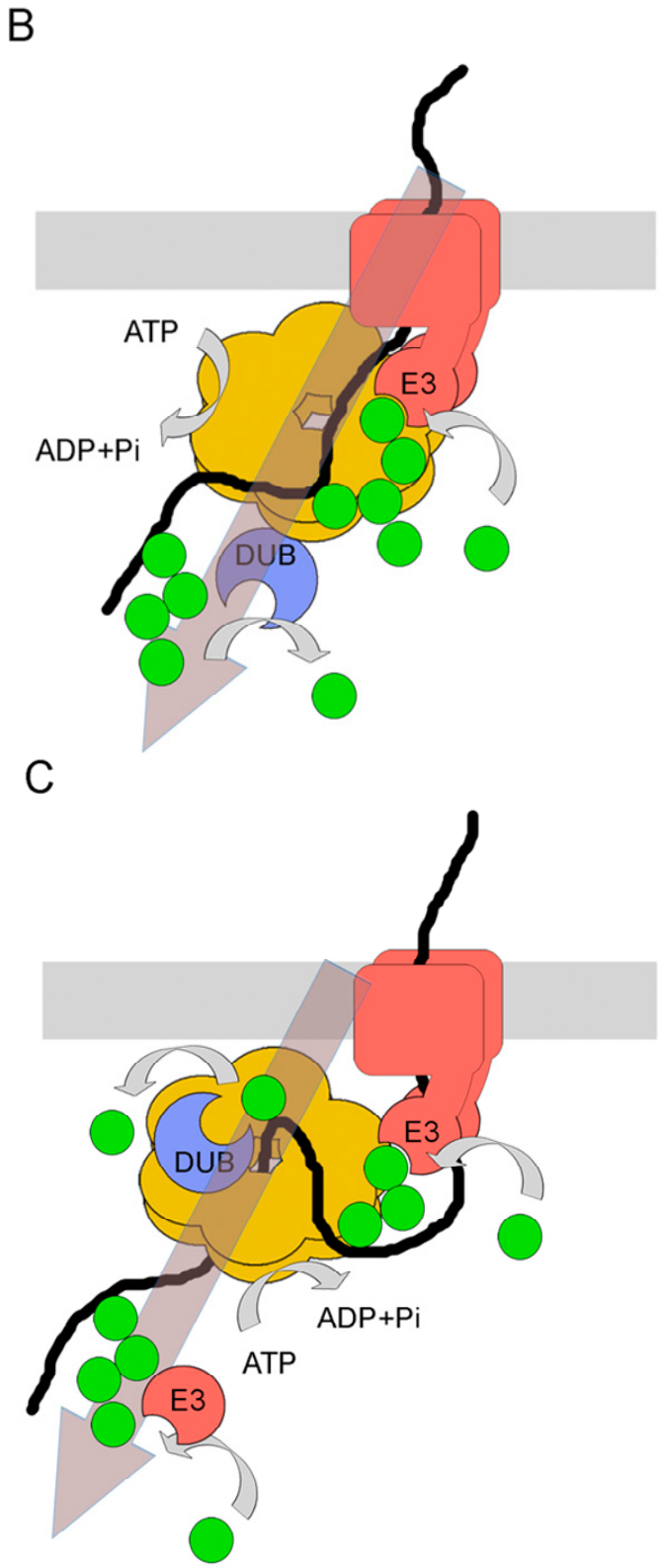

First studies that connected DUB activity to Cdc48p/p97 were not related to ERAD [53–55]. However, subsequent reports from mammalian cells showed that specific DUBs do have a role in ERAD [26–28,56]. Somewhat counterintuitive at first glance, DUB activity was found to be a positive regulator for substrate degradation [26,28]. The first p97-associated DUB that was proposed to have a

function in ERAD was Ataxin-3 [26]. The authors of this study proposed that the DUB would act downstream of p97-mediated retrotranslocation and would trim the PUCs on substrates if necessary to maintain an optimal signal for targeting to the proteasome, thereby streamlining protein retrotranslocation with their recognition by the proteasome (Figure 3B) [57]. Additional data came from work with YOD1, another DUB that was found to be associated with p97 [28]. YOD1 belongs to the OTU family of DUBs and was shown to prevent substrate degradation when expressed as a dominant negative version (YOD1 C160S) [28]. Important for mechanistic aspects of retrotranslocation, the model substrate used in this study was found poly-ubiquitinated and still associated with the ER membrane when the mutant DUB was expressed, suggesting that DUB activity was required to allow p97-mediated completion of substrate retrotranslocation [28]. To address this model in more detail, the same group expressed a highly active viral DUB from the Epstein-Barr virus (EBV-DUB) in the same system [58]. Two crucial observations were made. First, the degradation of various ERAD substrates was blocked under these conditions. Second, one particular substrate accumulated as a deglycosylated form in the cytosol, showing that is has been retrotranslocated but has not been forwarded to the proteasome [58]. The authors concluded that deubiquitination would influence ERAD, and in particular retrotranslocation, at distinct cellular stages, upstream and downstream of p97. In one model, initial ubiquitination of substrates by the ERAD ubiquitination machinery would trigger direct binding to p97. DUB-mediated PUC trimming or removal would then be needed to allow p97-mediated retrotranslocation. Subsequently, reubiquitination of substrates would facilitate their transfer to downstream components and targeting to the proteasome (Figure 3C) [59].

One speculative part of that model suggests that DUB activity upstream of p97 is required for threading the substrate through the pore in the center of p97 [28,58]. The evidence for this model is scarce at the moment and there are arguments in its favor and against it. The arguments in its favor concern the functional and structural analogies between Cdc48p/p97 and related AAA-ATPases like the regulatory particle of the proteasome and the *E.coli* protein ClpB. For instance, the regulatory particle of the proteasome threads substrates through its interior pore in an ATP-dependent manner and feeds it directly into the physically associated proteolytic chamber, the core particle, thereby coupling unfolding of the substrates with its subsequent degradation [60]. A similar mechanism of substrate translocation through the channel was shown for ClpB although, in contrast to its homologs ClpA and ClpX, it does not associate with the bacterial proteolytic chamber ClpP [61]. Thus, Cdc48p/p97-mediated protein unfolding might resemble a situation found in ClpB. Arguments against the threading model include structural studies with p97 mutants [62]. Only the central pore residues contributed by the D2 domain of the six p97 monomers but not the D1 domain were found to affect ERAD. To account for this phenomenon, it was proposed that substrates might enter and exit trough the same side of the channel, namely the part that is formed by the assembly of the D2 domains [62]. Alternatively, substrates might enter through the D2 pore and exit laterally between the D1 and D2 domains but proof for either of these models is currently lacking [62]. The threading model has also to be looked at with caution to account for the fact that some ERAD model substrates can apparently be retrotranslocated across the ER membrane in a partially or completely folded state, too big to envision that they would pass through the p97 pore during that process [63,64]. Although it has not been directly addressed whether p97 is involved in the retrotranslocation of these folded model substrates, it is required for ERAD of directly related proteins [65]. Therefore, threading of substrates through the pore of

Cdc48p/p97 might not always be mandatory. Clearly, more research is needed to clarify the mechanistic aspects of how Cdc48p/p97 promotes the retrotranlocation of substrates.

6. PUC Processing as a Mechanism for Targeting of Substrates to the Proteasome

Considering the currently available data for PUC processing on ERAD substrates during retrotranslocation it appears not unlikely that those PUCs that serve for recognition by the proteasome are generated specifically at later stages during ERAD, potentially after partial or complete removal of initial PUCs. The precise order of events might also depend on the specific cellular substrate and its requirements for retrotranslocation. PUCs for the recognition by the proteasome could be generated by the same ERAD-specific E3-ligases and DUBs involved in the initial retrotranslocation, or by additional components. Due to the general scarcity of available data for how PUCs with specific lengths and linkages are generated, these assumptions remain entirely speculative.

However, some models for how PUC processing at later stages during ERAD could ensure efficient substrate targeting to the proteasome have been put forward. They are mainly based on data obtained from work with yeast and, more specifically, from the functional characterization of Cdc48p-associated co-factors and of cytosolic "shuttle" factors of ERAD substrates. Important insight came from the discovery that Cdc48p recruits Ufd2p (Ufd2a), a specialized E3 ligase with an unusual ligase domain, the U-box, instead of a RING domain [66]. In connection with E1, E2 and E3 enzymes, Ufd2p promotes the extension of short ubiquitin chains, an activity that coined the term "E4 enzyme" [66]. Association of Cdc48p to Ufd2p leads to an increase in the binding affinity of Ufd2p for short PUCs, stimulates its E4 activity but also prevents excessive chain extension [67]. Importantly, the extended Ufd2p-generated PUCs contain preferentially K48-linkages [66,68]. Ufd2p was also reported to be required for the ERAD of several tested model substrates [67,69]. Ufd2p could thus mediate the generation of PUCs on ERAD substrates with an optimal length and linkage for proteasomal degradation.

An appealing mechanism of how Ufd2p would couple PUC extension on substrates with their efficient targeting to the proteasome was proposed by combining these findings with earlier data that revealed the involvement of specific cytosolic factors such as Rad23p and Dsk2p in ERAD [70,71]. The cytosolic factors Rad23p and Dsk2p were identified by a genetic screen in yeast for novel components with a function in ERAD [72]. A common structural hallmark is that they contain one or more of both an UBL (ubiquitin-like) and an UBA (ubiquitin-associated) domain. These features are conserved and were providing the name "UBL-UBA" to three protein families named after Rad23, Dsk2 and Ddi1, reviewed in [60]. So far, only members of the Rad23 and Dsk2 protein families were shown to play roles in ERAD. The UBL domain of Rad23p (HHR23A and HHR23B) was found to bind to Ufd2p or to the proteasomal ubiquitin receptor Rpn10p (hRpn10/S5a) in an exclusive manner [73–75]. In addition, the UBA domains of HHR23A and Rad23p were found to bind preferentially to PUCs with a chain length of 4-6 ubiquitins [76]. Binding to UBA domains was proposed to be an additional mechanism to regulate PUC length and to prevent excessive chain extension by E3 ligases [77,78]. Dual binding to the proteasome or to Cdc48p–associated components with their UBL domain and to substrates with their UBA domain is thought to put UBL-UBA proteins in the position to link specific PUCs on substrates with their targeting to the proteasome [67].

Although this simple model is not entirely free of controversy [79], there is also strong experimental evidence supporting it [80].

Interestingly, the regulatory particle of the proteasome is connected not only to DUBs but also to E3-ligases (Figure 4). Together they might thus have similar roles in PUC processing like the Cdc48p/p97-associated ubiquitin-modifying enzymes [70]. From the E3 ligases with reported associations with the proteasome, Hul5p (Hul5) is the most prominent example with stochiometric amounts bound to the proteasome in both yeast and mammals [81]. Other proteasome-associated E3 ligases include Ubr1p, Ufd4p and SCF, for review see [82]. Relevant for ERAD, Hul5p was shown to be required for the complete degradation of membrane-bound ERAD substrates [83]. Hul5p was shown to be tightly associated with the DUB Ubp6 (USP14) on the proteasome and both enzymes are thought to regulate the efficient degradation of substrates by keeping the balance of chain-extending and chain-trimming activities [81].

Figure 4. The 19S cap of the proteasome has functional and structural similarities with Cdc48p/p97. Like Cdc48p/p97, the hexameric 19S cap of the proteasome binds simultaneously to E3 ligases and to DUBs, suggesting that PUCs are processed at this stage, immediately before substrate degradation. This could be needed for the transfer of the substrate from the periphery of the proteasomal lid through its central pore and further into the proteolytic chamber of the proteasome. Immediately before passage through the pore of the l9S cap, structural data suggest that all PUCs are to be removed. See text for details.

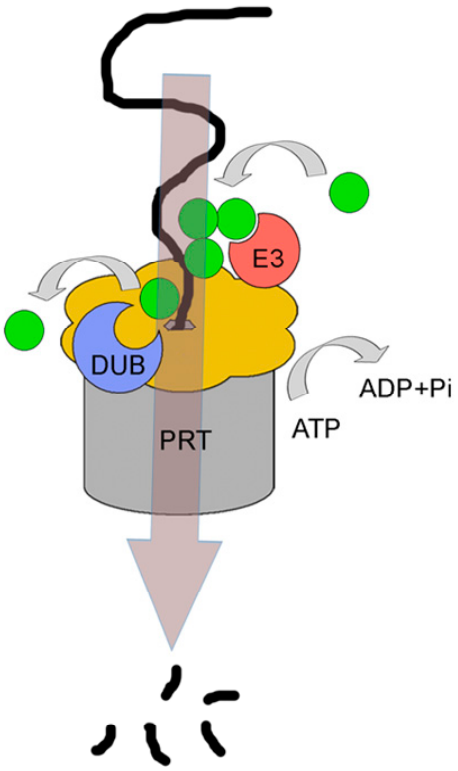

Complete removal of PUCs at the proteasome which would not be coupled to the insertion of substrates into the proteolytic chamber was also thought to provide an “ultimate rescue” of aberrantly ubiquitinated substrates [84]. Such a mechanism would thus be similar to the earlier described quality

control of ER membrane proteins where aberrantly ubiquitinated proteins can be spared from degradation by the activity of DUBs. However, although such a "rescue" might be useful for cytosolic or nuclear proteins, or for ER membrane proteins as part of their quality control, it should be of no use for ERAD substrates after they have been completely retrotranslocated or extracted from the membrane, because they could not re-enter the ER. Translocation of proteins into the ER lumen depends on an N-terminal signal sequence which is cleaved during or after translocation [1]. This impedes "a second" translocation into the ER. Membrane proteins, especially those with several transmembrane domains, are normally inserted into the ER membrane co-translationally, *i.e.*, with the synthesizing ribosome being docked onto the translocon [85]. Once extracted, "a second" post-translational insertion process seems mechanistically and energetically highly unlikely. Thus, specific combinations of DUBs and E3 ligases on the proteasome might allow for a quality control mechanism for certain substrates only. In general, however, PUC processing at the proteasome might be largely needed for initial substrate binding and for subsequent movement of substrates into the proteolytic chamber. For the first step, the generation of optimal PUCs was proposed to efficiently reduce the dissociation rates from ubiquitin receptors of the proteasome regulatory particle, Rpn10p (PSMD4) and Rpn13p (ADRM1) [81]. Rpn13p was shown to bind preferentially K48-linked-diubiquitins in comparison to other types of linkages [86,87]. Alternatively, PUC processing at this stage might also contribute to non-proteolytic functions of the proteasome [88,89].

Still, there is too little knowledge about the effects of specific PUCs with regard to the proteasomal degradation of a substrate. PUCs with homotypic K48-linked chains with at least four ubiquitins are known to provide an efficient signal for recognition by the proteasomal ubiquitin receptors [90]. However, as is becomes more apparent that the potential variety of PUCs with distinctive lengths and linkages has likely functional relevance *in vivo*, it is already evident that PUCs that encode a signal for degradation by the proteasome come in more flavors than 4–6 ubiquitins with a homotypic K48-linkage [91,92]. With the exception of K63-linkages, practically all possible modes of conjugations of ubiquitins in PUCs were found to support proteasomal degradation *in vivo* [93]. In selected cases, single ubiquitins on substrates were also shown to be sufficient for proteasomal degradation [94]. In addition, recent data show that branched PUCs with K11- and K48-linked chains provide a better signal for degradation by the proteasome than homotypic K11- or K48-linked chains [95]. Thus, a diversity of distinct PUCs can catalyze the degradation of substrates and the precise length and linkage of a particular PUC might influence kinetic aspects of turnover of particular substrates.

Apart from being the ultimate degradation machinery for ERAD substrates, the proteasome itself might actively participate in protein retrotranslocation or extraction of proteins from the ER membrane, similar to Cdc48p/p97. This is not too surprising, considering the remarkable structural and functional similarities between the regulatory particle of the proteasome and Cdc48p/p97. Both protein complexes can associate with multiple co-factors that can bind and process PUCs and both utilize ATP hydrolysis to undergo large conformational changes for the unfolding/movement of substrates, reviewed in [96]. The precise role of the proteasome in retrotranslocation likely depends on the substrate. The tail-anchored membrane protein Ubc6p, an E2 protein for the E3 ligase Doa10p, is continuously degraded by ERAD and its extraction from the ER membrane directly depends on the proteasome [97,98]. Thus, a recruitment of the proteasome to the ER membrane could be catalyzed by direct interaction with the cytosolic and ubiquitinated part of the ERAD substrates.

Interestingly, the proteasome was also found to bind to the ER membrane via association with the translocon [99,100]. The translocon, which constitutes the protein import machinery for the ER, was long considered a prime suspect for being the retrotranslocation channel as well [101–104]. Thus, there was a physiological relevance for the association with the proteasome. However, recent structural data suggest that the Sec61-channel cannot be easily accessed from the ER lumen for protein retrotranslocation [105]. Instead, members of the ER membrane-embedded ERAD-specific ubiquitination machineries such as Hrd1p and Der1p in yeast, and homologs in mammals, are more likely to constitute the conduit for protein retrotranslocation [106–109]. Interestingly, a recent report documents a role for the Hrd1-complex in freeing potentially obstructed translocons from stalled nascent chains by directing them to ERAD [110]. It could thus be that the observed association of the proteasome with the translocon is an indirect consequence of the ubiquitination of channel obstructing substrates by ERAD E3 ligases. In support of such a scenario, huge protein complexes, encompassing ERAD ubiquitination machinery components, ER luminal chaperones, cytosolic Cdc48p and the proteasome were shown to assemble under specific circumstances [111,112].

7. Ubiquitination and Deubiquitination of ERAD Machinery Components

Several recent studies started to reveal that ubiquitination and deubiquitination also occurs on ERAD machinery components [29,107,113]. Self-ubiquitination and subsequent degradation as one mode of regulation of cellular ubiquitination machineries has been known for some time, reviewed in [114]. One such example relevant for ERAD is the regulation of the E3 ubiquitin ligase Hrd1p in yeast. Hrd1p undergoes self-ubiquitination and degradation in dependence on its binding partners Hrd3p (Sel1) and Usa1p (Usa1) [115–117] (Figure 5A). Such a scenario might also involve additional regulating elements like DUBs. In support of this, the DUB YOD1 was recently shown to affect the turnover of a non-ubiquitinated ERAD substrate in mammalian cells, implying that this DUB might act on ERAD machinery components [113]. Since YOD1 is also known to act on PUCs on substrates, these results suggest that certain DUBs can process ubiquitins or PUCs on substrates and on ERAD machinery components. Another example relevant for ERAD links the failure of DUB activity and the following degradation of an aberrantly ubiquitinated machinery component with downregulation of ERAD in mammalian cells [29]. The authors of the study investigated the regulation of the Bag6 chaperone system which keeps aggregation-prone retrotranslocated and membrane-extracted ERAD substrates in a soluble yet unfolded state for targeting to the proteasome [118]. Bag6 is bound to the ER membrane by multiple interactions, but binds specifically to gp78, a membrane-embedded E3 ligase similar to Hrd1p in yeast [119]. Strikingly, Usp13, a DUB associated to p97, affected the stability of the Bag6 complex. Failure of Usp13 activity lead to the polyubiquitantion of the Bag6 complex component Ubl4A by gp78 [29]. As a result, Bag6 is degraded, leading to downregulation of ERAD (Figure 5A).

Figure 5. Models for ubiquitination and deubiquitination of ERAD machinery components as a mechanism to regulate ERAD. (**A**) Regulation through degradation. In the mammalian system, ubiquitination of the ERAD component Ubl4A by the E3 ligase gp78 leads to the degradation of the associated shuttling chaperone Bag6, thereby reducing efficient substrate targeting to the proteasome. Ubl4A ubiquitination is reversed by the DUB Usp13. A similar mechanism involves the self-ubiquitination of Hrd1p in yeast in absence of Hrd3p and Usa1p, leading to effective degradation of the E3 ligase. No DUB is currently known in this system. See text for details. (**B**) Regulation through conformational changes. Binding of a substrate to Hrd1p in the ER lumen induces oligomerization and self-ubiquitination of the E3 ligase (step 1). Subsequently, ATP hydrolysis by bound Cdc48p would result in conformational changes in the ATPase, which will consequently result in conformational changes in Hrd1p oligomers. This, in turn, would push the substrate through a postulated channel formed by Hrd1p oligomers (together with associated components like Der1p) until it is partially exposed to the cytosol (step 2). See text for details.

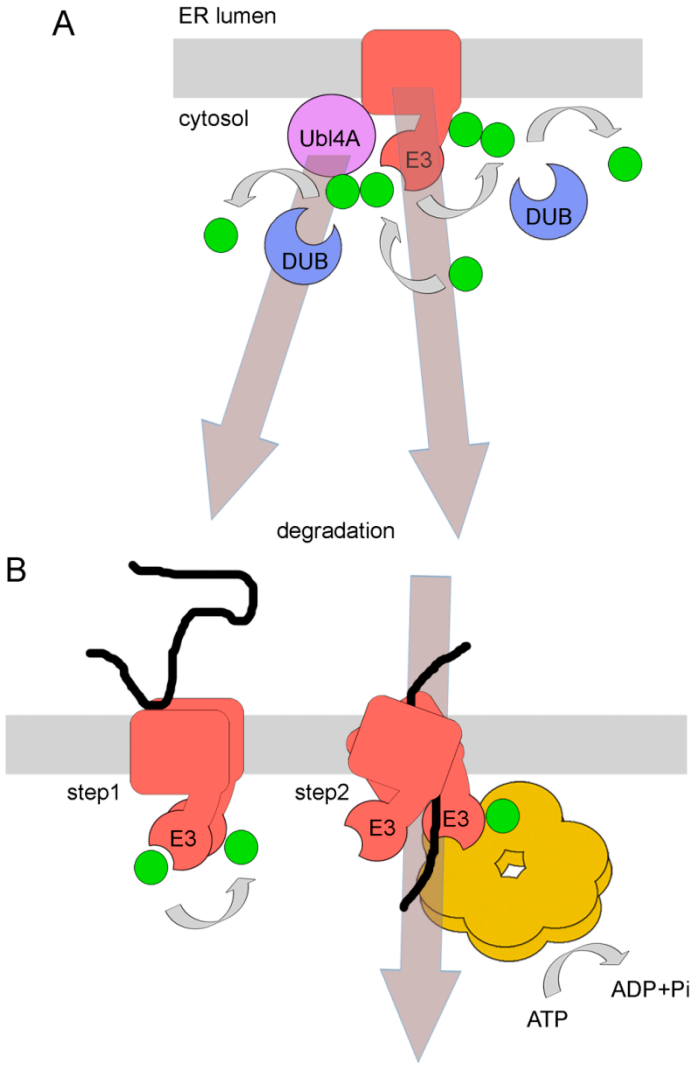

In addition to these classical examples for the role of ubiquitin in targeting proteins for degradation, a distinct ubiquitination event of the machinery component Hrd1p was proposed to regulate ERAD in additional ways. Hrd1p likely forms the main component of the retrotranslocation channel by

homo-oligomerization [107]. Interestingly, sustained substrate binding to Hrd1p on the luminal side of the ER membrane required its cytosolic E3 ligase activity [107]. The authors proposed a mechanism where substrate binding to Hrd1p on the luminal side leads to self-ubiquitination of Hrd1p on its cytosolic domain. Its ubiquitination, perhaps mono-ubiquitination, was proposed to activate the ATPase activity of the associated Cdc48p. Hydrolysis of ATP by Cdc48p would lead to conformational changes and structural rearrangements of the oligomerized Hrd1p, thereby aiding in initial phases of retrotranslocation until the substrate would be exposed to the cytosol and ubiquitinated by Hrd1p [107] (Figure 5B). Further work is needed to support this model, not the least because it remains currently unclear how deubiquitination of Hrd1p would be catalyzed.

Together, ubiquitination of ERAD machinery components can seemingly regulate ERAD in different ways. On the one hand, the regulation would be linked to cellular homeostasis (long term response) and involve the degradation of machinery components. On the other hand, regulation would be linked to mechanistic aspects of retrotranslocation (immediate response) and involve conformational changes of machinery components induced by activating ATP hydrolyzing machines like Cdc48p/p97.

8. Perspectives

The fact that DUBs can be positive regulators in ERAD has led to a new understanding for the roles of ubiquitin in the process of ERAD. It will be important to learn whether and at what stages of ERAD the processing of PUCs is following structural or kinetic aspects and what are the precise consequences with respect to the substrate. It seems clear that PUC processing on ERAD substrates most likely occurs when the substrates are connected to Cdc48p/p97 and to the proteasome during their journey to degradation. The temporal and spatial association of E3 ligases and DUBs with these huge ATP hydrolyzing machines is probably very dynamic and their activation is another parameter that will determine how PUCs are processed. It will be challenging to elucidate the molecular steps of PUC processing in a given environment and it would require the development of suitable *in vitro* assays with purified components. Similar systems should help to reveal the recently postulated functions of ubiquitination and deubiquitination in regulating ERAD machinery components through conformational changes. This could be very relevant for the mechanistic understanding of the actual retrotranslocation step in general but especially for soluble ER luminal proteins. These substrates do not expose any molecular “handle” to the cytosol prior to being at least partially retrotranslocated and the mechanisms that underlie the first steps of their transport back into the cytosol are therefore subject to intense research. The unambiguous identification of the exact composition of the postulated protein conducting channel would surely be a milestone in the field that would allow the tackling of these and related questions linked to a fascinating cellular pathway.

Acknowledgements

We thank Ralf Wellinger (Cabimer, Sevilla) for his comments and suggestions after critical reading of the manuscript. This work is supported by funds from the Ministry of Spain (BFU2009-07290) and the Junta de Andalucia (P09-CVI-4503).

Author Contributions

L.L. and V.G. wrote the paper. V.G. designed the figures.

Conflicts of Interest

The authors declare no conflict of interest.

References

1. Rapoport, T.A. Protein translocation across the eukaryotic endoplasmic reticulum and bacterial plasma membranes. *Nature* **2007**, *450*, 663–669.
2. Sommer, T.; Jentsch, S. A protein translocation defect linked to ubiquitin conjugation at the endoplasmic reticulum. *Nature* **1993**, *365*, 176–179.
3. Hiller, M.M.; Finger, A.; Schweiger, M.; Wolf, D.H. ER degradation of a misfolded luminal protein by the cytosolic ubiquitin-proteasome pathway. *Science* **1996**, *273*, 1725–1728.
4. Werner, E.D.; Brodsky, J.L.; McCracken, A.A. Proteasome-dependent endoplasmic reticulum-associated protein degradation: An unconventional route to a familiar fate. *Proc. Natl. Acad. Sci. USA* **1996**, *93*, 13797–13801.
5. Schulman, B.A.; Harper, J.W. Ubiquitin-like protein activation by E1 enzymes: The apex for downstream signalling pathways. *Nat. Rev. Mol. Cell. Biol.* **2009**, *10*, 319–331.
6. Ye, Y.; Rape, M. Building ubiquitin chains: E2 enzymes at work. *Nat. Rev. Mol. Cell. Biol.* **2009**, *10*, 755–764.
7. Deshaies, R.J.; Joazeiro, C.A. RING domain E3 ubiquitin ligases. *Annu. Rev. Biochem.* **2009**, *78*, 399–434.
8. Hampton, R.Y.; Gardner, R.G.; Rine, J. Role of 26S proteasome and HRD genes in the degradation of 3-hydroxy-3-methylglutaryl-CoA reductase, an integral endoplasmic reticulum membrane protein. *Mol. Biol. Cell.* **1996**, *7*, 2029–2044.
9. Swanson, R.; Locher, M.; Hochstrasser, M. A conserved ubiquitin ligase of the nuclear envelope/endoplasmic reticulum that functions in both ER-associated and Matalpha2 repressor degradation. *Genes Dev.* **2001**, *15*, 2660–2674.
10. Bordallo, J.; Plemper, R.K.; Finger, A.; Wolf, D.H. Der3p/Hrd1p is required for endoplasmic reticulum-associated degradation of misfolded lumenal and integral membrane proteins. *Mol. Biol. Cell.* **1998**, *9*, 209–222.
11. Hirsch, C.; Gauss, R.; Horn, S.C.; Neuber, O.; Sommer, T. The ubiquitylation machinery of the endoplasmic reticulum. *Nature* **2009**, *458*, 453–460.
12. Foresti, O.; Ruggiano, A.; Hannibal-Bach, H.K.; Ejsing, C.S.; Carvalho, P. Sterol homeostasis requires regulated degradation of squalene monooxygenase by the ubiquitin ligase Doa10/Teb4. *Elife* **2013**, *2*, e00953.
13. Vashist, S.; Ng, D.T. Misfolded proteins are sorted by a sequential checkpoint mechanism of ER quality control. *J. Cell. Biol.* **2004**, *165*, 41–52.
14. Carvalho, P.; Goder, V.; Rapoport, T.A. Distinct ubiquitin-ligase complexes define convergent pathways for the degradation of ER proteins. *Cell* **2006**, *126*, 361–373.

15. Horn, S.C.; Hanna, J.; Hirsch, C.; Volkwein, C.; Schutz, A.; Heinemann, U.; Sommer, T.; Jarosch, E. Usa1 functions as a scaffold of the HRD-ubiquitin ligase. *Mol. Cell.* **2009**, *36*, 782–793.
16. Sato, B.K.; Schulz, D.; Do, P.H.; Hampton, R.Y. Misfolded membrane proteins are specifically recognized by the transmembrane domain of the Hrd1p ubiquitin ligase. *Mol. Cell.* **2009**, *34*, 212–222.
17. Shimizu, Y.; Okuda-Shimizu, Y.; Hendershot, L.M. Ubiquitylation of an ERAD substrate occurs on multiple types of amino acids. *Mol. Cell.* **2010**, *40*, 917–926.
18. Ishikura, S.; Weissman, A.M.; Bonifacino, J.S. Serine residues in the cytosolic tail of the T-cell antigen receptor alpha-chain mediate ubiquitination and endoplasmic reticulum-associated degradation of the unassembled protein. *J. Biol. Chem.* **2010**, *285*, 23916–23924.
19. Wang, X.; Herr, R.A.; Chua, W.J.; Lybarger, L.; Wiertz, E.J.; Hansen, T.H. Ubiquitination of serine, threonine, or lysine residues on the cytoplasmic tail can induce ERAD of MHC-I by viral E3 ligase mK3. *J. Cell. Biol.* **2007**, *177*, 613–624.
20. Ikeda, F.; Dikic, I. Atypical ubiquitin chains: New molecular signals. *EMBO Rep.* **2008**, *9*, 536–542.
21. Ravid, T.; Hochstrasser, M. Autoregulation of an E2 enzyme by ubiquitin-chain assembly on its catalytic residue. *Nat. Cell. Biol.* **2007**, *9*, 422–427.
22. Li, W.; Tu, D.; Brunger, A.T.; Ye, Y. A ubiquitin ligase transfers preformed polyubiquitin chains from a conjugating enzyme to a substrate. *Nature* **2007**, *446*, 333–337.
23. Bazirgan, O.A.; Hampton, R.Y. Cue1p is an activator of Ubc7p E2 activity *in vitro* and *in vivo*. *J. Biol. Chem.* **2008**, *283*, 12797–12810.
24. Bagola, K.; von Delbruck, M.; Dittmar, G.; Scheffner, M.; Ziv, I.; Glickman, M.H.; Ciechanover, A.; Sommer, T. Ubiquitin binding by a CUE domain regulates ubiquitin chain formation by ERAD E3 ligases. *Mol. Cell.* **2013**, *50*, 528–539.
25. Komander, D.; Clague, M.J.; Urbe, S. Breaking the chains: Structure and function of the deubiquitinases. *Nat. Rev. Mol. Cell. Biol.* **2009**, *10*, 550–563.
26. Wang, Q.; Li, L.; Ye, Y. Regulation of retrotranslocation by p97-associated deubiquitinating enzyme ataxin-3. *J. Cell. Biol.* **2006**, *174*, 963–971.
27. Zhong, X.; Pittman, R.N. Ataxin-3 binds VCP/p97 and regulates retrotranslocation of ERAD substrates. *Hum. Mol. Genet.* **2006**, *15*, 2409–2420.
28. Ernst, R.; Mueller, B.; Ploegh, H.L.; Schlieker, C. The otubain YOD1 is a deubiquitinating enzyme that associates with p97 to facilitate protein dislocation from the ER. *Mol. Cell.* **2009**, *36*, 28–38.
29. Liu, Y.; Soetandyo, N.; Lee, J.G.; Liu, L.; Xu, Y.; Clemons, W.M., Jr.; Ye, Y. USP13 antagonizes gp78 to maintain functionality of a chaperone in ER-associated degradation. *Elife* **2014**, *3*, e01369.
30. Blount, J.R.; Burr, A.A.; Denuc, A.; Marfany, G.; Todi, S.V. Ubiquitin-specific protease 25 functions in Endoplasmic Reticulum-associated degradation. *PLoS One* **2012**, *7*, e36542.
31. Hassink, G.C.; Zhao, B.; Sompallae, R.; Altun, M.; Gastaldello, S.; Zinin, N.V.; Masucci, M.G.; Lindsten, K. The ER-resident ubiquitin-specific protease 19 participates in the UPR and rescues ERAD substrates. *EMBO Rep.* **2009**, *10*, 755–761.

32. Lee, J.G.; Kim, W.; Gygi, S.; Ye, Y. Characterization of the deubiquitinating activity of USP19 and its role in endoplasmic reticulum-associated degradation. *J. Biol. Chem.* **2014**, *289*, 3510–3517.
33. Sowa, M.E.; Bennett, E.J.; Gygi, S.P.; Harper, J.W. Defining the human deubiquitinating enzyme interaction landscape. *Cell* **2009**, *138*, 389–403.
34. Feldman, M.; van der Goot, F.G. Novel ubiquitin-dependent quality control in the endoplasmic reticulum. *Trends Cell. Biol.* **2009**, *19*, 357–363.
35. Abrami, L.; Kunz, B.; Iacovache, I.; van der Goot, F.G. Palmitoylation and ubiquitination regulate exit of the Wnt signaling protein LRP6 from the endoplasmic reticulum. *Proc. Natl. Acad. Sci. USA* **2008**, *105*, 5384–5389.
36. Ellgaard, L.; Helenius, A. Quality control in the endoplasmic reticulum. *Nat. Rev. Mol. Cell. Biol.* **2003**, *4*, 181–191.
37. Zhang, Z.R.; Bonifacino, J.S.; Hegde, R.S. Deubiquitinases sharpen substrate discrimination during membrane protein degradation from the ER. *Cell* **2013**, *154*, 609–622.
38. Ast, T.; Aviram, N.; Chuartzman, S.G.; Schuldiner, M. A cytosolic degradation pathway, prERAD, monitors pre-inserted secretory pathway proteins. *J. Cell. Sci.* **2014**, doi:10.1242/jcs.144386.
39. Yu, H.; Kopito, R.R. The role of multiubiquitination in dislocation and degradation of the alpha subunit of the T cell antigen receptor. *J. Biol. Chem.* **1999**, *274*, 36852–36858.
40. Kikkert, M.; Hassink, G.; Barel, M.; Hirsch, C.; van der Wal, F.J.; Wiertz, E. Ubiquitination is essential for human cytomegalovirus US11-mediated dislocation of MHC class I molecules from the endoplasmic reticulum to the cytosol. *Biochem. J.* **2001**, *358*, 369–377.
41. Shamu, C.E.; Flierman, D.; Ploegh, H.L.; Rapoport, T.A.; Chau, V. Polyubiquitination is required for US11-dependent movement of MHC class I heavy chain from endoplasmic reticulum into cytosol. *Mol. Biol. Cell.* **2001**, *12*, 2546–2555.
42. Ye, Y.; Meyer, H.H.; Rapoport, T.A. The AAA ATPase Cdc48/p97 and its partners transport proteins from the ER into the cytosol. *Nature* **2001**, *414*, 652–656.
43. Jarosch, E.; Taxis, C.; Volkwein, C.; Bordallo, J.; Finley, D.; Wolf, D.H.; Sommer, T. Protein dislocation from the ER requires polyubiquitination and the AAA-ATPase Cdc48. *Nat. Cell. Biol.* **2002**, *4*, 134–139.
44. Ye, Y. Diverse functions with a common regulator: Ubiquitin takes command of an AAA ATPase. *J. Struct. Biol.* **2006**, *156*, 29–40.
45. Ye, Y.; Meyer, H.H.; Rapoport, T.A. Function of the p97-Ufd1-Npl4 complex in retrotranslocation from the ER to the cytosol: Dual recognition of nonubiquitinated polypeptide segments and polyubiquitin chains. *J. Cell. Biol.* **2003**, *162*, 71–84.
46. Park, S.; Isaacson, R.; Kim, H.T.; Silver, P.A.; Wagner, G. Ufd1 exhibits the AAA-ATPase fold with two distinct ubiquitin interaction sites. *Structure* **2005**, *13*, 995–1005.
47. Ye, Y.; Shibata, Y.; Kikkert, M.; van Voorden, S.; Wiertz, E.; Rapoport, T.A. Inaugural Article: Recruitment of the p97 ATPase and ubiquitin ligases to the site of retrotranslocation at the endoplasmic reticulum membrane. *Proc. Natl. Acad. Sci. USA* **2005**, *102*, 14132–14138.
48. Neuber, O.; Jarosch, E.; Volkwein, C.; Walter, J.; Sommer, T. Ubx2 links the Cdc48 complex to ER-associated protein degradation. *Nat. Cell. Biol.* **2005**, *7*, 993–998.

49. Schuberth, C.; Buchberger, A. Membrane-bound Ubx2 recruits Cdc48 to ubiquitin ligases and their substrates to ensure efficient ER-associated protein degradation. *Nat. Cell. Biol.* **2005**, *7*, 999–1006.
50. Lilley, B.N.; Ploegh, H.L. Multiprotein complexes that link dislocation, ubiquitination, and extraction of misfolded proteins from the endoplasmic reticulum membrane. *Proc. Natl. Acad. Sci. USA* **2005**, *102*, 14296–14301.
51. Davies, J.M.; Tsuruta, H.; May, A.P.; Weis, W.I. Conformational changes of p97 during nucleotide hydrolysis determined by small-angle X-Ray scattering. *Structure* **2005**, *13*, 183–195.
52. Rouiller, I.; Butel, V.M.; Latterich, M.; Milligan, R.A.; Wilson-Kubalek, E.M. A major conformational change in p97 AAA ATPase upon ATP binding. *Mol. Cell.* **2000**, *6*, 1485–1490.
53. Rumpf, S.; Jentsch, S. Functional division of substrate processing cofactors of the ubiquitin-selective Cdc48 chaperone. *Mol. Cell.* **2006**, *21*, 261–269.
54. Doss-Pepe, E.W.; Stenroos, E.S.; Johnson, W.G.; Madura, K. Ataxin-3 interactions with rad23 and valosin-containing protein and its associations with ubiquitin chains and the proteasome are consistent with a role in ubiquitin-mediated proteolysis. *Mol. Cell. Biol.* **2003**, *23*, 6469–6483.
55. Boeddrich, A.; Gaumer, S.; Haacke, A.; Tzvetkov, N.; Albrecht, M.; Evert, B.O.; Muller, E.C.; Lurz, R.; Breuer, P.; Schugardt, N.; *et al.* An arginine/lysine-rich motif is crucial for VCP/p97-mediated modulation of ataxin-3 fibrillogenesis. *EMBO J.* **2006**, *25*, 1547–1558.
56. Locke, M.; Toth, J.I.; Petroski, M.D. Lys11- and Lys48-linked ubiquitin chains interact with p97 during endoplasmic-reticulum-associated degradation. *Biochem. J.* **2014**, *459*, 205–216.
57. Liu, Y.; Ye, Y. Roles of p97-associated deubiquitinases in protein quality control at the endoplasmic reticulum. *Curr. Protein Pept. Sci.* **2012**, *13*, 436–446.
58. Ernst, R.; Claessen, J.H.; Mueller, B.; Sanyal, S.; Spooner, E.; van der Veen, A.G.; Kirak, O.; Schlieker, C.D.; Weihofen, W.A.; Ploegh, H.L. Enzymatic blockade of the ubiquitin-proteasome pathway. *PLoS Biol.* **2011**, *8*, e1000605.
59. Claessen, J.H.; Kundrat, L.; Ploegh, H.L. Protein quality control in the ER: Balancing the ubiquitin checkbook. *Trends Cell. Biol.* **2012**, *22*, 22–32.
60. Finley, D. Recognition and processing of ubiquitin-protein conjugates by the proteasome. *Annu. Rev. Biochem.* **2009**, *78*, 477–513.
61. Weibezahn, J.; Tessarz, P.; Schlieker, C.; Zahn, R.; Maglica, Z.; Lee, S.; Zentgraf, H.; Weber-Ban, E.U.; Dougan, D.A.; Tsai, F.T.; *et al.* Thermotolerance requires refolding of aggregated proteins by substrate translocation through the central pore of ClpB. *Cell* **2004**, *119*, 653–665.
62. DeLaBarre, B.; Christianson, J.C.; Kopito, R.R.; Brunger, A.T. Central pore residues mediate the p97/VCP activity required for ERAD. *Mol. Cell.* **2006**, *22*, 451–462.
63. Tirosh, B.; Furman, M.H.; Tortorella, D.; Ploegh, H.L. Protein unfolding is not a prerequisite for endoplasmic reticulum-to-cytosol dislocation. *J. Biol. Chem.* **2003**, *278*, 6664–6672.
64. Fiebiger, E.; Story, C.; Ploegh, H.L.; Tortorella, D. Visualization of the ER-to-cytosol dislocation reaction of a type I membrane protein. *EMBO J.* **2002**, *21*, 1041–1053.
65. Wiertz, E.J.; Jones, T.R.; Sun, L.; Bogyo, M.; Geuze, H.J.; Ploegh, H.L. The human cytomegalovirus US11 gene product dislocates MHC class I heavy chains from the endoplasmic reticulum to the cytosol. *Cell* **1996**, *84*, 769–779.

66. Koegl, M.; Hoppe, T.; Schlenker, S.; Ulrich, H.D.; Mayer, T.U.; Jentsch, S. A novel ubiquitination factor, E4, is involved in multiubiquitin chain assembly. *Cell* **1999**, *96*, 635–644.
67. Richly, H.; Rape, M.; Braun, S.; Rumpf, S.; Hoege, C.; Jentsch, S. A series of ubiquitin binding factors connects CDC48/p97 to substrate multiubiquitylation and proteasomal targeting. *Cell* **2005**, *120*, 73–84.
68. Liu, C.; van Dyk, D.; Xu, P.; Choe, V.; Pan, H.; Peng, J.; Andrews, B.; Rao, H. Ubiquitin chain elongation enzyme Ufd2 regulates a subset of Doa10 substrates. *J. Biol. Chem.* **2010**, *285*, 10265–10272.
69. Nakatsukasa, K.; Huyer, G.; Michaelis, S.; Brodsky, J.L. Dissecting the ER-associated degradation of a misfolded polytopic membrane protein. *Cell* **2008**, *132*, 101–112.
70. Jentsch, S.; Rumpf, S. Cdc48 (p97): A "molecular gearbox" in the ubiquitin pathway? *Trends Biochem. Sci.* **2007**, *32*, 6–11.
71. Raasi, S.; Wolf, D.H. Ubiquitin receptors and ERAD: A network of pathways to the proteasome. *Semin. Cell. Dev. Biol.* **2007**, *18*, 780–791.
72. Medicherla, B.; Kostova, Z.; Schaefer, A.; Wolf, D.H. A genomic screen identifies Dsk2p and Rad23p as essential components of ER-associated degradation. *EMBO Rep.* **2004**, *5*, 692–697.
73. Kim, I.; Mi, K.; Rao, H. Multiple interactions of rad23 suggest a mechanism for ubiquitylated substrate delivery important in proteolysis. *Mol. Biol. Cell.* **2004**, *15*, 3357–3365.
74. Hiyama, H.; Yokoi, M.; Masutani, C.; Sugasawa, K.; Maekawa, T.; Tanaka, K.; Hoeijmakers, J.H.; Hanaoka, F. Interaction of hHR23 with S5a. The ubiquitin-like domain of hHR23 mediates interaction with S5a subunit of 26 S proteasome. *J. Biol. Chem.* **1999**, *274*, 28019–28025.
75. Schauber, C.; Chen, L.; Tongaonkar, P.; Vega, I.; Lambertson, D.; Potts, W.; Madura, K. Rad23 links DNA repair to the ubiquitin/proteasome pathway. *Nature* **1998**, *391*, 715–718.
76. Rao, H.; Sastry, A. Recognition of specific ubiquitin conjugates is important for the proteolytic functions of the ubiquitin-associated domain proteins Dsk2 and Rad23. *J. Biol. Chem.* **2002**, *277*, 11691–11695.
77. Raasi, S.; Pickart, C.M. Rad23 ubiquitin-associated domains (UBA) inhibit 26 S proteasome-catalyzed proteolysis by sequestering lysine 48-linked polyubiquitin chains. *J. Biol. Chem.* **2003**, *278*, 8951–8959.
78. Chen, L.; Shinde, U.; Ortolan, T.G.; Madura, K. Ubiquitin-associated (UBA) domains in Rad23 bind ubiquitin and promote inhibition of multi-ubiquitin chain assembly. *EMBO Rep.* **2001**, *2*, 933–938.
79. Raasi, S.; Orlov, I.; Fleming, K.G.; Pickart, C.M. Binding of polyubiquitin chains to ubiquitin-associated (UBA) domains of HHR23A. *J. Mol. Biol.* **2004**, *341*, 1367–1379.
80. Verma, R.; Oania, R.; Graumann, J.; Deshaies, R.J. Multiubiquitin chain receptors define a layer of substrate selectivity in the ubiquitin-proteasome system. *Cell* **2004**, *118*, 99–110.
81. Crosas, B.; Hanna, J.; Kirkpatrick, D.S.; Zhang, D.P.; Tone, Y.; Hathaway, N.A.; Buecker, C.; Leggett, D.S.; Schmidt, M.; King, R.W.; *et al.* Ubiquitin chains are remodeled at the proteasome by opposing ubiquitin ligase and deubiquitinating activities. *Cell* **2006**, *127*, 1401–1413.
82. Schmidt, M.; Hanna, J.; Elsasser, S.; Finley, D. Proteasome-associated proteins: Regulation of a proteolytic machine. *Biol. Chem.* **2005**, *386*, 725–737.

83. Kohlmann, S.; Schafer, A.; Wolf, D.H. Ubiquitin ligase Hul5 is required for fragment-specific substrate degradation in endoplasmic reticulum-associated degradation. *J. Biol. Chem.* **2008**, *283*, 16374–16383.
84. Lam, Y.A.; Xu, W.; DeMartino, G.N.; Cohen, R.E. Editing of ubiquitin conjugates by an isopeptidase in the 26S proteasome. *Nature* **1997**, *385*, 737–740.
85. Rapoport, T.A.; Goder, V.; Heinrich, S.U.; Matlack, K.E. Membrane-protein integration and the role of the translocation channel. *Trends Cell. Biol.* **2004**, *14*, 568–575.
86. Schreiner, P.; Chen, X.; Husnjak, K.; Randles, L.; Zhang, N.; Elsasser, S.; Finley, D.; Dikic, I.; Walters, K.J.; Groll, M. Ubiquitin docking at the proteasome through a novel pleckstrin-homology domain interaction. *Nature* **2008**, *453*, 548–552.
87. Husnjak, K.; Elsasser, S.; Zhang, N.; Chen, X.; Randles, L.; Shi, Y.; Hofmann, K.; Walters, K.J.; Finley, D.; Dikic, I. Proteasome subunit Rpn13 is a novel ubiquitin receptor. *Nature* **2008**, *453*, 481–488.
88. Huang, T.T.; D'Andrea, A.D. Regulation of DNA repair by ubiquitylation. *Nat. Rev. Mol. Cell. Biol.* **2006**, *7*, 323–334.
89. Collins, G.A.; Tansey, W.P. The proteasome: A utility tool for transcription? *Curr. Opin. Genet. Dev.* **2006**, *16*, 197–202.
90. Thrower, J.S.; Hoffman, L.; Rechsteiner, M.; Pickart, C.M. Recognition of the polyubiquitin proteolytic signal. *EMBO J.* **2000**, *19*, 94–102.
91. Williamson, A.; Werner, A.; Rape, M. The Colossus of ubiquitylation: Decrypting a cellular code. *Mol. Cell.* **2013**, *49*, 591–600.
92. Komander, D.; Rape, M. The ubiquitin code. *Annu. Rev. Biochem.* **2012**, *81*, 203–229.
93. Xu, P.; Duong, D.M.; Seyfried, N.T.; Cheng, D.; Xie, Y.; Robert, J.; Rush, J.; Hochstrasser, M.; Finley, D.; Peng, J. Quantitative proteomics reveals the function of unconventional ubiquitin chains in proteasomal degradation. *Cell* **2009**, *137*, 133–145.
94. Boutet, S.C.; Disatnik, M.H.; Chan, L.S.; Iori, K.; Rando, T.A. Regulation of Pax3 by proteasomal degradation of monoubiquitinated protein in skeletal muscle progenitors. *Cell* **2007**, *130*, 349–362.
95. Meyer, H.J.; Rape, M. Enhanced protein degradation by branched ubiquitin chains. *Cell* **2014**, *157*, 910–921.
96. Elsasser, S.; Finley, D. Delivery of ubiquitinated substrates to protein-unfolding machines. *Nat. Cell. Biol.* **2005**, *7*, 742–749.
97. Mayer, T.U.; Braun, T.; Jentsch, S. Role of the proteasome in membrane extraction of a short-lived ER-transmembrane protein. *EMBO J.* **1998**, *17*, 3251–3257.
98. Walter, J.; Urban, J.; Volkwein, C.; Sommer, T. Sec61p-independent degradation of the tail-anchored ER membrane protein Ubc6p. *EMBO J.* **2001**, *20*, 3124–3131.
99. Kalies, K.U.; Allan, S.; Sergeyenko, T.; Kroger, H.; Romisch, K. The protein translocation channel binds proteasomes to the endoplasmic reticulum membrane. *EMBO J.* **2005**, *24*, 2284–2293.
100. Ng, W.; Sergeyenko, T.; Zeng, N.; Brown, J.D.; Romisch, K. Characterization of the proteasome interaction with the Sec61 channel in the endoplasmic reticulum. *J. Cell. Sci.* **2007**, *120*, 682–691.

101. Wiertz, E.J.; Tortorella, D.; Bogyo, M.; Yu, J.; Mothes, W.; Jones, T.R.; Rapoport, T.A.; Ploegh, H.L. Sec61-mediated transfer of a membrane protein from the endoplasmic reticulum to the proteasome for destruction. *Nature* **1996**, *384*, 432–438.
102. Pilon, M.; Schekman, R.; Romisch, K. Sec61p mediates export of a misfolded secretory protein from the endoplasmic reticulum to the cytosol for degradation. *EMBO J.* **1997**, *16*, 4540–4548.
103. Plemper, R.K.; Bordallo, J.; Deak, P.M.; Taxis, C.; Hitt, R.; Wolf, D.H. Genetic interactions of Hrd3p and Der3p/Hrd1p with Sec61p suggest a retro-translocation complex mediating protein transport for ER degradation. *J. Cell. Sci.* **1999**, *112*, 4123–4134.
104. Huyer, G.; Piluek, W.F.; Fansler, Z.; Kreft, S.G.; Hochstrasser, M.; Brodsky, J.L.; Michaelis, S. Distinct machinery is required in Saccharomyces cerevisiae for the endoplasmic reticulum-associated degradation of a multispanning membrane protein and a soluble luminal protein. *J. Biol. Chem.* **2004**, *279*, 38369–38378.
105. Van den Berg, B.; Clemons, W.M., Jr.; Collinson, I.; Modis, Y.; Hartmann, E.; Harrison, S.C.; Rapoport, T.A. X-ray structure of a protein-conducting channel. *Nature* **2004**, *427*, 36–44.
106. Ye, Y.; Shibata, Y.; Yun, C.; Ron, D.; Rapoport, T.A. A membrane protein complex mediates retro-translocation from the ER lumen into the cytosol. *Nature* **2004**, *429*, 841–847.
107. Carvalho, P.; Stanley, A.M.; Rapoport, T.A. Retrotranslocation of a misfolded luminal ER protein by the ubiquitin-ligase Hrd1p. *Cell* **2010**, *143*, 579–591.
108. Mehnert, M.; Sommer, T.; Jarosch, E. Der1 promotes movement of misfolded proteins through the endoplasmic reticulum membrane. *Nat. Cell. Biol.* **2014**, *16*, 77–86.
109. Knop, M.; Finger, A.; Braun, T.; Hellmuth, K.; Wolf, D.H. Der1, a novel protein specifically required for endoplasmic reticulum degradation in yeast. *EMBO J.* **1996**, *15*, 753–763.
110. Rubenstein, E.M.; Kreft, S.G.; Greenblatt, W.; Swanson, R.; Hochstrasser, M. Aberrant substrate engagement of the ER translocon triggers degradation by the Hrd1 ubiquitin ligase. *J. Cell. Biol.* **2012**, *197*, 761–773.
111. Tcherpakov, M.; Broday, L.; Delaunay, A.; Kadoya, T.; Khurana, A.; Erdjument-Bromage, H.; Tempst, P.; Qiu, X.B.; DeMartino, G.N.; Ronai, Z. JAMP optimizes ERAD to protect cells from unfolded proteins. *Mol. Biol. Cell.* **2008**, *19*, 5019–5028.
112. Nakatsukasa, K.; Brodsky, J.L.; Kamura, T. A stalled retrotranslocation complex reveals physical linkage between substrate recognition and proteasomal degradation during ER-associated degradation. *Mol. Biol. Cell.* **2013**, *24*, 1765–1775.
113. Bernardi, K.M.; Williams, J.M.; Inoue, T.; Schultz, A.; Tsai, B. A deubiquitinase negatively regulates retro-translocation of nonubiquitinated substrates. *Mol. Biol. Cell.* **2013**, *24*, 3545–3556.
114. Weissman, A.M.; Shabek, N.; Ciechanover, A. The predator becomes the prey: Regulating the ubiquitin system by ubiquitylation and degradation. *Nat. Rev. Mol. Cell. Biol.* **2011**, *12*, 605–620.
115. Gardner, R.G.; Swarbrick, G.M.; Bays, N.W.; Cronin, S.R.; Wilhovsky, S.; Seelig, L.; Kim, C.; Hampton, R.Y. Endoplasmic reticulum degradation requires lumen to cytosol signaling. Transmembrane control of Hrd1p by Hrd3p. *J. Cell. Biol.* **2000**, *151*, 69–82.

116. Carroll, S.M.; Hampton, R.Y. Usa1p is required for optimal function and regulation of the Hrd1p endoplasmic reticulum-associated degradation ubiquitin ligase. *J. Biol. Chem.* **2010**, *285*, 5146–5156.
117. Iida, Y.; Fujimori, T.; Okawa, K.; Nagata, K.; Wada, I.; Hosokawa, N. SEL1L protein critically determines the stability of the HRD1-SEL1L endoplasmic reticulum-associated degradation (ERAD) complex to optimize the degradation kinetics of ERAD substrates. *J. Biol. Chem.* **2011**, *286*, 16929–16939.
118. Wang, Q; Liu, Y; Soetandyo, N; Baek, K; Hegde, R; Ye, Y. A ubiquitin ligase-associated chaperone holdase maintains polypeptides in soluble states for proteasome degradation. *Mol. Cell.* **2011**, *42*, 758–770.
119. Xu, Y; Liu, Y; Lee, J.G; Ye, Y. A ubiquitin-like domain recruits an oligomeric chaperone to a retrotranslocation complex in endoplasmic reticulum-associated degradation. *J. Biol. Chem.* **2013**, *288*, 18068–18076.

PART II

Role of the Endoplasmic Reticulum in Autophagy

Autophagy

Macroautophagy (here referred to as autophagy) is a catabolic and recycling process conserved in eukaryotic cells that promotes cellular homeostasis and its morphological hallmark is the sequestration of cytoplasmic components within cytosolic double membrane vesicles called autophagosomes, which eventually will fuse with lytic compartments (Reggiori and Klionsky, 2013).

Autophagy is triggered by nutrient starvation, stress and developmental signals in which proteins, cellular complexes, organelles and even invading pathogens are degraded in order to restore the cellular homeostasis or to cope with the specific stress condition. In addition to the signal-induced autophagy, there is a low level of constitutive autophagy important also for cellular homeostasis (Hara et al., 2006).

Moreover, depending on the cargo, autophagy has been divided in selective and nonselective. The first type make use of receptors that are specific for their cargos, and in the latter, bulk cytosol and other cytoplasm components are engulfed randomly (Kraft et al., 2009; Okamoto, 2014; Rubinsztein, 2015; Stolz et al., 2014).

Most proteins necessary for autophagy, termed Atg (autophagy-related), were first described in yeast (Klionsky and Ohsumi, 1999; Takeshige et al., 1992). Great efforts have been done to understand the interactions between these proteins and their actions on maturing autophagosomes in yeast and mammalian cells (Mizushima et al., 2011).

Autophagy-related proteins Atg8p/LC3 and Atg9p are two crucial players in the process of autophagosome biogenesis in both yeast and mammalian cells (Kirisako et al., 1999; Lang et al., 2000; Noda et al., 2000). Atg8p is a unique ubiquitin-like protein whose conjugation target is the lipid phosphatidylethanolamine (PE). The lipidation of Atg8 depends on the sequential action of the E1-activating-like enzyme (Atg7), E2-conjugating-like enzyme (Atg3) and the Atg12–Atg5–Atg16 complex acting as the E3-ubiquitin ligase-like enzyme (Hanada et al., 2007; Ichimura et al., 2000; Kaufmann et al., 2014; Suzuki et al., 2001).

Atg8 and its lipidated form are widely used as specific markers to monitor autophagosomes and autophagic activity (Kirisako et al., 1999). The amount of Atg8 increases significantly, when autophagy is induced (Huang et al., 2000). Therefore, autophagy flux can be estimated by measuring the turnover of Atg8-PE with and without vacuolar degradation (Klionsky et al., 2012; Mizushima et al., 2010).

Another autophagy-related marker is the only one multispanning membrane protein, Atg9p that is also essential for autophagy in yeast and mammals (Lang et al., 2000; Noda et al., 2000). It has been shown that Atg9p compartments participate in the generation of the PAS (Mari et al., 2010). Moreover, both Atg9p compartments and ER exit sites (ERES)[12] (Jensen and Schekman, 2011) participate in the initial assembly of the autophagy machinery (Graef et al., 2013; Sanchez-Wandelmer et al., 2015).

Considering that the ER has been proposed as one of the main source that provides membranes for the growing PAS and it is an extended membranous system that have contact with the vast majority of organelles inside the cell (Figure 12), we were interesting in determining which is the contribution of some ER fusion machineries in supplying membranes to the emerging autophagosomes upon autophagy induction.

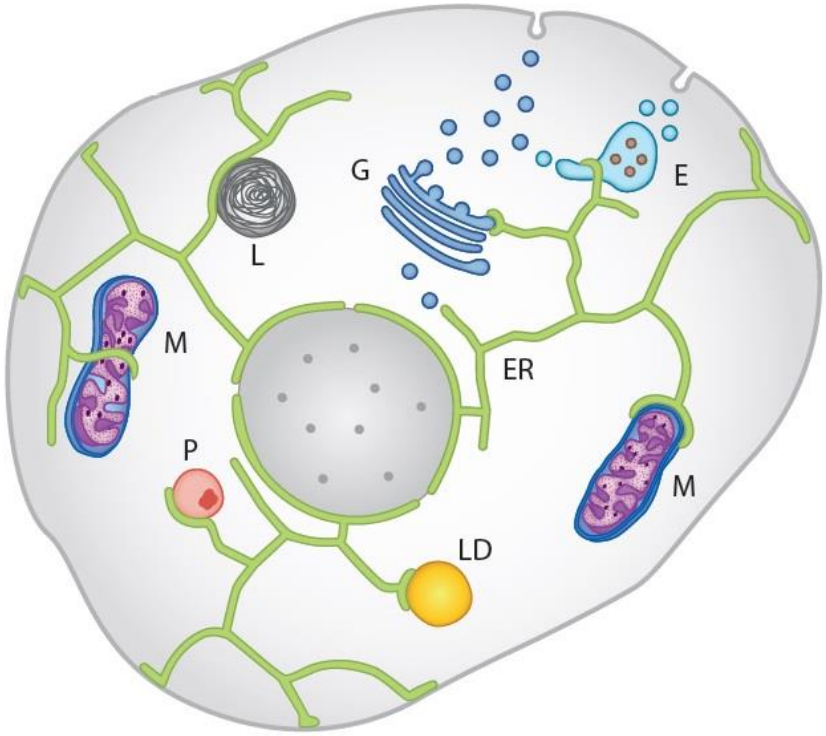

Figure 12 Broad localization of the ER (green) throughout the cytoplasm.
Depict of the ER contacts with other membranous organelles and with plasma membrane. Abbreviations: E, endosome; ER, endoplasmic reticulum; G, Golgi complex; L, lysosome; LD, lipid droplet; M, mitochondria; P, peroxisome (Saheki and De Camilli, 2017).

The cytoplasm-to-vacuole-targeting (Cvt) pathway is a non-induced autophagy-like pathway by means of which certain enzymes: vacuolar aminopeptidase 1 (Ape1), aspartyl aminopeptidase 4 (Ape4) and α-mannosidase 1 (Ams1), are transported to the

[12] ER region where proteins are sorted into the secretory system by COPII vesicles

vacuole where they mature and become active (Lynch-Day and Klionsky, 2010). It is known that Atg8 and Atg9 can be localized both in Cvt vesicles and in autophagosome membranes. Another goal in our research was to determine whether the ER fusion machineries that potentially could contribute with membranes in autophagy were also implicated in the formation of Cvt vesicles.

In order to asses all the questions we used biochemical, molecular biology and ultrastructural studies, for instances, co-immunoprecipitation assays, GFP-cleavage assay, fluorescence microscopy, thin-section electron microscopy and others (Lemus et al., 2016).

Autophagosome biogenesis.

Autophagosome (AP) biogenesis is triggered upon stress conditions, by the elongation of a flat membrane, called phagophore or isolation membrane, which wraps cytoplasmic components and will be completed by forming a closed double-membrane vesicle that eventually fuses with the vacuole/lysosome where components will be degraded and further recycled (Eskelinen, 2008).

The membrane source and the mechanism for the formation of autophagosomes has been a subject of intense research over the last decades. For a long time, it was assumed that autophagosome elongation was only dependent on *de novo* lipid addition. However, recent works have suggested that autophagosomes may derive membranes from multiple nonmutually exclusive sources, including the ER, Golgi, Atg9-containing compartment, plasma membrane, and mitochondria (Axe et al., 2008; Guo et al., 2012; Hailey et al., 2010; Hayashi-Nishino et al., 2009; Longatti and Tooze, 2009; Mari et al., 2010; Moreau and Rubinsztein, 2012; Ravikumar et al., 2010; van der Vaart et al., 2010; Yen et al., 2010; Yla-Anttila et al., 2009).

To date, it is known that APs are formed *de novo* at one or several pre-autophagosomal structure or phagophore assembly site (PAS). The PAS localizes proximal to the ERES, where autophagosome biogenesis has been localized (Graef et al., 2013; Suzuki et al., 2013). In mammals these sites are often referred to as omegasomes (Axe et al., 2008; Lamb et al., 2013). Glycoproteins exit the ER of the yeast *Saccharomyces cerevisiae* in coat protein complex II (COPII) coated vesicles. The coat consists of the essential proteins Sec23p, Sec24p, Sec13p, Sec31p, Sar1p and Sec16p. (Karhinen et. al., 2005).

How APs are formed? Which is the origin of their membranes? How do they become competent to fuse with endosomes and with the vacuole/lysosome? Those questions remain elusive. Moreover, the molecular mechanism to answer them is not quite clear yet. Nonetheless, much effort has been done in order to understand the mechanism of AP biogenesis (Reggiori and Ungermann, 2017).

In order to test whether Ufe1p, one of the ER fusion machineries, is involved in autophagosome biogenesis, we used several biochemical and ultrastructural approaches like Atg8 lipidation assay on Western blots, image analysis, transmission electron microscopy (TEM), etc. (Klionsky et al., 2012)

SNAREs and autophagy

In eukaryotic cells, traffic of proteins along the secretory pathway occurs by a process of vesicular budding and fusion within the endomembrane system (Ferro-Novick and Jahn, 1994). The docking and membrane fusion require the action of other proteins known as soluble N-ethylmaleimide-sensitive fusion (NSF) attachment protein receptors (SNARE) which are most transmembrane and in some cases can also lack the transmembrane domain (Kienle et al., 2009). Initially SNAREs were classified according to their functionality in two different types: v-SNAREs (on vesicles) and t-SNAREs (on the target membranes) (Sollner et al., 1993). Later on, they were classified as Q- or R-SNAREs, according to the aminoacid (aa) shared in the 0 layer of the bundle of SNARE motif, either glutamine (Q) or arginine (R) respectively (Fasshauer et al., 1998; Weimbs et al., 1997). Moreover, Q-SNARES have been subclassified into “a, b and c” based on other aa sequences of their SNARE domains (Bock et al., 2001; Hong, 2005; Kloepper et al., 2007). Finally, resulting in four-helix bundles comprising, in most cases, three Q-SNAREs ($Q_{a,b,\ and\ c}$) and one R-SNARE. However, this classification is not comprehensive yet.

For several years, it was assumed that SNAREs did not play a role in the biogenesis of autophagosome and that phagophore elongation was dependent on *de novo* lipid addition. However, recent studies have demonstrated that during autophagy multiple membrane fusion events take place, in which SNAREs play a key role, not only in mediating autophagosome-vacuole/lysosome fusion, but also in autophagosome formation and maturation, and in autophagosome-endosome fusion (Moreau et al., 2013) (Moreau et al., 2011; Nair et al., 2011; Takats et al., 2013; Wang et al., 2016) (Figure 13).

SNARE proteins Vam3 (Qa), Vti1 (Qb), Vam7(Qc), and Ykt6(R) have all been suggested to play a role in fusion of autophagosomes with the vacuole (Dilcher et al., 2001; Ishihara et al., 2001). Additionally, endocytic and secretory pathways are also involved in autophagosome formation (Kramer and Ungermann). We were aimed at determining whether Ufe1p interacts with some of the SNAREs and components of the endocytic pathway implicated in autophagosomes biogenesis in order to understand its molecular mechanism in this cellular process.

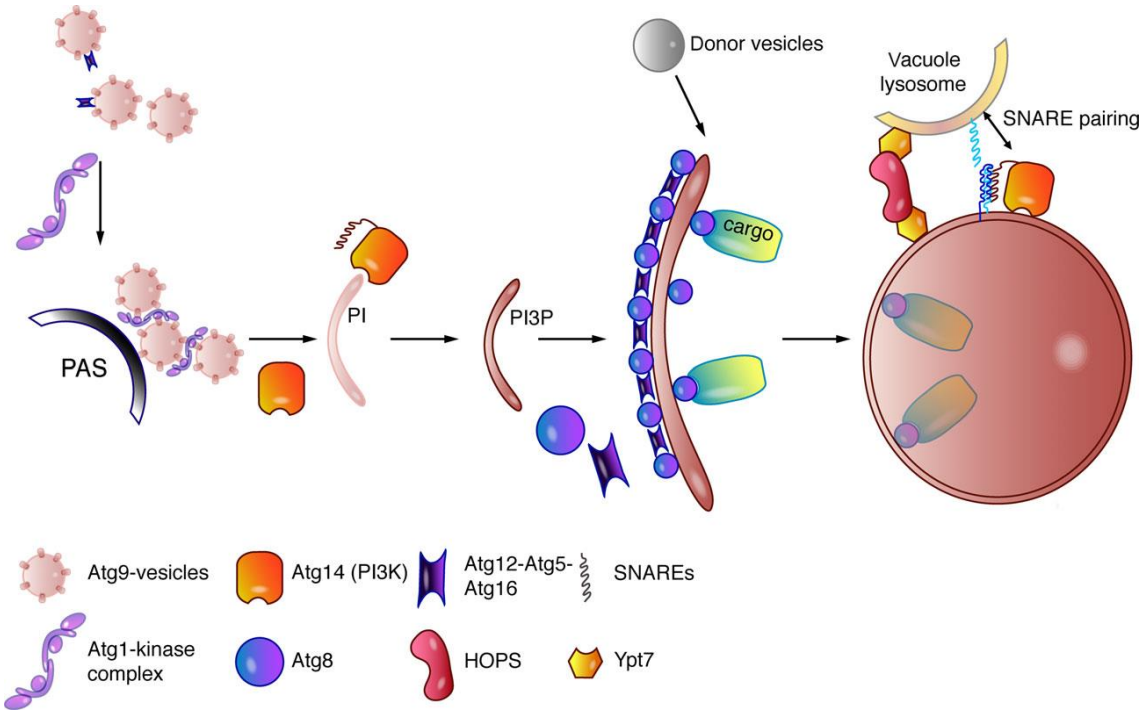

Figure 13. Autophagosome biogenesis and Membrane fusion is catalyzed by SNARE proteins.
Schematic representation of autophagosome formation and implication of other components like SNAREs, Atg9 reservoirs, Atg1-kinase complex, HOPS complex and tethering factors (Ypt7). (Rao et al., 2016)

Ufe1: an ER-localized SNARE.

Ufe1p is an essential Qa-SNARE that localizes to the ER (Lewis and Pelham, 1996). It forms a complex with the two other Q-SNAREs, Sec20p and Use1p, and the R-SNARE Sec22p completing the four partners that mediate retrograde transport and fusion of Golgi-derived vesicles at the ER (Dilcher et al., 2003; Lewis et al., 1997). Besides the above-mentioned heterotypic fusion, Ufe1p is also involved in homotypic ER-ER membrane fusion (Patel et al., 1998) together with the other Q-SNAREs (Sec20p and Use1p). Likewise, it has been shown that the dynamin-like GTPase Sey1p mediates homotypic ER fusion in *S. cerevisiae* (Anwar et al., 2012).

Considering all these previous results and taking into account that the ER is one of the main membrane sources in the autophagy process, we were wondering whether these two ER fusion machinery (Ufe1p and Sey1p) could contribute to membranes in AP biogenesis.

Given that AP formation implies membrane fusion from different sources, it has also been shown the key role of SNAREs -among other proteins- in the elongation, maturation and fusion of AP with other membranous structures (Nair et al., 2011) and compartments like endosomes and vacuole (Ishihara et al., 2001; Moreau et al., 2011; Puri et al., 2013). Therefore, we investigate the interaction and possible SNARE partner formation between Ufe1 and other SNAREs, known to be implicated in autophagy, for instance: the Qb-SNARE, Vti1p and the R-SNARE, Ykt6p (Ishihara et al., 2001).

Assuming that ER fusion machineries may be implicated in the biogenesis of AP, it is reasonable to consider that their components should be exported from the ER to the site of AP formation. ER export mostly depends on the early secretory pathway and is mediated by COPII vesicles (Miller and Schekman, 2013). Moreover, several studies have already shown a link between autophagy and the ER exit sites (ERES), where COPII-coated vesicles form, and its components contribute to autophagosome formation as well (Ge et al., 2013; Graef et al., 2013) (Suzuki et al., 2001).

Therefore, we were interested in determining whether components of the early secretory pathway were linked to the ER export of Ufe1p as well. In order to address these questions we tested Ufe1p export upon autophagy induction in several early secretory mutants.

Goals

General:

To investigate the role of the ER-localize SNARE, Ufe1p in autophagy.

Specifics:

1- To determine whether defective ufe1-1 cells impair either or both Cvt and autophagy pathways.

2- To investigate in which phase(s) of autophagy Ufe1p is playing a role.

3- To address the effect of autophagy in Ufe1 intracellular localization.

4- To demonstrate that Ufe1p interacts with key components (Atg8p, Atg9p) involved in the biogenesis of autophagosomes.

5- To quantify the defect in autophagosome biogenesis caused by ufe1-1 cells.

6- To analyze the physical interaction of Ufe1p with other SNAREs (Ykt6, Vti1, Nyv1, Vam7) implicated in autophagy.

7- To verify the hypersensitive phenotype of sec23-1 cells in the intracellular localization of Ufe1p upon starvation.

8- To confirm at the ultrastructural level using TEM, the effect of defective ufe1-1 and sec23-1 cells in the biogenesis of autophagosomes.

Results

Part II

Cell Rep. 2016 Feb 23;14(7):1710-22. doi: 10.1016/j.celrep.2016.01.047

An ER-Localized SNARE Protein Is Exported in Specific COPII Vesicles for Autophagosome Biogenesis.

Lemus L, Ribas JL, Sikorska N, Goder V.

Highlights of Lemus *et al.*, 2016.

We reported for the first time the following experimental evidences:

1. Ufe1p plays a role in autophagy but not in the Cvt pathway.
   The GFP cleavage assays showed that in cells defective for Ufe1p and expressing GFP-Atg8, there is no generation of GFP fragment (Fig. 1 B). This indicates that Ufe1p is required for autophagy. In contrast, the maturation of the aminopeptidase I (Ape1) in *ufe1-1* cells takes place as in WT indicating that Ufe1p is not involved in the Cvt pathway (Fig. S1, A). Therefore, the function of Ufe1p to target membranes to the vacuole is specific for autophagy.

2. Ufe1p function is not essential for initiation of autophagy.
   Fluorescence microscopy in cells defective for Ufe1p (*ufe1-1*) revealed that GFP-Atg8 is accumulated in puncta, what indicates that the initiation and/or elongation of autophagosomes is occurring (Fig. 1C). Likewise, the lipidation assay showed that Atg8p undergoes conjugation with PE (Fig. S1, D). Therefore, Ufe1p is not critical for the initiation of autophagy. However, the absence of fluorescence signal in the vacuole indicates that the vacuolar uptake of GFP-Atg8 is blocked in these conditional mutant cells. Hence, Ufe1p may play a role in the fusion of autophagosomes with the vacuole.

3. Ufe1p intracellular localization changes from cortical and perinuclear ER towards the vacuole upon starvation.

   Fluorescence microscopy images of GFP-Ufe1 before starvation revealed signal of Ufe1p in cortical and perinuclear ER. Strikingly, after 5 hours of starvation a strong vacuolar signal is detected in the cells, indicating an ER export of Ufe1p to the vacuole upon starvation (Fig. 2 C). In agreement with fluorescence microscopy, the GFP cleavage assays showed that in cells expressing GFP-Ufe1p, there is an increasing generation of GFP fragment upon starvation. Cleavage of GFP-Ufe1 is occurring in the vacuole since in *pep4*Δ cells there is no generation of GFP fragment (Fig. 2 E).

4. Ufe1p is targeted to sites of autophagosomes formation upon starvation.

   Co-localization analysis of GFP-Ufe1 and RFP-Atg8 revealed that after 3 hours of starvation the number of both proteins that colocalized and that are adjacent to each other increases significantly (Fig. 3A, 3B). In agreement with the co-localization analysis, co-immunoprecipitation (coIP) assays showed a physical interaction between Ufe1 and Atg8p that is starvation-dependent (Fig. 3C and S3).

5. Ufe1p is associated with Atg9 structures upon starvation.

   Following the same experimental procedures for determining co-localization and interaction of Ufe1p and Atg8p (described above), the same positive results were obtained for the co-localization (Fig. 4 A, B and C) and physical interaction between Ufe1p and Atg9p. (Fig. S4, B and C).

6. Vacuolar uptake of GFP-Ufe1 upon starvation depends on MVBs pathway.

   In the absence of Vps4 and Vps32 there is not generation of GFP fragment in cells expressing GFP-Ufe1, indicating that Ufe1 is transported along this pathway upon starvation (Fig S4, E and F).

7. Ufe1 has a role in autophagosome biogenesis.

   Thin-section transmission electron microscopy (TEM) reveal that in cells defective for Ufe1p the number and size of autophagosomes is significantly reduced. Likewise, the number of AB in the vacuole is significantly less, indicating a defect in the fusion with the vacuole (Fig. 5 A, B).

   In agreement with this data, the analysis by confocal scanning microscopy, in combination with 3D reconstruction also showed that *ufe1-1* cells have significantly less GFP-Atg8 fluorescence structures demonstrating the defect in AP biogenesis (Fig.5D and E).

   Moreover, in cells defective for Ufe1 the amount of Atg8 structures that were obtained in the pellet were less of the half of the amount obtained in WT cells (Fig. S5, C). This result also confirmd a defect in AP biogenesis in cells with non-functional Ufe1.

8. Qa-SNARE Ufe1p interact with non-ER SNAREs involved in autophagosome formation, but not with a SNARE involved in vacuolar fusion.

   Co-IP experiments showed that Ufe1p interacts physically with Ykt6p and Vti1p, which are SNAREs involved in AP biogenesis (Fig. S5, E). However, Ufe1 does not interact with Vam7, which is involved in fusion of autophagosomes with the vacuole. Therefore, the function of Ufe1 in decreasing the number of AB inside the vacuole could be an indirect effect (Fig. S5, F).

9. ER exit of Ufe1 depends on the early secretory pathway and on COPII vesicles.

   In thermosensitive mutants of both, the early secretory pathway (*sec18-1, sec22-3*) and the COPII vesicles (*sec13-1*), GFP-Ufe1 is visible in the vacuole upon starvation at the permissive temperature (22ºC) but not at 37ºC. Instead, at the restriction temperature (37ºC) the fluorescence signal in the ER was more intense, indicating the retention or the blocking of Ufe1 exit from the ER (Fig. 6A).

It is noteworthy the striking phenotype observed in the case of two COPII conditional mutants: *sec23-1* and *sec31-1.*

In the first case, blocking of ER exit of Ufe1 was observed even at the permissive temperature. However in the latter case, *sec31-1* cells do not show any restriction for the exiting of Ufe1, being visible the fluorescent signal in the vacuole at both permissive and restrictive temperature (Fig. 6A). These striking phenotypes indicate hypersensitivity in the exit of Ufe1 in *sec23-1* cells and a hyposensitivity in the case of .*sec31-1* cells.

The aforementioned fluorescent microscopy results were also confirmed by the GFP-cleavage assay, in which the generation of GFP fragment from GFP-Ufe1 is reduced (Fig. 6 B and C).

Similar results were obtained with *sec23-1* cells expressing GFP-Atg8 at 22ºC. Although this mutant has some visible vacuolar signal, the GFP-cleavage assay revealed a reduction in the generation of GFP-fragment in comparison to the WT (Fig S7, B, C and D), confirming the sensitivity of this conditional mutation in autophagy and its deficiency in autophagosomes biogenesis even at the permissive temperature.

Ultrastructural studies in *sec23-1* cells also confirmed the defect in autophagy even at the permissive temperature upon starvation. Thin-section transmission electron microscopy (TEM) revealed that the number of AB is significantly reduced in comparison to the WT (Fig. 7 C, E and F).

Article

Cell Reports

An ER-Localized SNARE Protein Is Exported in Specific COPII Vesicles for Autophagosome Biogenesis

Graphical Abstract

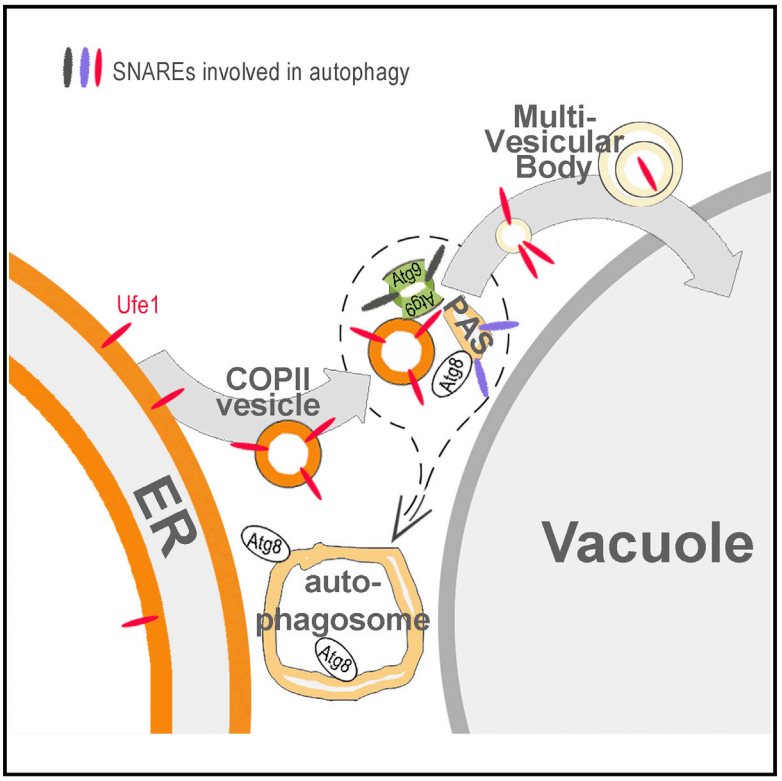

Highlights

- The ER SNARE protein Ufe1 has a role in autophagosome biogenesis in yeast
- Ufe1 is exported from the ER in specific COPII vesicles upon starvation
- Ufe1 is targeted to cellular structures containing Atg8 and Atg9
- Defective Ufe1 leads to fewer and smaller autophagosomes

Authors

Leticia Lemus, Juan Luis Ribas, Natalia Sikorska, Veit Goder

Correspondence

vgoder@us.es

In Brief

Lemus et al. show that starvation-induced autophagosome biogenesis in yeast involves the export of endoplasmic reticulum membranes together with the SNARE protein Ufe1 in specific COPII vesicles and their targeting to sites of autophagosome formation.

Lemus et al., 2016, Cell Reports *14*, 1710–1722
February 23, 2016
http://dx.doi.org/10.1016/j.celrep.2016.01.047

CellPress

OPEN ACCESS
CellPress

Cell Reports
Article

An ER-Localized SNARE Protein Is Exported in Specific COPII Vesicles for Autophagosome Biogenesis

Leticia Lemus,[1] Juan Luis Ribas,[2] Natalia Sikorska,[1,3] and Veit Goder[1,*]
[1]Department of Genetics, University of Seville, Avenue Reina Mercedes, s/n, 41012 Seville, Spain
[2]Centro de Investigación Tecnología e Innovación de la Universidad de Sevilla, Avenue Reina Mercedes, 41012 Seville, Spain
[3]Present address: Institut de Biologie Moléculaire des Plantes, Centre National de la Recherche Scientifique (CNRS), Université de Strasbourg, 67000 Strasbourg, France
*Correspondence: vgoder@us.es
http://dx.doi.org/10.1016/j.celrep.2016.01.047

SUMMARY

The de novo formation of autophagosomes for the targeting of cytosolic material to the vacuole/lysosome is upregulated upon starvation. How autophagosomes acquire membranes remains still unclear. Here, we report that, in yeast, the endoplasmic reticulum (ER)-localized Qa/t-SNARE Ufe1 has a role in autophagy. During starvation, Ufe1 is increasingly exported from the ER and targeted to intracellular sites that contain the autophagy markers Atg8 and Atg9. In addition, Ufe1 interacts with non-ER SNARE proteins implicated in autophagosome formation. Loss of Ufe1 function impairs autophagy and results in fewer and smaller autophagosomes. Unlike conventional cargo, the ER export of Ufe1 is significantly reduced in *sec23-1* cells, which affects the coat protein (COP)II complex, already at the permissive temperature. Under the same conditions, *sec23-1* cells are hypersensitive to starvation and deficient in autophagy. Our data suggest that ER membranes containing Ufe1 are delivered to sites of autophagosome formation in specific COPII vesicles.

INTRODUCTION

Macroautophagy (hereafter autophagy) is a conserved cellular process in response to starvation. A structure called "phagophore" forms in the cytosol at phagophore assembly sites (PAS), elongates while engulfing cytosolic material, and closes to form a double membrane-layered autophagosome that fuses with the vacuole/lysosome for material recycling (Klionsky, 2007; Ohsumi, 2001).

One key question of how autophagosomes are formed concerns the origin of their membranes (Chen and Klionsky, 2011). Growing evidence suggests that several cellular sources can contribute membranes by different and yet poorly understood mechanisms. There is consensus that the endoplasmic reticulum (ER) is a major source for autophagosomal membranes. Transient interconnections between phagophores and ER or specific ER subdomains have been observed both in yeast and mammalian cells and suggest that direct transfer of membranes to growing autophagosomes can occur (Biazik et al., 2015; Graef et al., 2013; Hamasaki et al., 2013; Hayashi-Nishino et al., 2009; Ylä-Anttila et al., 2009). Soluble N-ethylmaleimide-sensitive fusion (NSF) attachment protein receptors (SNARE) proteins with previously described functions in the endocytic and secretory pathways are also involved in autophagosome formation, suggesting that membranes can be equally delivered to autophagosomes through vesicular carriers (Moreau et al., 2011; Nair et al., 2011). Recently, conventional transport vesicles originating from the ER were indirectly (Graef et al., 2013) or directly (Tan et al., 2013) implicated in autophagosome formation in yeast. Together, these data also show that autophagosome formation involves membrane fusion mechanisms that function during conventional membrane traffic under rich growing conditions. During starvation, conventional transport vesicles can be diverted to sites of autophagosome formation by recruiting autophagy-specific modules to tethering complexes (Tan et al., 2013) or by relocalization of fusion activators of the Rab family (Popovic et al., 2012). Whether additional cellular mechanisms specify ER membranes to be used for autophagosome formation during starvation is unclear.

It is known that membrane fusion machineries themselves provide specificity for fusion reactions (McNew et al., 2000). Homo- and heterotypic membrane fusions at the ER are mediated by several distinct and conserved fusion machineries. In yeast, the cycling R/v-SNARE protein Sec22 and the Q/t-SNARE proteins Bet1 and Bos1 are incorporated into budding transport vesicles for fusion with the Golgi apparatus (Newman et al., 1990). The ER-localized Q/t-SNARE proteins Ufe1, Use1, and Sec20 catalyze homotypic ER-ER membrane fusion and heterotypic fusion of retrograde Sec22-containing vesicles with the ER (Anwar et al., 2012; Dilcher et al., 2003; Lewis et al., 1997; Patel et al., 1998). Another ER fusion machinery is Sey1, a dynamin-like GTPase that mediates homotypic ER-ER membrane fusion by an alternative mechanism (Anwar et al., 2012; Hu et al., 2009).

In this study, we addressed the function of specific ER membrane fusion machineries in autophagy in yeast. Our results uncover a cellular mechanism showing that the normally ER-localized SNARE protein Ufe1 is increasingly exported from the ER during starvation. Several independent sets of experiments

lead to a model where ER membranes containing Ufe1 participate in the generation of autophagosomal membranes.

RESULTS

We tested whether Sey1 or Ufe1, which belong to the ER-localized fusion machineries, play a role in autophagy. To this end, we used the GFP-Atg8 processing assay in combination with nitrogen starvation. Free GFP is generated as a result of autophagy-dependent vacuolar delivery of Atg8, which is an autophagosomal marker (Cheong and Klionsky, 2008). Cells with Sey1 deleted did not affect autophagy (Figure 1A). In contrast, cells with the temperature-sensitive *ufe1-1* allele generated free GFP at the permissive (30°C) but not at the non-permissive (37°C) temperature (Figure 1B). The block in autophagy at 37°C was not due to cell death (Figure 1B, lane 12). At the same time, loss of Ufe1 function did not block the autophagy-related constitutive cytoplasm-to-vacuole (Cvt)-pathway (Figure S1A). Although *SEY1* and *UFE1* interact genetically, overexpression of Sey1 could not rescue the autophagy defect in *ufe1-1* cells (Figures S1B and S1C). These data demonstrate that the function of Ufe1 but not of Sey1 is required for starvation-induced autophagy.

To address whether Ufe1 function is required for early or late stages of autophagy, we analyzed cells expressing GFP-Atg8 with live cell fluorescence microscopy. In agreement with the results from western blot analysis, Atg8 was seen inside large spherical structures, the typical pattern of vacuoles, after starving wild-type cells at 30°C or 37°C and *ufe1-1* cells at 30°C (Figure 1C). In *ufe1-1* cells at 37°C, GFP-Atg8 was only seen in punctuate structures after starvation (Figure 1C). Importantly, the number of Atg8 punctuates has multiplied compared to prior of starvation, indicating that autophagosomes or intermediates have formed but that their vacuolar uptake was blocked (Figure 1C). These punctuates were absent in Δ*atg16ufe1-1* cells ruling out autophagy-independent accumulation of Atg8 (Figure 1D). These data suggested that Ufe1 has no essential role in the initiation of autophagosome formation, a fact that was also supported by the finding that lipidation of Atg8 occurred in *ufe1-1* cells at 37°C (Figure S1D).

To analyze the intracellular localizations of Sey1 and Ufe1 before and after starvation, we constructed functional GFP-tagged versions (Figures 2A, S2A, and S2B). Both proteins were initially expressed from their endogenous promoters (EP) and showed weak fluorescence, indicative of low expression levels (Figures 2B and 2C). Under growing conditions, Sey1 was visible in the cortical ER (Figure 2B, "c") and also in the perinuclear ER (Figure 2B, "p"), in agreement with previous data (Hu et al., 2009). No change was visible after 5 hr of starvation (Figure 2B). Ufe1 showed a strikingly different behavior. Prior to starvation, GFP-Ufe1 was visible in the cortical ER (Figure 2C, "c") and also in the perinuclear ER when expressed from the stronger TDH3 promoter (TP-GFP-Ufe1) (Figure S2C). After 5 hr of starvation, most of the GFP-Ufe1 was vacuolar (Figures 2C, "v," and S2C). Thus, cellular starvation resulted in ER export and vacuolar targeting of a large fraction of Ufe1. We consistently observed a weak vacuolar signal with both EP-GFP-Ufe1 and TP-GFP-Ufe1 prior to starvation that indicates constitutive ER export of the protein at a low level under growing conditions (Figures 2C and S2C, "v"). Increased ER export of EP-GFP-Ufe1 also occurred when cells were treated with rapamycin, a drug that induces autophagy independently of starvation (Figure 2D). For a population-wide and semiquantitative assessment of Ufe1 traffic, we performed western blot analysis. Prior to starvation, a low amount of free GFP was observed in wild-type cells (Figure 2E, lane 1), in agreement with the microscopy data. After 2 hr and 5 hr of starvation, substantial amounts of free GFP had accumulated (Figure 2E, lanes 2 and 3). No free GFP was generated in Δ*pep4* cells, which lack vacuolar proteolysis, confirming that Ufe1 was routed to the vacuole upon starvation (Figure 2E, lanes 4–6). No free GFP was generated with EP-Sey1-GFP after up to 5 hr of starvation, in agreement with the microscopy data (Figure 2E, lanes 7–9). To rule out that the increase of Ufe1 export was caused by its tagging, we measured the vacuolar turnover of endogenous Ufe1 in absence and presence of starvation. Endogenous Ufe1 had a low turnover rate under normal growth conditions with only weak stabilization in the Δ*pep4* mutant, implying little or no targeting to the vacuole under these conditions, in agreement with previous data (Braun and Jentsch, 2007). Upon starvation, the turn-over of Ufe1 was enhanced and at the same time the protein was now almost fully stabilized in the Δ*pep4* mutant (Figures 2F, "SD-N," and 2G). Thus, endogenous Ufe1 shows an increase in ER export and targeting to the vacuole upon starvation as well, similar to GFP-Ufe1. It remains to be tested by more rigorous methods if endogenous Ufe1 is constitutively exported from the ER at a low level like GFP-Ufe1.

The increased ER export of Ufe1, but not of Sey1, upon starvation suggested this to be a selective process rather than bulk ER degradation or ER-phagy that occurs after extended times of starvation or ER stress (Bernales et al., 2007; Hamasaki et al., 2005; Mochida et al., 2015). To support this conclusion, we analyzed tagged versions of two additional and abundant ER membrane proteins, the translocon component Sec63, which is mostly found in ER sheets, and the reticulon protein Rtn1, which is mostly found in ER tubules (Voeltz et al., 2006). In contrast to Ufe1, only minute amounts of vacuolar signal were detected for both proteins after 5 hr of starvation (Figure S2D) and no free GFP was detected after 2 hr of starvation (Figure S2E). Thus, Ufe1 ER export is selective and precedes starvation-induced ER-phagy (Mochida et al., 2015). We also tested whether GFP-Ufe1 was a substrate of an autophagy-dependent constitutive ER quality control mechanism (Lipatova and Segev, 2015). This was not the case since free GFP was still increasingly generated from EP-GFP-Ufe1 upon short periods of starvation in autophagy mutants where this pathway is blocked (Figure S2F).

The same result also suggested that Ufe1 was not incorporated into autophagosomes, at least not permanently. However, the starvation-dependent ER export supported a function of Ufe1 in autophagy and furthermore suggested that this function might be outside the ER. We therefore tested if Ufe1 was targeted to sites of autophagosome formation by performing co-localization analysis with autophagosome markers using confocal fluorescence microscopy. EP-GFP-Ufe1 and an RFP-tagged version of Atg8 were co-expressed in Δ*ypt7* cells to prevent rapid fusion of autophagosomes with the vacuole (Kirisako et al., 1999). Under growing conditions, 0–1 Atg8-labeled

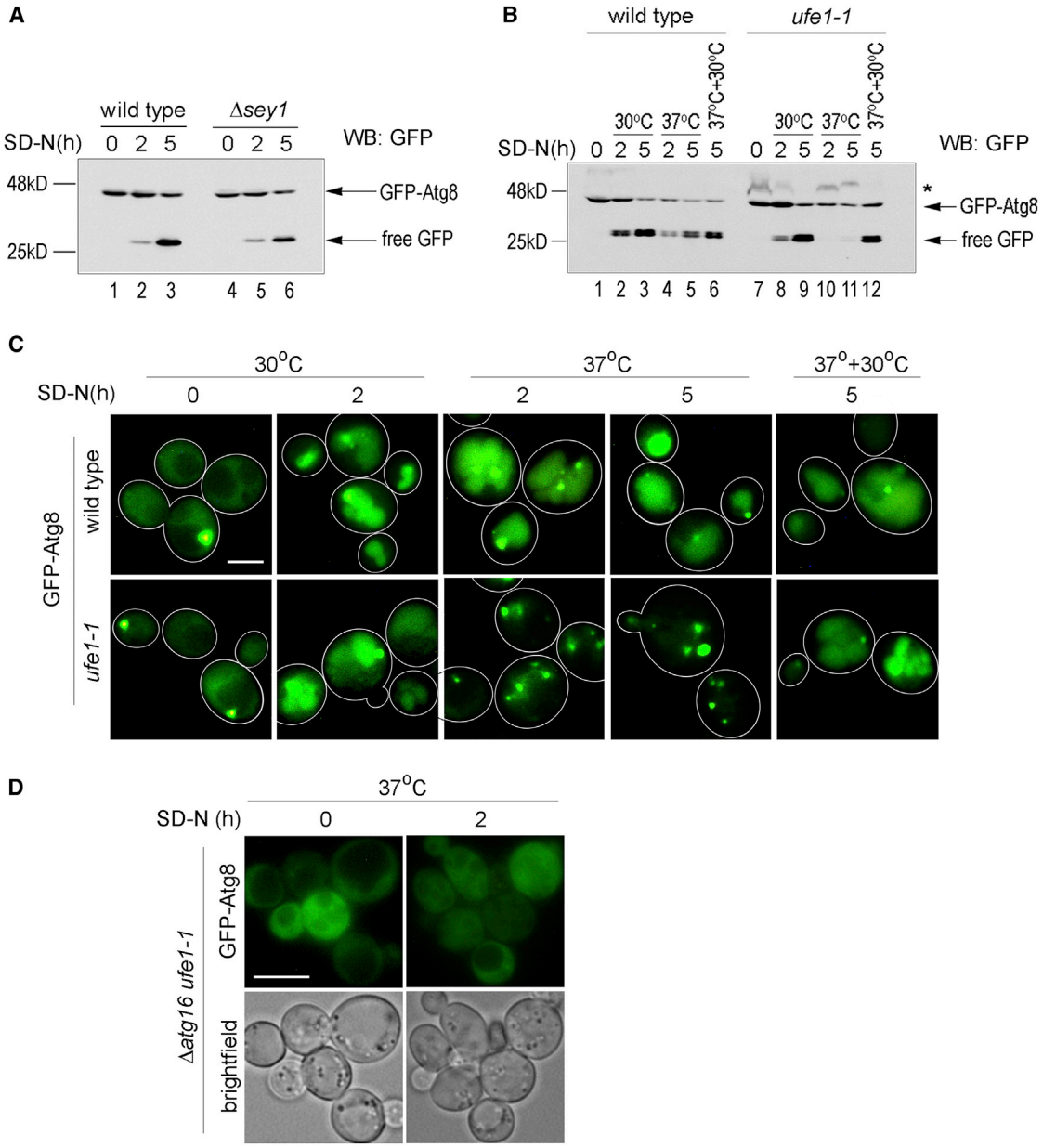

Figure 1. Ufe1 but Not Sey1 Has a Function in Autophagy

(A) GFP-Atg8 processing assay with wild-type cells and Δ*sey1* cells. Cells were grown to mid-log phase at 30°C and shifted to nitrogen starvation (SD-N) medium for the indicated periods of time. Equal amounts of cell lysates were analyzed by SDS-PAGE and western blotting (WB).

(B) GFP-Atg8 processing assay with wild-type cells and *ufe1-1* cells. Like in (A) but, if indicated, shift to 37°C simultaneously with shift to SD-N medium. Lanes 6 and 12: during starvation, cells were incubated for 2 hr at 37°C followed by 3 hr at 30°C. Asterisk indicates unspecific band.

(C) Live cell imaging of wild-type cells and *ufe1-1* cells expressing GFP-Atg8. Cells were treated like in (B). Scale bar, 2 μm. Outlines indicate cell borders.

(D) *Δatg16ufe1-1* cells expressing GFP-Atg8 were treated like in (B) and imaged before and 2 hr after shifting cells to SD-N medium. Scale bar, 5 μm.

See also Figure S1.

structures per cell were visible in a focal plane indicative of the location of the PAS (Figure 3A, "SD"). Ufe1 appeared in membranes and in additional puncta in Δ*ypt7* cells, the latter of which could represent the fraction of protein that is constitutively exported from the ER but fails to be targeted to the vacuole in this background. More than 60% of Atg8 (PAS) did not show contact with Ufe1 under these conditions (Figures 3A, "SD," and 3B). At the same time, more than 30% of Atg8-labeled structures were adjacent to Ufe1 (Figure 3B). After 3 hr of starvation, Atg8-labeled structures multiplied, indicative of formation and accumulation of autophagosomes (Figure 3A, "SD-N"). A combined 59% of Atg8 structures were now either adjacent to Ufe1

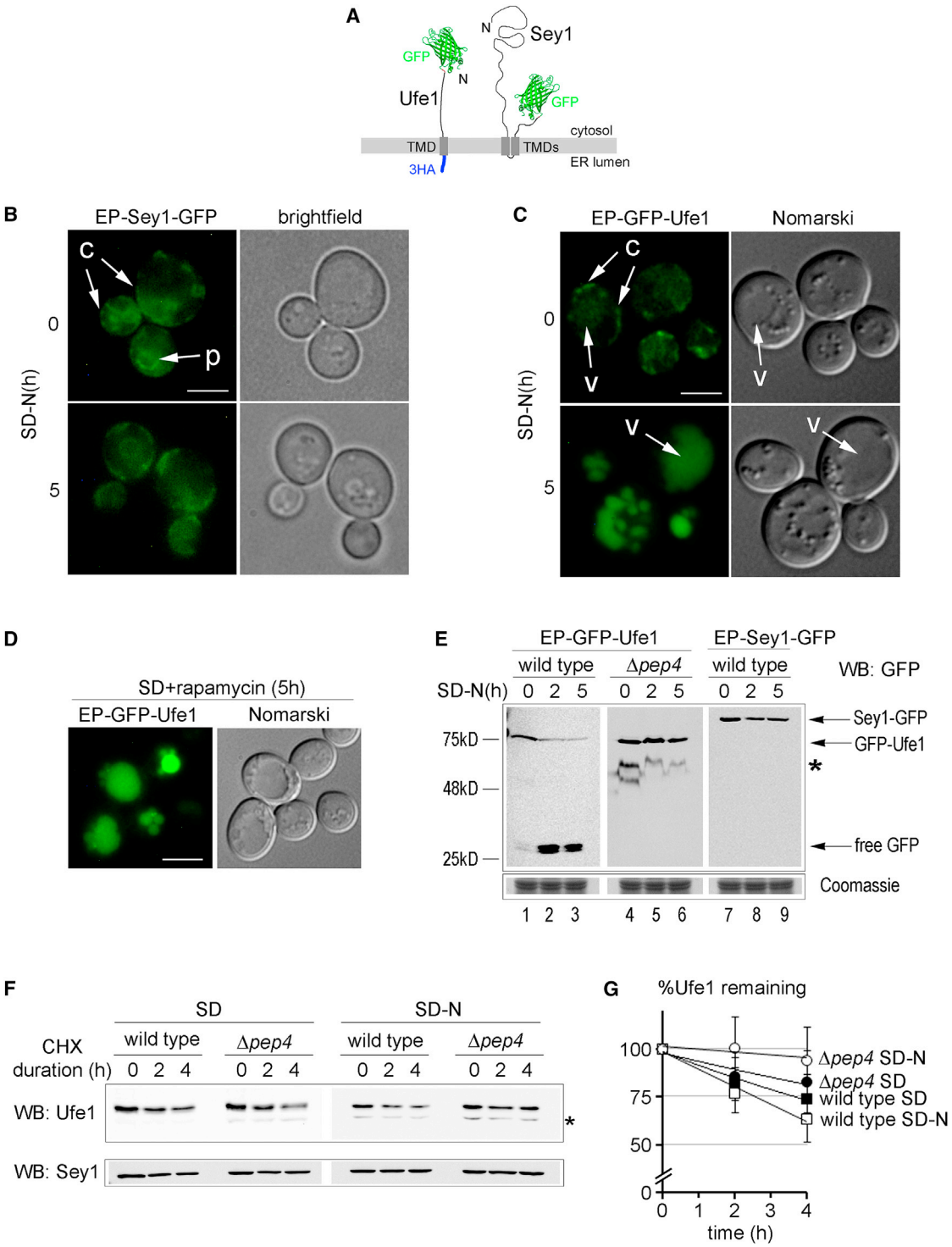

Figure 2. Ufe1 but Not Sey1 Is Increasingly Exported from the ER upon Cellular Starvation

(A) Schematic representation (not to scale) of tagged Ufe1 and Sey1 constructs. GFP was fused to the N terminus of Ufe1 and to the C terminus of Sey1. An additional triple-HA (3HA) tag was fused to the C terminus of Ufe1. TMD, transmembrane domain.

(B and C) Life cell imaging of wild-type cells expressing EP-Sey1-GFP or EP-GFP-Ufe1 before and after starvation at 30°C. c, cortical ER; p, perinuclear ER; v, vacuole. Scale bars, 2 μm.

(D) Life cell imaging of wild-type cells expressing EP-GFP-Ufe1 5 hr after the addition of 200 ng/ml of rapamycin at 30°C. Scale bar, 3 μm.

(legend continued on next page)

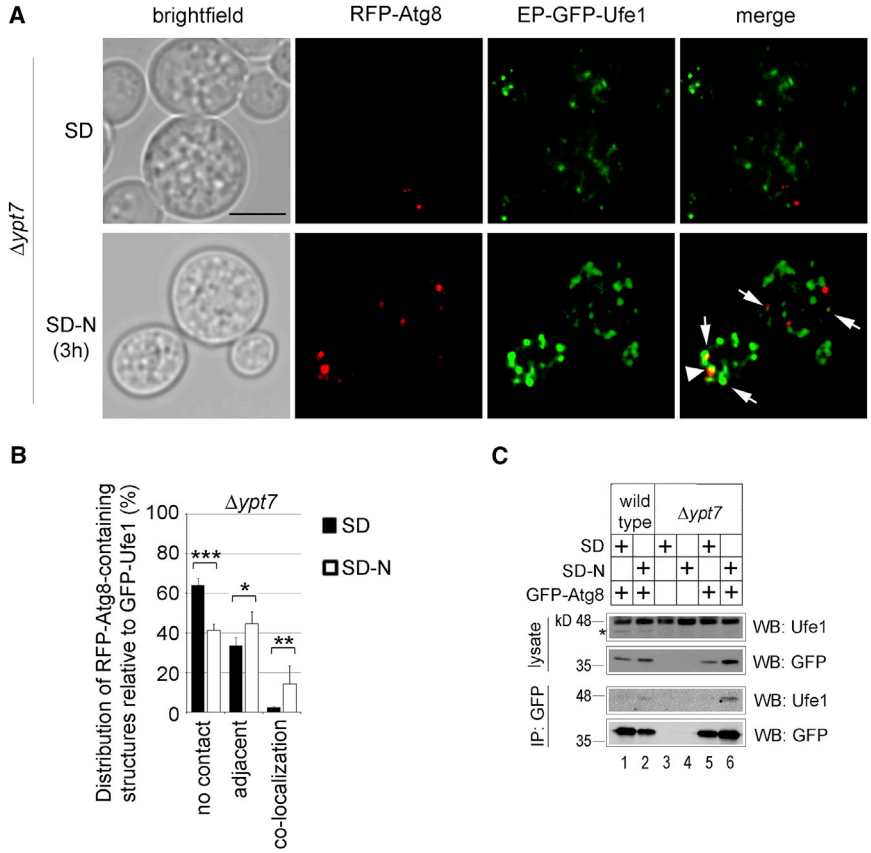

Figure 3. Starvation-Dependent Association of Ufe1 with Atg8

(A) Single scan confocal microscopy with Δ*ypt7* cells co-expressing EP-GFP-Ufe1 and RFP-Atg8 before (SD) and after starvation (SD-N) at 30°C. Arrows indicate Ufe1 and Atg8 in adjacent structures. Arrowhead indicates co-localization. Scale bar, 3 μm.

(B) Statistical analysis of the relative distribution from experiments shown in (A). RFP-Atg8 structures prior to starvation (96, n = 140) and after starvation (146, n = 88) were evaluated with respect to contact with GFP-Ufe1. n = number of cells. The mean values and SDs from four individual sets of assessments are shown, see Experimental Procedures. ***$p < 0.001$; **$p < 0.01$; *$p < 0.05$ (unpaired two-tailed Student's t test).

(C) Co-immunoprecipitation (coIP) of endogenous Ufe1 using GFP-Atg8 in combination with chemical crosslinking (see Experimental Procedures). Wild-type cells and Δ*ypt7* cells expressing GFP-Atg8 or control cells were used for coIP experiments before and after starvation followed by SDS-PAGE and western blotting (WB) with the indicated antibodies. Asterisk indicates an unspecific band.

See also Figure S3.

(45%) (Figures 3A, "SD-N," arrows, and 3B) or co-localized (14%) (Figures 3A, "SD-N," arrowhead, and 3B).

Using the same background, co-immunoprecipitation (coIP) experiments with cells co-expressing GFP-Atg8 and TP-Ufe1-3HA showed a starvation-dependent physical interaction between the two proteins (Figure S3). By using coIP in combination with in vivo crosslinking, we also found a starvation-dependent physical interaction between GFP-Atg8 and endogenous (non-tagged) Ufe1 (Figure 3C, lanes 3–6). A faint but reproducible physical interaction was also detectable in wild-type cells (Figure 3C, lanes 1 and 2), suggesting that the interaction is normally transient. Together with the microscopy data, it shows that Ufe1 is targeted in a starvation-dependent manner to cellular sites of autophagosome formation.

An important cytosolic pool of tubo-vesicular membranes for autophagosome formation contains the membrane protein Atg9 and is known to exchange material with the Golgi apparatus and with endosomes (Mari et al., 2010; Ohashi and Munro, 2010; Reggiori et al., 2004; Yamamoto et al., 2012). In yeast, cellular levels of Atg9 correlate with the number of autophagosomes that can be generated, supporting the ascribed role of Atg9 as a membrane carrier (Jin et al., 2014). To test whether Ufe1 comes into contact with Atg9, we performed a co-localization analysis in Δ*ypt7* cells co-expressing EP-GFP-Ufe1 and Atg9mCherry. Atg9 is synthesized at the ER but rapidly exported to the cytoplasmic membrane pool with no ER staining visible at steady state (Figure 4A, "SD") (Mari et al., 2010; Yamamoto et al., 2012). At growing conditions, only 5% of Atg9-containing structures co-localized with Ufe1 (Figures 4A, "SD," arrowhead, and 4B). A significant population of Atg9-containing structures (33%) was adjacent to Ufe1 puncta that are visible in the Δ*ypt7* background under the same conditions (Figures 4A, "SD," arrows, and 4B). After starvation, Atg9-containing structures that co-localized with Ufe1 increased to 32% (Figures 4A, "SD-N," arrowheads, and 4B) and those that were adjacent to Ufe1 to

(E) Wild-type cells and Δ*pep4* cells expressing EP-GFP-Ufe1 or EP-Sey1-GFP before and after different times of starvation were analyzed by SDS-PAGE and western blotting (WB). The same samples were run on a separate gel and stained with Coomassie to control for general protein content. Asterisk indicates unspecific bands.

(F) Vacuolar turnover of endogenous Ufe1 during normal cell growth (SD) and during starvation (SD-N) was measured using wild-type cells and Δ*pep4* cells in combination with cycloheximide (CHX) (see Experimental Procedures). Equal aliquots were removed from cell cultures at indicted times and analyzed by SDS-PAGE and western blotting (WB). Same membranes were cut and stained individually with antibodies against Ufe1 or Sey1. Asterisk indicates a non-specific band.

(G) Statistical analysis of remaining intracellular Ufe1 from experiments performed in (F). The mean values and SDs from four individual sets of experiments are shown.

See also Figure S2.

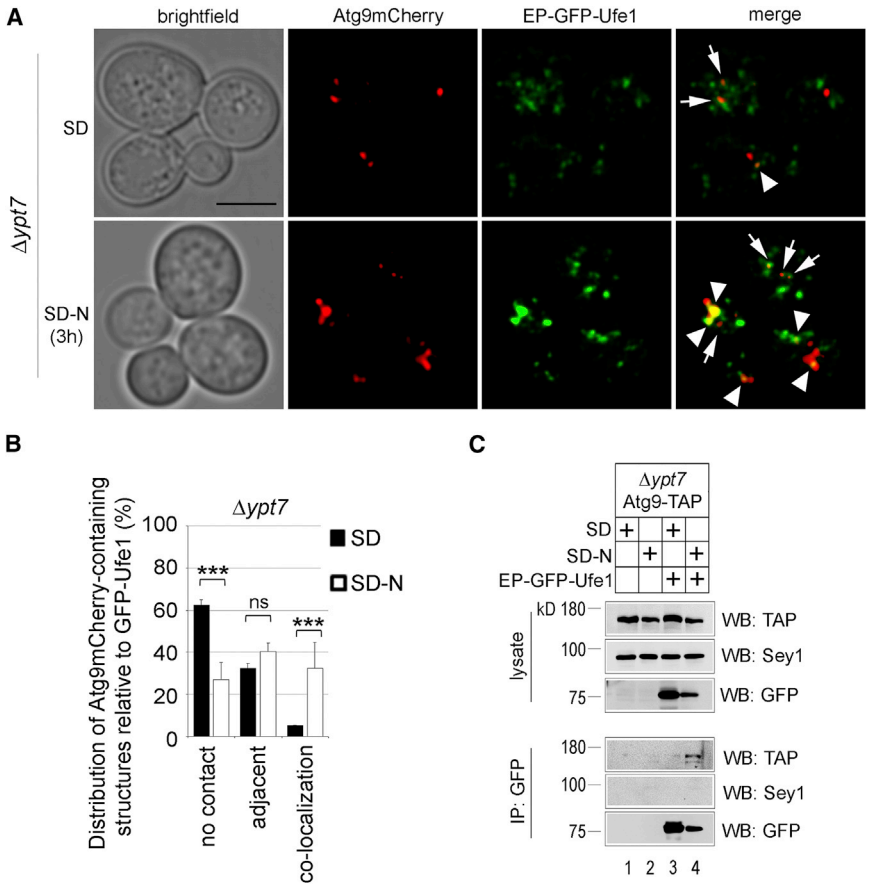

Figure 4. Starvation-Dependent Association of Ufe1 with Atg9

(A) Single scan confocal microscopy with Δ*ypt7* cells co-expressing EP-GFP-Ufe1 and Atg9mCherry before (SD) and after starvation (SD-N) at 30°C. Arrows indicate Ufe1 and Atg9 in adjacent structures. Arrowheads indicate co-localization. Scale bar, 3 μm.

(B) Statistical analysis of the relative distribution from experiments shown in (A). Atg9mCherry structures prior to starvation (243, n = 135) and after starvation (219, n = 65) were evaluated with respect to contact with GFP-Ufe1. n = number of cells. The mean values and SDs from four individual sets of assessments are shown (see Experimental Procedures). ***$p < 0.001$; not significant (NS) $p > 0.05$ (unpaired two-tailed Student's t test).

(C) CoIP of Atg9-TAP using EP-GFP-Ufe1. Δ*ypt7* cells co-expressing Atg9-TAP and EP-GFP-Ufe1 or control cells were used for coIP experiments (see Experimental Procedures) before and after starvation followed by SDS-PAGE and western blotting (WB). Same membranes were cut and individually stained with the indicated antibodies. See also Figure S4.

40% (Figures 4A, "SD-N," arrows, and 4B). This shows that during starvation, Ufe1-containing membranes increasingly target to sites that contain Atg9.

To test for a physical interaction, we co-expressed EP-GFP-Ufe1 and a chromosomally TAP-tagged version of Atg9 that was functional (Figure S4A) in Δ*ypt7* cells and performed coIP experiments. We could coIP both proteins in a starvation-dependent manner (Figure 4C, lanes 3 and 4). We did not detect Sey1 among the coIP proteins, showing a high level of specificity (Figures 4C and S4B). Physical interaction was also seen in the reverse pull-down using Atg9-TAP and TP-GFP-Ufe1 (Figure S4C). These data support a direct function for ER membranes containing Ufe1 in autophagosome formation. Although the physical interaction could suggest an exclusive functional link of Ufe1 to Atg9 during starvation, we did see clear differences in the behavior of GFP-Atg8 in Δ*atg9* cells compared to *ufe1-1* cells (Figure S4D, compare to Figure 1C), showing that the function of Ufe1 during autophagy is not linked exclusively to Atg9.

Since the ultimate vacuolar uptake of Ufe1 can occur independent of autophagosome formation (Figure S2F), we addressed the mechanism of Ufe1 transport from sites of autophagosome formation to the vacuole. The observation that Ufe1 accumulated in multiple puncta in Δ*ypt7* cells also after starvation suggested that vacuolar uptake could proceed through multivesicular bodies (MVBs), whose fusion with the vacuole also depends on Ypt7. When we expressed EP-GFP-Ufe1 in Δ*vps4* and Δ*vps32* cells, which are defective in the generation of MVBs, we did not detect free GFP (Figure S4E). The same result was obtained by fluorescence microcopy showing that vacuolar uptake after cellular starvation depends on MVBs (Figure S4F). This method also revealed that the minor fraction of GFP-Ufe1 that is constitutively exported under growing conditions accumulated in a single spot in Δ*vps32* cells, typical for a prevacuolar endocytic compartment formed in this mutant, termed the class E compartment (Figure S4F) (Piper et al., 1995). After starvation, Ufe1 was accumulated in multiple puncta per cell (Figure S4F) although the class E compartment is known to remain coalesced in a single spot (Müller et al., 2015). This supports the idea that starvation-dependent export of Ufe1 has a distinct cellular function compared to the constitutively exported minor fraction under growing conditions.

The regulation of autophagosome biogenesis affects autophagosome sizes and their numbers (Jin and Klionsky, 2014). Given the connection of Ufe1 to Atg9 and to general membrane traffic, we addressed whether Ufe1 function affects autophagosome sizes and/or their numbers. To measure sizes of autophagosomes, we performed thin-section electron microscopy. To prevent breakdown of autophagosomes inside the vacuole, cells where treated with the protease inhibitor PMSF during starvation. Larger numbers of autophagosomes inside the vacuole, also called autophagic bodies (ABs), were frequently seen in wild-type cells, as expected (Figure 5A, left panel, arrows). In agreement with fluorescence microscopy data, *ufe1-1* cells failed to

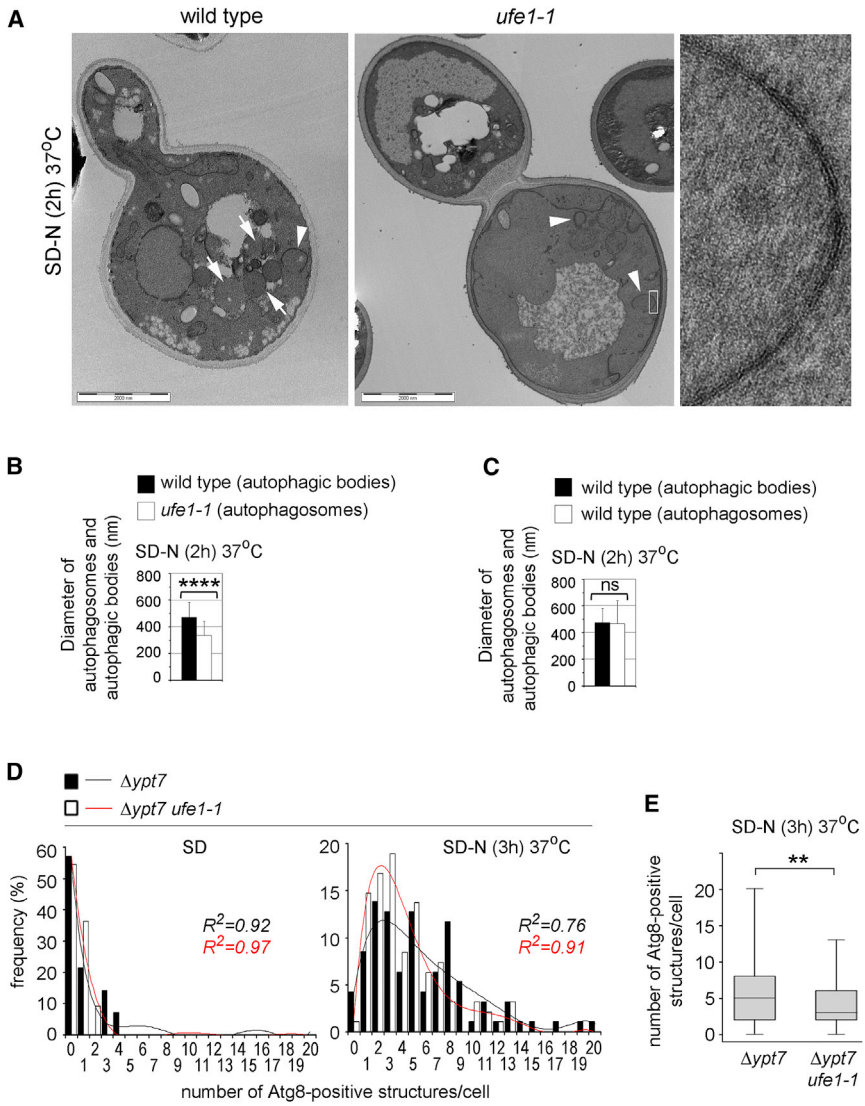

Figure 5. Ufe1 Function Affects Size and Number of Autophagosomes and Their Fusion with the Vacuole

(A) Analysis of wild-type cells and *ufe1-1* cells by electron microscopy after 2 hr of starvation at 37°C in presence of PMSF. Arrows indicate examples of autophagic bodies (ABs) inside the vacuole of a wild-type cell; arrowheads indicate cytosolic autophagosomes in a wild-type cell and in a *ufe1-1* cell. The boxed section of the middle panel is enlarged on the right to illustrate the autophagosomal double membrane. Scale bars, 2,000 nm.

(B) Diameters of ABs (n = 184) in wild-type cells and of autophagosomes (n = 52) in *ufe1-1* cells obtained from (A) were measured with iTEM software. The mean values and SDs are shown. ****$p < 0.0001$ (unpaired two-tailed Student's t test).

(C) Comparison of the diameters of occasionally visible autophagosomes (n = 15) (arrowhead in A) with ABs in wild-type cells. The mean values and SDs are shown. NS $p > 0.05$ (unpaired two-tailed Student's t test).

(D) Determination of numbers of Atg8-positive structures. Δ*ypt7* and Δ*ypt7ufe-1* cells expressing GFP-Atg8 were analyzed before and after starvation at 37°C using laser scanning fluorescence microscopy in combination with three-dimensional reconstruction (see Supplemental Experimental Procedures and Figure S5A). Scans from 14 and 94 Δ*ypt7* cells and from 22 and 95 Δ*ypt7ufe-1* cells were analyzed before and after starvation, respectively, at 37°C. The distribution of cells containing a particular number of GFP-Atg8-positive structures is shown in histograms together with polynomial regression lines and their respective R^2 values.

(E) Box plot together with statistical analysis of the results obtained from (D). **$p < 0.01$ (two-sample F-test for variances).

See also Figure S5.

show ABs but often showed cytosolic autophagosomes, identifiable by a double membrane that enclosed material with the same electron-density like the surrounding cytosol (Figure 5A, middle panel, arrow heads, right panel). The majority of cytosolic autophagosomes in *ufe1-1* cells appeared spherical and closed, revealing no formation defect. Confocal laser scanning microscopy in combination with 3D reconstruction with *ufe1-1* cells expressing GFP-Atg8 also showed hollow structures that were closed in cross section (Figures S5A and S5B). However, the diameters of autophagosomes in *ufe1-1* cells were significantly smaller (335 ± 107 nm) than ABs in wild-type cells (472 ± 112 nm) (Figure 5B). To exclude that ABs differed in size from cytosolic autophagosomes, we measured the occasionally detectable cytosolic autophagosomes in wild-type cells (Figure 5A, left panel, arrow head). Both were indistinguishable in size from one another: 472 ± 112 nm versus 466 ± 174 nm (Figure 5C).

To measure numbers of autophagosomes with used the Δ*ypt7* background, where autophagosomes accumulate in the cytosol. Δ*ypt7* and Δ*ypt7ufe1-1* cells expressing GFP-Atg8 were analyzed by confocal scanning microscopy in combination with 3D reconstruction before and after starvation for 3 hr at 37°C. The number of Atg8-positive structures per cell multiplied in both strains after starvation but cells with defective Ufe1 contained on average significantly fewer autophagosomes (Figures 5D and E). These data demonstrate that Ufe1 function also affects the number of autophagosomes.

To independently confirm our findings that Ufe1 function affects autophagosome biogenesis, we used a recently developed autophagosome pelleting assay where autophagosomes are accumulated in the Δ*ypt7* background and then pelleted with medium-speed density centrifugation, using GFP-Atg8 as marker (Yamamoto et al., 2012). Control experiments with wild-type cells, Δ*ypt7* cells, and Δ*atg16* cells showed the functionality of the assay (Figure S5C, lanes 1–9). We found that Δ*ypt7ufe1-1* cells showed reduction of more than 50% in pelleting efficiency when compared to Δ*ypt7* cells after starvation at

the non-permissive temperature (Figures S5C, lanes 10–15, and S5D), confirming a defect in autophagosome biogenesis under these conditions.

Together, our data show that cells with non-functional Ufe1 produce several distinct phenotypes with respect to autophagy: autophagosomes are reduced in size and number and they are unable to fuse with the vacuole. As a SNARE protein, Ufe1 might be important for all processes. Since Ufe1 is not permanently incorporated into autophagosomes, the observed defect in fusion with the vacuole could be indirect. In attempt to address in which membrane fusions relevant for autophagy Ufe1 participates, we tested the in vivo binding of the Qa-SNARE Ufe1 to non-ER Qb/c- or R-SNAREs with a role in autophagosome formation or in autophagosome vacuole fusion. The Qb-SNARE Vti1 and the R-SNARE Ykt6 are involved in autophagosome formation (Ishihara et al., 2001; Nair et al., 2011). Both SNARE proteins could be coIP with TP-GFP-Ufe1 after starvation (Figure S5E). In a control experiment, the R-SNARE protein Nyv1 with no role in autophagy (Nair et al., 2011) failed to bind to TP-GFP-Ufe1 (Figure S5E). Likewise, the Qb/c SNARE Vam7, with a well-established role in fusion of autophagosomes with the vacuole did not bind to Ufe1 (Figure S5F). Together, these results support a role for Ufe1 in the biogenesis of autophagosomes, whereas the fusion defect of autophagosomes with vacuoles could be indirect.

Next, we addressed the cellular pathway for the export of Ufe1 from the ER. Export of cargo from the ER mostly depends on the early secretory pathway and is mediated by COPII vesicles (Miller and Schekman, 2013). We expressed EP-GFP-Ufe1 in temperature-sensitive mutants of the early secretory pathway (*sec18-1*, *sec22-3*) part of which were COPII mutants (*sec13-1*, *sec23-1*, *sec31-1*) and performed fluorescence microscopy. After starvation, Ufe1 was visible inside the vacuole at the permissive (22°C) and at the non-permissive temperature (37°C) in wild-type cells (Figure 6A). In *sec22-3*, *sec13-1*, and *sec18-1* cells, vacuolar signal was visible at 22°C but not at 37°C, indicating that the ER exit of Ufe1 relied on the early secretory pathway and on COPII vesicles (Figure 6A). Two mutants produced unusual phenotypes. In *sec23-1* cells, ER exit of Ufe1 appeared to be blocked even after starvation at 22°C (Figure 6A). In *sec31-1* cells, ER exit of Ufe1 still occurred even at 37°C, and Ufe1 was visible inside the vacuole to an elevated extent also prior to starvation (Figure 6A). Western blot analysis with cell lysates from the same experiments confirmed that *sec23-1* cells produced severely reduced amounts of free GFP at 22°C compared to control cells, whereas *sec31-1* cells showed elevated levels of free GFP prior to starvation and increasing amounts of free GFP after starvation at 37°C, comparable with wild-type cells, in agreement with the microscopy data (Figures 6B and 6C). In contrast to these phenotypes during starvation, both mutants show normal growth at 22°C, indicating a functional secretory pathway, and no growth at 37°C, indicating a blocked secretory pathway, as expected (Figure S6A). However, it was known previously that the *sec31-1* mutant is less restrictive at 37°C during starvation, probably as a result of a compensatory mechanism (Hamasaki et al., 2003). At the same time, it is unknown whether *sec23-1* cells possess a similar starvation-dependent difference in sensitivity at 22°C. To address this issue, we measured the ER export of the model substrate CPY during starvation in *sec23-1* and *sec31-1* cells. In agreement with published data (Hamasaki et al., 2003), *sec31-1* cells showed CPY maturation comparable with that of wild-type cells at 37°C, showing that the observed Ufe1 export is part of a general phenomenon seen with *sec31-1* cells (Figures S6B and S6C). On the other hand, CPY maturation was comparable between wild-type cells and *sec23-1* cells at 22°C, suggesting that the observed reduction in Ufe1 export under the same conditions is not a general phenomenon (Figures S6B and S6C). To confirm this finding, we tested another substrate. KWW, a chimeric membrane protein, behaved like CPY: its ER export was unaffected at 22°C and reduced at 37°C during starvation (Figures S6D and S6E). Together, these data demonstrate that *sec23-1* cells display a specific ER export defect for Ufe1 at the permissive temperature during starvation.

These findings provided us with a tool to test for the correlation of Ufe1 transport with functional autophagy under conditions where the secretory pathway is intact. As expected, the co-localization of GFP-Ufe1 with Atg9mCherry after starvation was strongly reduced in Δ*ypt7sec23-1* cells at 22°C compared to Δ*ypt7* cells (Figure S7A). To test whether *sec23-1* cells are deficient for autophagy at 22°C, we plated cells on starvation medium in combination with the vital dye Phloxine B (Tsukada and Ohsumi, 1993). Indeed, of all mutants tested, only *sec23-1* cells showed increased sensitivity to starvation over a time course of several days (Figures 7A and 7B). Although autophagy seemed not deficient in *sec23-1* cells during shorter periods of starvation when judged visually by transport of GFP-Atg8 to the vacuole with fluorescence microscopy (Figure S7B), it became apparent when we used the GFP-Atg8 processing assay, which yielded fewer free GFP in *sec23-1* cells compared to wild-type cells and *sec18-1* cells at 22°C (Figures S7C and S7D). These results prompted us to analyze *sec23-1* cells at the ultrastructural level. Cells were starved at 22°C in the presence of PMSF and analyzed by electron microscopy. ABs were visible inside the vacuoles of both wild-type cells and *sec23-1* cells (Figure 7C). The diameters of ABs that were generated under these conditions and in this background did not differ significantly between wild-type cells (320 ± 61 nm) and *sec23-1* cells (345 ± 95 nm) (Figure 7D). However, *sec23-1* cells contained on average markedly fewer ABs than wild-type cells (Figure 7E). A statistical analysis for which we included results obtained with *sec18-1* cells revealed that the reduction in the number of autophagosomes in *sec23-1* cells was significant (Figure 7F). Together, these data reveal that *sec23-1* cells are deficient in autophagosome biogenesis at the permissive temperature. This deficiency correlates with the observed specific reduction in export of Ufe1 from the ER and lend independent support to a role of Ufe1-containing ER membranes in the biogenesis of autophagosomes.

DISCUSSION

Our data show that the Qa/t-SNARE Ufe1 plays a role in autophagy. In combination with the observed particular itinerary of Ufe1 during starvation, our findings reveal that autophagy-specific regulation of membrane traffic involves the mobilization of

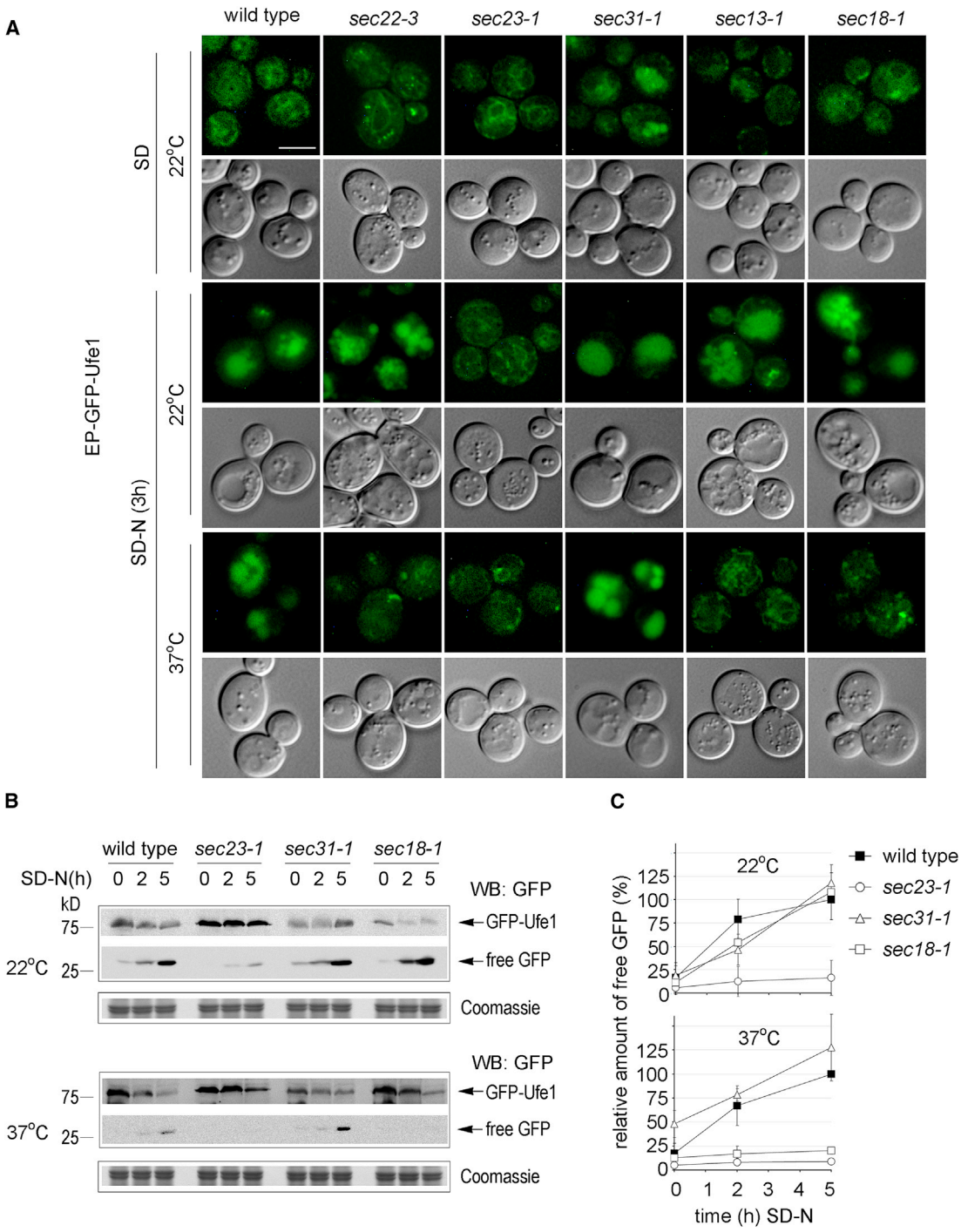

Figure 6. ER Export of Ufe1 Depends on the Secretory Pathway and Is Hypersensitive to the *sec23-1* Mutation

(A) Live cell fluorescence microscopy of wild-type cells and the indicated mutant strains expressing EP-GFP-Ufe1 before and after starvation at the indicated temperatures. Scale bar, 3 μm.

(B) GFP processing assay. The indicated mutants expressing EP-GFP-Ufe1 were starved at the indicated temperatures and analyzed by SDS-PAGE and western blotting (WB). The upper parts of the membranes were overexposed to reveal the fainter GFP-Ufe1 bands. A lower part of the gel was stained with Coomassie as loading control.

(C) Quantifications of free GFP generated in wild-type cells and mutant cells from experiments shown in (B). The amount of free GFP generated in individual strains at different times was normalized to the amount of free GFP generated after 5 hr starvation in wild-type cells (set to 100%) within the same set of experiments. The mean values and SDs from at least three independent sets of experiments are shown.

See also Figure S6.

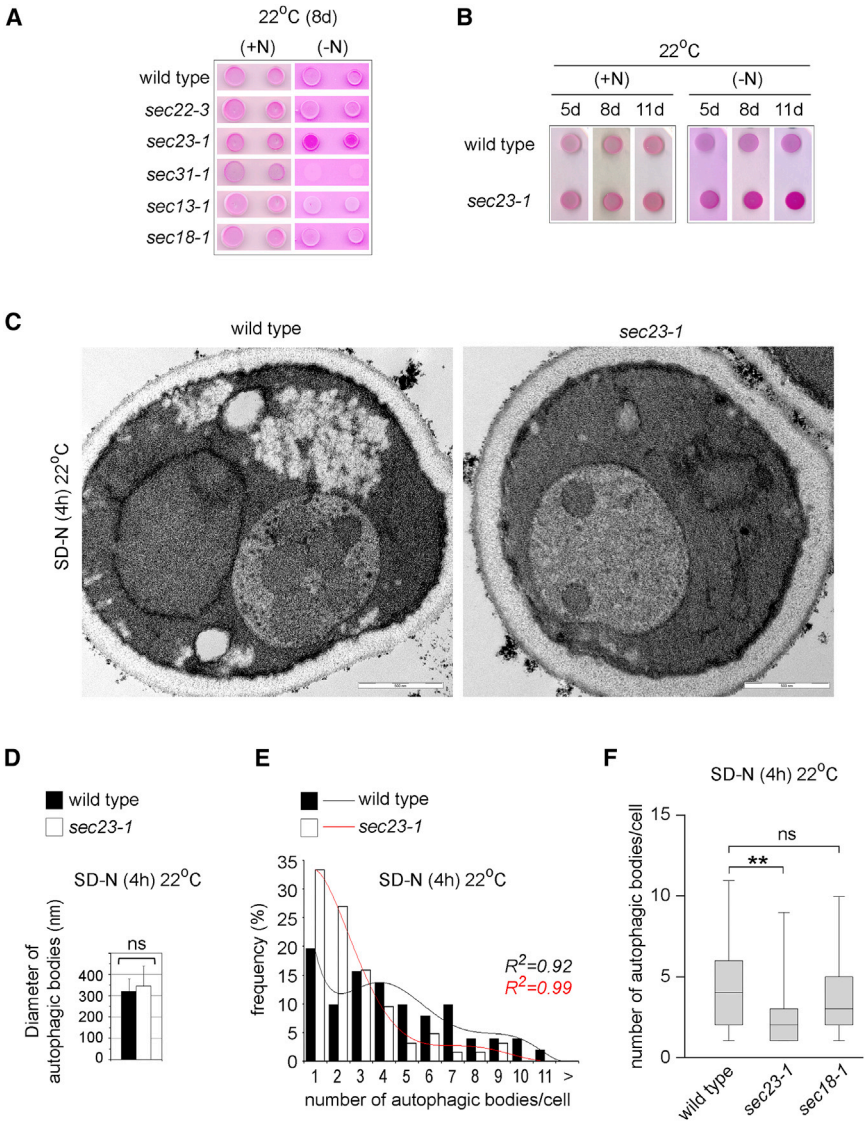

Figure 7. The *sec23-1* Mutant Is Deficient in Autophagy at the Permissive Temperature

(A) Wild-type cells and the indicated mutant cells were spotted in two distinct dilutions onto plates containing minimal medium and the vital dye Phloxine B in presence (+N) or absence (−N) of ammonium sulfate and incubated at 22°C. Plates were imaged after 8 days.

(B) Wild-type cells and *sec23-1* cells were spotted on plates like in (A) and repeatedly imaged after the indicated number of days.

(C) Analysis of wild-type cells and *sec23-1* cells by electron microscopy after 4 hr of starvation at 22°C in presence of PMSF. Representative examples of cells with visible ABs are shown. Scale bars, 500 nm.

(D) The diameters of individual ABs in wild-type cells and in *sec23-1* cells obtained from (C) were measured with iTEM software. The mean values and SDs are shown. NS $p > 0.05$ (unpaired two-tailed Student's t test).

(E) Histogram showing the distribution of cells with a particular number of ABs together with polynomial regression lines and their respective R^2 values. Fifty-one wild-type cells and 63 *sec23-1* cells with at least one AB inside the vacuole from experiments in (C) were imaged and their individual number of ABs counted.

(F). Box plot together with statistical analysis of the results obtained from (E) and including results obtained from the parallel analysis of 37 *sec18-1* cells. NS $p > 0.05$, $^{**}p < 0.01$ (two-sample F test for variances).

See also Figure S7.

SNARE proteins that are at the core of most membrane fusion machineries and that, in case of Ufe1, are thought to be organelle-specific. This mechanism adds a layer of regulation to the previous findings that starvation leads to a relocalization of membrane fusion regulators of the Rab protein family and to a modulation of membrane tethers in order to direct particular membrane traffic to sites of autophagosome formation (Popovic et al., 2012; Tan et al., 2013).

Our findings suggest that the export of membranes from the ER for the purpose of autophagosome formation depends on specific COPII vesicles. Although we have only limited data, the incorporation of Ufe1 and the particular sensitivity to the *sec23-1* allele for their ER export clearly separate them from "more conventional" transport vesicles. The sensitivity to the *sec23-1* allele, which affects the inner layer of the COPII coat, could reflect specific conformational requirements for coat proteins for the formation of vesicles with different shapes (Miller and Schekman, 2013). Interestingly, in mammalian cells, specific (in this case unusually small) COPII vesicles are generated during starvation for the biogenesis of autophagosomes (Ge et al., 2013).

Which membrane fusion steps are catalyzed by Ufe1 during autophagosome biogenesis remains to be elucidated and needs testing in suitable in vitro assays together with candidate partner SNAREs. Our finding that Ufe1 interacts physically with Ykt6 and Vti1 in vivo under conditions of starvation is consistent with the formation of SNARE complexes that do not form under growing conditions but might catalyze particular membrane fusions during starvation, such as for the elongation of phagophores. The common phenotype with respect to autophagosome biogenesis that we have obtained with *ufe1-1* cells at 37°C and with *sec23-1* cells at 22°C was a reduction in the number of autophagosomes. Previous work has established a link between the number of autophagosomes and the available membrane supply for autophagosome biogenesis (Jin et al., 2014). In agreement with these data, inefficient supply of Ufe1-containing membranes in *sec23-1* cells or their inefficient integration into membrane pools for the biogenesis of autophagosomes in *ufe1-1* cells can explain the observed reduction in the number of autophagosomes in

both cases. The additional phenotype of smaller autophagosomes seen in *ufe1-1* cells at 37°C could reflect a consequence of the SNARE to misfold after having been localized to sites relevant for the biogenesis of autophagosomes.

Whereas several independent results support a role of Ufe1 in autophagosome biogenesis, we do not have results supporting a role of Ufe1 in the fusion of autophagosomes with the vacuole. Although the failure of binding to Vam7 is a negative evidence, we also could not observe Ufe1 on the vacuolar rim as the expected post-fusion localization. It might be that rapid retrieval followed by targeting to MVBs prevented the detection. In mammalian cells, the Qa/t-SNARE protein syntaxin 17 (STX17) was shown to have an exclusive role in mediating the fusion of autophagosomes with the lysosome (Itakura et al., 2012). Although STX17 is not the sequence homolog of Ufe1, a fraction of the protein is likewise found in the ER membrane where it has a role in initiation of autophagosome formation (Hamasaki et al., 2013). However, for fusing autophagosomes with lysosomes, STX17 is recruited directly to autophagosomes from a cytosolic pool (Itakura et al., 2012). It thus remains to be tested whether the known functions of Ufe1 and STX17 during autophagy contain common and evolutionary conserved features.

Rapid retrieval of Ufe1 from autophagosomal membranes could reflect a cellular mechanism to define membrane identity; it would also serve to permit several rounds of fusion. The ultimate targeting of Ufe1 to the vacuole via MVBs might not be surprising considering the close structural and functional connections of autophagosomes with the endosomal system (Biazik et al., 2015; Müller et al., 2015). Endosomes can exchange lipids and probably other material with Atg9 vesicles (Mari et al., 2010; Ohashi and Munro, 2010). Endosomes are also important suppliers of membranes for autophagosome formation in mammalian cells (Puri et al., 2013).

Our findings open a series of questions that are currently being addressed. Foremost, how is Ufe1 incorporated into ER vesicles and how is it regulated? Are the other ER-localized SNAREs similarly exported during autophagy? What else distinguishes the specific COPII vesicles for the autophagosome biogenesis from vesicles transporting cargo along the secretory pathway? Which membrane fusion reactions are catalyzed by Ufe1 during for the formation of autophagosomes, and what are the partner SNARE proteins for these fusions? Answers to these questions will provide a detailed picture of the contribution of the ER to autophagosome formation by vesicular transport.

EXPERIMENTAL PROCEDURES

Construction of Plasmids and Yeast Strains Used in This Study

A description for the construction of plasmids is given in the Supplemental Experimental Procedures. Yeast strains are listed in Table S1.

Electron Microscopy

Cells were grown to optical density (OD) 600 of 0.5, washed, resuspended in starvation (SD-N) medium (1.7% yeast nitrogen base without amino acids and ammonium sulfate, with 2% glucose) containing 1 mM PMSF and incubated for the indicated times at the indicated temperatures. Cultures were harvested by centrifugation, fixed in 1.5% $KMnO_4$ in water for 20 min at 24°C, washed, and stained with 2% uranyl acetate for 1 hr, dehydrated through a graded series of ethanol and propylene oxide, embedded in Epon resin (Ted Pella), and polymerized at 60°C for 2 days. Thin sections were cut with an ultramicrotome (Leica UC7) using a diamond knife (Diatome 45°) and examined in a Philips CM10 transmission electron microscope operating at 80 kV. Digital images were acquired with a side port 4 Mpx camera (Veleta, Olympus). The size of autophagosomes was analyzed with iTEM software (Olympus).

GFP-Processing Assays

Cells were grown overnight, diluted to OD 0.2, and regrown for 5 hr, washed, resuspended in SD-N medium, and continued. Removed aliquots were lysed by alkaline treatment (Kushnirov, 2000), resuspended in a cell-density normalized volume of loading buffer, followed by SDS-PAGE and western blotting using anti-GFP antibody (Roche), HRP-conjugated anti-mouse secondary antibody (Roche), and ECL (Pierce) as substrate. Images were taken with a LAS-3000 mini imaging system (Fujifilm) and bands were quantified using Multi-Gauge software (Fujifilm).

Fluorescence Microscopy

Cells were grown to OD 600 of 0.2 at the permissive temperature, washed, resuspended in SD-N medium, incubated for the indicated times, and immediately analyzed by live cell imaging using an Olympus BX61 microscope equipped with a 100×/1.4 PlanApo oil-immersion lens and a conventional FITC cube as well as a DIC prism and polarizer for Normarksi imaging. Images were acquired with a DP70 camera and the DPcontroller software (Olympus). Mutants with temperature-sensitive alleles were shifted to the non-permissive temperature simultaneously with the start of starvation.

Confocal Microscopy

Cells were mildly fixed by addition of 2% of paraformaldehyde (PFA) for 30 min, washed, resuspended in PBS, and scanned with a laser-scanning confocal microscope from Zeiss (LSM 7 Duo) equipped with a binary GaAsP (BiG) module using a Plan-Apochromat objective 63×/1,40 Oil DIC. A 488 nm argon laser (GFP) and a 594 nm helium-neon laser were used (RFP and mCherry).

Co-localization Analysis

For statistical analysis of co-localization ZEN software (ZEISS) was used to project images from individual channels. Structures that entirely overlapped were defined as co-localized, partially overlapping or contacting structures were defined as adjacent, otherwise they were defined as no contact. Counting was performed independently by two individuals and repeated twice.

Cycloheximide Shut-Off Experiments

The shut-off was started by addition of 200 μg/ml cycloheximide (CHX) to exponentially growing or starving cells, as indicated. Equal volume aliquots of cell culture were removed at indicated time points and lysed by alkaline treatment (Kushnirov, 2000). Samples were analyzed by SDS-PAGE followed by western blotting with the indicated antibodies.

CoIP

Cell cultures (200 ml) were grown to mid-log phase, washed, and starved, lysed by grinding in liquid nitrogen (1× PBS, 1 mM EDTA, 1 mM PMSF, and protein inhibitor cocktail [Roche]). Lysates were cleared, solubilized by addition of 1% digitonin (Calbiochem) for 30 min, cleared by centrifugation for 20 min at 100,000 × *g* followed by incubation with GFP-trap resin (Chromotek) or with IgG-coupled magnetic beads (Life Technologies). Washing was done in lysis buffer with 0.5% digitonin followed by elution in SDS-loading buffer.

Chemical crosslinking prior to coIP was done according to Müller et al. (2011). Briefly, freshly prepared PFA was added to cells prior to lysis to a final concentration of 1%, incubated for 20 min at 30°C. Cells were moved to ice for 15 min and PFA was quenched by addition of 500 mM glycine. Cells were lysed, membranes solubilized with 1% Triton X-100 (Sigma) for 30 min, and samples were processed like described above. Prior to performing SDS-PAGE, crosslinks were reversed by incubation of samples at 100°C for 30 min.

Phloxine B Plating Assay

Cells were grown in liquid culture in rich medium and spotted onto plates containing 20 μg/ml Phloxine B (Sigma) in synthetic medium with auxotrophic nutrients and nitrogen base with or without ammonium sulfate.

SUPPLEMENTAL INFORMATION

Supplemental Information includes Supplemental Experimental Procedures, seven figures, and one table and can be found with this article online at http://dx.doi.org/10.1016/j.celrep.2016.01.047.

AUTHOR CONTRIBUTIONS

Acquisition of Data, L.L., J.L.R., N.S., and V.G.; Analysis and Interpretation of Data, L.L. and V.G.; Drafting or Revising the Article, L.L. and V.G.; Conception and Design, V.G.

ACKNOWLEDGMENTS

We thank Randy Schekman, Bil Wickner, Amy Orr, Will Prinz, Hugh Pelham, Mike Lewis, Junji Hu, Sebastian Chávez, Manolo Muñiz, Pedro Carvalho, Stefan Jentsch, Daniel Klionsky, Maria Jesus Mazon, Henning Arlt, Fulvio Reggori, and Jose Luis Crespo for yeast strains, antibodies, reagents, and advice; Javier Manzano and Eeva-Liisa Eskelinen for suggestions for electron microscopy; and Pedro Carvalho, Alexander Stein, and Tom Rapoport for critical reading of the manuscript. L.L. was supported by an EMBO short-term fellowship (EMBO ASTF 293-2015). This work was supported by grants of the Spanish Ministry of Science (BFU2009-07290) and the Ramón y Cajal program to V.G, and (BFU2014-59309-P).

Received: January 12, 2015
Revised: November 11, 2015
Accepted: January 13, 2016
Published: February 11, 2016

REFERENCES

Anwar, K., Klemm, R.W., Condon, A., Severin, K.N., Zhang, M., Ghirlando, R., Hu, J., Rapoport, T.A., and Prinz, W.A. (2012). The dynamin-like GTPase Sey1p mediates homotypic ER fusion in S. cerevisiae. J. Cell Biol. *197*, 209–217.

Bernales, S., Schuck, S., and Walter, P. (2007). ER-phagy: selective autophagy of the endoplasmic reticulum. Autophagy *3*, 285–287.

Biazik, J., Ylä-Anttila, P., Vihinen, H., Jokitalo, E., and Eskelinen, E.L. (2015). Ultrastructural relationship of the phagophore with surrounding organelles. Autophagy *11*, 439–451.

Braun, S., and Jentsch, S. (2007). SM-protein-controlled ER-associated degradation discriminates between different SNAREs. EMBO Rep. *8*, 1176–1182.

Chen, Y., and Klionsky, D.J. (2011). The regulation of autophagy - unanswered questions. J. Cell Sci. *124*, 161–170.

Cheong, H., and Klionsky, D.J. (2008). Biochemical methods to monitor autophagy-related processes in yeast. Methods Enzymol. *451*, 1–26.

Dilcher, M., Veith, B., Chidambaram, S., Hartmann, E., Schmitt, H.D., and Fischer von Mollard, G. (2003). Use1p is a yeast SNARE protein required for retrograde traffic to the ER. EMBO J. *22*, 3664–3674.

Ge, L., Melville, D., Zhang, M., and Schekman, R. (2013). The ER-Golgi intermediate compartment is a key membrane source for the LC3 lipidation step of autophagosome biogenesis. eLife *2*, e00947.

Graef, M., Friedman, J.R., Graham, C., Babu, M., and Nunnari, J. (2013). ER exit sites are physical and functional core autophagosome biogenesis components. Mol. Biol. Cell *24*, 2918–2931.

Hamasaki, M., Noda, T., and Ohsumi, Y. (2003). The early secretory pathway contributes to autophagy in yeast. Cell Struct. Funct. *28*, 49–54.

Hamasaki, M., Noda, T., Baba, M., and Ohsumi, Y. (2005). Starvation triggers the delivery of the endoplasmic reticulum to the vacuole via autophagy in yeast. Traffic *6*, 56–65.

Hamasaki, M., Furuta, N., Matsuda, A., Nezu, A., Yamamoto, A., Fujita, N., Oomori, H., Noda, T., Haraguchi, T., Hiraoka, Y., et al. (2013). Autophagosomes form at ER-mitochondria contact sites. Nature *495*, 389–393.

Hayashi-Nishino, M., Fujita, N., Noda, T., Yamaguchi, A., Yoshimori, T., and Yamamoto, A. (2009). A subdomain of the endoplasmic reticulum forms a cradle for autophagosome formation. Nat. Cell Biol. *11*, 1433–1437.

Hu, J., Shibata, Y., Zhu, P.P., Voss, C., Rismanchi, N., Prinz, W.A., Rapoport, T.A., and Blackstone, C. (2009). A class of dynamin-like GTPases involved in the generation of the tubular ER network. Cell *138*, 549–561.

Ishihara, N., Hamasaki, M., Yokota, S., Suzuki, K., Kamada, Y., Kihara, A., Yoshimori, T., Noda, T., and Ohsumi, Y. (2001). Autophagosome requires specific early Sec proteins for its formation and NSF/SNARE for vacuolar fusion. Mol. Biol. Cell *12*, 3690–3702.

Itakura, E., Kishi-Itakura, C., and Mizushima, N. (2012). The hairpin-type tail-anchored SNARE syntaxin 17 targets to autophagosomes for fusion with endosomes/lysosomes. Cell *151*, 1256–1269.

Jin, M., and Klionsky, D.J. (2014). Regulation of autophagy: modulation of the size and number of autophagosomes. FEBS Lett. *588*, 2457–2463.

Jin, M., He, D., Backues, S.K., Freeberg, M.A., Liu, X., Kim, J.K., and Klionsky, D.J. (2014). Transcriptional regulation by Pho23 modulates the frequency of autophagosome formation. Curr. Biol. *24*, 1314–1322.

Kirisako, T., Baba, M., Ishihara, N., Miyazawa, K., Ohsumi, M., Yoshimori, T., Noda, T., and Ohsumi, Y. (1999). Formation process of autophagosome is traced with Apg8/Aut7p in yeast. J. Cell Biol. *147*, 435–446.

Klionsky, D.J. (2007). Autophagy: from phenomenology to molecular understanding in less than a decade. Nat. Rev. Mol. Cell Biol. *8*, 931–937.

Kushnirov, V.V. (2000). Rapid and reliable protein extraction from yeast. Yeast *16*, 857–860.

Lewis, M.J., Rayner, J.C., and Pelham, H.R. (1997). A novel SNARE complex implicated in vesicle fusion with the endoplasmic reticulum. EMBO J. *16*, 3017–3024.

Lipatova, Z., and Segev, N. (2015). A role for macro-ER-phagy in ER quality control. PLoS Genet. *11*, e1005390.

Mari, M., Griffith, J., Rieter, E., Krishnappa, L., Klionsky, D.J., and Reggiori, F. (2010). An Atg9-containing compartment that functions in the early steps of autophagosome biogenesis. J. Cell Biol. *190*, 1005–1022.

McNew, J.A., Parlati, F., Fukuda, R., Johnston, R.J., Paz, K., Paumet, F., Söllner, T.H., and Rothman, J.E. (2000). Compartmental specificity of cellular membrane fusion encoded in SNARE proteins. Nature *407*, 153–159.

Miller, E.A., and Schekman, R. (2013). COPII - a flexible vesicle formation system. Curr. Opin. Cell Biol. *25*, 420–427.

Mochida, K., Oikawa, Y., Kimura, Y., Kirisako, H., Hirano, H., Ohsumi, Y., and Nakatogawa, H. (2015). Receptor-mediated selective autophagy degrades the endoplasmic reticulum and the nucleus. Nature *522*, 359–362.

Moreau, K., Ravikumar, B., Renna, M., Puri, C., and Rubinsztein, D.C. (2011). Autophagosome precursor maturation requires homotypic fusion. Cell *146*, 303–317.

Müller, V.S., Jungblut, P.R., Meyer, T.F., and Hunke, S. (2011). Membrane-SPINE: an improved method to identify protein-protein interaction partners of membrane proteins in vivo. Proteomics *11*, 2124–2128.

Müller, M., Schmidt, O., Angelova, M., Faserl, K., Weys, S., Kremser, L., Pfaffenwimmer, T., Dalik, T., Kraft, C., Trajanoski, Z., et al. (2015). The coordinated action of the MVB pathway and autophagy ensures cell survival during starvation. eLife *4*, e07736.

Nair, U., Jotwani, A., Geng, J., Gammoh, N., Richerson, D., Yen, W.L., Griffith, J., Nag, S., Wang, K., Moss, T., et al. (2011). SNARE proteins are required for macroautophagy. Cell *146*, 290–302.

Newman, A.P., Shim, J., and Ferro-Novick, S. (1990). BET1, BOS1, and SEC22 are members of a group of interacting yeast genes required for transport from the endoplasmic reticulum to the Golgi complex. Mol. Cell. Biol. *10*, 3405–3414.

Ohashi, Y., and Munro, S. (2010). Membrane delivery to the yeast autophagosome from the Golgi-endosomal system. Mol. Biol. Cell *21*, 3998–4008.

Ohsumi, Y. (2001). Molecular dissection of autophagy: two ubiquitin-like systems. Nat. Rev. Mol. Cell Biol. *2*, 211–216.

Patel, S.K., Indig, F.E., Olivieri, N., Levine, N.D., and Latterich, M. (1998). Organelle membrane fusion: a novel function for the syntaxin homolog Ufe1p in ER membrane fusion. Cell *92*, 611–620.

Piper, R.C., Cooper, A.A., Yang, H., and Stevens, T.H. (1995). VPS27 controls vacuolar and endocytic traffic through a prevacuolar compartment in Saccharomyces cerevisiae. J. Cell Biol. *131*, 603–617.

Popovic, D., Akutsu, M., Novak, I., Harper, J.W., Behrends, C., and Dikic, I. (2012). Rab GTPase-activating proteins in autophagy: regulation of endocytic and autophagy pathways by direct binding to human ATG8 modifiers. Mol. Cell. Biol. *32*, 1733–1744.

Puri, C., Renna, M., Bento, C.F., Moreau, K., and Rubinsztein, D.C. (2013). Diverse autophagosome membrane sources coalesce in recycling endosomes. Cell *154*, 1285–1299.

Reggiori, F., Wang, C.W., Nair, U., Shintani, T., Abeliovich, H., and Klionsky, D.J. (2004). Early stages of the secretory pathway, but not endosomes, are required for Cvt vesicle and autophagosome assembly in Saccharomyces cerevisiae. Mol. Biol. Cell *15*, 2189–2204.

Tan, D., Cai, Y., Wang, J., Zhang, J., Menon, S., Chou, H.T., Ferro-Novick, S., Reinisch, K.M., and Walz, T. (2013). The EM structure of the TRAPPIII complex leads to the identification of a requirement for COPII vesicles on the macroautophagy pathway. Proc. Natl. Acad. Sci. USA *110*, 19432–19437.

Tsukada, M., and Ohsumi, Y. (1993). Isolation and characterization of autophagy-defective mutants of Saccharomyces cerevisiae. FEBS Lett. *333*, 169–174.

Voeltz, G.K., Prinz, W.A., Shibata, Y., Rist, J.M., and Rapoport, T.A. (2006). A class of membrane proteins shaping the tubular endoplasmic reticulum. Cell *124*, 573–586.

Yamamoto, H., Kakuta, S., Watanabe, T.M., Kitamura, A., Sekito, T., Kondo-Kakuta, C., Ichikawa, R., Kinjo, M., and Ohsumi, Y. (2012). Atg9 vesicles are an important membrane source during early steps of autophagosome formation. J. Cell Biol. *198*, 219–233.

Ylä-Anttila, P., Vihinen, H., Jokitalo, E., and Eskelinen, E.L. (2009). 3D tomography reveals connections between the phagophore and endoplasmic reticulum. Autophagy *5*, 1180–1185.

Cell Reports, Volume *14*

Supplemental Information

An ER-Localized SNARE Protein Is Exported in Specific COPII Vesicles for Autophagosome Biogenesis

Leticia Lemus, Juan Luis Ribas, Natalia Sikorska, and Veit Goder

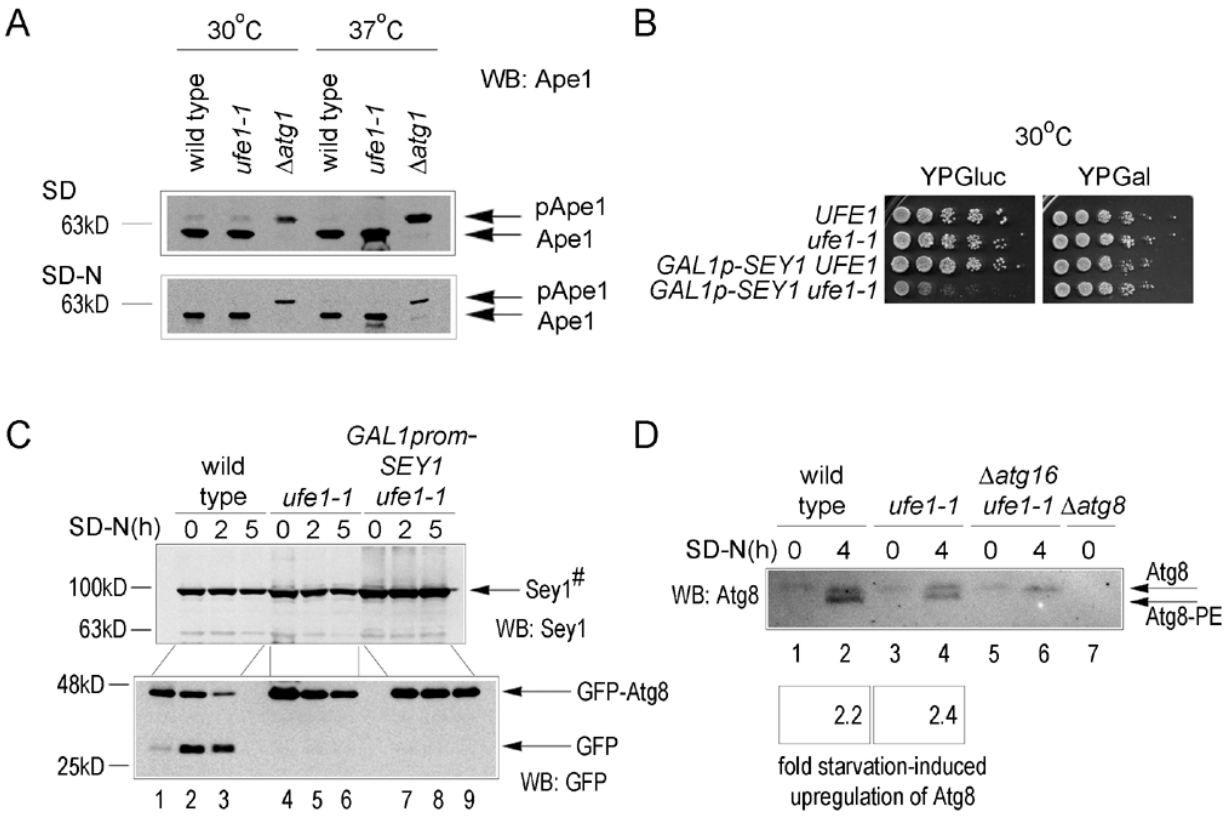

Figure S1, related to Figure 1. (A) Ufe1 does not belong to the core machinery of the Cvt-pathway. Wild type cells, *ufe1-1* cells and *Δatg1* cells, which are defective in the Cvt-pathway, were grown in rich (SD) medium at 30°C to mid-log phase and split. Equal fractions were continued to grow in SD medium or shifted to starvation (SD-N) medium and incubated at 30°C or at 37°C for 3 hours. Equal amounts of cells were lysed and cell lysates were analyzed by SDS-PAGE and Western blotting (WB). pApe1 indicates the cytosolic precursor form; Ape1 indicates the vacuolar mature form that appears after vacuolar import through the Cvt pathway. **(B)** Genetic interaction between *UFE1* and *SEY1*. Wild type cells (*UFE1*) and the indicated mutant cells with or without a genomic insertion of the Gal1 promoter (*GAL1p*) in front of the *SEY1* locus were spotted in dilution series on plates containing Glucose (YPGluc) or Galactose (YPGal) as carbon source and incubated for 2 days at 30°C. Glucose-mediated repression of *SEY1* causes a growth defect in combination with *ufe1-1*, indicating genetic interaction. **(C)** Overexpressing Sey1 does not rescue the defect in autophagy in *ufe1-1* cells. Wild type cells and the indicated mutant cells were grown overnight in rich media containing Raffinose as carbon source at 30°C. 2% Galactose was added to all strains to induce overexpression of *SEY1* in the *GAL1prom-SEY1 ufe1-1* strain. After incubation for 3 hours cells were shifted to 37°C and to SD-N medium containing Galactose. Equal amounts of cell lysates were removed after the indicated periods of time and analyzed by SDS-PAGE and Western blotting with either anti-Sey1 antibody or anti-GFP antibody. # The steady-state amount of Sey1 increased approximately 4.3 fold upon overexpression compared to wild type cells and *ufe1-1* cells. **(D)** Atg8 lipidation assay. Wild type cells and the indicated mutants were grown in rich medium to mid-log phase at 30°C and shifted to starvation medium at 37°C for 4 hours. Equal amounts of cell lysates were analyzed by SDS-PAGE containing 6M urea and by Western blotting with anti-Atg8 antibody. Lipidated Atg8 (Atg8-PE) is generated in wild type as well as in *ufe1-1* cells after starvation at 37°C but not in *ufe1-1Δatg16* cells. *Δatg8* cells served as control for antibody specificity. The amount of total Atg8 before and after starvation in wild type cells and in *ufe1-1* cells was quantified from Western Blot signal with Multi-Gauge software.

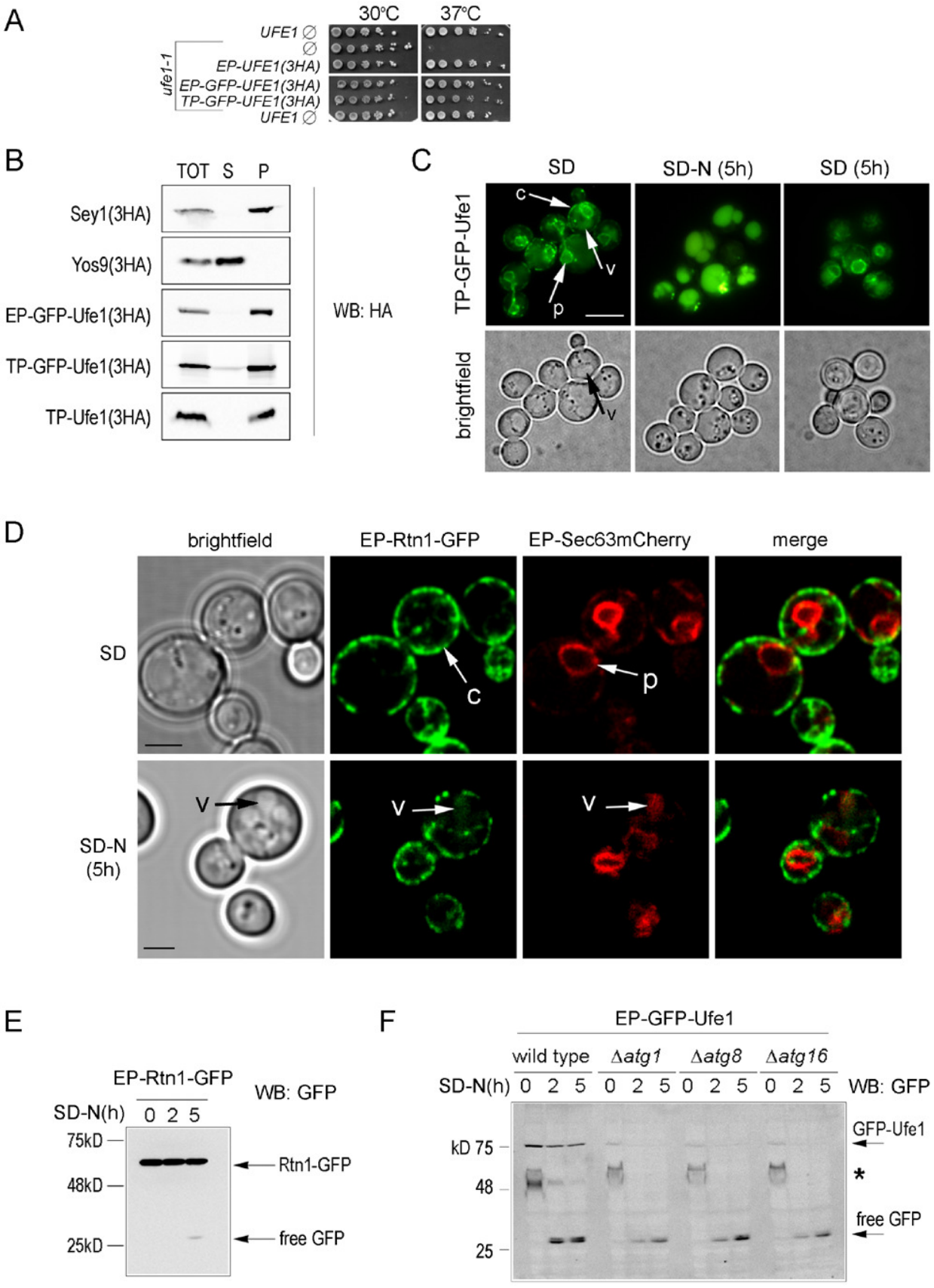
A
30°C
37°C
UFE1 ∅
∅
EP-UFE1(3HA)
ufe1-1
EP-GFP-UFE1(3HA)
TP-GFP-UFE1(3HA)
UFE1 ∅
B
TOT S P
Sey1(3HA)
Yos9(3HA)
EP-GFP-Ufe1(3HA)
TP-GFP-Ufe1(3HA)
TP-Ufe1(3HA)
WB: HA
C
SD
SD-N (5h)
SD (5h)
TP-GFP-Ufe1
brightfield
c
v
p
D
brightfield
EP-Rtn1-GFP
EP-Sec63mCherry
merge
SD
SD-N (5h)
c
p
v
E
EP-Rtn1-GFP
WB: GFP
SD-N(h) 0 2 5
75kD
48kD
25kD
Rtn1-GFP
free GFP
F
EP-GFP-Ufe1
wild type
Δatg1
Δatg8
Δatg16
SD-N(h) 0 2 5 0 2 5 0 2 5 0 2 5
WB: GFP
kD 75
48
25
GFP-Ufe1
*
free GFP

Figure S2, related to Figure 2. (A) Functionality tests of distinct tagged versions of Ufe1 by complementation analysis. Wild type cells (*UFE1*) and *ufe1-1* cells harboring an empty plasmid (Ø) or a CEN plasmid expressing the indicated construct were spotted in dilution series onto plates with synthetic media lacking uracil and incubated for 2 days at the indicated temperatures. The constructs were expressed under the control of the endogenous Ufe1 promoter (*EP*) or the TDH3 promoter (*TP*). EP-GFP-Sey1 was expressed from its chromosomal locus under the control of its endogenous promoter and was previously shown to be functional (Hu et al., 2009). **(B)** Membrane integration test of the distinct Ufe1 constructs by alkaline extraction. *ufe1-1* cells expressing the indicated Ufe1 constructs and control cells expressing a tagged version of the membrane integrated protein Sey1 (Sey1(3HA)) or the soluble ER luminal protein Yos9 (Yos9(3HA)) were treated like described in Supplemental Experimental Procedures and the distinct fractions were analyzed by SDS-PAGE and Western blotting with anti-HA antibodies. TOT=total, S=supernatant, P=pellet. **(C)** Starvation-dependent increase in ER exit of TP-GFP-Ufe1. TP-GFP-Ufe1 was functional (see Figures S2A and B). Wild type cells expressing TP-GFP-Ufe1 were grown to midlog phase at 30^{o}C in SD medium. At steady state, TP-GFP-Ufe1 was visible in the perinuclear (p) and cortical (c) ER as well as inside the vacuole (v). After 5 hours of starvation (SD-N (5h)) the vacuolar signal had increased dramatically and was dominant. Continuing growth in SD medium for 5 hours still showed a dominant signal from the perinuclear ER (SD (5h)). Scale bar: 5µm. **(D)** Additional ER-resident proteins were tested for starvation-dependent ER exit. A chromosomally GFP-tagged version of Rtn1 expressed from its endogenous promoter (EP-Rtn1-GFP) and a plasmid-borne mCherry-tagged version of Sec63 expressed from its endogenous promoter (EP-Sec63mCherry) were co-expressed in wild type cells. Cells were grown to midlog phase at 30^{o}C in SD medium and imaged (SD). Rtn1 was mainly visible in cortical ER (arrow, "c") and in tubules, whereas Sec63 was mainly visible in the perinuclear ER (arrow, "p"). After 5 hours of starvation (SD-N (5h)), dominant signals were still visible from cortical (Rtn1) and perinuclear (Sec63) ER. Few cells in the entire population started to show faint signals from both proteins inside the vacuole (arrow, "v"), indicating onset of starvation-dependent ER-phagy. Scale bars: 2µm. **(E)** Population-wide quantification of Rtn1-GFP targeting to the vacuole using the GFP processing assay. Wild type cells expressing chromosomally GFP-tagged Rtn1 (EP-Rtn1-GFP) were grown to midlog phase at 30^{o}C in SD medium and shifted to starvation. At the indicated times after start of starvation, aliquots were taken and analyzed by SDS-PAGE and Western Blotting (WB). Less than 1% of free GFP compared to total signal was measured after 5 hours of starvation, in agreement with the microscopy data. **(F)** EP-GFP-Ufe1 is targeted to the vacuole in a starvation-dependent manner in autophagy mutants. Wild type cells and the indicated mutant strains expressing EP-GFP-Ufe1 were grown in SD medium to mid-log phase and shifted to SD-N medium for the indicated periods of time and analyzed by SDS-PAGE and Western Blot (WB). Asterisk indicates unspecific bands.

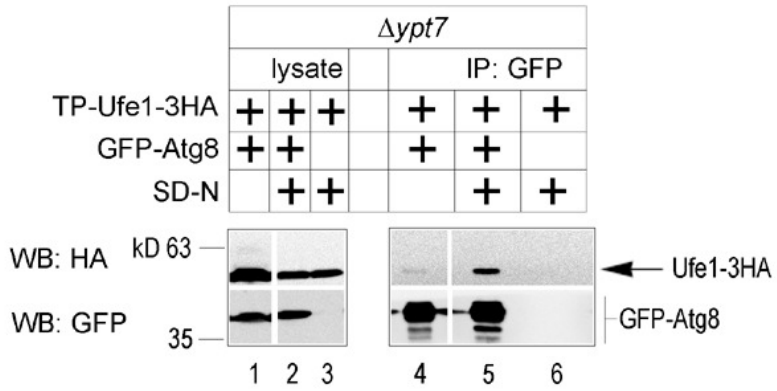

Figure S3, related to Figure 3. Starvation-dependent interaction of TP-Ufe1-3HA with GFP-Atg8. *Δypt7* cells expressing TP-Ufe1-3HA or co-expressing TP-Ufe1-3HA and GFP-Atg8 were grown at 30°C in SD medium to mid-log phase and, if indicated, were shifted to SD-N medium for 2 hours. Cells were lysed and membranes solubilized with digitonin, followed by immunoprecipition (IP) with anti-GFP beads, SDS-PAGE and Western Blotting (WB) with the indicated antibodies.

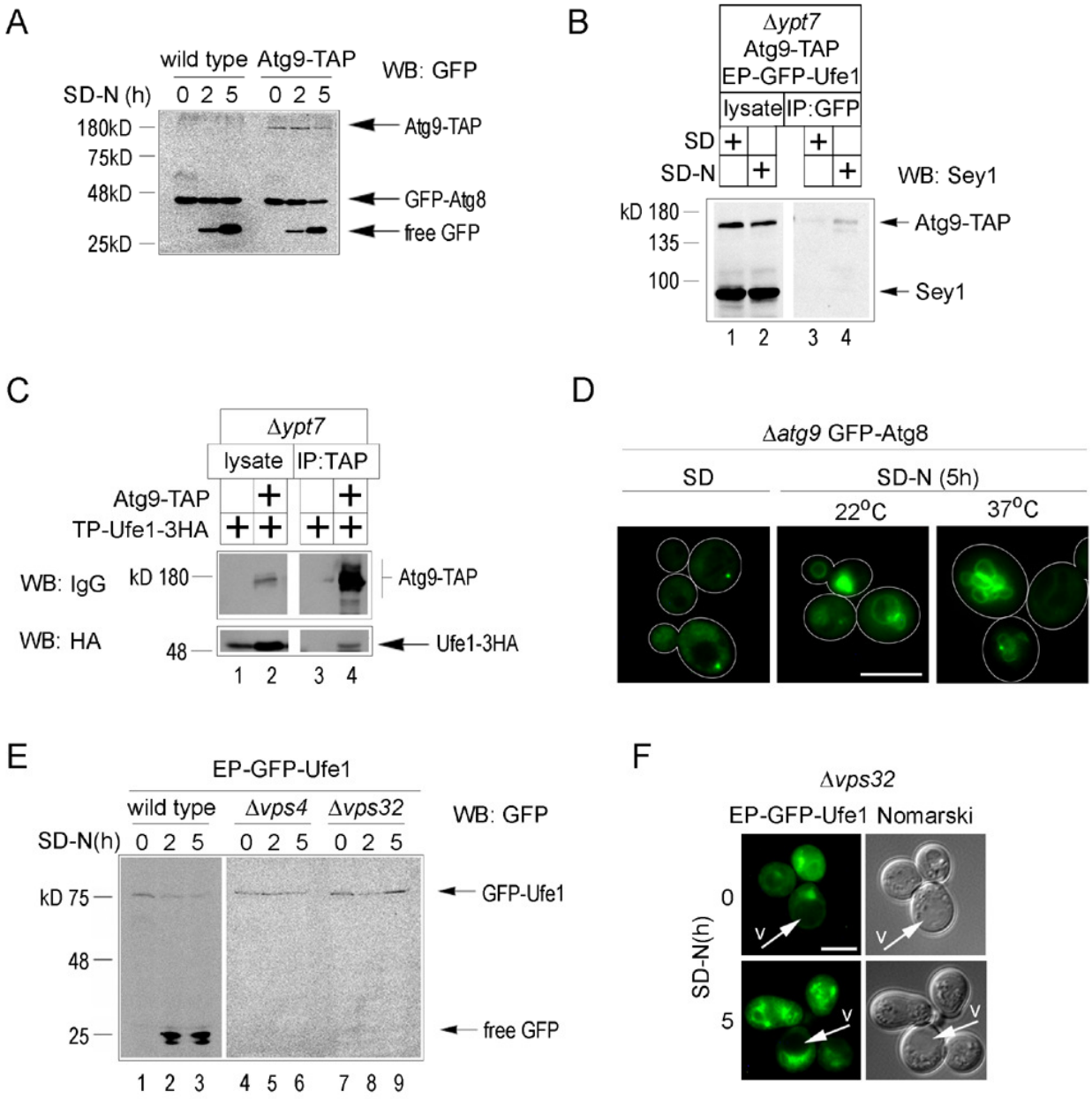

Figure S4, related to Figure 4. **(A)** Functionality test for TAP-tagged Atg9. Wild type cells and cells with chromosomally TAP-tagged Atg9 expressing GFP-Atg8 were grown in SD medium to mid-log phase and shifted to SD-N medium for the indicated periods of time before being analyzed by SDS-PAGE and Western Blotting. The TAP tag of Atg9 was recognized by the secondary antibody against the anti-GFP antibody. Note that GFP-Atg8 processing in cells expressing Atg9-TAP was comparable to that in wild type cells, showing that Atg9-TAP is functional for autophagy. **(B)** Physical interaction of Atg9-TAP with EP-GFP-Ufe1. Lysates and immunoprecipitates from the experiments with cells co-expressing Atg9-TAP with EP-GFP-Ufe1 performed in Figure 4C were re-analyzed by SDS-PAGE and Western Blotting (WB). Instead of cutting the membrane for incubating the individual parts with distinct antibodies, the entire membrane was incubated with antibodies against Sey1. On the same membrane, the TAP tag of Atg9 that was recognized only by the secondary antibody was clearly detectable in the IP fraction after starvation whereas Sey1 that was recognized by a combination of

primary and secondary antibody was only detectable in the lysate fractions. Together these results show the specificity of the interaction of Ufe1 with Atg9 under conditions of starvation. **(C)** Reverse co-IP of TP-GFP-Ufe1 with Atg9-TAP. Cells expressing Atg9-TAP and, if indicated, co-expressing TP-GFP-Ufe1 were grown to midlog phase in SD medium and shifted to SD-N medium for 2 hours. Cells were lysed and membranes solubilized with digitonin, followed by immunoprecipitation with IgG-coupled magnetic beads followed by SDS-PAGE and Western Blotting (WB) with the indicated antibodies. Physical interaction between Atg9 and Ufe1 was detected under these conditions (lane 4). **(D)** The function of Ufe1 in autophagy is not exclusively linked to Atg9. *Δatg9* cells expressing GFP-Atg8 were grown at 22°C in SD medium to mid-log phase before being shifted to SD-N medium. Cells were incubated for 5 hours at either 22°C or at 37°C and analyzed by fluorescence microscopy. Whereas *ufe1-1* cells showed GFP-Atg8 in puncta under these conditions (Figure 1C) GFP-Atg8 is seen in multiple ring-like structures, which have previously been reported to be the vacuolar rim (Suzuki et al., 2004). This demonstrates that *ufe1-1* and *Δatg9* cells produce different autophagy-specific phenotypes. Outlines indicate cell borders. Scale bar: 5 μm. **(E)** EP-GFP-Ufe1 is not processed in mutants of the MVB pathway. Wild type cells and the indicated mutants expressing EP-GFP-Ufe1 were grown in SD medium to mid-log phase at 30°C and shifted to SD-N medium. Equal amount of cells were lysed at the indicated time points after start of starvation and analyzed by SDS-PAGE and Western Blotting (WB). In contrast to wild type cells (lanes 1-3), no free GFP was generated in *Δvps4* and *Δvps32* cells (lanes 4-9). **(F)** No fluorescent signal was detectable inside vacuoles when EP-GFP-Ufe1 was expressed in *Δvps32* cells. Cells were grown in SD medium to mid-log phase at 30°C and shifted to starvation conditions for 5 hours, followed by live cells fluorescence microscopy. Prior to starvation (SD-N, 0h), EP-GFP-Ufe1 was seen in single perivacuolar puncta, typical for an aberrant structure called the class E compartment in this background. No signal was detected inside the vacuole (arrow, "v"). After starvation (SD-N, 5h), Ufe1 was visible in multiple cellular puncta, yet no signal was detectable inside the vacuole (arrow, "v"), in agreement with the data from WB analysis. Scale bar: 3 μm.

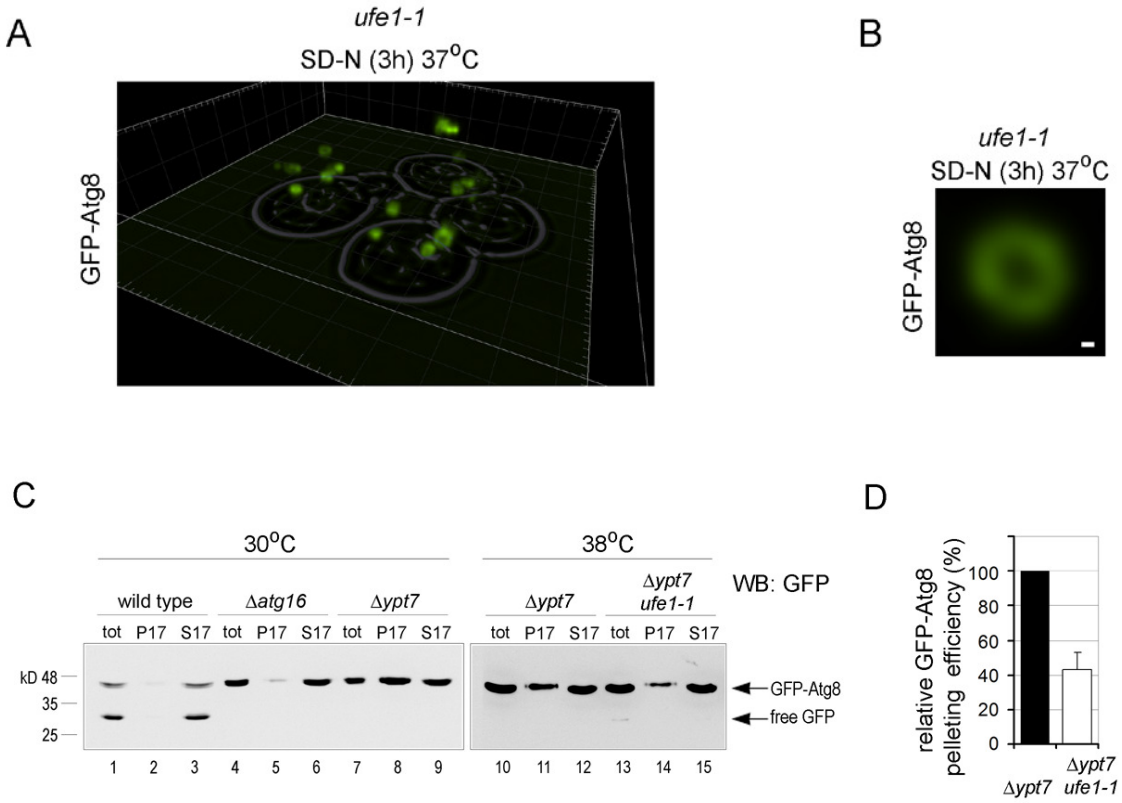

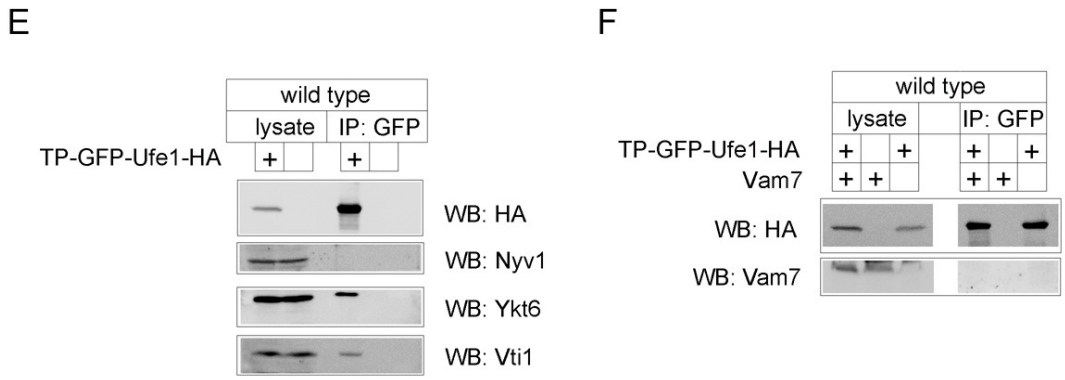

Figure S5, related to Figure 5. (A) Hollow Atg8-positive structures accumulate in *ufe1-1* cells at 37°C. *ufe1-1* cells expressing GFP-Atg8 were grown to mid-log phase in SD medium at 30°C, shifted to starvation medium and incubated for 2 hours at 37°C before being mildly fixed and analyzed by laser scanning fluorescence microscopy (see Supplemental Experimental Procedures). The image shows a three-dimensional reconstruction of deconvolved z-stacked images containing several cells. A two-dimensional projection of the brightfield image is displayed to indicate the positions of individual cells. Several Atg8-positive hollow structures are visible in every cell. **(B)** A representative single scan from a z-stacked series of images from experiments described in (A)

shows a cross section of a closed Atg8-positive structure, indicating the formation of an autophagosome. Scale bar: 100nm. **(C)** Autophagosome pelleting assay. Cells were grown to mid-log phase in SD medium at 30°C, shifted to starvation medium for 3.5 hours at the indicated temperatures, lysed and analyzed by medium-speed centrifugation (see Supplemental Experimental Procedures) followed by SDS-PAGE and Western Blotting. (tot): total, (P17): pellet and (S17): supernatant. Lanes 1-9: indicated strains were starved for 3.5 hours at 30°C. A significant amount of GFP-Atg8 was pelleted in *Δypt7* cells, whereas only residual pelleting was seen under the same conditions in wild type cells, due to rapid fusion of autophagosomes with the vacuole, or in *Δatg16* cells, where autophagosome formation was prevented. Lanes 10-15: indicated strains were starved for 3.5 hours at 38°C. A notable reduction in pelleting efficiency is visible in *Δypt7ufe1-1* cells (lanes 14 and 15) compared to *Δypt7* cells (lanes 11 and 12). **(D)** Statistical analysis of results obtained in (C) with *Δypt7* cells and *Δypt7ufe1-1* cells after starvation at 38°C. The pelleting efficiency of GFP-Atg8 in *Δypt7* cells at 38°C, as determined from the ratio between fractions P17 and S17, was set to 100% and compared to the efficiency of pelleting in *Δypt7ufe1-1* cells at the same conditions. The mean value and SD from 3 independent experiments are shown. **(E)** Test for physical interaction between selected SNARE proteins and TP-GFP-Ufe1 upon starvation. Wild type cells expressing TP-GFP-Ufe1 or control cells were grown in rich medium (SD) and then starved for 2 hours, lysed and their membranes solubilized with digitonin, followed by immunoprecipitation with anti-GFP beads, SDS-PAGE and Western Blotting (WB) with the indicated antibodies. **(F)** Test for physical interaction between Vam7 and TP-GFP-Ufe1. Wild type cells and *Δvam7* cells expressing TP-GFP-Ufe1 and control cells were treated and processed like in (E).

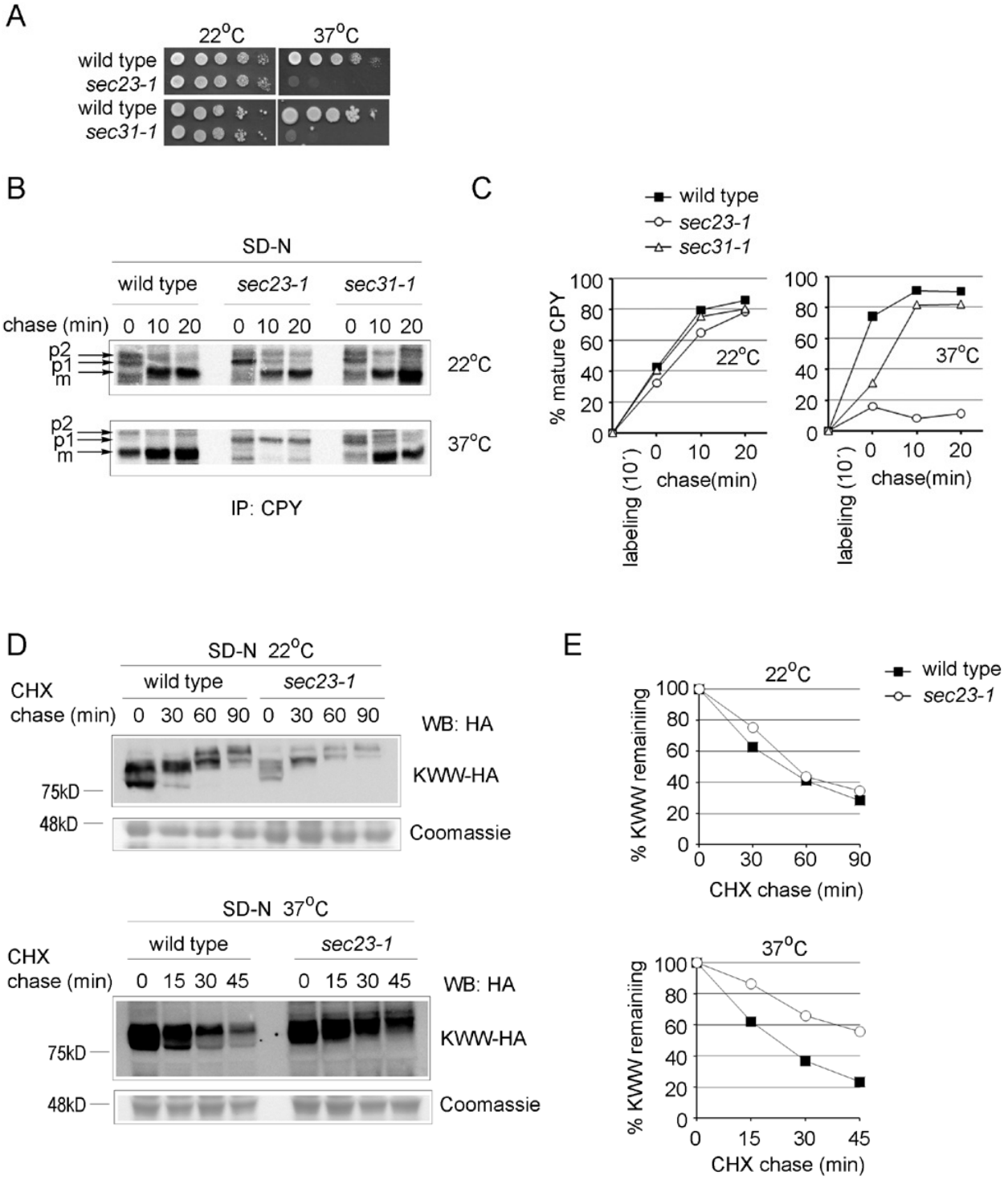

Figure S6, related to Figure 6. **(A)** Growth phenotypes of *sec23-1* and *sec31-1* cells. Wild type cells, *sec23-1* and *sec31-1* cells were spotted in dilution series on YPD plates and incubated for 3 days at 22°C and for 2 days at 37°C, respectively. The growth phenotypes at 22°C indicated full functionality of both alleles at this temperature,

whereas 37°C caused cell death in both cases, as expected. **(B)** ER export kinetics of carboxypeptidase Y (CPY) in *sec23-1* and *sec31-1* cells at 22°C and at 37°C under starvation conditions. Cells were grown to mid-log phase in SD medium at 22°C and starved for 1 hour prior to ^{35}S-methionine pulse-labeling and chased for the indicated periods of time, followed by cells lysis and immunoprecipitation of CPY (see Supplemental Experimental Procedures), followed by SDS-PAGE and autoradiography. The CPY precursor forms (p1 and p2) and the mature vacuolar form (m) are indicated. **(C)** Graphs illustrating the conversion of CPY to the mature vacuolar form at 22°C and at 37°C in wild type cells, *sec23-1* and *sec31-1* cells, from the experiment shown in (B). **(D)** Degradation of KWW in wild type cells and *sec23-1* cells. KWW is a glycosylated chimeric protein that misfolds and becomes ultimately a substrate for ERAD (ER-associated protein degradation). A large fraction of the protein is first exported in COP II vesicles and only degraded after retrieval from the Golgi (Vashist and Ng, 2004). Blocking of ER export was shown to reduce the degradation rate of KWW, therefore its degradation rate can be used to measure ER export efficiency of KWW (Vashist and Ng, 2004). Cells expressing KWW were grown to midlog phase at 22°C, split and starved for nitrogen for 3 hours followed by incubation with 200ug/ml cycloheximide (CHX). 1 hour prior to incubation with CHX, one fraction of cells was shifted to 37°C. Equal volumes were taken after the indicated periods of time and analyzed by SDS-PAGE and Western Blotting. A region of the lower part of the gel was stained with Coomassie as loading control. The increase in molecular weight is due to an increase O-mannosylation of the protein after longer chase times (Vashist and Ng, 2004). **(E)** Graphs illustrating the degradation of KWW at 22°C and at 37°C in wild type cells and *sec23-1* cells from experiments shown in (D). The mean values of two independent sets of experiments are plotted.

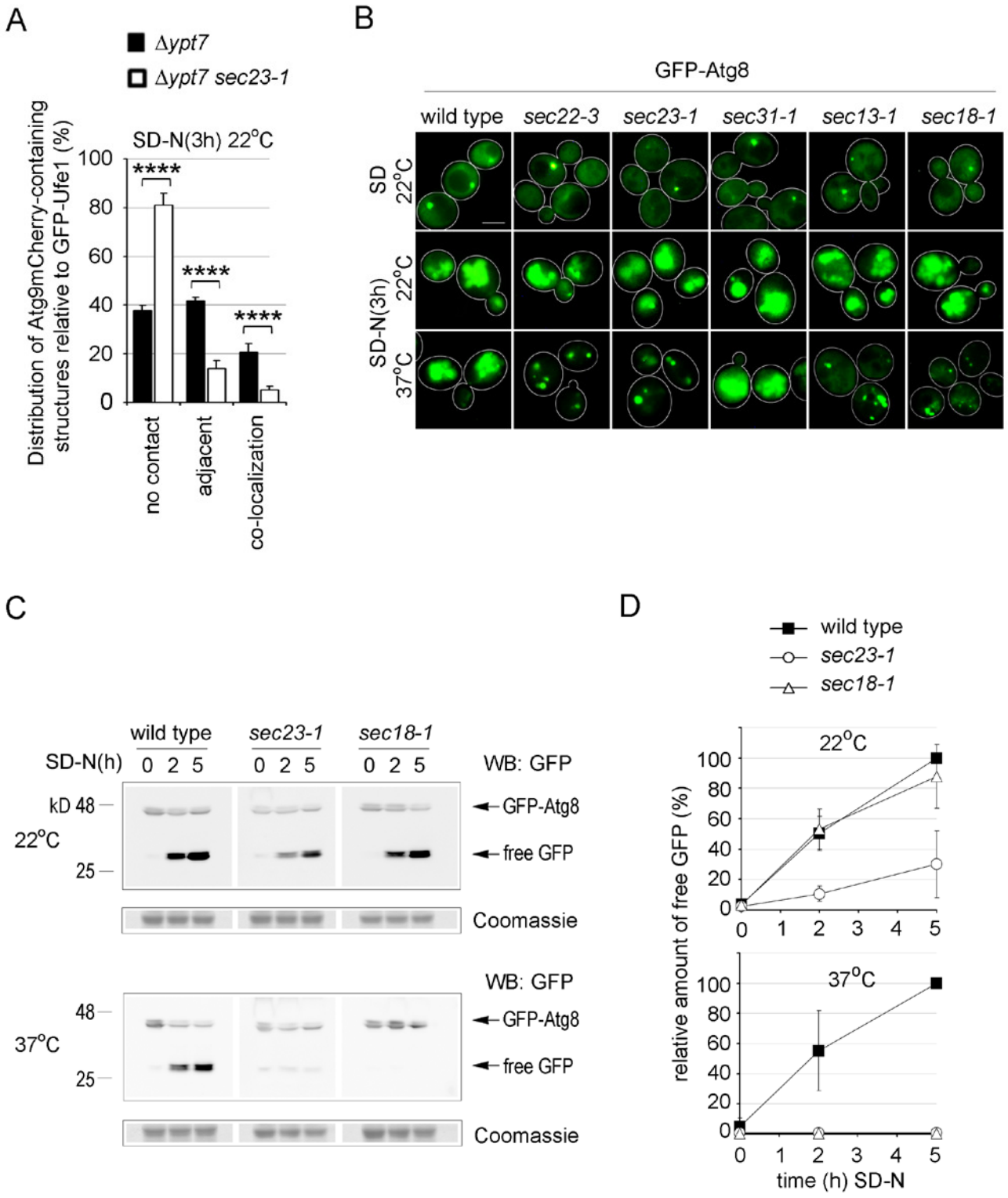
A
Δypt7
Δypt7 sec23-1
SD-N(3h) 22°C
Distribution of Atg9mCherry-containing structures relative to GFP-Ufe1 (%)
100
80
60
40
20
0
****
****
****
no contact
adjacent
co-localization
B
GFP-Atg8
wild type
sec22-3
sec23-1
sec31-1
sec13-1
sec18-1
SD 22°C
SD-N(3h) 22°C
37°C
C
wild type
sec23-1
sec18-1
SD-N(h) 0 2 5 0 2 5 0 2 5
WB: GFP
kD 48
22°C
25
GFP-Atg8
free GFP
Coomassie
WB: GFP
48
37°C
25
GFP-Atg8
free GFP
Coomassie
D
wild type
sec23-1
sec18-1
22°C
37°C
relative amount of free GFP (%)
100
80
60
40
20
0
0 1 2 3 4 5
time (h) SD-N

Figure S7, related to Figure 7. (A) Statistical analysis of the distribution of Atg9mCherry-containing structures with respect to GFP-Ufe1 in *Δypt7* cells and in *Δypt7sec23-1* cells after 3 hours of starvation at 22°C. The experiments were performed as described in Figure 4A. 166/53 (total number of Atg9mCherry structures/ in number of cells) in *Δypt7*cells and 190/78 in *Δypt7sec23-1* were evaluated with respect to contact with GFP-Ufe1. The mean values and SDs from 4 individual sets of assessments are shown, see Experimental Procedures. ****p<0.0001 (unpaired two-tailed Student's t-test). **(B)** Live cell imaging of wild type cells and *sec* mutant cells expressing GFP-Atg8. Cells were grown in SD medium to mid-log phase at 22°C and imaged with fluorescence microscopy before and after shifting cells to SD-N medium for 3 hours at the indicated temperatures. Prior to starvation, GFP-Atg8 was absent from vacuoles and visible in single puncta, representing the PAS. After starvation at 22°C all cells showed the staining pattern typical for vacuoles, including *sec23-1* cells, which did not reveal a marked reduction in vacuolar staining. After starvation at 37°C only wild type cells and *sec31-1* cells showed vacuolar staining. The result obtained with *sec31-1* cells correlated with the general ER export being largely unaffected in this strain under these conditions (Figures 6 and S6). All other mutants fail to show GFP-Atg8 inside the vacuole, as expected. Outlines indicate cell borders. Scale bar: 2µm. **(C)** GFP-Atg8 processing assay. Wild type cells and the indicated mutants expressing GFP-Atg8 were grown in SD medium to mid-log phase at 22°C and shifted to starvation conditions for the indicated periods of time at 22°C or at 37°C. Equal aliquots were analyzed by SDS-PAGE and Western Blotting (WB). (**D)** Quantifications of free GFP generated in wild type cells and mutant cells from experiments shown in (C). The amount of free GFP generated in individual strains at different times was normalized to the amount of free GFP generated after 5 hours starvation in wild type cells (set to 100%) within the same set of experiments. The mean values and SDs from at least 3 independent set of experiments are shown.

Table S1

Yeast strains used in this study are listed in an accompanying Excel file. Related to Experimental Procedures.

Chromosomal tagging of proteins and gene deletions were performed using standard PCR-based homologous recombination techniques.

Supplemental Experimental Procedures:

Construction of plasmids used in this study

VGp101 is pRS316. VGp160 contains *GFP-ATG8* and was a gift from the Yoshinori Ohsumi lab (Suzuki et al., 2001). VGp172 contains *TP-UFE1-3HA*. First, *UFE1* was chromosomally tagged in VGY100 on its C-terminus with 3 hemagglutinin tags yielding VGY1192. *UFE1-3HA* was amplified from VGY1192 using the primers GCGTCTAGAATGATGTCTGATTTAACACC and GCGCTCGAGGGTGTGGTCAATAAGAGCG, cut with XbaI/XhoI and ligated into pRS416 cut with the same enzymes; yielding VGp136. The *TDH3* promoter was amplified from VGY1192 using CGCGAGCTCCAGTTCGAGTTTATCATTATC and GCGTCTAGATTTGTTTGTTTATGTGTGTTT, cut with SacI/XbaI and ligated into VGp136 cut with the same enzymes, yielding VGc285. VGc285 was cut with SacI/XhoI and ligated into pRS315 cut with the same enzymes; yielding VGp172. VGp185 contains *ss-RFP-HDEL* and was a gift from the Will Prinz lab (referenced as pLKE037). VGc334 contains *TP-GFP-Ufe1-3HA*. First, *GFP* was amplified from pKT127 (EUROSCARF collection) using the primers CGCGCTAGCATGTCTAAAGGTGAAGAATTA and CGCGCTAGCTTTGTACAATTCATCCATACC, cut with NheI and ligated into VGc285 cut with XbaI; yielding VGc334. VGc336 contains *EP-UFE1-3HA*. *UFE1-3HA* was amplified from VGY1192 using the primers GCGTCTAGATTGGCCTTTTCCAATGAAAC and GCGCTCGAGGGTGTGGTCAATAAGAGCG, cut with XbaI/XhoI and ligated into pRS316 cut with the same enzymes, yielding VGc336. VGc340 contains *EP-GFP-UFE1-3HA*. First, *GFP* was amplified from pKT127 (EUROSCARF collection) using the primers CGCATCGATTCTAAAGGTGAAGAATTATTC and CGCATCGATTTTGTACAATTCATCCATACC, cut with ClaI and ligated into VGc336 cut with the same enzyme, yielding VGc340. VGc344 contains *TP-RFP-UFE1-3HA*. First, *RFP* was amplified from VGp170 (containing *RFP*) using the primers CGCGCTAGCATGGCCTCCTCCGAGGACG and CGCGCTAGCGGCGCCGGTGGAGTGG, cut with NheI and ligated into VGp172 cut with XbaI, yielding VGc344. VGc351 contains *EP-UFE1-3HA*. First, VGc336 was cut with SacI/XhoI and the resulting fragment was ligated into pRS315 cut with the same enzymes, yielding VGc351. Plasmid VGp241 contains Sec63mCherry, a gift from Pedro Carvalho, CRG, Barcelona.

Alkaline extraction

Cells were lysed in lysis buffer consisting of PBS, 1mM EDTA, 1mM PMSF and protein inhibitor cocktail (Roche) using glass beads and bead beating. Lysates were freed from debris by centrifugation. The total lysate was split in equal parts. Both parts were treated with carbonate pH 11.5 on ice for 15 minutes and one part was subsequently centrifuged at 100000g for 20 minutes. The obtained supernatant was treated as extractable fraction whereas the pellet was considered membrane fraction. The pellet was supplemented with carbonate solution and both fractions where centrifuged again. The non-centrifuged sample was considered total.

Confocal laser scanning microscopy and 3D reconstruction

Cells were mildly fixed by addition of 2 % of paraformaldehyde for 30 minutes, washed, resuspended in PBS and scanned with a Laser Scanning Confocal Microscope from Zeiss (LSM 7 Duo) using a Plan-Apochromat objective 63x/1,40 Oil DIC and a 488nm Argon Laser (used for GFP). Z-stacks were acquired using optimized automated optical sectioning. For 3D imaging, image series were deconvolved using the Huygens Deconvolution Software by Scientific Volume Imaging (http://www.svi.nl). 3D images were reconstructed with IMARIS software (Bitplane; Switzerland).

Pulse-Chase experiments

Cells were grown exponentially at 22°C and shifted to starvation conditions 1 hour prior to starting the pulse. For pulsing, cells equivalent to 5 OD were resuspended in 1ml medium lacking methionine and labeled for 10 min with 100 µCi/ml [^{35}S]methionine (Perkin Elmers) at 22°C or 37°C, as indicated. Cells were kept at these temperatures until the end of the chase period. After the pulse, cells were diluted to OD 0.8 and supplemented with methionine. Aliquots were taken at indicated times, cells were moved to ice and supplemented with 10 mM azide, pelleted, resuspended in 50 mM Tris, pH 7.5, 5 mM EDTA, 1 mM PMSF, and lysed with glass beads for 7 min in a bead-beater, supplemented with 1% SDS, and heated at 65°C for 10 min. Cell remnants were removed by centrifugation for 10 min in a microfuge, and the supernatant was used for immunoprecipitation using anti-CPY antibodies. Immune complexes were isolated with protein A-Sepharose (GE Healthcare) and analyzed by SDS-gel electrophoresis and autoradiography using a PhosphorImager (Fuji).

Autophagosome pelleting

The experiments were essentially done as described in (Yamamoto et al., 2012). Cells were grown to mid-log phase and starved for 3.5 hours, treated with 10mM DTT for 15 min at RT, converted to spheroplasts by incubation with 100ug/ml Zymolase 20T for 60 min at RT in spheroplasting buffer (20mM Tris pH7.5, 1.2M Sorbitol, 1mM DTT, 100mM NaCl) and lysed by 30 strokes with a Dounce-homogenizer in lysis buffer (20mM Tris pH7.5, 100mM Sorbitol, 1mM DTT, 100mM NaCl) in presence of protein-inhibitor cocktail (Roche). Lysates were cleared by 2x spinning for 5 min at 1000g, and split in two equal parts. One part was centrifuged for 15 min at 17400g. Supernatant and pellet were separated and respun or washed in lysis buffer, respectively. The pellet was resuspended in lysis buffer and all fractions were subjected to precipitation with 15% tri-chloro-acetic acid, centrifugation, followed by 3 wash steps in acetone, and analysis by SDS-PAGE and Western Blotting. For experiments at the non-permissive temperature, cells were first converted to spheroplasts like described above. Spheroplasts were resuspended in nitrogen starvation medium containing 1.2M sorbitol and grown for 3.5 hours at the non-permissive temperature. Spheroplasts were pelleted and processed like described above.

Supplemental References:

Hu, J., Y. Shibata, P.P. Zhu, C. Voss, N. Rismanchi, W.A. Prinz, T.A. Rapoport, and C. Blackstone. (2009). A class of dynamin-like GTPases involved in the generation of the tubular ER network. Cell. *138*, 549-61.

Suzuki, K., T. Kirisako, Y. Kamada, N. Mizushima, T. Noda, and Y. Ohsumi. (2001). The pre-autophagosomal structure organized by concerted functions of APG genes is essential for autophagosome formation. Embo J. *20*, 5971-81.

Suzuki, K., T. Noda, and Y. Ohsumi. (2004). Interrelationships among Atg proteins during autophagy in Saccharomyces cerevisiae. Yeast. *21*, 1057-65.

Vashist, S., and D.T. Ng. (2004). Misfolded proteins are sorted by a sequential checkpoint mechanism of ER quality control. J Cell Biol. *165*, 41-52.

Yamamoto, H., S. Kakuta, T.M. Watanabe, A. Kitamura, T. Sekito, C. Kondo-Kakuta, R. Ichikawa, M. Kinjo, and Y. Ohsumi. (2012). Atg9 vesicles are an important membrane source during early steps of autophagosome formation. J Cell Biol. *198*, 219-33.

Autophagy. 2016 Jun 2;12(6):1049-50. doi: 10.1080/15548627.2016.1164368.

A SNARE and specific COPII requirements define ER-derived vesicles for the biogenesis of autophagosomes.

Lemus L, Goder V.

Autophagy

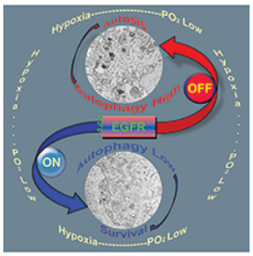

Autophagy

ISSN: 1554-8627 (Print) 1554-8635 (Online) Journal homepage: http://www.tandfonline.com/loi/kaup20

A SNARE and specific COPII requirements define ER-derived vesicles for the biogenesis of autophagosomes

Leticia Lemus & Veit Goder

To cite this article: Leticia Lemus & Veit Goder (2016) A SNARE and specific COPII requirements define ER-derived vesicles for the biogenesis of autophagosomes, Autophagy, 12:6, 1049-1050, DOI: 10.1080/15548627.2016.1164368

To link to this article: http://dx.doi.org/10.1080/15548627.2016.1164368

Published online: 28 Apr 2016.

AUTOPHAGY
2016, VOL. 12, NO. 6, 1049–1050
http://dx.doi.org/10.1080/15548627.2016.1164368

Taylor & Francis
Taylor & Francis Group

AUTOPHAGIC PUNCTUM

A SNARE and specific COPII requirements define ER-derived vesicles for the biogenesis of autophagosomes

Leticia Lemus and Veit Goder

Department of Genetics, University of Seville, Avda Reina Mercedes, Seville, Spain

ABSTRACT
The endoplasmic reticulum (ER) is a major source for the generation of autophagosomes during macroautophagy. Our recent work in yeast shows that particular ER-derived vesicles are generated for the biogenesis of autophagosomes. These vesicles not only incorporate a SNARE protein that is largely ER-resident under nonstarving conditions, but also display COPII requirements for ER-exit that differ from conventional cargo-transporting vesicles. Our results suggest that specific intracellular traffic is launched at the ER for the transport of membranes to sites of autophagosome formation.

ARTICLE HISTORY
Received 2 March 2016
Revised 5 March 2016
Accepted 7 March 2016

KEYWORDS
autophagy; COPII; membrane fusion; membrane traffic; SNARE proteins

The elaborate cellular ER network is a hallmark of all eukaryotic cells and is the hub for COPII vesicles that transport lipids as well as membrane proteins and soluble cargo from the ER to the Golgi apparatus. It is also known that the ER plays an important role for the biogenesis of autophagosomes, which have a characteristic double-layered membrane and form increasingly during periods of starvation. Our recent work with the yeast *S. cerevisiae* revealed a particular cellular trafficking pathway that emanates from the ER and constitutes one source of membranes for the formation of autophagosomes.

By investigating whether distinct ER membrane fusion machineries play a role in autophagy we found that the SNARE protein Ufe1, but not the atlastin-like Sey1, is required for this process. Interestingly, Ufe1, which was considered an ER-resident SNARE protein with known functions in ER-ER membrane fusion as well as in fusion of retrograde vesicles with the ER, is increasingly exported from the ER upon conditions that induce autophagy and ends up inside the vacuole. In mutants that block the vacuolar uptake of multivesicular bodies (MVBs), Ufe1 accumulates in extravacuolar structures. In *ypt7Δ* cells, where vacuolar uptake of both autophagosomes and of MVBs is blocked, Ufe1 colocalizes with Atg8 and Atg9 in punctate structures and shows physical interaction with these autophagy markers. These results combined lead to the hypothesis that Ufe1-containing ER vesicles are targeted to sites of autophagsome formation where they contribute membranes to emerging autophagosomes. Membrane fusion during these processes would be catalyzed in part by Ufe1, which would subsequently be forwarded to the vacuole via MVBs.

We performed a number of experiments to test our hypothesis. Previously published work from the laboratories of Fulvio Reggiori, Yoshinori Ohsumi and Daniel Klionsky demonstrated that the availability of membranes for autophagosome formation, in these cases Atg9-containing membranes, correlates with the number and size of autophagosomes. With this in mind we used thin-section electron microscopy and confocal laser scanning microscopy in combination with 3-dimensional reconstruction and measured the number and size of autophagosomes dependent on functional Ufe1. In cells with a temperature-sensitive allele of Ufe1 both the number and size of autophagosomes are reduced at the restrictive temperature when compared to control cells, showing a function of Ufe1 in membrane supply relevant for autophagosome biogenesis. Additional evidence came from the observed physical interactions of Ufe1 with SNARE proteins previously implicated in this process. We found that Ufe1, a Qa-SNARE, binds to Vti1 (Qb) and Ykt6 (R), both non-ER SNAREs, under conditions that induce autophagy.

In another series of experiments we addressed the requirements for ER exit of Ufe1 during starvation. Not too surprisingly, formation of vesicles that carry Ufe1 depend on the COPII complex. A connection of COPII vesicles to autophagosome formation in yeast has been demonstrated previously by the laboratories of Jodi Nunnari and Susan Ferro-Novick. We made the additional observation that the ER exit of Ufe1 is hypersensitive to the *sec23-1* allele, which affects the inner layer of the COPII coat. At the permissive temperature the ER exit of conventional cargo is unaffected in *sec23-1* cells upon starvation, whereas the ER exit of Ufe1 is strongly reduced. This provided us with a tool to test the correlation between the ER export of Ufe1 and the biogenesis of autophagosomes under conditions where the early secretory pathway is intact. Strikingly, we observed that *sec23-1* cells are deficient in autophagy at the permissive temperature. On a subcellular level, using thin-section electron microscopy, we detected a decreased number of autophagosomes in *sec23-1* cells when compared to wild-type cells or additional control cells, revealing a deficiency in membrane supply to autophagosome biogenesis.

The observed correlation between the specific COPII-dependent ER exit of Ufe1 during starvation and the number of generated autophagosomes in *sec23-1* cells supports the model that one way of transporting membranes to sites of autophagosome

CONTACT Veit Goder vgoder@us.es Department of Genetics, University of Seville, Ave Reina Mercedes, Seville, E-41012, Spain

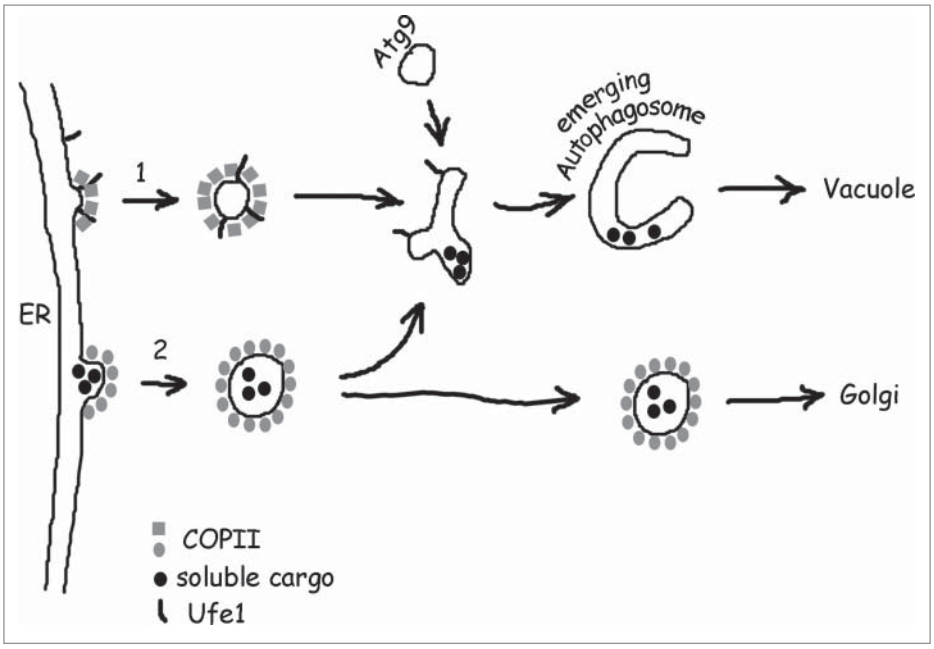

Figure 1. Current models for the contribution of ER-derived COPII vesicles to autophagosome biogenesis. (1) Upon cellular starvation, vesicles are produced that differ from conventional transport vesicles in several aspects. Our work suggests that in yeast, such vesicles incorporate the Qa-SNARE Ufe1 and have specific COPII requirements for budding, maybe due to subtle differences in coat arrangement. Likewise in mammals, starvation-specific and unusually small COPII vesicles are produced at the ERGIC. Based on these findings and the assumed functional role of such vesicles it is possible that they constitute a class of ER vesicles that is free of lumenal cargo and carries mainly membranes and fusion machinery instead, but evidence for this assumption is lacking. (2) Previous work with yeast suggests an alternative mechanism for the contribution of COPII vesicles to autophagosome biogenesis. In this scenario, transport vesicles are generated normally, but are diverted from their route to the Golgi and are targeted to sites of autophagosome formation by virtue of a starvation-specific membrane tethering factor. As a consequence, lumenal cargo might end up in between the 2 membranes that form an autophagosome.

formation relies on vesicles that contain Ufe1. Our data also indicate that these vesicles are specific COPII vesicles and that they differ from those that contain cargo destined for various places along the secretory pathway. One possibility for the observed sensitivity of formation of autophagy-specific COPII vesicles to the *sec23-1* allele is that it might reflect subtle differences in coat arrangement. A recent report from work with mammalian cells could indicate that a similar system is also present in higher eukaryotes: the Schekman lab isolated specific COPII vesicles for the biogenesis of autophagosomes that bud from the ERGIC, an intermediate structure in mammalian cells that is functionally comparable to yeast ER exit sites. A striking feature of these autophagy-specific COPII vesicles is their markedly reduced diameter compared to COPII transport vesicles destined for the Golgi.

On a speculative note, we think it is possible that one class of ER vesicles routed to sites of autophagosome formation is generally free of lumenal cargo (Fig. 1, step 1). This could account for the observed differences in biophysical and structural features compared to cargo transporting vesicles destined for the Golgi. The main purpose of these vesicles would be to carry membranes along with the appropriate fusion machinery rather than lumenal cargo. Conversely, results from the group of Susan Ferro-Novick suggest that conventional transport vesicles en route to the Golgi can be diverted and used for autophagosome biogenesis as well (Fig. 1, step 2). An interesting and testable consequence of this scenario would be that ER lumenal cargo ends up permanently in between the autophagosomal membranes, or temporarily in case it is recycled from intermediate structures (Fig. 1). It remains to be seen whether the observed differences in COPII vesicles that are used for autophagosome biogenesis in distinct cell types or under distinct conditions indeed reflect different cellular pathways. Other interesting questions concern the mechanism of Ufe1 incorporation into ER vesicles and the particular fusion reactions that are catalyzed in connection with this SNARE protein, all of which will lead to crucial insight into the contribution of the ER to autophagosome formation by vesicular transport and its regulation.

Disclosure of potential conflicts of interest

No potential conflicts of interest were disclosed.

Funding

This work has been supported by an EMBO short-term fellowship (EMBO ASTF 293-2015) to L.L. and by grants of the Spanish Ministry of Science (BFU2009-07290) and (BFU2014-59309-P).

DISCUSSION

Interplay between Endoplasmic Reticulum and Cellular Homeostasis

It was previously shown that GPI-lipid remodeling, by the action of Bst1p, Per1p, and Gup1p, is required for transport of GPI-APs from the ER in yeast (Bosson et al., 2006; Castillon et al., 2009; Fujita et al., 2006a). Likewise, it was also shown that GPI-glycan remodeling by Ted1p is necessary for its recognition by the p24 complex and its subsequent ER export (Manzano-Lopez et al., 2015).

These two previous works were carried out using native GPI-APs though. As we were interested in determining the degradation fate of the misfolded Gas1* we verified its identity by checking whether it also contains a GPI moiety and if it is remodeled or not. GPI-APs are known to be incorporated into detergent-resistant membrane (DRM) in the ER in yeast (Bagnat et al., 2000) and have been biochemically isolated from it (Fujita and Jigami, 2008; Pittet and Conzelmann, 2007). DRMs are enriched in ceramides and float into the upper fraction of the density gradient. Accordingly, the density gradient ultracentrifugation assay showed that Gas1*, despite being misfolded, is partitioned in the DRM fraction and consequently it is also GPI-anchored and undergoes remodeling like the native Gas1p.

Therefore, when the GPI-lipid remodeling is impaired, which is the case for *bst1*Δ cells (Fujita et al., 2006b) the distribution of the GPI-AP in the density gradient is changed and now it is not found in the upper fraction together with the DRM. Instead, GPI-APs are found in the bottom fraction that is lacking of DRM and ceramides. Thus, we obtained this result in *bst1*Δ cells not only for the native protein Gas1p, but also for the misfolded version Gas1*p. This result indicates that both correctly folded and misfolded GPI-APs undergo GPI remodeling and consequently the misfolded Gas1*, is GPI-anchored as well.

Consequently, Gas1*, though being misfolded, undergoes GPI-anchor remodeling and it is prone to be recognized by the p24 complex and exported from the ER. Hence, when GPI moiety remodeling is impaired, its recognition by p24 complex will be compromised and more protein will be processed by ERAD.

Despite those previous data suggesting that misfolded GPI-APs are rather poor ERAD substrates, it has been previously shown that the degradation of Gas1*p is a dynamic

process, involving components of both ERAD and p24 complex (Castillon et al., 2011; Goder and Melero, 2011; Hirayama et al., 2008). However, details for the mechanism of targeting to ERAD and/or to the vacuole remained elusive.

We have demonstrated that Gas1* can be preferentially degraded by ERAD when GPI remodeling is impaired (Sikorska et al., 2016).

On our second study related to the contribution of the ER-localized SNARE Ufe1p, our data show that it plays a role in autophagy. Our findings reveal that autophagy-specific regulation of membrane traffic involves the mobilization of SNARE proteins that are at the core of most membrane fusion machineries and that, in case of Ufe1, are thought to be organelle-specific. This mechanism adds a layer of regulation to the previous findings that starvation leads to a relocalization of membrane fusion regulators of the Rab protein family and to a modulation of membrane tethers in order to direct particular membrane traffic to sites of autophagosome formation (Popovic et al., 2012; Tan et al., 2013).

Our findings suggest that the export of membranes from the ER for the purpose of autophagosome formation depends on specific COPII vesicles. Although we have only limited data, the incorporation of Ufe1 and the particular sensitivity to the sec23-1 allele for their ER export clearly separate them from ‘‘more conventional’’ transport vesicles.

Moreover, our data, obtained by conventional transmission electron microscopy confirmed that Ufe1p plays an important role in determining the magnitude of the autophagic response, judging from the decrease in number and size of autophagosomes in the cytosol and the no accumulation of autophagic bodies in the vacuole in cells depleted of Ufe1p activity. This could reflect a consequence of the SNARE to misfold after having been localized to sites relevant for the biogenesis of autophagosomes.

Our findings open a series of questions that are currently being addressed. Foremost, how is Ufe1 incorporated into ER vesicles and how is it regulated? Are the other ER-localized SNAREs similarly exported during autophagy? What else distinguishes the specific COPII vesicles for the autophagosome biogenesis from vesicles transporting cargo along the secretory pathway? Which membrane fusion reactions are catalyzed by Ufe1 during for the formation of autophagosomes, and what are the partner SNARE

proteins for these fusions? Answers to these questions will provide a detailed picture of the contribution of the ER to autophagosome formation by vesicular transport.

CONCLUSIONS

Part I

1. Remodeled GPI moiety functions as an ER export signal even for misfolded GPI-APs, limiting its retention in the ER and consequently its turnover by ERAD.

Part II

1. The Qa-SNARE, Ufe1p plays a role in autophagy, contributing with ER membrane in the biogenesis of autophagosomes and their fusion with the vacuole.

2. The function of Ufe1p in autophagy is linked to other SNAREs and early secretory proteins that play a role in autophagy as well.

REFERENCES

Anwar, K., Klemm, R. W., Condon, A., Severin, K. N., Zhang, M., Ghirlando, R., Hu, J., Rapoport, T. A., and Prinz, W. A. (2012). The dynamin-like GTPase Sey1p mediates homotypic ER fusion in S. cerevisiae. J Cell Biol *197*, 209-217.

Arakawa, S., Yunoki, K., Izawa, T., Tamura, Y., Nishikawa, S.-i., and Endo, T. (2016). Quality control of nonstop membrane proteins at the ER membrane and in the cytosol. Scientific Reports *6 DO - 10.1038/srep30795 AN - PMC4969602*, 30795.

Arvan, P., Zhao, X., Ramos-Castaneda, J., and Chang, A. (2002). Secretory pathway quality control operating in Golgi, plasmalemmal, and endosomal systems. Traffic *3*, 771-780.

Ashok, A., and Hegde, R. S. (2008). Retrotranslocation of prion proteins from the endoplasmic reticulum by preventing GPI signal transamidation. Mol Biol Cell *19*, 3463-3476.

Axe, E. L., Walker, S. A., Manifava, M., Chandra, P., Roderick, H. L., Habermann, A., Griffiths, G., and Ktistakis, N. T. (2008). Autophagosome formation from membrane compartments enriched in phosphatidylinositol 3-phosphate and dynamically connected to the endoplasmic reticulum. J Cell Biol *182*, 685-701.

Baba, M., Takeshige, K., Baba, N., and Ohsumi, Y. (1994). Ultrastructural analysis of the autophagic process in yeast: detection of autophagosomes and their characterization. J Cell Biol *124*, 903-913.

Bagnat, M., KerÃ¤nen, S., Shevchenko, A., Shevchenko, A., and Simons, K. (2000). Lipid rafts function in biosynthetic delivery of proteins to the cell surface in yeast. Proceedings of the National Academy of Sciences of the United States of America *97*, 3254-3259.

Bernasconi, R., Galli, C., Calanca, V., Nakajima, T., and Molinari, M. (2010). Stringent requirement for HRD1, SEL1L, and OS-9/XTP3-B for disposal of ERAD-Ls substrates. J Cell Biol *188*, 223 LP - 235.

Bock, J. B., Matern, H. T., Peden, A. A., and Scheller, R. H. (2001). A genomic perspective on membrane compartment organization. *409*, 839-841.

Bonifacino, J. S., and Lippincott-Schwartz, J. (1991). Degradation of proteins within the endoplasmic reticulum., pp. 592-600.

Bonifacino, J. S., Suzuki, C. K., Lippincott-Schwartz, J., Weissman, A. M., and Klausner, R. D. (1989). Pre-Golgi degradation of newly synthesized T-cell antigen receptor chains: intrinsic sensitivity and the role of subunit assembly. J Cell Biol *109*, 73-83.

Bosson, R. g., Jaquenoud, M., and Conzelmann, A. (2006). GUP1 of Saccharomyces cerevisiae Encodes an O-Acyltransferase Involved in Remodeling of the GPI Anchor. Molecular Biology of the Cell *17*, 2636-2645.

Butikofer, P., Malherbe, T., Boschung, M., and Roditi, I. (2001). GPI-anchored proteins: now you see 'em, now you don't. Faseb J *15*, 545-548.

Caro, L. G., and Palade, G. E. (1964). Protein Synthesis, Storage, and Discharge in the Pancreatic Exocrine Cell. An Autoradiographic Study. J Cell Biol *20*, 473-495.

Carvalho, P., Goder, V., and Rapoport, T. A. (2006). Distinct ubiquitin-ligase complexes define convergent pathways for the degradation of ER proteins. Cell *126*, 361-373.

Castillon, G. A., Aguilera-Romero, A., Manzano-Lopez, J., Epstein, S., Kajiwara, K., Funato, K., Watanabe, R., Riezman, H., and Muniz, M. (2011). The yeast p24 complex regulates GPI-anchored protein transport and quality control by monitoring anchor remodeling. Mol Biol Cell *22*, 2924-2936.

Castillon, G. A., Watanabe, R., Taylor, M., Schwabe, T. M., and Riezman, H. (2009). Concentration of GPI-anchored proteins upon ER exit in yeast. Traffic *10*, 186-200.

Ciechanover, A. (2012). Intracellular protein degradation: From a vague idea thru the lysosome and the ubiquitin-proteasome system and onto human diseases and drug targeting. Biochimica et Biophysica Acta (BBA) - Proteins and Proteomics Proteolysis 50 years after the discovery of lysosome *1824*, 3-13.

Coughlan, C. M., Walker, J. L., Cochran, J. C., Wittrup, K. D., and Brodsky, J. L. (2004). Degradation of mutated bovine pancreatic trypsin inhibitor in the yeast vacuole suggests post-endoplasmic reticulum protein quality control. J Biol Chem *279*, 15289-15297.

Cox, J. S., and Walter, P. (1996). A novel mechanism for regulating activity of a transcription factor that controls the unfolded protein response. Cell *87*, 391-404.

de Duve, C. (1963). In Ciba Foundation Symposium on Lysosomes, A. V. S. C. in de Reuck, M. P. (eds), ed. (London, J. & A. Churchill Ltd).

Diehn, M., Bhattacharya, R., Botstein, D., and Brown, P. O. (2006). Genome-Scale Identification of Membrane-Associated Human mRNAs. PLoS Genetics *2*, e11.

Dilcher, M., Köhler, B., and Von Mollard, G. F. (2001). Genetic Interactions with the Yeast Q-SNARE VTI1 Reveal Novel Functions for the R-SNARE YKT6. Journal of Biological Chemistry *276*, 34537-34544.

Dilcher, M., Veith, B., Chidambaram, S., Hartmann, E., Schmitt, H. D., and Fischer von Mollard, G. (2003). Use1p is a yeast SNARE protein required for retrograde traffic to the ER. Embo J *22*, 3664-3674.

Ellgaard, L., and Helenius, A. (2003). Quality control in the endoplasmic reticulum. Nat Rev Mol Cell Biol *4*, 181-191.

Ellgaard, L., McCaul, N., Chatsisvili, A., and Braakman, I. (2016). Co- and Post-Translational Protein Folding in the ER. Traffic *17*, 615-638.

Eskelinen, E. L. (2008). Fine structure of the autophagosome. Methods Mol Biol *445*, 11-28.

Fankhauser, C., Homans, S. W., Thomas-Oates, J. E., McConville, M. J., Desponds, C., Conzelmann, A., and Ferguson, M. A. (1993). Structures of glycosylphosphatidylinositol membrane anchors from Saccharomyces cerevisiae. J Biol Chem *268*, 26365-26374.

Fasshauer, D., Sutton, R. B., Brunger, A. T., and Jahn, R. (1998). Conserved structural features of the synaptic fusion complex: SNARE proteins reclassified as Q- and R-SNAREs. Proc Natl Acad Sci U S A *95*, 15781-15786.

Ferguson, M. A., Homans, S. W., Dwek, R. A., and Rademacher, T. W. (1988). Glycosyl-phosphatidylinositol moiety that anchors Trypanosoma brucei variant surface glycoprotein to the membrane. Science *239*, 753-759.

Ferguson, M. A. J., Kinoshita, T., and Hart, G. W. (2009). Glycosylphosphatidylinositol Anchors. In: Varki A, Cummings RD, Esko JD, et al., editors. Essentials of Glycobiology. 2nd edition. Cold Spring Harbor (NY): Cold Spring Harbor Laboratory Press. Chapter 11.

Ferro-Novick, S., and Jahn, R. (1994). Vesicle fusion from yeast to man. Nature *370*, 191-193.

Foresti, O., Rodriguez-Vaello, V., Funaya, C., and Carvalho, P. (2014). Quality control of inner nuclear membrane proteins by the Asi complex. Science *346*, 751-755.

Fujita, M., Gao, X.-D., and Kinoshita, T. (2015). Glycan-Mediated Protein Transport from the Endoplasmic Reticulum

Sugar Chains: Decoding the Functions of Glycans. In, T. Suzuki, K. Ohtsubo, and N. Taniguchi, eds. (Tokyo, Springer Japan), pp. 21-34.

Fujita, M., and Jigami, Y. (2008). Lipid remodeling of GPI-anchored proteins and its function. Biochim Biophys Acta *1780*, 410-420.

Fujita, M., and Kinoshita, T. (2010). Structural remodeling of GPI anchors during biosynthesis and after attachment to proteins. FEBS Lett *584*, 1670-1677.

Fujita, M., and Kinoshita, T. (2012). GPI-anchor remodeling: potential functions of GPI-anchors in intracellular trafficking and membrane dynamics. Biochim Biophys Acta *1821*, 1050-1058.

Fujita, M., Maeda, Y., Ra, M., Yamaguchi, Y., Taguchi, R., and Kinoshita, T. (2009). GPI glycan remodeling by PGAP5 regulates transport of GPI-anchored proteins from the ER to the Golgi. Cell *139*, 352-365.

Fujita, M., Umemura, M., Yoko-o, T., and Jigami, Y. (2006a). PER1 Is Required for GPI-Phospholipase A(2) Activity and Involved in Lipid Remodeling of GPI-anchored Proteins. Molecular Biology of the Cell *17*, 5253-5264.

Fujita, M., Yoko, O. T., and Jigami, Y. (2006b). Inositol deacylation by Bst1p is required for the quality control of glycosylphosphatidylinositol-anchored proteins. Mol Biol Cell *17*, 834-850.

Futerman, A. H., Low, M. G., Ackermann, K. E., Sherman, W. R., and Silman, I. (1985). Identification of covalently bound inositol in the hydrophobic membrane-anchoring domain of Torpedo acetylcholinesterase. Biochemical and Biophysical Research Communications *129*, 312-317.

Ge, L., Melville, D., Zhang, M., and Schekman, R. (2013). The ER-Golgi intermediate compartment is a key membrane source for the LC3 lipidation step of autophagosome biogenesis. Elife *2*, e00947.

Goder, V., and Melero, A. (2011). Protein O-mannosyltransferases participate in ER protein quality control. J Cell Sci *124*, 144-153.

Graef, M., Friedman, J. R., Graham, C., Babu, M., and Nunnari, J. (2013). ER exit sites are physical and functional core autophagosome biogenesis components. Mol Biol Cell.

Guerriero, C. J., and Brodsky, J. L. (2012). The Delicate Balance Between Secreted Protein Folding and Endoplasmic Reticulum-Associated. Degradation in Human Physiology. Physiol Rev *92*, 537 LP - 576.

Guo, Y., Chang, C., Huang, R., Liu, B., Bao, L., and Liu, W. (2012). AP1 is essential for generation of autophagosomes from the trans-Golgi network. J Cell Sci *125*, 1706-1715.

Hailey, D. W., Rambold, A. S., Satpute-Krishnan, P., Mitra, K., Sougrat, R., Kim, P. K., and Lippincott-Schwartz, J. (2010). Mitochondria supply membranes for autophagosome biogenesis during starvation. Cell *141*, 656-667.

Halperin, L., Jung, J., and Michalak, M. D.-i. (2014). The many functions of the endoplasmic reticulum chaperones and folding enzymes. In IUBMB Life (Wiley Online Library), pp. 318-326.

Hammond, C., Braakman, I., and Helenius, A. (1994). Role of N-linked oligosaccharide recognition, glucose trimming, and calnexin in glycoprotein folding and quality control. Proc Natl Acad Sci U S A *91*, 913-917.

Hampton, R. Y., Gardner, R. G., and Rine, J. (1996). Role of 26S proteasome and HRD genes in the degradation of 3-hydroxy-3-methylglutaryl-CoA reductase, an integral endoplasmic reticulum membrane protein. Mol Biol Cell *7*, 2029-2044.

Hanada, T., Noda, N. N., Satomi, Y., Ichimura, Y., Fujioka, Y., Takao, T., Inagaki, F., and Ohsumi, Y. (2007). The Atg12-Atg5 Conjugate Has a Novel E3-like Activity for Protein Lipidation in Autophagy. Journal of Biological Chemistry *282*, 37298-37302.

Hara, T., Nakamura, K., Matsui, M., Yamamoto, A., Nakahara, Y., Suzuki-Migishima, R., Yokoyama, M., Mishima, K., Saito, I., Okano, H., and Mizushima, N. (2006). Suppression of basal autophagy in neural cells causes neurodegenerative disease in mice. Nature *441*, 885-889.

Hayashi-Nishino, M., Fujita, N., Noda, T., Yamaguchi, A., Yoshimori, T., and Yamamoto, A. (2009). A subdomain of the endoplasmic reticulum forms a cradle for autophagosome formation. Nat Cell Biol *11*, 1433-1437.

Hebert, D. N., Bernasconi, R., and Molinari, M. (2010). ERAD substrates: Which way out? Seminars in Cell & Developmental Biology Quality control in the endoplasmic reticulum *21*, 526-532.

Hebert, D. N., Foellmer, B., and Helenius, A. (1995). Glucose trimming and reglucosylation determine glycoprotein association with calnexin in the endoplasmic reticulum. Cell *81*, 425-433.

Hershko, A., and Ciechanover, A. (1998). The ubiquitin system. Annu Rev Biochem *67*, 425-479.

Hiller, M. M., Finger, A., Schweiger, M., and Wolf, D. H. (1996). ER degradation of a misfolded luminal protein by the cytosolic ubiquitin-proteasome pathway. Science *273*, 1725-1728.

Hirayama, H., Fujita, M., Yoko-o, T., and Jigami, Y. (2008). O-mannosylation is required for degradation of the endoplasmic reticulum-associated degradation substrate Gas1*p via the ubiquitin/proteasome pathway in Saccharomyces cerevisiae. J Biochem *143*, 555-567.

Hirsch, C., Gauss, R., Horn, S. C., Neuber, O., and Sommer, T. (2009). The ubiquitylation machinery of the endoplasmic reticulum. Nature *458*, 453-460.

Hong, E., Davidson, A. R., and Kaiser, C. A. (1996). A pathway for targeting soluble misfolded proteins to the yeast vacuole. J Cell Biol *135*, 623-633.

Hong, W. (2005). SNAREs and traffic. Biochim Biophys Acta *1744*, 120-144.

Hoseki, J., Ushioda, R., and Nagata, K. (2010). Mechanism and components of endoplasmic reticulum-associated degradation. J Biochem *147*, 19-25.

Houck, S. A., and Cyr, D. M. (2012). Mechanisms for quality control of misfolded transmembrane proteins. Biochimica et Biophysica Acta (BBA) - Biomembranes Protein Folding in Membranes *1818*, 1108-1114.

Huang, W. P., Scott, S. V., Kim, J., and Klionsky, D. J. (2000). The itinerary of a vesicle component, Aut7p/Cvt5p, terminates in the yeast vacuole via the autophagy/Cvt pathways. J Biol Chem *275*, 5845-5851.

Ichimura, Y., Kirisako, T., Takao, T., Satomi, Y., Shimonishi, Y., Ishihara, N., Mizushima, N., Tanida, I., Kominami, E., Ohsumi, M.*, et al.* (2000). A ubiquitin-like system mediates protein lipidation. Nature *408*, 488-492.

Ishihara, N., Hamasaki, M., Yokota, S., Suzuki, K., Kamada, Y., Kihara, A., Yoshimori, T., Noda, T., and Ohsumi, Y. (2001). Autophagosome requires specific early Sec proteins for its formation and NSF/SNARE for vacuolar fusion. Mol Biol Cell *12*, 3690-3702.

Jakob, C. A., Bodmer, D., Spirig, U., Battig, P., Marcil, A., Dignard, D., Bergeron, J. J., Thomas, D. Y., and Aebi, M. (2001). Htm1p, a mannosidase-like protein, is involved in glycoprotein degradation in yeast. EMBO Rep *2*, 423-430.

Jensen, D., and Schekman, R. (2011). COPII-mediated vesicle formation at a glance. J Cell Sci *124*, 1-4.

Kadowaki, H., Nagai, A., Maruyama, T., Takami, Y., Satrimafitrah, P., Kato, H., Honda, A., Hatta, T., Natsume, T., Sato, T.*, et al.* (2015). Pre-emptive Quality Control Protects the ER from Protein Overload via the Proximity of ERAD Components and SRP. Cell Reports *13*, 944-956.

Kato, M., Saitsu, H., Murakami, Y., Kikuchi, K., Watanabe, S., Iai, M., Miya, K., Matsuura, R., Takayama, R., Ohba, C.*, et al.* (2014). PIGA mutations cause early-onset epileptic encephalopathies and distinctive features. Neurology *82*, 1587-1596.

Kaufmann, A., Beier, V., Franquelim, H. G., and Wollert, T. (2014). Molecular Mechanism of Autophagic Membrane-Scaffold Assembly and Disassembly. Cell *156*, 469-481.

Khoury, G. A., Baliban, R. C., and Floudas, C. A. (2011). Proteome-wide post-translational modification statistics: frequency analysis and curation of the swiss-prot database. Scientific Reports *1 DO - 10.1038/srep00090 AN - PMC3201773*, 90.

Kienle, N., Kloepper, T. H., and Fasshauer, D. (2009). Phylogeny of the SNARE vesicle fusion machinery yields insights into the conservation of the secretory pathway in fungi. BMC Evol Biol *9*, 19.

Kincaid, M. M., and Cooper, A. A. (2007). Misfolded proteins traffic from the endoplasmic reticulum (ER) due to ER export signals. Mol Biol Cell *18*, 455-463.

Kinoshita, T. (2014). Biosynthesis and deficiencies of glycosylphosphatidylinositol. Proc Jpn Acad Ser B Phys Biol Sci *90*, 130-143.

Kinoshita, T., and Fujita, M. (2016). Biosynthesis of GPI-anchored proteins: special emphasis on GPI lipid remodeling. Journal of Lipid Research *57*, 6-24.

Kirisako, T., Baba, M., Ishihara, N., Miyazawa, K., Ohsumi, M., Yoshimori, T., Noda, T., and Ohsumi, Y. (1999). Formation process of autophagosome is traced with Apg8/Aut7p in yeast. J Cell Biol *147*, 435-446.

Klionsky, D. J., Abdalla, F. C., Abeliovich, H., Abraham, R. T., Acevedo-Arozena, A., Adeli, K., Agholme, L., Agnello, M., Agostinis, P., Aguirre-Ghiso, J. A.*, et al.* (2012). Guidelines for the use and interpretation of assays for monitoring autophagy. Autophagy *8*, 445-544.

Klionsky, D. J., and Ohsumi, Y. (1999). Vacuolar import of proteins and organelles from the cytoplasm. Annu Rev Cell Dev Biol *15*, 1-32.

Kloepper, T. H., Kienle, C. N., and Fasshauer, D. (2007). An Elaborate Classification of SNARE Proteins Sheds Light on the Conservation of the Eukaryotic Endomembrane System. Molecular Biology of the Cell *18*, 3463-3471 DO - 3410.1091/mbc.E3407-3403-0193.

Komander, D., and Rape, M. (2012). The ubiquitin code. Annu Rev Biochem *81*, 203-229.

Korennykh, A., and Walter, P. (2012). Structural basis of the unfolded protein response. Annu Rev Cell Dev Biol *28*, 251-277.

Kraft, C., Reggiori, F., and Peter, M. (2009). Selective types of autophagy in yeast. Biochim Biophys Acta *1793*, 1404-1412.

Kramer, L., and Ungermann, C. (2011). HOPS drives vacuole fusion by binding the vacuolar SNARE complex and the Vam7 PX domain via two distinct sites. Mol Biol Cell *22*, 2601-2611.

Lamb, C. A., Yoshimori, T., and Tooze, S. A. (2013). The autophagosome: origins unknown, biogenesis complex. Nat Rev Mol Cell Biol *14*, 759-774.

Lang, T., Reiche, S., Straub, M., Bredschneider, M., and Thumm, M. (2000). Autophagy and the cvt pathway both depend on AUT9. J Bacteriol *182*, 2125-2133.

Lemus, L., and Goder, V. (2014). Regulation of Endoplasmic Reticulum-Associated Protein Degradation (ERAD) by Ubiquitin. Cells *3*, 824-847.

Lemus, L., Ribas, J. L., Sikorska, N., and Goder, V. (2016). An ER-Localized SNARE Protein Is Exported in Specific COPII Vesicles for Autophagosome Biogenesis. Cell Rep *14*, 1710-1722.

Lewis, M. J., and Pelham, H. R. (1996). SNARE-mediated retrograde traffic from the Golgi complex to the endoplasmic reticulum. Cell *85*, 205-215.

Lewis, M. J., Rayner, J. C., and Pelham, H. R. (1997). A novel SNARE complex implicated in vesicle fusion with the endoplasmic reticulum. Embo J *16*, 3017-3024.

Lippincott-Schwartz, J., Bonifacino, J. S., Yuan, L. C., and Klausner, R. D. (1988). Degradation from the endoplasmic reticulum: Disposing of newly synthesized proteins. Cell *54*, 209-220.

Loizides-Mangold, U., David, F. P., Nesatyy, V. J., Kinoshita, T., and Riezman, H. (2012). Glycosylphosphatidylinositol anchors regulate glycosphingolipid levels. J Lipid Res *53*, 1522-1534.

Longatti, A., and Tooze, S. A. (2009). Vesicular trafficking and autophagosome formation. Cell Death Differ *16*, 956-965.

Low, M., and Saltiel, A. (1988). Structural and functional roles of glycosyl-phosphatidylinositol in membranes. Science *239*, 268 LP - 275.

Lynch-Day, M. A., and Klionsky, D. J. (2010). The Cvt pathway as a model for selective autophagy. FEBS letters *584*, 1359-1366.

Lynes, E. M., and Simmen, T. (2011). Urban planning of the endoplasmic reticulum (ER): how diverse mechanisms segregate the many functions of the ER. Biochim Biophys Acta *1813*, 1893-1905.

Ma, J., and Lindquist, S. (2001). Wild-type PrP and a mutant associated with prion disease are subject to retrograde transport and proteasome degradation. Proc Natl Acad Sci U S A *98*, 14955-14960.

Maeda, Y., Tashima, Y., Houjou, T., Fujita, M., Yoko-o, T., Jigami, Y., Taguchi, R., and Kinoshita, T. (2007). Fatty Acid Remodeling of GPI-anchored Proteins Is Required for Their Raft Association. Molecular Biology of the Cell *18*, 1497-1506.

Manzano-Lopez, J., Perez-Linero, A. M., Aguilera-Romero, A., Martin, M. E., Okano, T., Silva, D. V., Seeberger, P. H., Riezman, H., Funato, K., Goder, V.*, et al.* (2015). COPII Coat Composition Is Actively Regulated by Luminal Cargo Maturation. Curr Biol *25*, 152-162.

Mari, M., Griffith, J., Rieter, E., Krishnappa, L., Klionsky, D. J., and Reggiori, F. (2010). An Atg9-containing compartment that functions in the early steps of autophagosome biogenesis. J Cell Biol *190*, 1005-1022.

Mayor, S., and Riezman, H. (2004). Sorting GPI-anchored proteins. Nat Rev Mol Cell Biol *5*, 110-120.

Mehnert, M., Sommer, T., and Jarosch, E. (2010). ERAD ubiquitin ligases: multifunctional tools for protein quality control and waste disposal in the endoplasmic reticulum. Bioessays *32*, 905-913.

Metzger, M. B., Hristova, V. A., and Weissman, A. M. (2012). HECT and RING finger families of E3 ubiquitin ligases at a glance. J Cell Sci *125*, 531 LP - 537.

Metzger, M. B., Pruneda, J. N., Klevit, R. E., and Weissman, A. M. (2014). RING-type E3 ligases: Master manipulators of E2 ubiquitin-conjugating enzymes and ubiquitination. Biochimica et Biophysica Acta (BBA) - Molecular Cell Research Ubiquitin-Proteasome System *1843*, 47-60.

Meusser, B., Hirsch, C., Jarosch, E., and Sommer, T. (2005). ERAD: the long road to destruction. Nat Cell Biol *7*, 766-772.

Miller, E. A., and Schekman, R. (2013). COPII - a flexible vesicle formation system. Curr Opin Cell Biol *25*, 420-427.

Mizushima, N., Yoshimori, T., and Levine, B. (2010). Methods in mammalian autophagy research. Cell *140*, 313-326.

Mizushima, N., Yoshimori, T., and Ohsumi, Y. (2011). The role of Atg proteins in autophagosome formation. Annu Rev Cell Dev Biol *27*, 107-132.

Moreau, K., Ravikumar, B., Renna, M., Puri, C., and Rubinsztein, D. C. (2011). Autophagosome precursor maturation requires homotypic fusion. Cell *146*, 303-317.

Moreau, K., Renna, M., and Rubinsztein, D. C. (2013). Connections between SNAREs and autophagy. Trends Biochem Sci *38*, 57-63.

Moreau, K., and Rubinsztein, D. C. (2012). The plasma membrane as a control center for autophagy. Autophagy *8*, 861-863.

Muniz, M., Nuoffer, C., Hauri, H. P., and Riezman, H. (2000). The Emp24 complex recruits a specific cargo molecule into endoplasmic reticulum-derived vesicles. J Cell Biol *148*, 925-930.

Nair, U., Jotwani, A., Geng, J., Gammoh, N., Richerson, D., Yen, W. L., Griffith, J., Nag, S., Wang, K., Moss, T., *et al.* (2011). SNARE proteins are required for macroautophagy. Cell *146*, 290-302.

Nakatsukasa, K., Okada, S., Umebayashi, K., Fukuda, R., Nishikawa, S., and Endo, T. (2004). Roles of O-mannosylation of aberrant proteins in reduction of the load for endoplasmic reticulum chaperones in yeast. J Biol Chem *279*, 49762-49772.

Nedelsky, N. B., Todd, P. K., and Taylor, J. P. (2008). Autophagy and the ubiquitin-proteasome system: Collaborators in neuroprotection. Biochimica et Biophysica Acta (BBA) - Molecular Basis of Disease Ubiquitin, Proteasomes, and Disease *1782*, 691-699.

Needham, P. G., and Brodsky, J. L. (2013). How early studies on secreted and membrane protein quality control gave rise to the ER associated degradation (ERAD) pathway: The early history of ERAD. Biochimica et biophysica acta *1833*, 2447-2457.

Ng, B. G., Hackmann, K., Jones, M. A., Eroshkin, A. M., He, P., Wiliams, R., Bhide, S., Cantagrel, V., Gleeson, J. G., Paller, A. S.*, et al.* (2012). Mutations in the glycosylphosphatidylinositol gene PIGL cause CHIME syndrome. Am J Hum Genet *90*, 685-688.

Nishikawa, S., Brodsky, J. L., and Nakatsukasa, K. (2005). Roles of molecular chaperones in endoplasmic reticulum (ER) quality control and ER-associated degradation (ERAD). J Biochem *137*, 551-555.

Nishikawa, S. I., Fewell, S. W., Kato, Y., Brodsky, J. L., and Endo, T. (2001). Molecular chaperones in the yeast endoplasmic reticulum maintain the solubility of proteins for retrotranslocation and degradation. J Cell Biol *153*, 1061-1070.

Noda, T., Kim, J., Huang, W. P., Baba, M., Tokunaga, C., Ohsumi, Y., and Klionsky, D. J. (2000). Apg9p/Cvt7p is an integral membrane protein required for transport vesicle formation in the Cvt and autophagy pathways. J Cell Biol *148*, 465-480.

Ogg, S. C., Poritz, M. A., and Walter, P. (1992). Signal recognition particle receptor is important for cell growth and protein secretion in Saccharomyces cerevisiae. Mol Biol Cell *3*, 895-911.

Ohsumi, Y. (2014). Historical landmarks of autophagy research. Cell Research *24*, 9-23.

Okamoto, K. (2014). Organellophagy: Eliminating cellular building blocks via selective autophagy. Journal of Cell Biology *205*, 435-445.

Olzmann, J. A., Kopito, R. R., and Christianson, J. C. (2013). The Mammalian Endoplasmic Reticulum-Associated Degradation System. Cold Spring Harbor perspectives in biology *5*, 10.1101/cshperspect.a013185 a013185.

Palade, G. (1975). Intracellular aspects of the process of protein synthesis. Science *189*, 867.

Palade, G. E. (1956). Intracisternal granules in the exocrine cells of the pancreas. J Biophys Biochem Cytol *2*, 417-422.

Paladino, S., Lebreton, S., and Zurzolo, C. (2015). Chapter Eight - Trafficking and Membrane Organization of GPI-Anchored Proteins in Health and Diseases. Current Topics in Membranes. In Lipid Domains, A. K. Kenworthy, ed. (Academic Press), pp. 269-303.

Patel, S. K., Indig, F. E., Olivieri, N., Levine, N. D., and Latterich, M. (1998). Organelle membrane fusion: a novel function for the syntaxin homolog Ufe1p in ER membrane fusion. Cell *92*, 611-620.

Paulick, M. G., and Bertozzi, C. R. (2008). The glycosylphosphatidylinositol anchor: a complex membrane-anchoring structure for proteins. Biochemistry *47*, 6991-7000.

Pincus, D. (2016). Size doesn't matter in the heat shock response. Current Genetics, 1-4.

Pisoni, G., and Molinari, M. (2016). Five Questions (with their Answers) on ER-Associated Degradation. Traffic *17*, 341-350.

Pittet, M., and Conzelmann, A. (2007). Biosynthesis and function of GPI proteins in the yeast Saccharomyces cerevisiae. Biochim Biophys Acta *1771*, 405-420.

Popovic, D., Akutsu, M., Novak, I., Harper, J. W., Behrends, C., and Dikic, I. (2012). Rab GTPase-activating proteins in autophagy: regulation of endocytic and autophagy pathways by direct binding to human ATG8 modifiers. Mol Cell Biol *32*, 1733-1744.

Puri, C., Renna, M., Bento, C. F., Moreau, K., and Rubinsztein, D. C. (2013). Diverse autophagosome membrane sources coalesce in recycling endosomes. Cell *154*, 1285-1299.

Rao, Y., Matscheko, N., and Wollert, T. (2016). Autophagy in the test tube: In vitro reconstitution of aspects of autophagosome biogenesis. The FEBS Journal *283*, 2034-2043.

Rapoport, T. A. (2007). Protein translocation across the eukaryotic endoplasmic reticulum and bacterial plasma membranes. Nature *450*, 663-669.

Ravikumar, B., Moreau, K., Jahreiss, L., Puri, C., and Rubinsztein, D. C. (2010). Plasma membrane contributes to the formation of pre-autophagosomal structures. Nat Cell Biol *12*, 747-757.

Reggiori, F., Canivenc-Gansel, E., and Conzelmann, A. (1997). Lipid remodeling leads to the introduction and exchange of defined ceramides on GPI proteins in the ER and Golgi of Saccharomyces cerevisiae. Embo J *16*, 3506-3518.

Reggiori, F., and Klionsky, D. J. (2013). Autophagic processes in yeast: mechanism, machinery and regulation. Genetics *194*, 341-361.

Reggiori, F., and Ungermann, C. (2017). Autophagosome maturation and fusion. Journal of Molecular Biology.

Rubinsztein, D. C. (2015). Cell biology: Receptors for selective recycling. Nature *522*, 291-292.

Saha, S., Anilkumar, A. A., and Mayor, S. (2015). GPI-anchored protein organization and dynamics at the cell surface. J Lipid Res *57*, 159-175.

Saheki, Y., and De Camilli, P. (2017). Endoplasmic Reticulum-Plasma Membrane Contact Sites. Annu Rev Biochem *86*.

Sanchez-Wandelmer, J., Ktistakis, N. T., and Reggiori, F. (2015). ERES: sites for autophagosome biogenesis and maturation? J Cell Sci *128*, 185-192.

Satpute-Krishnan, P., Ajinkya, M., Bhat, S., Itakura, E., Hegde, R. S., and Lippincott-Schwartz, J. (2014). ER stress-induced clearance of misfolded GPI-anchored proteins via the secretory pathway. Cell *158*, 522-533.

Schubert, U., Antón, L. C., Gibbs, J., Norbury, C. C., Yewdell, J. W., and Bennink, J. R. (2000). Rapid degradation of a large fraction of newly synthesized proteins by proteasomes. Nature *404*, 770-774.

Senft, D., and Ronai, Z. e. A. (2015). UPR, autophagy and mitochondria crosstalk underlies the ER stress response. Trends in biochemical sciences *40*, 141-148.

Seong, J., Wang, Y., Kinoshita, T., and Maeda, Y. (2013). Implications of lipid moiety in oligomerization and immunoreactivities of GPI-anchored proteins. J Lipid Res *54*, 1077-1091.

Shibata, Y., Voeltz, G. K., and Rapoport, T. A. (2006). Rough sheets and smooth tubules. Cell *126*, 435-439.

Siekevitz, P., and Palade, G. E. (1962). Cytochemical study on the pancreas of the guinea pig. VII. Effects of spermine on ribosomes. J Cell Biol *13*, 217-232.

Sikorska, N., Lemus, L., Aguilera-Romero, A., Manzano-Lopez, J., Riezman, H., Muniz, M., and Goder, V. (2016). Limited ER quality control for GPI-anchored proteins. J Cell Biol *213*, 693-704.

Smith, H. W., and Marshall, C. J. (2010). Regulation of cell signalling by uPAR. *11*, 23-36.

Sollner, T., Whiteheart, S. W., Brunner, M., Erdjument-Bromage, H., Geromanos, S., Tempst, P., and Rothman, J. E. (1993). SNAP receptors implicated in vesicle targeting and fusion. *362*, 318-324.

Sommer, T., and Jentsch, S. (1993). A protein translocation defect linked to ubiquitin conjugation at the endoplasmic reticulum. Nature *365*, 176-179.

Sommer, T., and Wolf, D. H. (1997). Endoplasmic reticulum degradation: reverse protein flow of no return. Faseb J *11*, 1227-1233.

Stefanova, I., Horejsi, V., Ansotegui, I., Knapp, W., and Stockinger, H. (1991). GPI-anchored cell-surface molecules complexed to protein tyrosine kinases. Science *254*, 1016 LP - 1019.

Stolz, A., Ernst, A., and Dikic, I. (2014). Cargo recognition and trafficking in selective autophagy. Nat Cell Biol *16*, 495-501.

Stolz, A., and Wolf, D. H. (2010). Endoplasmic reticulum associated protein degradation: a chaperone assisted journey to hell. Biochim Biophys Acta *1803*, 694-705.

Suzuki, K., Akioka, M., Kondo-Kakuta, C., Yamamoto, H., and Ohsumi, Y. (2013). Fine mapping of autophagy-related proteins during autophagosome formation in Saccharomyces cerevisiae. J Cell Sci *126*, 2534-2544.

Suzuki, K., Kirisako, T., Kamada, Y., Mizushima, N., Noda, T., and Ohsumi, Y. (2001). The pre-autophagosomal structure organized by concerted functions of APG genes is essential for autophagosome formation. Embo J *20*, 5971-5981.

Suzuki, K. G., Fujiwara, T. K., Sanematsu, F., Iino, R., Edidin, M., and Kusumi, A. (2007). GPI-anchored receptor clusters transiently recruit Lyn and Galpha for temporary cluster immobilization and Lyn activation: single-molecule tracking study 1. The Journal of Cell Biology *177*, 717-730.

Swanson, R., Locher, M., and Hochstrasser, M. (2001). A conserved ubiquitin ligase of the nuclear envelope/endoplasmic reticulum that functions in both ER-associated and Matalpha2 repressor degradation. Genes Dev *15*, 2660-2674.

Takats, S., Nagy, P., Varga, A., Pircs, K., Karpati, M., Varga, K., Kovacs, A. L., Hegedus, K., and Juhasz, G. (2013). Autophagosomal Syntaxin17-dependent lysosomal degradation maintains neuronal function in Drosophila. J Cell Biol *201*, 531-539.

Takeshige, K., Baba, M., Tsuboi, S., Noda, T., and Ohsumi, Y. (1992). Autophagy in yeast demonstrated with proteinase-deficient mutants and conditions for its induction. J Cell Biol *119*, 301-311.

Tan, D., Cai, Y., Wang, J., Zhang, J., Menon, S., Chou, H. T., Ferro-Novick, S., Reinisch, K. M., and Walz, T. (2013). The EM structure of the TRAPPIII complex leads to the identification of a requirement for COPII vesicles on the macroautophagy pathway. Proc Natl Acad Sci U S A *110*, 19432-19437.

Tashima, Y., Taguchi, R., Murata, C., Ashida, H., Kinoshita, T., and Maeda, Y. (2006). PGAP2 is essential for correct processing and stable expression of GPI-anchored proteins. Mol Biol Cell *17*, 1410-1420.

Travers, K. J., Patil, C. K., Wodicka, L., Lockhart, D. J., Weissman, J. S., and Walter, P. (2000). Functional and genomic analyses reveal an essential coordination between the unfolded protein response and ER-associated degradation. Cell *101*, 249-258.

Tripodi, F., Nicastro, R., Reghellin, V., and Coccetti, P. (2015). Post-translational modifications on yeast carbon metabolism: Regulatory mechanisms beyond transcriptional control. Biochimica et Biophysica Acta (BBA) - General Subjects *1850*, 620-627.

Tse, A., Barclay, A., Watts, A., and Williams, A. (1985). A glycophospholipid tail at the carboxyl terminus of the Thy-1 glycoprotein of neurons and thymocytes. Science *230*, 1003 LP - 1008.

Umemura, M., Fujita, M., Yoko, O. T., Fukamizu, A., and Jigami, Y. (2007). Saccharomyces cerevisiae CWH43 is involved in the remodeling of the lipid moiety of GPI anchors to ceramides. Mol Biol Cell *18*, 4304-4316.

van der Vaart, A., Griffith, J., and Reggiori, F. (2010). Exit from the Golgi is required for the expansion of the autophagosomal phagophore in yeast Saccharomyces cerevisiae. Mol Biol Cell *21*, 2270-2284.

Varma, R., and Mayor, S. (1998). GPI-anchored proteins are organized in submicron domains at the cell surface. *394*, 798-801.

Vashist, S., and Ng, D. T. (2004). Misfolded proteins are sorted by a sequential checkpoint mechanism of ER quality control. J Cell Biol *165*, 41-52.

Vembar, S. S., and Brodsky, J. L. (2008). One step at a time: endoplasmic reticulum-associated degradation. Nat Rev Mol Cell Biol *9*, 944-957.

Voeltz, G. K., Rolls, M. M., and Rapoport, T. A. (2002). Structural organization of the endoplasmic reticulum. EMBO Rep *3*, 944-950.

Walsh, C. A. (2006). Posttranslational modification of proteins : expanding nature's inventory., Englewood, Colo.: Roberts and Co. Publishers).

Wang, S., and Ng, D. T. (2010). Evasion of endoplasmic reticulum surveillance makes Wsc1p an obligate substrate of Golgi quality control. Mol Biol Cell *21*, 1153-1165.

Wang, Y., Li, L., Hou, C., Lai, Y., Long, J., Liu, J., Zhong, Q., and Diao, J. (2016). SNARE-mediated membrane fusion in autophagy. Seminars in Cell & Developmental Biology *60*, 97-104.

Wang, Y. J., Tayo, B. O., Bandyopadhyay, A., Wang, H., Feng, T., Franceschini, N., Tang, H., Gao, J., Sung, Y. J., Elston, R. C.*, et al.* (2014). The association of the vanin-1 N131S variant with blood pressure is mediated by endoplasmic reticulum-associated degradation and loss of function. PLoS Genet *10*, e1004641.

Watanabe, R., and Riezman, H. (2004). Differential ER exit in yeast and mammalian cells. Curr Opin Cell Biol *16*, 350-355.

Weimbs, T., Low, S. H., Chapin, S. J., Mostov, K. E., Bucher, P., and Hofmann, K. (1997). A conserved domain is present in different families of vesicular fusion proteins: a new superfamily. Proc Natl Acad Sci U S A *94*, 3046-3051.

Werner, E. D., Brodsky, J. L., and McCracken, A. A. (1996). Proteasome-dependent endoplasmic reticulum-associated protein degradation: an

unconventional route to a familiar fate. Proc Natl Acad Sci U S A *93*, 13797-13801.

Whatley, B. R., Li, L., and Chin, L.-S. (2008). The ubiquitin-proteasome system in spongiform degenerative disorders. Biochimica et Biophysica Acta (BBA) - Molecular Basis of Disease Ubiquitin, Proteasomes, and Disease *1782*, 700-712.

Xu, C., and Ng, D. T. W. (2015). Glycosylation-directed quality control of protein folding. Nat Rev Mol Cell Biol *16*, 742-752.

Yen, W. L., Shintani, T., Nair, U., Cao, Y., Richardson, B. C., Li, Z., Hughson, F. M., Baba, M., and Klionsky, D. J. (2010). The conserved oligomeric Golgi complex is involved in double-membrane vesicle formation during autophagy. J Cell Biol *188*, 101-114.

Yla-Anttila, P., Vihinen, H., Jokitalo, E., and Eskelinen, E. L. (2009). 3D tomography reveals connections between the phagophore and endoplasmic reticulum. Autophagy *5*, 1180-1185.

Zhang F, Crise B, Su B, Hou Y, Rose JK, Bothwell A, and K, J. (1991). Lateral diffusion of membrane-spanning and glycosylphosphatidylinositol- linked proteins: toward establishing rules governing the lateral mobility of membrane proteins. The Journal of Cell Biology *115*, 75-84.

Zhao, Y., Macgurn, J. A., Liu, M., and Emr, S. (2013). The ART-Rsp5 ubiquitin ligase network comprises a plasma membrane quality control system that protects yeast cells from proteotoxic stress. Elife *2*, e00459.